Robust layer-resolving methods for various Prandtl Problems

by

John Butler

B.A. (Mod.) (Hons.)M.Sc.

A Thesis submitted to
The University of Dublin
for the degree of

PhD

Department of Mathematics
University of Dublin
Trinity College
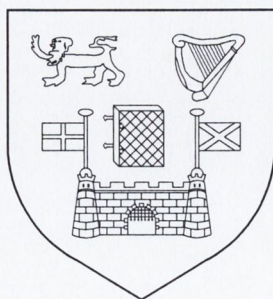
October, 2004
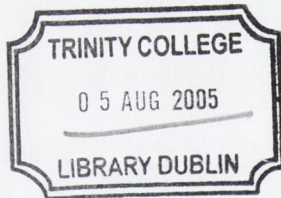
Declaration

This thesis has not been submitted as an exercise for a degree at any other University. Except where otherwise stated, the work described herein has been carried out by the author alone. This thesis may be borrowed or copied upon request with the permission of the Librarian, University of Dublin, Trinity College. The copyright belongs jointly to the University of Dublin and John Butler.

Signature of Author . . . .

John Butler
31 October, 2004

Abstract

Robust layer-resolving methods for various Prandtl Problems.
John Simon Butler

Abstract In this thesis we deal with four Prandtl boundary layer problems for incompressible laminar flow. When the Reynolds and Prandtl numbers are large the solution of each problem has parabolic boundary layers. For each problem we construct a direct numerical method for computing approximations to the solution of the problem using a piecewise uniform fitted mesh technique appropriate to the parabolic boundary layer. We use the numerical method to approximate the self–similar solution of the Prandtl problem in a finite rectangle excluding the leading edge of the wedge, which is the source of an additional singularity caused by incompatibility of the problem data. We verify that the constructed numerical method is robust in the sense that the computed errors for the components and their derivatives in the discrete maximum norm are parameter uniform. For each problem we construct and apply a special numerical method related to the Blasius technique to compute a reference solution for the error analysis of the components and their derivatives. By means of extensive numerical experiments we show that the constructed direct numerical methods are parameter–uniform.

Summary

In this thesis we construct robust layer-resolving methods for various Prandtl problems. Chapter 1 introduces the Prandtl problem and gives a brief history of the numerical methods for singularly perturbed equations.

In Chapter 2 we construct a uniform numerical method for the Prandtl problem for flow past a flat plate. We show the shortcomings of this method.

In Chapters 3-10 we construct four parameter-uniform numerical methods for four Prandtl boundary layer problems for incompressible laminar flow. The problems are:

- the Prandtl problem for flow past a wedge (discussed in Chapters 3 and 4).

- the Prandtl problem for flow past a three dimensional yawed wedge (discussed in Chapters 5 and 6).

- the Prandtl problem for flow past a wedge with heat transfer (discussed in Chapters 7 and 8).

- the Prandtl problem for flow past a wedge with mass transfer (discussed in Chapters 9 and 10)

Each problem is dealt with in a similar fashion. We divide the problem into two chapters.

In the first chapter we construct a semi–analytical reference solution for the components and their derivatives. In the second chapter we construct a direct numerical method for computing approximations to the solution of the problem using a piecewise uniform fitted mesh technique appropriate to the parabolic boundary layers. We use the numerical method to approximate the self–similar solution of the Prandtl problem in a finite rectangle excluding the leading edge of the wedge, which is the source of an additional singularity caused by incompatibility of the problem data. We verify that the constructed numerical method is robust in the sense that the computed errors for the components and their derivatives in the discrete maximum norm are parameter uniform. We also use the reference solution for error analysis of the components and their derivatives. By means of extensive numerical experiments we show that the constructed direct numerical method is parameter–uniform.

To my family

Acknowledgements

I would like to thank Prof J J H Miller my supervisor for his support, knowledge, guidence and grammar.

I would like to thank Prof G I Shishkin for his excitement, energy and vast knowledge of singularly perturbed equations.

I would like to thank my lawyer Brian Mc Elligott for going above and beyond the call of duty.

In alphabetical order I would like to thank my proof readers Eabhnat Ni Fhloinn, Steven Watterson, and Emilie Pine who are generous with time and corrections.

I would like to thank Prof L Crane, Dr S. Ryan, Dr D. O'Donovan and Dr E. O'Riordan for encouraging and interesting chats.

I would like to thank Mary Geraghty, Daire O'Broin, Dave Long, Derek McHugh, Chris Swift, Marco Conte, Dennis Curry, Tom O'Brien and Treasa Ni Mhiochain for a good time.

I have been in the maths dept a long time so I should thank Karen O'Doherty, Justin Foley, Norah Daly, Al Mathews, Michael Cooney, Alan O'Cais and Don Moynihan for being there as well.

I would like to thank Peter Ashe for an opinion on everything.

Last but not least I would like to thank Edel Flynn.

Contents

List of Figures

List of Tables

Chapter 1

Introduction

As a barge glides down the canal it cuts the water like a wedge. The water glides past the bow, and for a brief period before turbulence, before separation, before transitional flow we have laminar flow at the bow of the barge.

In this thesis we deal with laminar flow.

1.1 Ludwig Prandtl

A century ago, in August 1904 at the Third International Congress of Mathematicians, Ludwig Prandtl presented a paper 'On the motion of fluids of very small viscosity'. With the aid of theoretical considerations and several simple experiments, he proved that the flow about a solid body can be divided into two regions: a very thin layer in the neighbourhood of the body (*boundary layer*) where friction plays an essential part, and the remaining region outside this layer, where friction can be neglected.

The boundary layer theory finds its application in the calculation of the skin-friction drag which acts on a body as it is moved through a fluid: for example, the drag experienced by a flat plate at zero incidence, the drag of a ship, of an aeroplane wing or turbine blades. Boundary layer flow has the peculiar property that under certain conditions the flow in the immediate neighbourhood of a solid cell becomes reversed causing the boundary layer to separate from it. This is accompanied by a more or less pronounced formation of eddies in the wake of the body (see Figure 1-1).

Problems of heat transfer between a solid body and a fluid flowing past it also belong to the class of problems in which boundary layer phenomena play a decisive part.
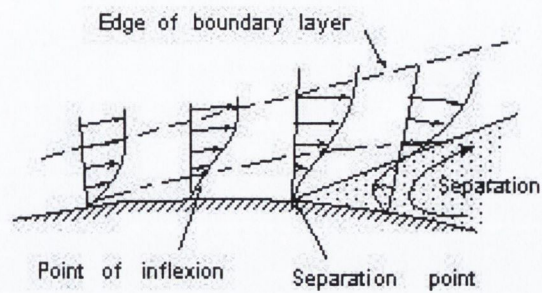
Figure 1-1: Point of separation

1.2 Navier Stokes

An incompressible fluid is a fluid whose density is not changed by external forces acting on the fluid. Most steady state incompressible fluid systems can be modelled using the Navier-Stokes equations.

$$(P_{NS}) \begin{cases} \text{momentum equation} \\ -\nu \triangle^2 \mathbf{u}_{NS} + \mathbf{u}_{NS} \cdot \nabla \mathbf{u_{NS}} = -\frac{1}{\rho} \nabla p_{NS} \\ \\ \text{continuity equation} \\ \nabla . \mathbf{u}_{NS} = 0 \\ \\ \text{temperature (energy) equation} \\ -\frac{\nu}{k c_p} \triangle^2 t_{NS} + \mathbf{u}_{NS} . \nabla t_{NS} = 0 \end{cases}$$

where

- ν is the kinematic viscosity,

- ρ is the density,

- k is thermal conductivity,

- c_p is the specific heat for a constant pressure,

- p_{NS} is the pressure field,

- $\mathbf{u}_{NS} = (U_{NS}, V_{NS}, W_{NS})$ is the unknown velocity component,

- T_{NS} is the unknown temperature (energy) component.

Written out in full, the differential equations are

$$
(P_{NS}) \begin{cases}
\text{X-component of the momentum equation} \\
-\nu\left(\frac{\partial^2 U_{NS}}{\partial X^2} + \frac{\partial^2 U_{NS}}{\partial Y^2} + \frac{\partial^2 U_{NS}}{\partial Z^2}\right) + u_{NS}\frac{\partial U_{NS}}{\partial X} + v_{NS}\frac{\partial U_{NS}}{\partial Y} + w_{NS}\frac{\partial U_{NS}}{\partial Z} + \frac{1}{\rho}\frac{\partial p_{NS}}{\partial X} = 0 \\
\text{y-component of the momentum equation} \\
-\nu\left(\frac{\partial^2 V_{NS}}{\partial X^2} + \frac{\partial^2 V_{NS}}{\partial Y^2} + \frac{\partial^2 V_{NS}}{\partial Z^2}\right) + u_{NS}\frac{\partial V_{NS}}{\partial X} + v_{NS}\frac{\partial V_{NS}}{\partial Y} + w_{NS}\frac{\partial V_{NS}}{\partial Z} + \frac{1}{\rho}\frac{\partial p_{NS}}{\partial Y} = 0 \\
\text{z-component of the momentum equation} \\
-\nu\left(\frac{\partial^2 W_{NS}}{\partial X^2} + \frac{\partial^2 W_{NS}}{\partial Y^2} + \frac{\partial^2 W_{NS}}{\partial Z^2}\right) + u_{NS}\frac{\partial W_{NS}}{\partial X} + v_{NS}\frac{\partial W_{NS}}{\partial Y} + w_{NS}\frac{\partial W_{NS}}{\partial Z} + \frac{1}{\rho}\frac{\partial p_{NS}}{\partial Z} = 0 \\
\text{continuity equation} \\
\frac{\partial U_{NS}}{\partial X} + \frac{\partial V_{NS}}{\partial Y} + \frac{\partial W_{NS}}{\partial Z} = 0 \\
\text{temperature (energy) equation} \\
-\frac{\nu}{kc_p}\left(\frac{\partial^2 T_{NS}}{\partial X^2} + \frac{\partial^2 T_{NS}}{\partial Y^2} + \frac{\partial^2 T_{NS}}{\partial Z^2}\right) + U_{NS}\frac{\partial T_{NS}}{\partial X} + V_{NS}\frac{\partial T_{NS}}{\partial Y} + W_{NS}\frac{\partial T_{NS}}{\partial Z} = 0.
\end{cases}
$$

Using Prandtl's approach the vertical momentum equation is omitted and the horizontal momentum equation is simplified, see [46] and [1]. The dimensionless Prandtl Problem is

$$
(P_P) \begin{cases}
-\frac{1}{Re}\frac{\partial^2 u_P}{\partial y^2} + u_P\frac{\partial u_P}{\partial x} + v_P\frac{\partial u_P}{\partial y} + w_P\frac{\partial u_P}{\partial z} = U\frac{dU}{dx} \\[2mm]
-\frac{1}{Re}\frac{\partial^2 v_P}{\partial y^2} + u_P\frac{\partial v_P}{\partial x} + v_P\frac{\partial v_P}{\partial y} + w_P\frac{\partial v_P}{\partial z} = V\frac{dV}{dy} \\[2mm]
-\frac{1}{Re}\frac{\partial^2 w_P}{\partial y^2} + u_P\frac{\partial w_P}{\partial x} + v_P\frac{\partial w_P}{\partial y} + w_P\frac{\partial w_P}{\partial z} = W\frac{dW}{dz} \\[2mm]
\frac{\partial u_P}{\partial x} + \frac{\partial v_P}{\partial y} + \frac{\partial w_P}{\partial z} = 0 \\[2mm]
-\frac{1}{Re}\frac{1}{Pr}\frac{\partial^2 t_P}{\partial y^2} + \mathbf{u}_P.\nabla t_P = 0
\end{cases}
$$

with boundary conditions

$$
\begin{aligned}
y = 0, \quad & u_P = w_P = 0, \quad v_p = v_0(x) \text{ and } t_p = 1 \\
y \to \infty, \quad & u_P = w_P = 1 \text{ and } t_p = 0
\end{aligned}
$$

where $\mathbf{U} = (U, V, W)$ is the potential flow. $Re = \frac{U_0 L}{\mu}$ is the Reynolds number, where U_0 and L, represent velocity and length scales in the system. $Pr = \frac{\mu c_p}{k}$ is the Prandtl number, where μ represents the viscosity. $x = \frac{X}{L}$, $y = \frac{Y}{L}$ and $z = \frac{Z}{L}$ are dimensionless coordinates.

Since there is only one second order derivative in the momentum equations in (P_P), this is a parabolic equation, in contrast to the elliptic equation in (P_{NS}). From

Prandtl's work it is known that the solution of (P_P) is a good approximation to the solution of (P_{NS}) in a subdomain excluding the leading edge region, provided that the flow remains laminar and that no separation occurs.

As the momentum equation is nonlinear it is difficult to calculate analytic solutions therefore we attack the problem using numerical methods.

The momentum equations are singularly perturbed with respect to the Reynolds number (Re). The energy equation is singularly perturbed with respect to the Reynolds number (Re) and the Prandtl number (Pr). It is well known that for flow problems with large Reynolds and Prandtl numbers boundary layers arise. Also, when classical numerical methods are applied to these problems large errors occur, especially in approximations of the derivatives, which grow unboundedly as the Reynolds and Prandtl numbers increase. For this reason robust layer-resolving numerical methods, in which the error is independent of the singular perturbation parameter, are required. We want to solve the Prandtl problem in a region including the parabolic boundary layer. We restrict our research to the Prandtl boundary layer equations and the energy equation.

1.3   Numerical methods for singularly perturbed equations

Linearization of (P_P) is typically of the fom

$$-\varepsilon \triangle \mathbf{u} + \mathbf{b} \cdot \nabla \mathbf{u} + c\mathbf{u} = \mathbf{f},$$

where $\mathbf{b}$ is independent of u. This is a convection-diffusion problem. The convection diffusion problem is singularly perturbed with respect to ε.

A review of some classical uniform methods for boundary and interior layers is given in [16] and [17]. In [44] H.-G. Roos, M. Stynes and L. Tobiska give a review of numerical methods for singularly perturbed equations.

The difficulty with standard numerical methods which employ uniform meshes is a lack of robustness with respect to the perturbation parameter ε. Since the layer contracts as ε becomes smaller, the mesh needs to be refined substantially to capture the dynamics within the diminishing layer; this is illustrated in Chapter 2 of this thesis. An ingenious solution to this problem is a piece-wise mesh has been proposed by Shishkin [39]. This mesh, together with an appropriate difference scheme, gives solutions that are robust with respect to the perturbation parameter ε. Proofs of

theoretical results for linear singularly perturbed equations using Shishkin meshes
are in [39] and [26]. Experimental results for non-linear singularly perturbed equa-
tions using Shishkin meshes are in [39]. As the Prandtl boundary layer equations
are non-linear, theoretical results are difficult to prove. There have been promising
computational results done for Prandtl's problem for flow past a flat plate in the
book [26] and in the papers [23], [24] and [25].

In his thesis [3] A. Ansari investigated the Prandtl problem for a two dimensional
laminar jet. The numerical results shown in his thesis are parameter uniform. He
also investigated a convection diffusion problem with mixed boundary conditions in
1-D.

In the paper [38] Miller *et al* present computational results for a Reynolds uniform
numerical method for the Prandtl solution and its derivatives for stagnation line flow.
These computational methods are the basis of the thesis.

1.4   Definitions

Numerical methods that converge uniformly for all values of the parameter, ε in the
range $(0, 1]$ and that require a parameter–uniform amount of computational work to
compute each numerical solution are known as parameter–uniform or ε–uniform. If
a method is ε–uniform the dfference between the exact solution u_ε and the numerical
solution U_ε^N satisfies an estimate of the following form: for some positive integer N_0,
all integers $N \geq N_0$ and all $\varepsilon \in (0, 1]$, we have

$$\|\overline{U}_\varepsilon^N - u_\varepsilon\|_{\overline{\Omega}} \leq CN^{-p},$$

where C, N_0 and p are positive constants independent of ε and N. Here $\overline{U_\varepsilon^N}$ denotes
the piecewise linear interpolant on the whole domain $\overline{\Omega}$ of the mesh function U_ε^N
defined on the mesh $\overline{\Omega}^N$ and $\|.\|_{\overline{\Omega}}$ denotes the maximum norm on the whole domain
$\overline{\Omega}$.

Definition Let (P_ε) be a family of mathematical problems parameterized by a singu-
lar perturbation parameter ε, where ε satisfies $0 < \varepsilon \leq 1$. Assume that each problem
in (P_ε) has a unique solution denoted by u_ε, and that each u_ε is approximated by a
sequence of numerical solutions $\{U_\varepsilon^N, \overline{\Omega}^N\}_{N=1}^\infty$ obtained using a monotone numerical
method (P_ε^N), where U_ε^N is defined on the mesh $\overline{\Omega}^N$ and N is a discretization param-
eter. Let $\overline{U^N}_\varepsilon$ denote the piecewise linear interpolant over $\overline{\Omega}$ of the discrete solution
U_ε^N. Then (P_ε^N) is said to be a robust layer–resolving method if the numerical solu-
tions are computable with an ε–uniform amount of computational work and converge

ε-uniformly, in the sense that there exists a positive integer N_0, and positive numbers C and p, where N_0, C and p are independent of N and ε, such that for all $N \geq N_0$

$$\sup_{0<\varepsilon\leq 1} ||\overline{U^N}_\varepsilon - u_\varepsilon||_{\overline{\Omega}} \leq CN^{-p}.$$

1.5   Thesis outline

Chapter 2 describes a numerical method on a uniform mesh for the Prandtl problem for flow past a flat plate. The chapter shows that a numerical method on a uniform mesh will not yield Re-uniform results.

In Chapters 3-10 we construct four parameter-uniform numerical methods for four Prandtl problems. Each problem is dealt with in two chapters; the first chapter solving the Blasius form and the second solving the Prandtl problem. We use Chapters 11 and 12 in [26] as the blueprint for these four problems. While each problem can stand alone, it is better to view it as an organic progression. When constructing each method we use the knowledge gained from the previous numerical methods.

In Chapters 3 and 4 we construct a Re-uniform numerical method for the Prandtl boundary layer problem for flow past a semi-infinite wedge (see [46], [1] and [20]). In Chapter 3 we numerically solve the Falkner–Skan problem [43] for f and its derivatives, and then use a variant of the semi-analytic approach of Falkner–Skan to generate numerical approximations of guaranteed pointwise accuracy to the velocity components and their scaled derivatives. In Chapter 4 we construct a direct numerical method for the Prandtl problem to generate numerical approximations of guaranteed accuracy to the velocity components and their scaled derivatives for all Reynolds and angles of the wedge considered.

In Chapters 5 and 6 we construct a Re-uniform numerical method for the Prandtl boundary layer problem for flow past a three dimensional semi-infinite wedge (see [46] and [45]). Similarly to Chapter 3, in Chapter 5 we numerically solve the Blasius problem [45] for f, g and their derivatives, and then use a variant of the semi-analytic approach of Blasius to generate numerical approximations of guaranteed pointwise accuracy to the velocity components and their scaled derivatives. Similar to Chapter 4, in Chapter 6 we construct a direct numerical method for the Prandtl problem to generate numerical approximations of guaranteed accuracy to the velocity components and their scaled derivatives for all Reynolds and angles of the wedge considered.

In Chapters 7 and 8 we construct a Re and Pr uniform numerical method for the Prandtl boundary layer problem for flow past a semi-infinite wedge with heat–transfer

(see [18], [51], [20] and [36]). In Chapter 7 we numerically solve the Blasius problem for f, θ and their derivatives, and then use a variant of the semi-analytic approach of Blasius to generate numerical approximations of guaranteed pointwise accuracy to the velocity components, temperature component and their scaled derivatives. In Chapter 8 we use the knowledge gained in the previous chapters to construct a direct numerical method for the Prandtl problem to generate numerical approximations of guaranteed accuracy to the velocity components, the temperature component and their scaled derivatives for all Reynolds, all Prandtl and angles of the wedge considered for a constant wall temperature and constant heat flux.

In Chapters 9 and 10 we construct a Re uniform numerical method for the Prandtl boundary layer problem for flow past a semi-infinite wedge with mass–transfer (see [46] and [43]). In Chapter 9 we numerically solve the Blasius problem for f, and its derivatives, and then use a variant of the semi-analytic approach of Blasius to generate numerical approximations of guaranteed pointwise accuracy to the velocity components and its scaled derivatives. In Chapter 10 we use the knowledge gained in the previous chapters to construct a direct numerical method for the Prandtl problem to generate numerical approximations of guaranteed accuracy to the velocity components and its scaled derivatives for all Reynolds, angles of the wedge and mass-transfer.

All the code in this thesis was written in C and run on the work-stations in the mathematics department in Trinity College Dublin.

Chapter 2

Prandtl flow past a flat plate - uniform mesh

2.1 Introduction

In this chapter we investigate the use of a numerical method on a uniform mesh for the Prandtl problem for flow past a flat plate.

We want to solve the Prandtl problem in a region that includes the parabolic boundary layer. Since the solution of the problem has a singularity at the leading edge of the plate, we take as the computational domain the finite rectangle $\Omega = (0.1, 1.1) \times (0, 1)$ on the upper side of the plate, which is sufficiently far from the leading edge that the leading edge singularity does not cause problems for the numerical method. We denote the boundary of Ω by $\Gamma = \Gamma_L \bigcup \Gamma_T \bigcup \Gamma_B \bigcup \Gamma_R$ where Γ_L, Γ_T, Γ_B and Γ_R denote, respectively, the left-hand, top, bottom and right-hand edges of Ω.

The Prandtl boundary layer problem in Ω is

$$(P_u) \begin{cases} \text{Find } \mathbf{u}_\varepsilon = (u_\varepsilon, v_\varepsilon) \text{ such that for all } (x, y) \in \Omega \\ \mathbf{u}_\varepsilon \text{ satisfies the differential equation} \\ \\ -\frac{1}{Re}\frac{\partial^2 u_\varepsilon}{\partial^2 y} + \mathbf{u}_\varepsilon.\nabla u_\varepsilon = 0 \\ \\ \nabla.\mathbf{u}_\varepsilon = 0 \\ \\ \text{with the boundary conditions} \\ \mathbf{u}_\varepsilon = 0 \text{ on } \Gamma_B \\ \mathbf{u}_\varepsilon = \mathbf{u}_P \text{ on } \Gamma_L \bigcup \Gamma_T. \end{cases}$$

where u_P is the exact solution of (P_P). The goal of this chapter is to show that a numerical method on a uniform mesh will give error bounds for the solution components and their derivatives, that depend on the value of Re, for $Re \in [1, \infty)$. The numerical method on a uniform mesh is **not** (Re)–uniform.

2.2   Blasius solution

Using the transformation described in [43], (P_u) can be simplified to the well–known Blasius problem, involving a non-linear ordinary differential equation, which we now describe. Writing

$$\eta = y\sqrt{\frac{Re}{2x}}$$

the velocity components have the form

$$u_{UB}(x, y) = f'(\eta)$$

$$v_{UB}(x, y) = -\sqrt{\frac{1}{2x}\frac{1}{Re}}\,(f - \eta f')\,.$$

where f is the solution of the Blasius problem

$$(P_{UB}) \begin{cases} \text{For } \eta \in (0, \infty) \text{ find } f \in C^3(0, \infty) \\[2mm] f''' + ff'' = 0 \\[2mm] \text{with boundary conditions} \\[2mm] f(0) = f'(0) = 0, \qquad\qquad \lim_{\eta \to \infty} f'(\eta) = 1. \end{cases}$$

To find the components $u_{UB}(x, y)$, $v_{UB}(x, y)$ of $\mathbf{u_{UB}}$, and their derivatives, we need to solve (P_{UB}) numerically for $f(\eta)$ and its derivatives on the semi-infinite domain $[0, \infty)$ and then we apply post-processing to determine numerical approximations to $\mathbf{u_u}$. This process is described in detail in Chapter 11 of [26] for flow past a flat plate. The method used is expanded upon in Chapter 3 of this thesis.

The purpose of finding this computed Blasius solution of the Prandtl problem is that we can use it as a reference solution for the unknown exact solution in the expression for the error and for the unknown boundary condtions, when we estimate the error in the numerical method on the uniform mesh of the next section. In this way, since the computed Blasius solution is known to converge Reynolds–uniformly to the so-

lution of the Prandtl problem, we can estimate guaranteed error bounds for it. For this purpose we use the computed Blasius solution for (P_{UB}) when $N=8192$, namely $\mathbf{U}_{UB}^{8192}$, which provides the required accuracy for the velocity components U_{UB}^{8192} and V_{UB}^{8192}.

2.3   The Prandtl Problem

The aim of this section is to construct a numerical method on a uniform to solve the Prandtl problem (P_u). Because the computational domain is rectangular, the uniform mesh Ω_u^N is a tensor product of two one–dimensional meshes. The mesh in the x direction is the uniform mesh

$$\Omega_u^{N_x} = \{x_i : x_i = 0.1 + iN_x^{-1}, 0 \le i \le N_x\}.$$

The mesh in the y-direction is the uniform mesh

$$\Omega_u^{N_y} = \{y_i : y_i = N_y^{-1}, 0 \le i \le N_y\}.$$

The rectangular mesh is then the tensor product $\Omega_u^{\mathbf{N}} = \Omega_u^{N_x} \times \Omega_u^{N_y}$, where $\mathbf{N}=(N_x, N_y)$. For simplicity we take $N_x = N_y = N$.

The problem (P_u) is discretized by the following non-linear upwind finite difference method on the uniform mesh $\Omega_u^{\mathbf{N}}$

$$(P_u^{\mathbf{N}}) \begin{cases} \text{Find } \mathbf{U_u} = (U_u, V_u) \text{ such that for all } (x_i, y_j) \in \Omega_u^{\mathbf{N}} \\ \mathbf{U_u} \text{ satisfies the finite difference equations} \\[2mm] -\varepsilon\delta_y^2 U_u(x_i, y_j) + U_u(x_i, y_j)D_x^- U_u(x_i, y_j) + \\[2mm] V_u(x_i, y_j)D_y^- U_u(x_i, y_j) = 0 \\[2mm] D_x^- U_u(x_i, y_j) + D_y^- V_u(x_i, y_j) = 0 \\[2mm] \text{with the boundary conditions} \\ \mathbf{U_u} = 0 \text{ on } \Gamma_B \\ \mathbf{U_u} = \mathbf{U}_{UB} \text{ on } \Gamma_L \bigcup \Gamma_T. \end{cases}$$

δ_y^2 is the standard second order centered difference operator in the y direction. D_x^- and D_y^- are the standard first order backward finite difference operators, respectively, in the x and y directions.

Since the problem $(P_u^{\mathbf{N}})$ is a nonlinear system, an iterative method is required for its solution. This is obtained by replacing the system of nonlinear equations with a sequence of systems of linear equations. The systems of linearized equations are

$$(A_u^{\mathbf{N}}) \begin{cases} \text{With the boundary condition } \mathbf{U_u^M} = \mathbf{U_{UB}^{8192}} \text{ on } \Gamma_{\mathrm{L}}, \\[4pt] \text{for each } i, 1 \le i \le N, \text{ use the initial guess } \mathbf{U}_u^0|_{X_i} = \mathbf{U}_u^{M_{i-1}}|_{X_{i-1}} \\[4pt] \text{and for } m = 1, \ldots, M_i \text{ solve the following} \\[4pt] \text{two point boundary value problem for } U_u^m(x_i, y_j) \\[10pt] (-\varepsilon\delta_y^2 + \mathbf{U}_u^{m-1} \cdot \mathbf{D}^-)U_u^m(x_i, y_j) = 0, \quad 1 \le j \le N-1 \\[10pt] \text{with the boundary conditions } U_u^m = U_{\mathrm{UB}} \text{ on } \Gamma_{\mathrm{B}} \cup \Gamma_{\mathrm{T}}, \\[4pt] \text{and the initial guess for } V_u^0|_{X_1} = 0. \\[4pt] \text{Also, solve the initial value problem for } V_u^m(x_i, y_j) \\[10pt] (\mathbf{D}^- \cdot \mathbf{U}_i^m)(x_i, y_j) = 0, \\[10pt] \text{with initial condition } V_u^m = 0 \text{ on } \Gamma_{\mathrm{B}}. \\[4pt] \text{Continue to iterate between the equations for } \mathbf{U}_u^m \text{ until } m = M_i, \\[4pt] \text{where } M_i \text{ is such that} \\[10pt] \max\left(|U_u^{M_i} - U_u^{M_i-1}|_{\overline{X}_i}, \tfrac{1}{\sqrt{\varepsilon}}|V_u^{M_i} - V_u^{M_i-1}|_{\overline{X}_i}\right) \le tol \text{ or } M_i = 3001. \end{cases}$$

For notational simplicity, we suppress explicit mention of the iteration superscript M_i henceforth, and we write simply $\mathbf{U}_u$ for the solution generated by $(A_u^{\mathbf{N}})$. We take $tol = 10^{-6}$ in the computations. The introduction of an upper-limit of iterations is needed as the iterative process might fail to converge. We note that there are no known theoretical results concerning the convergence of the solutions $\mathbf{U}_u$ of $(P_u^{\mathbf{N}})$ to the solution $\mathbf{u}_u$ of (P_u) and no theoretical estimate for the pointwise error $(\mathbf{U}_u - \mathbf{u}_u)(x_i, y_j)$.

2.4   Error Analysis

In this section we compute ε–uniform maximum pointwise differences for the approximations generated by the numerical method on a uniform mesh described in Section 2.3.

For this case, we compare the parameter uniform maximum pointwise differences for the approximations generated by the numerical method on a uniform mesh with the corresponding values of $\mathbf{U}_{UB}^{8192}$.

Before we look at the maximum pointwise differences, it is important to investigate whether or not the numerical method on a uniform mesh converges. The experimentally determined results in Table 2.1 show the total number of one dimensional linear solver iterations $\sum_{i=1}^{N}$. We see that the number of iterations required increases as ε decreases. In Table 2.1 the * entries indicate when the method failed to converge within the allotted number of iterations. The numerical method on a uniform mesh does not converge within the allotted iterations when $\sqrt{\varepsilon}\varepsilon N < 1$. For the numerical method on a uniform mesh to converge we require $N \geq \sqrt{\varepsilon}$, which becomes computationally expensive for small ε.

$\varepsilon \backslash N$	32	64	128	256	512
2^{-0}	308	698	1489	2933	5323
2^{-2}	552	1044	1967	3693	6844
2^{-4}	707	1257	2310	4301	8030
2^{-6}	917	1499	2619	4758	8776
2^{-8}	1523	2058	3223	5500	9829
2^{-10}	4846	3951	4832	7088	11674
2^{-12}	*	11606	11310	12041	15998
2^{-14}	*	*	30747	35450	32516
2^{-16}	*	*	*	90045	118888
2^{-18}	*	*	*	*	285956
2^{-20}	*	*	*	*	*

Table 2.1: Number of one dimensional linear solver iterations required for convergence for method A_u^N applied to problem (P_u) for various values of ε and N.

The scaled maximum pointwise differences $||U_u - \overline{U}_{UB}^{8192}||_{\overline{\Omega}_u^N}$ and $\frac{1}{\sqrt{\varepsilon}}||V_u - \overline{V}_{UB}^{8192}||_{\overline{\Omega}_u^N \backslash \Gamma_L}$ for various values of N and ε are given in Tables 2.2 and 2.3, respectively. In Tables 2.2 and 2.3 the * entries indicate when the numerical method on a uniform mesh failed to converge. In Tables 2.2 and 2.3 when ε decreases by 2^{-2} the differences

increase by at least a factor of 2. The entries in Tables 2.2 and 2.3 in *italics* are along the diagonal for $1 \leq \sqrt{\varepsilon}N \leq 2$. In Table 2.2 we read that the italic entries have differences of about 18% for $\sqrt{\varepsilon}N = 2$ and of about 70% for $\sqrt{\varepsilon}N = 1$ for $\|U_u - \overline{U}_{UB}^{8192}\|_{\overline{\Omega}_u^N}$. In Table 2.3 the entries in italics are tellingly large. Thus, Tables 2.2 and 2.3 suggest that the numerical method on a uniform mesh is not ε-uniform.

$\varepsilon \backslash N$	32	64	128	256	512
2^{-0}	2.87e-03	1.66e-03	8.98e-04	4.50e-04	2.11e-04
2^{-2}	1.24e-02	6.22e-03	3.12e-03	1.57e-03	7.92e-04
2^{-4}	3.52e-02	1.67e-02	8.17e-03	4.04e-03	2.02e-03
2^{-6}	7.25e-02	3.26e-02	1.56e-02	7.62e-03	3.78e-03
2^{-8}	*1.89e-01*	6.96e-02	3.16e-02	1.51e-02	7.42e-03
2^{-10}	*7.49e-01*	*1.86e-01*	6.84e-02	3.12e-02	1.50e-02
2^{-12}	*	*7.49e-01*	*1.86e-01*	6.79e-02	3.10e-02
2^{-14}	*	*	*7.49e-01*	*1.86e-01*	6.76e-02
2^{-16}	*	*	*	*7.48e-01*	*1.86e-01*
2^{-18}	*	*	*	*	*7.48e-01*
2^{-20}	*	*	*	*	*

Table 2.2: Computed maximum pointwise difference $\|U_u - U_{UB}^{8192}\|_{\overline{\Omega}_u^N}$ generated by $(A_u^{\mathbf{N}})$ for various values of ε and N.

$\varepsilon \backslash N$	32	64	128	256	512
2^{-0}	2.13e-01	1.08e-01	5.36e-02	2.68e-02	1.42e-02
2^{-2}	3.71e-01	1.94e-01	1.01e-01	5.31e-02	2.86e-02
2^{-4}	7.63e-01	3.82e-01	1.97e-01	1.04e-01	5.62e-02
2^{-6}	1.93e+00	8.49e-01	4.16e-01	2.15e-01	1.14e-01
2^{-8}	*9.49e+00*	2.51e+00	1.01e+00	4.77e-01	2.41e-01
2^{-10}	*1.89e+02*	*1.63e+01*	3.49e+00	1.24e+00	5.52e-01
2^{-12}	*	*3.75e+02*	*2.98e+01*	5.22e+00	1.57e+00
2^{-14}	*	*	*7.43e+02*	*5.68e+01*	8.46e+00
2^{-16}	*	*	*	*1.48e+03*	*1.11e+02*
2^{-18}	*	*	*	*	*2.96e+03*
2^{-20}	*	*	*	*	*

Table 2.3: Computed maximum pointwise difference $\frac{1}{\sqrt{\varepsilon}}\|V_u - V_{UB}^{8192}\|_{\overline{\Omega}_u^N \backslash \Gamma_L}$ generated by $(A_u^{\mathbf{N}})$ for various values of ε and N.

Graphs of the scaled velocity components U_u and $\frac{1}{\sqrt{\varepsilon}}V_u$ of the Prandtl solutions are shown in Figure 2-1 for $\varepsilon = 2^{-10}$ and N=32. The graph of U_u has no non-physical jumps but it appears not to resolve the boundary layer. The graph of V_u has a non-physical jump from Γ_L to X_1. The results of V_u on X_1 dwarf all other results in the domain.
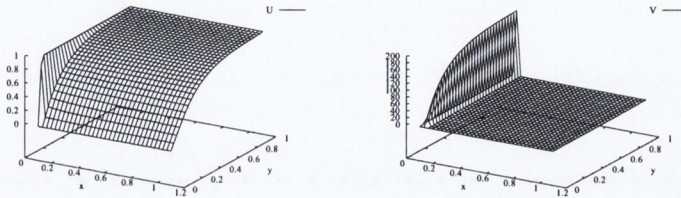
Figure 2-1: Graphs of U_u and $\frac{1}{\sqrt{\varepsilon}}V_u$ for $\varepsilon = 2^{-10}$ and N=32.

Graphs of the differences $U_u - U_{UB}^{8192}$ and $\frac{1}{\sqrt{\varepsilon}}(V_u - V_{UB}^{8192})$ between the scaled velocity components of the Prandtl and computed Blasius solutions are shown in Figure 2-2 for $\varepsilon = 2^{-10}$ and N=32. In Figure 2-2 we see that, unsurprisingly, the largest differences occur along the plate for U_u. This is due to the numerical method on a uniform mesh diffusing the region of rapid change in the boundary layer. From the graph of $\frac{1}{\sqrt{\varepsilon}}(V_u - V_{UB}^{8192})$ we see the largest difference is along X_1.
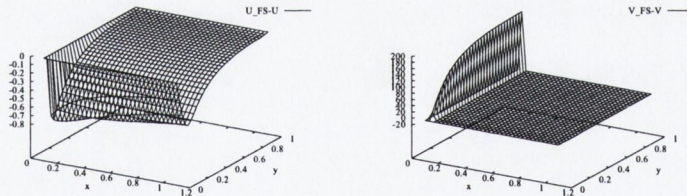
Figure 2-2: Graphs of $U_u - U_{UB}^{8192}$ and $\frac{1}{\sqrt{\varepsilon}}(V_u - V_{UB}^{8192})$ for $\varepsilon = 2^{-10}$ and N=32.

Due to the severe nature of the differences of $\frac{1}{\sqrt{\varepsilon}}(V_u - V_{UB}^{8192})$ along X_1 we investigate the differences $\frac{1}{\sqrt{\varepsilon}}\|V_u - V_{UB}^{8192}\|$ in the subdomain $(\overline{\Omega}_u^N \backslash \Gamma_L) \bigcap [0.2, 1.1] \times [0, 1]$. The scaled maximum pointwise differences $\frac{1}{\sqrt{\varepsilon}}\|V_u - \overline{V_{UB}}^{8192}\|$ in the subdomain $(\overline{\Omega}_u^N \backslash \Gamma_L) \bigcap [0.2, 1.1] \times [0, 1]$ for various values of N and ε are given in Table 2.4. The * entries indicate when the numerical method on a uniform mesh failed to converge. Notice that the differences increase as ε decreases. The entries in Table

2.4 in *italics* are along the diagonal of the table for $1 \le \sqrt{\varepsilon}N \le 2$. In Table 2.4 we read that the italic entries have differences of about 65% for $\sqrt{\varepsilon}N = 2$ and of about 150% for $\sqrt{\varepsilon}N = 1$ for $\frac{1}{\sqrt{\varepsilon}}||V_u - V_{UB}^{8192}||$. These results are unacceptable.

$\varepsilon\backslash N$	32	64	128	256	512
2^{-0}	1.08e-01	5.99e-02	3.14e-02	1.52e-02	7.16e-03
2^{-2}	1.82e-01	9.93e-02	5.16e-02	2.53e-02	1.23e-02
2^{-4}	3.44e-01	1.73e-01	8.62e-02	4.17e-02	2.02e-02
2^{-6}	5.61e-01	2.79e-01	1.37e-01	6.60e-02	3.20e-02
2^{-8}	*7.76e-01*	4.86e-01	2.42e-01	1.15e-01	5.58e-02
2^{-10}	*1.42e+00*	*6.84e-01*	4.44e-01	2.15e-01	1.04e-01
2^{-12}	*	*1.52e+00*	*6.31e-01*	4.07e-01	2.01e-01
2^{-14}	*	*	*1.57e+00*	*5.78e-01*	3.89e-01
2^{-16}	*	*	*	*1.58e+00*	*5.52e-01*
2^{-18}	*	*	*	*	*1.58e+00*
2^{-20}	*	*	*	*	*

Table 2.4: Computed maximum pointwise difference $\frac{1}{\sqrt{\varepsilon}}||V_u - V_{UB}^{8192}||$ in the subdomain $(\overline{\Omega}_u^N \backslash \Gamma_L) \bigcap [0.2, 1.1] \times [0, 1]$ generated by (A_u^N) for various values of ε and N.

A graph of the differences $\frac{1}{\sqrt{\varepsilon}}(V_u - V_{UB}^{8192})$ between the scaled components of the Prandtl and computed Blasius solutions in the subdomain $(\overline{\Omega}_u^N \backslash \Gamma_L) \bigcap [0.2, 1.1] \times [0, 1]$ is shown in Figure 2-3 for $\varepsilon = 2^{-10}$ and N=32. We see that the largest differences occur along the plate, where the boundary layer is located.
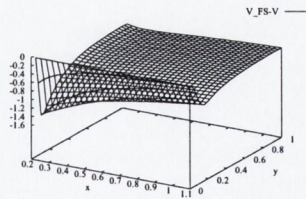
Figure 2-3: Graphs of $\frac{1}{\sqrt{\varepsilon}}(V_u - V_{UB}^{8192})$ in the subdomain $(\overline{\Omega}_u^N \backslash \Gamma_L) \bigcap [0.2, 1.1] \times [0, 1]$ for $\varepsilon = 2^{-10}$ and N=32.

2.5   Conclusion

We have shown that a numerical method on a uniform mesh will give error bounds for the solution components and their derivatives, which do depend on the value of Re, for $Re \in [1, \infty)$. We have also shown that the iterative method fails to converge for $\sqrt{\varepsilon}N < 1$. The results suggest that if you wish to have accuracy better than 18% for $U_u - U_{UB}^{8192}$ and better than 50% for $\frac{1}{\sqrt{\varepsilon}}(V_u - V_{UB}^{8192})$ you need $N \geq \frac{4}{\sqrt{\varepsilon}}$. Thus the numerical method on a uniform mesh will not yield Reynolds uniform results.

Chapter 3

Prandtl flow past a wedge – Falkner–Skan method

3.1 Prandtl boundary layer equations

In this chapter and the next we use and adapt the numerical methods developed in [26] and apply them to the Prandtl boundary layer equations for flow past a semi-infinite wedge.

In the present chapter, we use a variant of the semi-analytic approach of Falkner–Skan to generate numerical approximations of guaranteed pointwise accuracy to the flow velocities and their scaled derivatives. We use the approximate solution, which has known accuracy, to estimate the error to the approximates obtained later by the direct numerical method.

In the next chapter, we construct a direct numerical method to generate numerical approximations of guaranteed accuracy to the flow variables and their scaled derivatives. Although there are, at present, no theoretical error estimates for the resulting numerical solutions, we determine accuracy by means of extensive numerical experiments and comparisons with the previously determined semi–analytic approximations. We show that the numerical approximations are pointwise accurate and that they satisfy pointwise error estimates that are uniform with respect to the Reynolds number and the angle of the wedge.

As we intend to solve the Prandtl boundary layer numerically we must compute the approximate solution on a finite domain Ω. The Prandtl boundary layer problem on

a finite domain, Ω, is

$$(P_W) \begin{cases} \text{Find } \mathbf{u_W} = (u_W, v_W) \text{ such that for all } (x,y) \in \Omega \\ \mathbf{u}_W \text{ satisfies the differential equation} \\ \\ -\frac{1}{Re}\frac{\partial^2 u_W}{\partial^2 y} + \mathbf{u}_W.\nabla u_W = U(x)\frac{dU(x)}{dx} \\ \\ \nabla.\mathbf{u}_W = 0 \\ \\ \text{with boundary conditions} \\ \mathbf{u}_W = 0 \text{ for all } x \geq 0 \\ \\ u_W = u_P \text{ on } \Gamma_L\bigcup\Gamma_T \end{cases}$$

where $(U(x) = x^m, 0)$ is the solution of the reduced problem and $m = \frac{\beta}{2-\beta}$, where $\beta\pi$ is the angle in radians of the wedge and u_P is the exact solution of (P_P), see Chapter 1.

It is well known (see [43]) that the problem (P_W) has a self similar solution in the open subdomain $\{(x,y) : x > 0, |y| > 0\}$. By symmetry, it suffices to study the problem in the open quarter plane $\{(x,y) : x > 0, y > 0\}$. To avoid the more complicated behaviour of the flow near the leading edge of the wedge, we compute numerical approximations to the solution (P_W) on a finite rectangle, which does not contain the leading edge. More precisely, we take as the computational domain Ω a finite rectangle, which is a fixed distance away from the leading edge along the wedge. We can take this domain to be as close to the leading edge and as large as desired, provided that its location and size are independent of the Reynolds number and the angle of the wedge. An appropriate domain is $\Omega = (a, A) \times (0, B)$, where a, A and B are fixed and independent of the Reynolds number, Re, and the angle of the wedge, β. In all of the numerical computations in this and the next chapter we use the specific values

$$a = 0.1 + \gamma(\beta), \quad A = 1.1 + \gamma(\beta), \quad B = 1, \quad Re \in [1, \infty) \text{ and } \beta \in [0.0, 1.5].$$

We choose

$$\gamma(\beta) = \begin{cases} 0 & \text{for } \beta \in [0, 1.0] \\ \frac{\sin(\frac{\beta-1}{2.0}\pi)}{\sin(1-\frac{\beta}{2.0}\pi)} & \text{for } \beta \in (1.0, 1.5] \end{cases} \qquad (3.1)$$

such that Ω does not cross the line of symmetry.

Let us illustrate several of these flows. For $\beta = 0.0$, the problem reduces to fluid flow over a flat plate with $x = 0$ at the leading edge, see Figure 3-1. This is extensively dealt with by Farrell et al. in [26]. When $\beta = 0.5$ the angle of the wedge is $\frac{\pi}{2}$ radians with $x = 0$ at the leading edge of the wedge, see Figure 3-2.
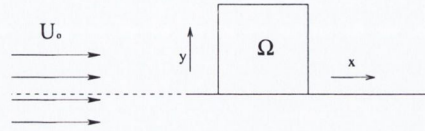
Figure 3-1: Flow past a semi–infinite flat plate.
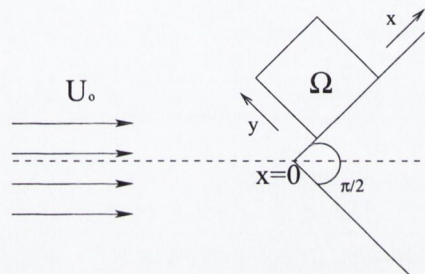
Figure 3-2: Flow past a semi–infinite wedge, of angle $\frac{\pi}{2}$.

For $\beta = 1.0$, we have the two dimensional stagnation point flow with $x = 0$ at the stagnation point of the flow, see Figure 3-3. When $\beta = 1.5$, we have an obtuse angled wedge with $x = 0$ tip, see Figure 3-4. While it is difficult to visualise or reproduce in experiment the flow for obtuse angles of the wedge, it is helpful to view the flow as being dragged along a conveyer belt represented by the line of symmetry.
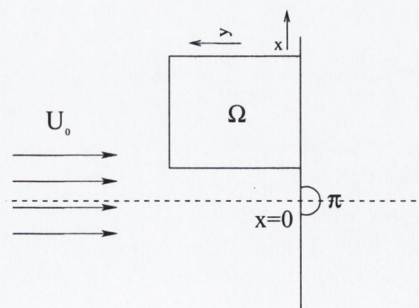
Figure 3-3: Stagnation flow.
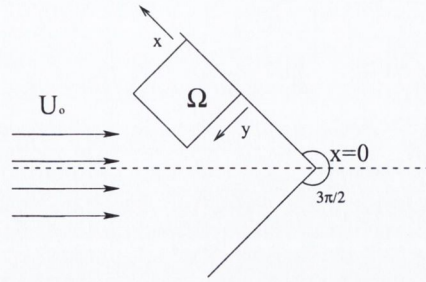
Figure 3-4: Flow past a semi–infinite wedge, of angle $\frac{3\pi}{2}$.

Our goal in Chapters 3 and 4 is to model the flow for all Reynolds numbers, $Re \in [1, \infty)$, and angles of the wedge, $\beta \in [0.0, 1.5]$, for which the flow remains laminar and no separation occurs on the wedge.

3.2 Falkner–Skan solution

Using the similarity transformation described in [1]

$$\eta = y\sqrt{\frac{(m+1)Re}{2}\frac{U}{x}} \tag{3.2}$$

the velocity components of the Falkner–Skan solution $\mathbf{u}_{FS}$ of (P_W) are given by

$$u_{FS}(x, y) = x^m f'(\eta) = U f'(\eta) \tag{3.3}$$

$$v_{FS}(x, y) = -\sqrt{\frac{m+1}{2x}\frac{U}{Re}}\left(f(\eta) + \frac{m-1}{m+1}\eta f'(\eta)\right). \tag{3.4}$$

where f is the solution of the non–linear ordinary differential equation

$$(P_{FS}) \begin{cases} \text{For } \eta \in (0, \infty) \text{ find } f \in C^3(0, \infty) \\[2mm] f''' + ff'' + \beta(1 - f'^2) = 0 \\[2mm] \text{with boundary conditions} \\ f(0) = f'(0) = 0, \qquad\qquad \lim_{\eta \to \infty} f'(\eta) = 1. \end{cases}$$

The problem (P_{FS}) is known as the Falkner–Skan problem and in what follows we refer to $\mathbf{u}_{FS}$ as the Falkner–Skan solution of (P_W).

The equation in (P_{FS}) is a third order non–linear ordinary differential equation on the semi-infinite domain $(0, \infty)$. Note that the case for $\beta = 0$ is dealt with in [26]. The existence and uniqueness of f are discussed in [41] and [47]. The exact solution of (P_{FS}) can be obtained in the form of a series expansion [20]. It can also be solved numerically on any bounded domain I of $(0, \infty)$. In what follows we solve the Falkner–Skan problem (P_{FS}) numerically for the function f and its derivatives. We then use the analytic relations (3.3) and (3.4) to construct Reynolds uniform analytic approximations with guaranteed accuracy, to the solution $\mathbf{u}_W$ of (P_W) for all relevant values of the Reynolds number and values of the angles of the wedge at all points of the domain Ω.

To achieve this it is clear that we need Reynolds uniform pointwise accuracy of $f(\eta)$, $f'(\eta)$ and $f''(\eta)$ for all $\eta \in (0, \infty)$. We know of no standard numerical method for computing approximations of f, f' and f'' that fulfill these requirements. Therefore we construct a new numerical method using the techniques discussed in [26], which enables us to generate such (Re, β)–uniform approximations.

3.3 Singularly perturbed nature of Falkner–Skan problem

Using similar arguments to [26] we show that (P_{FS}) has a singularly perturbed nature. In the next section we use this observation to motivate the construction of the numerical method for solving (P_{FS}).

We observe that, while we need the solution of (P_{FS}) on an infinite interval, in practice we can find numerical solutions only on a finite interval. For this reason, we introduce a one-parameter family of problems related to (P_{FS}) on the finite interval $(0, L)$ where the length L of the interval is taken as the parameter of the family. The typical problem in this family is defined for each value of L in the range $1 \le L \le \infty$ by

$$f_L'''(\eta) + f_L(\eta) f_L''(\eta) + \beta(1 - f_L'^2(\eta)) = 0 \quad \eta \in [0, L)$$
$$f_L(0) = f_L'(0) = 0, \qquad f_L'(L) = 1. \tag{3.5}$$

When we reformulate (3.5) as a singularly perturbed problem, it transpires that $\frac{1}{L}$ is the singular perturbation parameter and so it is appropriate to introduce the temporary notation $\varepsilon = \frac{1}{L}$. Then the problem (3.5) can be written in the form

$$f_\varepsilon'''(\eta) + f_\varepsilon(\eta) f_\varepsilon''(\eta) + \beta(1 - f_\varepsilon'^2(\eta)) = 0, \quad f_\varepsilon(0) = f_\varepsilon'(0) = 0, \quad f_\varepsilon'(\frac{1}{\varepsilon}) = 1.$$

Putting $g_\varepsilon = f'_\varepsilon$, this problem becomes

$$g''_\varepsilon(\eta) + f_\varepsilon(\eta)g'_\varepsilon(\eta) + \beta(1 - g_\varepsilon^2(\eta)) = 0, \qquad g_\varepsilon(0) = 0, \qquad g_\varepsilon(\frac{1}{\varepsilon}) = 1.$$

Changing variables from η to $\xi = \varepsilon\eta$ which is equivalent to a mapping of the interval $[0, \frac{1}{\varepsilon}]$ to the unit interval $[0, 1]$, and writing $k_\varepsilon(\xi) = g_\varepsilon(\eta)$ and $h(\xi) = f_\varepsilon(\eta)$, we obtain

$$\varepsilon k''_\varepsilon(\xi) + h_\varepsilon(\xi)k'_\varepsilon(\xi) + \beta(1 - k_\varepsilon^2(\xi)) = 0, \qquad k_\varepsilon(0) = 0, \qquad k_\varepsilon(1) = 1 \qquad (3.6)$$

where $h(0) = 0$ and $h(\xi) = O(\xi)$ for all $\xi \geq \epsilon$. This is a singularly perturbed problem for k_ε with a boundary layer at $\xi = 0$. Consequently, to construct an ε-uniform method for problem (3.6), we need to choose the appropriate transition parameter σ_ξ. The transition parameter σ_ξ in the piecewise uniform fitted mesh is defined as $\sigma_\xi = \sigma_\xi(\varepsilon, N) = \varepsilon\Phi(N)$ where $\Phi(N) \to \infty$ as $N \to \infty$. From [26] we take $\Phi(N) = \ln N$, which in terms of the original variable η gives $\sigma_\eta = \ln N$.

In what follows it is natural to refer to L-uniform methods for (3.5). These are defined in an analogous way to ε-uniform methods.

3.4 Robust layer resolving method for Falkner–Skan problem

Our strategy for computing L-uniform approximations to the solution of (P_{FS}) is to obtain a numerical solution F_L for problem (3.5), on the interval $[0, L]$, for an increasing sequence of values of the length L. Since for each L we need the values of f_L, f'_L and f''_L at all points of the interval $(0, \infty)$, we extend the domain of f_L, f'_L and f''_L from $[0, L]$ to the semi-infinite interval $[0, \infty)$ by defining the following extrapolations

$$f''(\eta) = 0, \text{ for all } \eta \geq L \qquad (3.7)$$
$$f'(\eta) = 1, \text{ for all } \eta \geq L \qquad (3.8)$$
$$f(\eta) = (\eta - L_N) + f(L_N), \text{ for all } \eta \geq L \qquad (3.9)$$

where (3.9) is obtained by integrating both sides of (3.8) from L to η.

We now describe our numerical method for finding approximations to the solution and its derivatives of problem (P_{FS}). For each fixed N we write $L_N = \ln N$ and we divide the interval into the two subintervals $[0, L_N]$ and $[L_N, \infty)$. We construct a

uniform mesh

$$\overline{I}_u^N = \{\eta_i : \eta_i = iN^{-1}\ln N, 0 \le i \le N\}_0^N$$

on the subinterval $[0, L_N]$ and we determine numerical approximations F, D^+F and D^+D^+F to f_L, f_L' and f_L'', respectively, at the mesh points $\overline{I}_u^N$, using the nonlinear finite difference method

$$(P_{FS}^N) \begin{cases} \text{Find } F \text{ on } I_u^N \text{such that, for all } \eta \in I_u^N, \ 2 \le i \le N-1 \\ \\ \delta^2(D^-F_i) + F_i(D^+(D^-F_i)) + \beta(1 - (D^-F_i)(D^-F_i)) = 0 \\ \\ \text{with boundary conditions} \\ F(0) = D^+F(0) = 0, \qquad\qquad D^0F(\eta_{N-1}) = 1. \end{cases}$$

3.4.1 The monotone nature of the discrete Falkner–Skan equation

The Falkner–Skan problem can be represented as a lower Hessenberg matrix. we cannot easily deduce the nature of F_i from the problem (P_{FS}^N) To learn more about F_i we must investigate the discrete derivative $D^-F_i^m$ and their operator matrix. Let

$$G_i^m = D^-F_i^m = \frac{F_i^m - F_{i-1}^m}{x_i - x_{i-1}}. \tag{3.10}$$

Rewriting the Falkner–Skan equation with respect to (3.10)

$$\delta^2(G_i^m) + F_i^{m-1}D^+(G_i^m) + \beta(1 - G_i^{m-1}G_i^m) = 0 \tag{3.11}$$

with boundary conditions

$$G_1 = 0, \qquad\qquad \frac{G_N + G_{N-1}}{2} = 1.$$

This system of equations is expressed in a tridiagonal matrix, with a negative diagonal and two positive off diagonals which are defined as:

Upper diagonal

$$\frac{1}{h^2} + \frac{F_i^{m-1}}{h}$$

Diagonal

$$-\frac{2}{h^2} - \frac{F_i^{m-1}}{h} - \beta G_i^{m-1}$$

Lower diagonal

$$\frac{1}{h^2}$$

This system of equations is diagonally dominant but to ensure monotonicity we need it to be strictly diagonally dominant. Thus we introduce a new term in to the equation which tends to zero as m gets larger. Equation (3.10) is now written as:

$$\delta^2(G_i^m) + F_i^{m-1}D^+(G_i^m) + \beta(1 - G_i^{m-1}G_i^m) - (\beta + 1)(G_i^m - G_i^{m-1}) = 0 \qquad (3.12)$$

with boundary conditions

$$G_1 = 0, \qquad \frac{G_N + G_{N-1}}{2} = 1$$

The tridiagonal matrix is strictly diagonally dominant and it satisfies the conditions to be an M-matrix, which are:

1. The off diagonal elements of $-A \leq 0$ and the diagonal of $-A > 0$;

2. A is irreducible ie the directed graph for $G(A)$ is strongly connected this is true for all non-negative tridiagonal matrices;

3. A is diagonally dominant for each row, which is true;

4. And is strict for at least one row, which is also true;

We know that this matrix is monotone - since M-matrices are a subset of monotone matrices - therefore G_i^m is always non-negative. We can also deduce F_i^m is always non-negative since its derivative is non-negative and the boundary conditions are all ≥ 0.

In practice, since (P_{FS}^N) is non–linear, we need a non–linear solver to compute its solution. Using a variation of the continuation algorithm defined in [26] we use the

following continuation algorithm with the continuation parameter m

$$(A_{FS}^N) \begin{cases} \text{For each integer } m, \ 1 \le m \le M \text{ find } F^m \text{ on } I_u^N \\ \text{such that, for all } \eta \in I_u^N, \ 2 \le i \le N-1 \\ \\ \delta^2(D^- F_i^m) + F_i^{m-1}(D^+(D^- F_i^m)) + \beta(1 - (D^- F_i^{m-1})(D^- F_i^m)) \\ -(1+\beta)(D^- F_i^m - D^- F_i^{m-1}) = 0 \\ \\ \text{with boundary conditions} \\ F(0) = D^+F(0) = 0, \qquad\qquad D^0 F(x_{N-1}) = 1 \\ \\ \text{and the initial guess } F^0(\eta_i) = \eta_i. \end{cases}$$

To avoid cumbersome notation we suppress explicit mention of N and M and we denote the final output of (A_{FS}^N) simply by F. In what follows the finest mesh is taken to be $I_u^{N^*}$, with N^* chosen sufficiently large so that the asymptotic nature of the numerical solutions is observed on several meshes I_u^N for which $N < N^*$. For our purpose $N^* = 65,536$ suffices and we use the numerical solution F on the mesh $I_u^{65,536}$ to replace the unknown exact solution in the expression for the pointwise error.

We assign the values $D^+F(\eta_N) = 1$ and $D^+D^+F(\eta_N) = D^+D^+F(\eta_{N-1}) = 0$, so that F, D^+F and D^+D^+F are defined at all points of the mesh $\overline{I}_u^N$. We then use piecewise linear interpolation to interpolate from $\overline{I}_u^N$ to each point of the subinterval $[0, L_N]$. We denote the corresponding interpolants by $\overline{F}$, $\overline{D^+F}$ and $\overline{D^+D^+F}$. We extend these functions to the whole of the semi-infinite interval $[0, \infty)$ in an analogous way to the extensions (3.7)-(3.9) of their continuous counterparts, that is

$$\overline{D^+D^+F}(\eta) = 0, \text{ for all } \eta \in [L_N, \infty) \tag{3.13}$$

$$\overline{D^+F}(\eta) = 1, \text{ for all } \eta \in [L_N, \infty) \tag{3.14}$$

$$\overline{F}(\eta) = (\eta - L_N) + \overline{F}(L_N), \text{ for all } \eta \in [L_N, \infty). \tag{3.15}$$

We take the values of F, D^+F and D^+D^+F, respectively, to be the required numerical approximations to the exact values f, f' and f'' of the Blasius solution and its derivatives on the semi-infinite interval $[0, \infty)$.

3.5   Numerical solution of Falkner–Skan problem

The computed pointwise maximum errors with respect to the finest mesh $N^* = 65,536$ are defined by

$$E^N = ||F^N - \overline{F}^{N^*}||_{I_u^N}$$

and the pointwise two mesh differences are defined by

$$D^N = ||F^N - \overline{F}^{2N}||_{I_u^N}$$

for all N satisfying $N, 2N \leq N^*$. From these values we find the two mesh orders of convergence by

$$p^N = \log_2 \frac{D^N}{D^{2N}}.$$

For the sake of brevity we show the errors for only three typical values of the angle of the wedge $\beta = 0.5, \beta = 1.0$ and $\beta = 1.5$. For $\beta = 0.5, 1.0$ and 1.5 the computed maximum pointwise error E^N, the computed two mesh difference D^N and the computed order of convergence p^N for $\overline{F}$, $\overline{D^+F}$ and $\overline{D^+D^+F}$, are given by Tables 3.1, 3.2 and 3.3, respectively. The main conclusion to be drawn from the numerical results in Tables 3.1-3.3 is that method (P_{FS}^N), in conjunction with algorithm (A_{FS}^N), is in practice a robust layer-resolving method for problem (3.5) for all admissible values of β. By this we mean that it is L-uniform and that the L-uniform order of convergence on $[0, L_N]$ of the numerical solution F to the exact f_L and of the discrete derivatives D^+F and D^+D^+F to the derivatives f_L' and f_L'', respectively, is, in practice, better than 0.8 for all $N \geq 512$ and all β considered.

				$\beta = 0.5$				
N	128	256	512	1024	2048	4096	8192	16384
E^N	0.019535	0.011099	0.006192	0.003397	0.001828	0.000957	0.000479	0.000217
D^N	0.008438	0.004906	0.002795	0.001569	0.000871	0.000479	0.000261	0.000141
p^N	0.78	0.81	0.83	0.85	0.86	0.87	0.88	0.89
				$\beta = 1.0$				
E^N	0.019455	0.011033	0.006152	0.003374	0.001815	0.000951	0.000475	0.000216
D^N	0.008438	0.004906	0.002795	0.001569	0.000871	0.000479	0.000261	0.000141
p^N	0.78	0.81	0.83	0.85	0.86	0.87	0.88	0.89
				$\beta = 1.5$				
E^N	0.019404	0.010995	0.006128	0.003361	0.001808	0.000946	0.000473	0.000215
D^N	0.008409	0.004866	0.002768	0.001553	0.000861	0.000473	0.000258	0.000140
p^N	0.79	0.81	0.83	0.85	0.86	0.88	0.88	0.89

Table 3.1: Computed maximum pointwise error E^N, the computed two mesh difference D^N and the computed order of convergence p^N for $\overline{F}$ on $\overline{I}_u^N$ generated by (A_{FS}^N) with $M = 8 \ln N$ applied to problem (P_{FS}) for various values of N and β.

				$\beta = 0.5$				
N	128	256	512	1024	2048	4096	8192	16384
E^N	0.000739	0.000422	0.000236	0.000130	0.000070	0.000037	0.000018	0.000008
D^N	0.000317	0.000186	0.000106	0.000060	0.000033	0.000018	0.000010	0.000005
p^N	0.76	0.81	0.83	0.85	0.86	0.87	0.88	0.89
				$\beta = 1.0$				
E^N	0.000550	0.000311	0.000173	0.000095	0.000051	0.000027	0.000013	0.000006
D^N	0.000256	0.000142	0.000079	0.000044	0.000024	0.000013	0.000007	0.000004
p^N	0.85	0.85	0.84	0.85	0.86	0.88	0.89	0.89
				$\beta = 1.5$				
E^N	0.000451	0.000253	0.000140	0.000077	0.000042	0.000022	0.000011	0.000005
D^N	0.000249	0.000128	0.000069	0.000037	0.000020	0.000011	0.000006	0.000003
p^N	0.96	0.89	0.88	0.87	0.88	0.88	0.89	0.90

Table 3.2: Computed maximum pointwise error E^N, the computed two mesh difference D^N and the computed order of convergence p^N for $\overline{D^+F}$ on $\overline{I}_u^N \backslash \{\eta_N\}$ generated by (A_{FS}^N) with $M = 8 \ln N$ applied to problem (P_{FS}) for various values of N and β.

				$\beta = 0.5$				
N	128	256	512	1024	2048	4096	8192	16384
E^N	0.009555	0.005437	0.003038	0.001668	0.000898	0.000470	0.000235	0.000107
D^N	0.004125	0.002401	0.001371	0.000770	0.000428	0.000235	0.000128	0.000069
p^N	0.78	0.81	0.83	0.85	0.86	0.87	0.88	0.89
				$\beta = 1.0$				
E^N	0.017131	0.009740	0.005440	0.002987	0.001608	0.000842	0.000421	0.000191
D^N	0.007398	0.004301	0.002454	0.001379	0.000766	0.000421	0.000230	0.000124
p^N	0.78	0.81	0.83	0.85	0.86	0.87	0.88	0.89
				$\beta = 1.5$				
E^N	0.026508	0.015100	0.008442	0.004637	0.002497	0.001308	0.000654	0.000297
D^N	0.011425	0.006661	0.003805	0.002140	0.001189	0.000654	0.000357	0.000193
p^N	0.78	0.81	0.83	0.85	0.86	0.87	0.88	0.89

Table 3.3: Computed maximum pointwise error E^N, the computed two mesh difference D^N and the computed order of convergence p^N for $\overline{D^+D^+F}$ on $\overline{I}_u^N \setminus \{\eta_{N-1}, \eta_N\}$ generated by (A_{FS}^N) with $M = 8nN$ applied to problem (P_{FS}) for various values of N and β.

It is important to observe that, when $N > 2048$, the effect of rounding error is significant in the calculations of the computed pointwise errors, the two mesh differences and the two mesh order of convergence. This is due, in part, to the fact that the discretization matrix is lower Hessenberg with two lower diagonals. In addition, we use a very fine mesh. Consequently, we need quadruple precision to achieve the L-uniform convergence in all the Tables in this chapter.

Comparison of the entries in the order of convergence p^N rows of Tables 3.1, 3.2 and 3.3 with the Table of theoretical behavior for $N^{-1}nN$ and $N^{-1}(nN)^2$ of the order of convergence defined p^N in Appendix B suggests strongly that the computed order of L-uniform convergence p^N corresponds to the theoretical behavior $N^{-1}nN$.

Graphs of $\overline{F}$ for $N = 8192$ and various values of β on $[0, L_N]$ are given in Figure 3-5. These graphs show that there is a region of activity near $\eta = 0$.
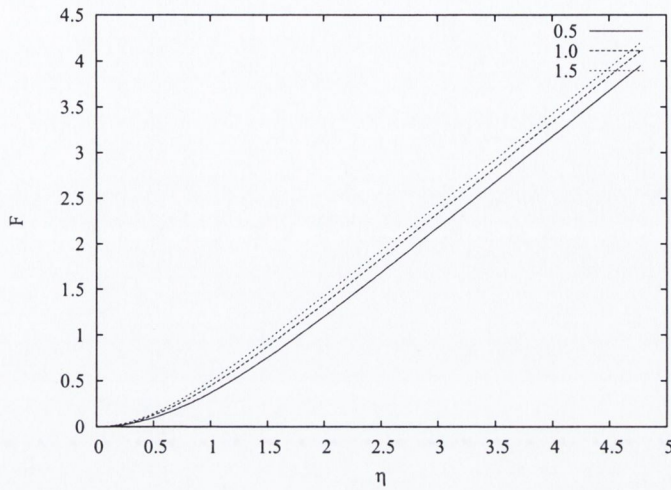
Figure 3-5: Solution $\overline{F}$ generated by method (A_{FS}^N) applied to problem P_{FS} with $M = 8nN$, $N = 8192$ and various values of β.

Graphs of $\overline{D^+F}$ and $\overline{D^+D^+F}$ for $N = 8192$ and various values of β on $[0, L_N]$ are given in Figures 3-6 and 3-7, respectively. In Figures 3-6 and 3-7 we can make out more clearly than in Figure 3-5 the region of rapid change near $\eta = 0$.
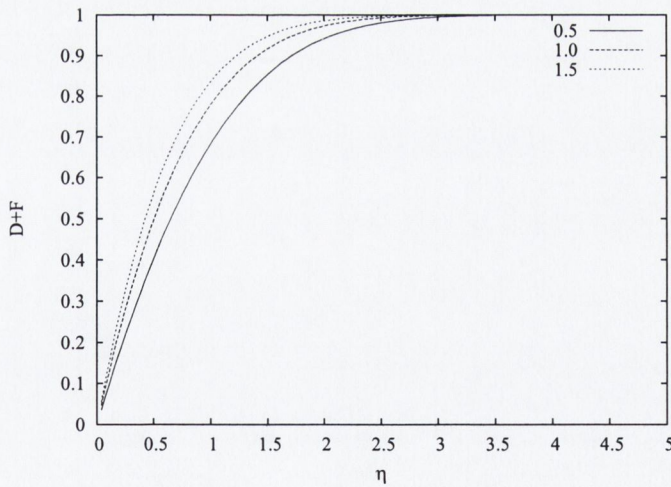
Figure 3-6: Solution $\overline{D^+F}$ generated by method (A_{FS}^N) applied to problem P_{FS} with $M = 8nN$, $N = 8192$ and various values of β.
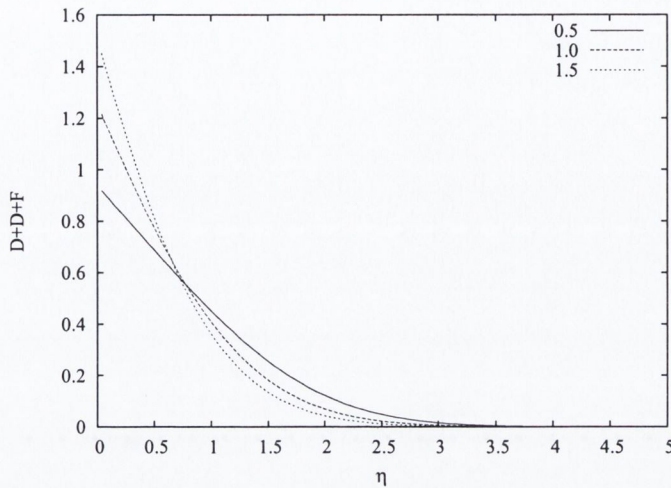
Figure 3-7: Solution $\overline{D^+D^+F}$ generated by method (A_{FS}^N) applied to problem P_{FS} with $M = 8nN$, $N = 8192$ and various values of β.

3.6 Computed error estimates for Falkner–Skan problem

Theoretical estimates in [26] indicate that, for all $N \geq N_0$, the approximations of $\overline{F}$, $\overline{D^+F}$ and $\overline{D^+D^+F}$, respectively, to the exact solution of the Falkner–Skan problem (P_{FS}) and its derivatives satisfy error bounds of the form

$$||\overline{F} - f||_{[0,\infty)} \leq C_p N^{-p}$$
$$||\overline{D^+F} - f||_{[0,\infty)} \leq C_p N^{-p}$$
$$||\overline{D^+D^+F} - f||_{[0,\infty)} \leq C_p N^{-p}$$

where the error parameters are unknown. We now use the experimental techniques to estimate the global error constant by modifying the technique touched upon in the previous section.

The computed two–mesh difference is defined by

$$\overline{D}^N = ||\overline{F}^N - \overline{F}^{2N}||_{[0,\infty)}$$

for all N satisfying $N, 2N \leq N^*$. From these values we compute the computed order of convergence to be

$$\overline{p}^N = \log_2 \frac{\overline{D}^N}{\overline{D}^{2N}}$$

and we take the computed global order of convergence to be

$$\overline{p}^* = \min_N \overline{p}^N.$$

Corresponding to this value of $\overline{p}^*$ we define

$$\overline{C}_{\overline{p}^*}^N = \frac{\overline{D}^N N^{p^*}}{1 - 2^{-\overline{p}^*}}$$

and we take the computed global error constant to be

$$\overline{C}_{\overline{p}^*}^* = \max_N \overline{C}_{\overline{p}^*}^N.$$

We now use the experimental techniques to obtain computed L-uniform global error parameters for the function $\overline{F}$ on the semi-infinite interval $[0, \infty)$ for various β. To determine the two mesh differences $\overline{D}^N$ and hence the computed order of convergence $\overline{p}^N$ and the constant of convergence $\overline{C}_{\overline{p}^*}^N$ for a pair of meshes with N and 2N points respectively, we have to consider the 3 subintervals $[0, L_N)$, $[L_N, L_{2N})$ and $[L_{2N}, \infty)$ separately. For $\eta \in [L_N, L_{2N})$ the two mesh difference at η for $\overline{F}$ is $\overline{F}^{2N}(\eta) - F^N(L_n) - (\eta - L_N)$, for $\overline{D^+F}$ is $\overline{D^+F}^{2N}(\eta) - 1$ and for $\overline{D^+D^+F}$ is $\overline{D^+D^+F}^{2N}(\eta)$. In the subinterval $[L_{2N}, \infty)$, the two mesh difference at η for $\overline{F}$ is $\overline{F}^{2N}(L_{2N}) - F^N(L_n) - ln2$ and for $\overline{D^+F}$ and $\overline{D^+D^+F}$ it is zero. The resulting computed global two-mesh difference $\overline{D}$, the computed order of convergence $\overline{p}^N$ and the constant of convergence $\overline{C}_{\overline{p}^*}^N$ for $\overline{F}$, $\overline{D^+F}$ and $\overline{D^+D^+F}$ for various values of N and β are given in Tables 3.4, 3.5 and 3.6.

N	128	256	512	1024	2048	4096	8192	16384
				$\beta = 0.5$				
$\overline{D}^N$	0.008438	0.004906	0.002795	0.001569	0.000871	0.000479	0.000261	0.000141
$\overline{p}^N$	0.78	0.81	0.83	0.85	0.86	0.87	0.88	0.89
$\overline{C}^N_{0.86}$	1.235767	1.307253	1.354761	1.383781	1.397106	1.397106	1.385923	1.365481
				$\beta = 1.0$				
$\overline{D}^N$	0.008422	0.004881	0.002778	0.001559	0.000865	0.000475	0.000259	0.000140
$\overline{p}^N$	0.79	0.81	0.83	0.85	0.86	0.88	0.88	0.89
$\overline{C}^N_{0.86}$	1.234450	1.301607	1.347867	1.376316	1.389417	1.389417	1.378381	1.358180
				$\beta = 1.5$				
$\overline{D}^N$	0.008409	0.004866	0.002768	0.001553	0.000861	0.000473	0.000258	0.000140
$\overline{p}^N$	0.79	0.81	0.83	0.85	0.86	0.88	0.88	0.89
$\overline{C}^N_{0.86}$	1.233350	1.298834	1.344259	1.372281	1.385214	1.385214	1.374283	1.354252

Table 3.4: Computed two mesh difference $\overline{D}^N$, order of convergence $\overline{p}^N$ and constant of convergence $\overline{C}^N_{\overline{p}^*}$ for $\overline{F}$ on $[0, \infty)$ generated by (A^N_{FS}) with $M = 8nN$ applied to problem (P_{FS}) for various values of N and β.

N	128	256	512	1024	2048	4096	8192	16384
				$\beta = 0.5$				
$\overline{D}^N$	0.000317	0.000186	0.000106	0.000060	0.000033	0.000018	0.000010	0.000005
$\overline{p}^N$	0.76	0.81	0.83	0.85	0.86	0.87	0.88	0.89
$\overline{C}^N_{0.86}$	0.046309	0.049604	0.051499	0.052652	0.053187	0.053187	0.052771	0.051989
				$\beta = 1.0$				
$\overline{D}^N$	0.000256	0.000142	0.000079	0.000044	0.000024	0.000013	0.000007	0.000004
$\overline{p}^N$	0.85	0.85	0.84	0.85	0.86	0.88	0.89	0.89
$C^N_{0.86}$	0.037595	0.037895	0.038284	0.038884	0.039246	0.039246	0.038945	0.038389
				$\beta = 1.5$				
$\overline{D}^N$	0.000249	0.000128	0.000069	0.000037	0.000020	0.000011	0.000006	0.000003
$\overline{p}^N$	0.96	0.89	0.88	0.87	0.88	0.88	0.89	0.90
$\overline{C}^N_{0.88}$	0.038560	0.036424	0.036027	0.036023	0.036117	0.036117	0.035992	0.035718

Table 3.5: Computed two mesh difference $\overline{D}^N$, order of convergence $\overline{p}^N$ and constant of convergence $\overline{C}^N_{\overline{p}^*}$ for $\overline{D^+F}$ on $[0, \infty)$ generated by (A^N_{FS}) with $M = 8nN$ applied to problem (P_{FS}) for various values of N and β.

N	128	256	512	1024	2048	4096	8192	16384
				$\beta = 0.5$				
$\overline{D}^N$	0.004125	0.002401	0.001371	0.000770	0.000428	0.000235	0.000128	0.000069
$\overline{p}^N$	0.78	0.81	0.83	0.85	0.86	0.87	0.88	0.89
$\overline{C}_{0.86}^N$	0.603032	0.638212	0.662605	0.677204	0.683940	0.683940	0.678361	0.668200
				$\beta = 1.0$				
$\overline{D}^N$	0.007398	0.004301	0.002454	0.001379	0.000766	0.000421	0.000230	0.000124
$\overline{p}^N$	0.78	0.81	0.83	0.85	0.86	0.87	0.88	0.89
$\overline{C}_{0.86}^N$	1.081445	1.143468	1.186393	1.212510	1.224457	1.224457	1.214482	1.196298
				$\beta = 1.5$				
$\overline{D}^N$	0.011425	0.006661	0.003805	0.002140	0.001189	0.000654	0.000357	0.000193
$\overline{p}^N$	0.78	0.81	0.83	0.85	0.86	0.87	0.88	0.89
$\overline{C}_{0.86}^N$	1.668108	1.768405	1.836877	1.878426	1.897330	1.897330	1.881687	1.853234

Table 3.6: Computed two mesh difference $\overline{D}^N$, order of convergence $\overline{p}^N$ and constant of convergence $\overline{C}_{\overline{p}^*}^N$ for $\overline{D^+D^+F}$ on $[0,\infty)$ generated by (A_{FS}^N) with $M = 8nN$ applied to problem (P_{FS}) for various values of N and β.

The computed global error can be used to calculate the global error bounds for all values of $N \geq 256$, but in the next chapter we need them only for the value $N = 8192$. For this number of nodes, we use the Tables 3.4-3.6 and the experimental techniques to obtain the following error bounds for $N \geq 2048$

$$
\begin{aligned}
\beta = 0.5 \quad & ||\overline{F} - f||_{[0,\infty)} \leq 1.40N^{-0.86} \\
\beta = 1.0 \quad & ||\overline{F} - f||_{[0,\infty)} \leq 1.38N^{-0.86} \\
\beta = 1.5 \quad & ||\overline{F} - f||_{[0,\infty)} \leq 1.38N^{-0.86}
\end{aligned}
\tag{3.16}
$$

$$
\begin{aligned}
\beta = 0.5 \quad & ||\overline{D^+F} - f'||_{[0,\infty)} \leq 0.05N^{-0.86} \\
\beta = 1.0 \quad & ||\overline{D^+F} - f'||_{[0,\infty)} \leq 0.04N^{-0.86} \\
\beta = 1.5 \quad & ||\overline{D^+F} - f'||_{[0,\infty)} \leq 0.04N^{-0.86}
\end{aligned}
\tag{3.17}
$$

$$
\begin{aligned}
\beta = 0.5 \quad & ||\overline{D^+D^+F} - f''||_{[0,\infty)} \leq 0.68N^{-0.86} \\
\beta = 1.0 \quad & ||\overline{D^+D^+F} - f''||_{[0,\infty)} \leq 1.22N^{-0.86} \\
\beta = 1.5 \quad & ||\overline{D^+D^+F} - f''||_{[0,\infty)} \leq 1.90N^{-0.86}.
\end{aligned}
\tag{3.18}
$$

In the specific case of $N = 8192$ we get the bounds

$$
\begin{aligned}
\beta = 0.5 \quad & ||\overline{F} - f||_{[0,\infty)} \leq 6.034 \times 10^{-4} \\
\beta = 1.0 \quad & ||\overline{F} - f||_{[0,\infty)} \leq 5.948 \times 10^{-4} \\
\beta = 1.5 \quad & ||\overline{F} - f||_{[0,\infty)} \leq 5.948 \times 10^{-4}
\end{aligned}
\tag{3.19}
$$

$$
\begin{aligned}
\beta = 0.5 \quad & ||\overline{D^+F} - f'||_{[0,\infty)} \leq 2.155 \times 10^{-5} \\
\beta = 1.0 \quad & ||\overline{D^+F} - f'||_{[0,\infty)} \leq 1.724 \times 10^{-5} \\
\beta = 1.5 \quad & ||\overline{D^+F} - f'||_{[0,\infty)} \leq 1.724 \times 10^{-5}
\end{aligned}
\tag{3.20}
$$

$$\beta = 0.5 \quad ||\overline{D^+D^+F} - f''||_{[0,\infty)} \leq 2.931 \times 10^{-4}$$
$$\beta = 1.0 \quad ||\overline{D^+D^+F} - f''||_{[0,\infty)} \leq 5.258 \times 10^{-4} \qquad (3.21)$$
$$\beta = 1.5 \quad ||\overline{D^+D^+F} - f''||_{[0,\infty)} \leq 8.189 \times 10^{-4}.$$

We observe from (3.3) and (3.4) that u_{FS}, v_{FS}, ∇u_{FS} and ∇v_{FS} involve the expression $\eta f''$ and $\beta f' + \frac{m-1}{m+1}\eta f''$. Therefore, we compute the global error bounds for $\eta\overline{D^+D^+F}$ and $\beta\overline{D^+F} + \frac{m-1}{m+1}\eta\overline{D^+D^+F}$, respectively, using the techniques described at the beginning of the section and the data in Tables 3.7 and 3.8. The resulting computed global error bounds, which hold for all $N \geq 2048$, are

$$\beta = 0.5 \quad ||\beta\overline{D^+F} + \tfrac{m-1}{m+1}\eta\overline{D^+D^+F} - \beta f' + \tfrac{m-1}{m+1}\eta f''||_{[0,\infty)} \leq 0.399N^{-0.86}$$
$$\beta = 1.0 \quad ||\beta\overline{D^+F} + \tfrac{m-1}{m+1}\eta\overline{D^+D^+F} - \beta f' + \tfrac{m-1}{m+1}\eta f''||_{[0,\infty)} \leq 0.039N^{-0.86} \quad (3.22)$$
$$\beta = 1.5 \quad ||\beta\overline{D^+F} + \tfrac{m-1}{m+1}\eta\overline{D^+D^+F} - \beta f' + \tfrac{m-1}{m+1}\eta f''||_{[0,\infty)} \leq 0.472N^{-0.86}$$

$$\beta = 0.5 \quad ||\eta\overline{D^+D^+F} - \eta f''||_{[0,\infty)} \leq 0.804N^{-0.86}$$
$$\beta = 1.0 \quad ||\eta\overline{D^+D^+F} - \eta f''||_{[0,\infty)} \leq 0.864N^{-0.86} \qquad (3.23)$$
$$\beta = 1.5 \quad ||\eta\overline{D^+D^+F} - \eta f''||_{[0,\infty)} \leq 0.952N^{-0.86}.$$

N	128	256	512	1024	2048	4096	8192	16384
				$\beta = 0.5$				
D^N	0.004785	0.002817	0.001622	0.000915	0.000509	0.000280	0.000153	0.000083
p^N	0.76	0.80	0.83	0.85	0.86	0.87	0.88	0.89
$C^N_{0.86}$	0.694194	0.742389	0.776245	0.795746	0.804352	0.804352	0.797310	0.784639
				$\beta = 1.0$				
D^N	0.005145	0.003028	0.001742	0.000983	0.000547	0.000301	0.000164	0.000089
p^N	0.76	0.80	0.83	0.85	0.86	0.87	0.88	0.89
$C^N_{0.86}$	0.746665	0.798205	0.834075	0.854937	0.864309	0.864309	0.856764	0.843187
				$\beta = 1.5$				
D^N	0.005629	0.003333	0.001921	0.001084	0.000604	0.000332	0.000181	0.000098
p^N	0.76	0.80	0.83	0.84	0.86	0.87	0.88	0.89
$C^N_{0.86}$	0.816612	0.878354	0.919281	0.942096	0.952838	0.952838	0.944518	0.929504

Table 3.7: Computed two mesh difference $\overline{D}^N$, order of convergence $\overline{p}^N$ and constant of convergence $\overline{C}^N_{\overline{p}^*}$ for $\eta\overline{D^+D^+F}$ on $[0,\infty)$ generated by (A^N_{FS}) with $M = 8nN$ applied to problem (P_{FS}) for various values of N and β.

				$\beta = 0.5$				
N	128	256	512	1024	2048	4096	8192	16384
D^N	0.002380	0.001399	0.000803	0.000453	0.000252	0.000139	0.000076	0.000041
p^N	0.77	0.80	0.83	0.85	0.86	0.87	0.88	0.89
$C^N_{0.86}$	0.345965	0.369496	0.385191	0.394629	0.398846	0.398846	0.395435	0.389253
				$\beta = 1.0$				
D^N	0.000256	0.000142	0.000079	0.000044	0.000024	0.000013	0.000007	0.000004
p^N	0.85	0.85	0.84	0.85	0.86	0.88	0.89	0.89
$C^N_{0.86}$	0.037595	0.037895	0.038284	0.038884	0.039246	0.039246	0.038945	0.038389
				$\beta = 1.5$				
D^N	0.002824	0.001655	0.000950	0.000535	0.000298	0.000164	0.000089	0.000048
p^N	0.77	0.80	0.83	0.85	0.86	0.87	0.88	0.89
$C^N_{0.86}$	0.410474	0.437191	0.455736	0.466901	0.472029	0.472029	0.467952	0.460620

Table 3.8: Computed two mesh difference $\overline{D}^N$, order of convergence $\overline{p}^N$ and constant of convergence $\overline{C}^N_{\overline{p}^*}$ for $\beta \overline{D^+F} + \frac{m-1}{m+1}\eta\overline{D^+D^+F}$ on $[0, \infty)$ generated by (A^N_{FS}) with $M = 8nN$ applied to problem (P_{FS}) for various values of N and β.

In the specific case of $N = 8192$ we get the bounds

$$\beta = 0.5 \quad ||\eta\overline{D^+D^+F} - \eta f''||_{[0,\infty)} \leq 3.465 \times 10^{-4}$$
$$\beta = 1.0 \quad ||\eta\overline{D^+D^+F} - \eta f''||_{[0,\infty)} \leq 3.724 \times 10^{-4} \qquad (3.24)$$
$$\beta = 1.5 \quad ||\eta\overline{D^+D^+F} - \eta f''||_{[0,\infty)} \leq 4.103 \times 10^{-4}$$

$$\beta = 0.5 \quad ||\beta\overline{D^+F} + \frac{m-1}{m+1}\eta\overline{D^+D^+F} - \beta f' + \frac{m-1}{m+1}\eta f''||_{[0,\infty)} \leq 1.720 \times 10^{-4}$$
$$\beta = 1.0 \quad ||\beta\overline{D^+F} + \frac{m-1}{m+1}\eta\overline{D^+D^+F} - \beta f' + \frac{m-1}{m+1}\eta f''||_{[0,\infty)} \leq 1.681 \times 10^{-5} \qquad (3.25)$$
$$\beta = 1.5 \quad ||\beta\overline{D^+F} + \frac{m-1}{m+1}\eta\overline{D^+D^+F} - \beta f' + \frac{m-1}{m+1}\eta f''||_{[0,\infty)} \leq 2.034 \times 10^{-4}.$$

3.7 Computed global error estimates for Falkner–Skan solution

We now obtain approximate expressions $\mathbf{U}_{FS} = (U_{FS}, V_{FS})$ for the Falkner–Skan solution u_{FS} of (P_W) by substituting into the relations (3.3) and (3.4) the approximations $\overline{F}$ and $\overline{D^+F}$ for f and f', computed by (A^N_{FS}). Thus for each (x, y) in the rectangle $\overline{\Omega}$ we define

$$U_{FS}(x, y) = x^m\overline{D^+F}(\eta) = U(x)\overline{D^+F}(\eta) \qquad (3.26)$$

$$V_{FS}(x, y) = -\sqrt{\frac{m+1}{2x}\frac{U(x)}{Re}}\left(\overline{F}(\eta) + \frac{m-1}{m+1}\eta\overline{D^+F}(\eta)\right) \qquad (3.27)$$

where $\eta \in [0, \infty)$ is given by (3.2).

Preliminary analytical investigations in [26] indicate that for all $N \geq N_0$ and some

unknown constants p_1, p_2, C_{p_1} and C_{p_2}, the following theoretical bounds hold for the approximations $(U_{FS}, \frac{1}{V^*}V_{FS})$ to the scaled velocity $(u_{FS}, \frac{1}{V_*}v_{FS})$

$$||U_{FS} - u_{FS}||_{\overline{\Omega}} \leq C_{p_1}N^{-p_1}, \quad p_1 > 0 \tag{3.28}$$

$$||V_{FS} - v_{FS}||_{\overline{\Omega}} \leq C_{p_2}N^{-p_2}, \quad p_2 > 0 \tag{3.29}$$

where $\mathbf{U}_{FS}$ is the computed Falkner–Skan solution of the Prandtl problem on $\overline{\Omega}$ given by (3.26) and (3.27) and $(\mathbf{u}_{FS})$ is the exact solution of (P_W). Here N_0 and the error parameters p_1, p_2, C_{p_1} and C_{p_2} are independent of N and M. We have chosen

$$V^* = \begin{cases} \sqrt{\varepsilon} & \text{for } \beta = 0 \\ 1 & \text{for } \beta \in (0, 1.5]. \end{cases} \tag{3.30}$$

this is discussed in Appendix A.

In what follows, we use the experimental techniques from Section 3.6 to determine realistic error bounds of the form (3.28) and (3.29).

For the x-component U_{FS} of the velocity we obtain from (3.26) and (3.21) the following computed error bound for all $N \geq 2048$

$$\begin{aligned} \beta = 0.5 \quad ||U_{FS} - u_{FS}||_{\overline{\Omega}} &\leq 1.1^{0.333}(0.05N^{-0.86}) \\ \beta = 1.0 \quad ||U_{FS} - u_{FS}||_{\overline{\Omega}} &\leq 1.1^{1}(0.04N^{-0.86}) \\ \beta = 1.5 \quad ||U_{FS} - u_{FS}||_{\overline{\Omega}} &\leq 2.1^{3}(0.04N^{-0.86}). \end{aligned}$$

In the specific case of $N = 8192$ we have

$$\begin{aligned} \beta = 0.5 \quad ||U_{FS} - u_{FS}||_{\overline{\Omega}} &\leq 2.225 \times 10^{-5} \\ \beta = 1.0 \quad ||U_{FS} - u_{FS}||_{\overline{\Omega}} &\leq 1.896 \times 10^{-5} \\ \beta = 1.5 \quad ||U_{FS} - u_{FS}||_{\overline{\Omega}} &\leq 1.597 \times 10^{-4}. \end{aligned} \tag{3.31}$$

Similarly for the y-component $\frac{1}{V^*}V_{FS}$ of the velocity we obtain from (3.27), (3.19) and (3.21) the following computed error bound for all $N \geq 2048$ (also see Appendix A)

$$\begin{aligned} ||V_{FS} - v_{FS}||_{\overline{\Omega}} &= \sqrt{\frac{m+1}{2x}\frac{U(x)}{Re}}||\overline{F}(\eta) + \frac{m-1}{m+1}\eta\overline{D^+F}(\eta) \\ &\quad -(f(\eta) + \frac{m-1}{m+1}\eta f')|| \\ &\leq \sqrt{\frac{m+1}{2x}U(x)}(||\overline{F}(\eta) - f(\eta)||) \\ &\quad +U(x)\frac{m-1}{2x}y||\overline{D^+F}(\eta) - f'|| \end{aligned} \tag{3.32}$$

$$\beta = 0.5 \quad \|V_{FS} - v_{FS}\|_{\overline{\Omega}} \leq \sqrt{\tfrac{m+1}{2x}U(x)}(1.40N^{-0.86}) + U(x)\tfrac{m-1}{2x}y(0.05N^{-0.86})$$
$$\beta = 1.0 \quad \|V_{FS} - v_{FS}\|_{\overline{\Omega}} \leq \sqrt{\tfrac{m+1}{2(x)}U(x)}(1.38N^{-0.86}) + U(x)\tfrac{m-1}{2x}y(0.04N^{-0.86})$$
$$\beta = 1.5 \quad \|V_{FS} - v_{FS}\|_{\overline{\Omega}} \leq \sqrt{\tfrac{m+1}{2x}U(x)}(1.38N^{-0.86}) + U(x)\tfrac{m-1}{2x}y(0.04N^{-0.86}).$$

In the specific case of $N = 8192$ we have

$$\begin{aligned}
\beta = 0.5 \quad \|V_{FS} - v_{FS}\|_{\overline{\Omega}} &\leq 2.885 \times 10^{-4} \\
\beta = 1.0 \quad \|V_{FS} - v_{FS}\|_{\overline{\Omega}} &\leq 5.948 \times 10^{-4} \\
\beta = 1.5 \quad \|V_{FS} - v_{FS}\|_{\overline{\Omega}} &\leq 2.869 \times 10^{-3}.
\end{aligned} \tag{3.33}$$

In a similar manner, we calculate computed error bounds for approximations of the scaled first derivatives by scaled discrete derivatives

$$\partial_y U_{FS} = \frac{\eta}{y}U(x)\overline{D^+ D^+}F(\eta) \tag{3.34}$$

$$\partial_y V_{FS} = -\frac{\eta}{y}\left(\sqrt{\frac{(m+1)U(x)}{2xRe}}\left(\beta\overline{D^+}F + \frac{m-1}{m+1}\eta\overline{D^+ D^+}F\right)\right) \tag{3.35}$$

$$\partial_x U_{FS} = -\partial_y V_{FS} \tag{3.36}$$

$$\partial_x V_{FS} = \frac{m-1.0}{2x}\left(V_{FS} - \sqrt{\frac{(m+1)U(x)}{(2xRe)}}\left(\eta\overline{D^+}F + \eta\frac{m-1.0}{m+1.0}\left(\overline{D^+}F + \eta\overline{D^+ D^+}F\right)\right)\right). \tag{3.37}$$

For $\frac{1}{\sqrt{Re}}D_y U_{FS}$ of the velocity we obtain from (3.34) and (3.18) the following computed error bound for all $N \geq 2048$

$$\frac{1}{\sqrt{Re}}\|\partial_y U_{FS} - \frac{\partial u_{FS}}{\partial y}\|_{\overline{\Omega}} = \frac{1}{\sqrt{Re}}\sqrt{\frac{(m+1)Re\,U(x)}{2}}\frac{U(x)}{x}U(x)\|\overline{D^+ D^+}F - f''\|_{[0,\infty)} \tag{3.38}$$

$$\begin{aligned}
\beta = 0.5 \quad \tfrac{1}{\sqrt{Re}}\|\partial_y U_{FS} - \tfrac{\partial u_{FS}}{\partial y}\|_{\overline{\Omega}} &\leq \sqrt{\tfrac{(1.333)}{2}\tfrac{1.1^{0.333}}{1.1}}1.1^{0.333}(1.40N^{-0.86}) \\
\beta = 1.0 \quad \tfrac{1}{\sqrt{Re}}\|\partial_y U_{FS} - \tfrac{\partial u_{FS}}{\partial y}\|_{\overline{\Omega}} &\leq \sqrt{\tfrac{(1)}{2}\tfrac{1.1^1}{1.1}}1.1^1(1.22N^{-0.86}) \\
\beta = 1.5 \quad \tfrac{1}{\sqrt{Re}}\|\partial_y U_{FS} - \tfrac{\partial u_{FS}}{\partial y}\|_{\overline{\Omega}} &\leq \sqrt{\tfrac{(4)}{2}\tfrac{2.1^3}{2.1}}2.1^4(1.90N^{-0.86}).
\end{aligned} \tag{3.39}$$

In the specific case of $N = 8192$ we have

$$\begin{aligned}
\beta = 0.5 \quad \tfrac{1}{\sqrt{Re}}\|\partial_y U_{FS} - \tfrac{\partial u_{FS}}{\partial y}\|_{\overline{\Omega}} &\leq 4.773 \times 10^{-4} \\
\beta = 1.0 \quad \tfrac{1}{\sqrt{Re}}\|\partial_y U_{FS} - \tfrac{\partial u_{FS}}{\partial y}\|_{\overline{\Omega}} &\leq 5.258 \times 10^{-4} \\
\beta = 1.5 \quad \tfrac{1}{\sqrt{Re}}\|\partial_y U_{FS} - \tfrac{\partial u_{FS}}{\partial y}\|_{\overline{\Omega}} &\leq 2.432 \times 10^{-3}.
\end{aligned} \tag{3.40}$$

For $D_y V_{FS}$ of the velocity we obtain from (3.35) and (3.22) the following computed

error bound for all $N \geq 2048$

$$\|\partial_y V_{FS} - \frac{\partial v_{FS}}{\partial y}\|_{\overline{\Omega}} = \sqrt{\frac{(m+1)Re}{2}\frac{U(x)}{x}} \left(\sqrt{\frac{(m+1)U(x)}{2xRe}} \|\beta \overline{D^+F} \right.$$
$$\left. + \frac{m-1}{m+1}\eta \overline{D^+D^+F} - \beta f' - \frac{m-1}{m+1}\eta f''\|_{[0,\infty)} \right) \tag{3.41}$$

$$\beta = 0.5 \quad \|\partial_y V_{FS} - \frac{\partial v_{FS}}{\partial y}\|_{\overline{\Omega}} \leq \frac{(1.333)1.1^{0.333}}{2(1.1)}(0.399N^{-0.86})$$
$$\beta = 1.0 \quad \|\partial_y V_{FS} - \frac{\partial v_{FS}}{\partial y}\|_{\overline{\Omega}} \leq \frac{(1.333)1.1^{0.333}}{2(1.1)}(0.039N^{-0.86}) \tag{3.42}$$
$$\beta = 1.5 \quad \|\partial_y V_{FS} - \frac{\partial v_{FS}}{\partial y}\|_{\overline{\Omega}} \leq \frac{(1.333)2.1^{0.333}}{2(2.1)}(0.472N^{-0.86}).$$

In the specific case of $N = 8192$ we have

$$\beta = 0.5 \quad \|\partial_y V_{FS} - \frac{\partial v_{FS}}{\partial y}\|_{\overline{\Omega}} \leq 1.076 \times 10^{-4}$$
$$\beta = 1.0 \quad \|\partial_y V_{FS} - \frac{\partial v_{FS}}{\partial y}\|_{\overline{\Omega}} \leq 1.681 \times 10^{-5} \tag{3.43}$$
$$\beta = 1.5 \quad \|\partial_y V_{FS} - \frac{\partial v_{FS}}{\partial y}\|_{\overline{\Omega}} \leq 1.794 \times 10^{-3}.$$

For $\frac{1}{V_*}D_x V_{FS}$ of the velocity we obtain from (3.37), (3.19), (3.21) and (3.23) the following computed error bound for all $N \geq 2048$

$$\frac{1}{V_*}\|\partial_x V_{FS} - \frac{\partial v_{FS}}{\partial x}\|_{\overline{\Omega}} = \frac{m-1.0}{2x}\left(\|V_{FS} - \sqrt{\frac{(m+1)U(x)}{(2xRe)}}\left(\eta\overline{D^+F} + \eta\frac{m-1.0}{m+1.0}\left(\overline{D^+F} + \eta\overline{D^+D^+F}\right)\right)\right.$$
$$\left. -v_{FS} + \sqrt{\frac{(m+1)U(x)}{(2xRe)}}\left(\eta f' + \eta\frac{m-1.0}{m+1.0}\left(f' + \eta f''\right)\right)\|\right)$$
$$\leq \frac{m-1.0}{2x}\left(\|V_{FS} - v_{FS}\|_{\overline{\Omega}}\right.$$
$$+\frac{m+1}{2x}U(x)\beta\|\overline{D^+F} - f'\|_{[0,\infty)}$$
$$\left. +\frac{m-1}{m+1}\|\eta\overline{D^+D^+F} - \eta f''\|_{[0,\infty)}\right) \tag{3.44}$$

$$\beta = 0.5 \quad \frac{1}{V_*}\|\partial_x V_{FS} - \frac{\partial v_{FS}}{\partial x}\|_{\overline{\Omega}} \leq \frac{m-1.0}{2x}\left(\sqrt{\frac{2x}{m+1}}U(x)(1.40N^{-0.86}) + U(x)\frac{m-1}{2x}y(0.05N^{-0.86})\right.$$
$$+\frac{m+1}{2x}U(x)\beta(0.399N^{-0.86})$$
$$\left. +\frac{m-1}{m+1}(0.804N^{-0.86})\right)$$

$$\beta = 1.0 \quad \frac{1}{V_*}\|\partial_x V_{FS} - \frac{\partial v_{FS}}{\partial x}\|_{\overline{\Omega}} = 0$$

$$\beta = 1.5 \quad \frac{1}{V_*}\|\partial_x V_{FS} - \frac{\partial v_{FS}}{\partial x}\|_{\overline{\Omega}} \leq \frac{|m-1.0|}{2x}\left(\sqrt{\frac{2x}{m+1}}U(x)(1.38N^{-0.86}) + U(x)\frac{m-1}{2x}y(0.04N^{-0.86})\right.$$
$$+\frac{m+1}{2x}U(x)\beta(0.472N^{-0.86})$$
$$\left. +\frac{|m-1|}{m+1}(0.952N^{-0.86})\right). \tag{3.45}$$

In the specific case of $N = 8192$ we have

$$\beta = 0.5 \quad \frac{1}{V_*}\|\partial_x V_{FS} - \frac{\partial v_{FS}}{\partial x}\|_{\overline{\Omega}} \leq 2.114 \times 10^{-4}$$
$$\beta = 1.0 \quad \frac{1}{V_*}\|\partial_x V_{FS} - \frac{\partial v_{FS}}{\partial x}\|_{\overline{\Omega}} = 0 \tag{3.46}$$
$$\beta = 1.5 \quad \frac{1}{V_*}\|\partial_x V_{FS} - \frac{\partial v_{FS}}{\partial x}\|_{\overline{\Omega}} \leq 1.973 \times 10^{-3}.$$

Chapter 4

A Reynolds–uniform numerical method for the Prandtl boundary layer problem for flow past a wedge – direct method

4.1   Introduction

In this chapter we make use of the computed Falkner–Skan similarity solution of the Prandtl problem calculated in Chapter 3 in two ways. Firstly, we use it to provide the unknown boundary conditions that are required on the boundary of Ω in the direct numerical method for the Prandtl problem. Secondly, we use the reference solution for the unknown exact solution in the expression for the error. It is convenient to introduce the notation $\varepsilon = \frac{1}{Re}$, to emphasis the singularly perturbed nature of the

problem. The problem (P_W) in Chapter 3 is now written as

$$(P_\varepsilon) \begin{cases} \text{Find } \mathbf{u}_\varepsilon = (u_\varepsilon, v_\varepsilon) \text{ such that for all } (x, y) \in \Omega \\ \mathbf{u}_\varepsilon \text{ satisfies the differential equation} \\[2mm] -\varepsilon \frac{\partial^2 u_\varepsilon}{\partial^2 y} + \mathbf{u}_\varepsilon . \nabla u_\varepsilon = U(x) \frac{dU(x)}{dx} \\[2mm] \nabla . \mathbf{u}_\varepsilon = 0 \\[2mm] \text{with boundary conditions} \\[2mm] \mathbf{u}_\varepsilon = 0 \text{ on } \Gamma_B \\ \mathbf{u}_\varepsilon = \mathbf{u}_{FS} \text{ on } \Gamma_L \bigcup \Gamma_T \end{cases}$$

where $(U(x) = x^m, 0)$ is the solution of the reduced problem and $m = \frac{\beta}{2-\beta}$, where $\beta\pi$ is the angle in radians of the wedge.

Since the computed Falkner-Skan solution in Chapter 3 is known to converge Reynolds uniformly to the solution of the Prandtl problem, we can compute Reynolds uniform error bounds. For this purpose we use the computed Falkner–Skan solution for (P_{FS}) with $N = 8192$; namely $\mathbf{U}_{FS}^{8192}$. This provides the required accuracy for the velocity components U_{FS}^{8192}, V_{FS}^{8192} and their scaled derivatives $\sqrt{\varepsilon} D_y U_{FS}^{8192}$, $D_x V_{FS}^{8192}$ and $D_y V_{FS}^{8192}$.

4.2 The Prandtl Problem for flow past a wedge

The aim of this section is to construct a robust numerical method to solve the Prandtl problem (P_ε) for all values of $\beta \in [0.0, 1.5]$ and Reynolds numbers $Re \in [1, \infty)$.

When constructing a mesh in the rectangle Ω, it is important to note where the boundary layer occurs in order to define an appropriate transition point from the coarse to the fine mesh. Because the computational domain is rectangular the piecewise–uniform fitted mesh Ω_ε^N is a tensor product of two one–dimensional meshes. The mesh in the x direction is the uniform mesh (see Fig. 4-1)

$$\Omega_u^{N_x} = \{x_i : x_i = 0.1 + \gamma(\beta) + iN_x^{-1}, 0 \le i \le N_x\}$$

where $\gamma(\beta)$ is (3.1). The mesh in the y-direction is a piecewise–uniform fitted mesh,

which is defined by

$$\Omega_\varepsilon^{N_y} = \{y_j : y_j = \sigma j \frac{2}{N_y}, 0 \le j \le \frac{N_y}{2}; y_j = \sigma + (1-\sigma)(j - \frac{N_y}{2})\frac{2}{N_y}, \frac{N_y}{2} \le j \le N_y\}.$$

The transition point σ is chosen so that there is a fine mesh in the boundary layer when required. The appropriate choice in this case is

$$\sigma = \min\{\frac{1}{2}, C\sqrt{\varepsilon} \ln N_y\}.$$

The factor $\sqrt{\varepsilon}$ may be motivated from from asymptotic analysis [46].
C is an experimental constant to optimize the results the choice of C is discussed in Appendix C. We choose

$$C = \begin{cases} 1.2 & \text{for } \beta \in [0, 1.3] \\ 0.75 & \text{for } \beta \in (1.3, 1.5]. \end{cases}$$

The rectangular mesh is then the tensor product $\Omega_\varepsilon^{\mathbf{N}} = \Omega_u^{N_x} \times \Omega_\varepsilon^{N_y}$, where $\mathbf{N}=(N_x, N_y)$. For simplicity we take $N_x = N_y = N$.
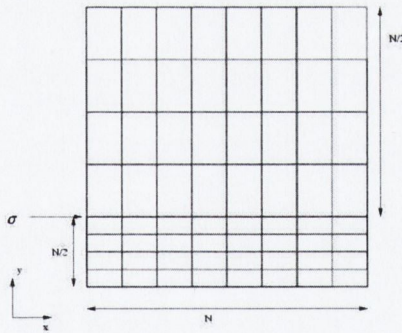
Figure 4-1: 2-d mesh constructed from a tensor product

The problem (P_ε) is discretized by the following non-linear upwind finite difference

method on the piecewise uniform fitted mesh Ω_ε^N

$$(P_\varepsilon^N) \begin{cases} \text{Find } \mathbf{U}_\varepsilon = (U_\varepsilon, V_\varepsilon) \text{ such that for all } (x_i, y_j) \in \Omega_\varepsilon^N \\ \mathbf{U}_\varepsilon \text{ satisfies the finite difference equations} \\[2mm] -\varepsilon\delta_y^2 U_\varepsilon(x_i, y_j) + U_\varepsilon(x_i, y_j) D_x^- U_\varepsilon(x_i, y_j) + \\ V_\varepsilon(x_i, y_j) D_y^u U_\varepsilon(x_i, y_j) = U(x_i)\frac{dU}{dx}(x_i) \\[3mm] D_x^- U_\varepsilon(x_i, y_j) + D_y^- V_\varepsilon(x_i, y_j) = 0 \\[3mm] \text{with boundary conditions} \\ \mathbf{U}_\varepsilon = 0 \text{ on } \Gamma_B \\ \mathbf{U}_\varepsilon = \mathbf{U}_{FS}^{8192} \text{ on } \Gamma_L \bigcup \Gamma_T \end{cases}$$

where D_x^-, D_x^+ and D_y^-, D_y^+ are the standard first–ordered backward and forward finite difference operators, respectively, in the x and y directions. For any continuous function $V_\varepsilon(x_i, y_j)$ on the domain Ω_ε^N, D_y^u is defined by

$$V_\varepsilon(x_i, y_j) D_y^u U_\varepsilon(x_i, y_j) = \begin{cases} V_\varepsilon(x_i, y_j) D_y^- U_\varepsilon(x_i, y_j) & \text{if } V_\varepsilon(x_i, y_j) \geq 0; \\ V_\varepsilon(x_i, y_j) D_y^+ U_\varepsilon(x_i, y_j) & \text{if } V_\varepsilon(x_i, y_j) < 0 \end{cases}$$

δ_y^2 is the standard second order centered difference operator in the y direction.

The need for changes between forward and backward differences is due to the fact that, at values of $\beta > 0.1$, V_ε is initially negative and then becomes positive. Without these changes, the tridiagonal system would no longer be diagonally dominant and the continuation algorithm would fail to converge.

Since the problem (P_ε^N) is a nonlinear system, an iterative method is required for its solution. This is obtained by replacing the system of nonlinear equations with a sequence of systems of linear equations. The systems of linearized equations are

$(A_\varepsilon^{\mathbf{N}})$
$\begin{cases}
\text{With the boundary condition } \mathbf{U}_\varepsilon^M = \mathbf{U}_{\text{FS}}^{8192} \text{ on } \Gamma_{\text{L}}, \\[4pt]
\text{for each } i, 1 \le i \le N, \text{ use the initial guess } \mathbf{U}_\varepsilon^0|_{X_i} = \mathbf{U}_\varepsilon^0|_{X_{i-1}} \\[4pt]
\text{and for } m = 1, \ldots, M \text{ solve the following} \\[4pt]
\text{two point boundary value problem for } U_\varepsilon^m(x_i, y_j) \\[12pt]
-\varepsilon \delta_y^2 U_\varepsilon^m(x_i, y_j) + U_\varepsilon^{m-1}(x_i, y_j) D_x^- U_\varepsilon^m(x_i, y_j) + \\[4pt]
V_\varepsilon^{m-1}(x_i, y_j) D_y^u U_\varepsilon^m(x_i, y_j) = U(x_i)\frac{dU}{dx}(x_i) \\[12pt]
\text{with the boundary conditions } U_\varepsilon^m = U_{\text{FS}} \text{ on } \Gamma_{\text{B}} \cup \Gamma_{\text{T}}, \\[4pt]
\text{and the initial guess for } V_\varepsilon^0|_{X_1} = 0. \\[4pt]
\text{Also, solve the initial value problem for } V_\varepsilon^m(x_i, y_j) \\[12pt]
(\mathbf{D}^- \cdot \mathbf{U}_\varepsilon^m)(x_i, y_j) = 0, \\[12pt]
\text{with initial condition } V_\varepsilon^m = 0 \text{ on } \Gamma_{\text{B}}. \\[4pt]
\text{Continue to iterate between the equations for } \mathbf{U}_\varepsilon^m \text{ until } m = M, \\[4pt]
\text{where } M \text{ is such that} \\[4pt]
\max\left(|U_\varepsilon^M - U_\varepsilon^{M-1}|_{\overline{\Omega}_\varepsilon^N}, \frac{1}{V^*}|V_\varepsilon^M - V_\varepsilon^{M-1}|_{\overline{\Omega}_\varepsilon^N}\right) \le tol.
\end{cases}$

For notational simplicity we suppress explicit mention of the iteration superscript M henceforth, and we write simply $\mathbf{U}_\varepsilon$ for the solution generated by $(A_\varepsilon^{\mathbf{N}})$. We take $tol = 10^{-6}$ in the computations. We note that there are no known theoretical results concerning the convergence of the solutions $\mathbf{U}_\varepsilon$ of $(P_\varepsilon^{\mathbf{N}})$ to the solution $\mathbf{u}_\varepsilon$ of (P_ε) and no theoretical estimate for the pointwise error $(\mathbf{U}_\varepsilon - \mathbf{u}_\varepsilon)(x_i, y_j)$. It is for this reason that we are forced to apply controllable experimental techniques that are adapted to the problem under consideration. They are of crucial value to our understanding of the computational problems and are the topic of the next two sections. The scaling factor for V_ε^N, V^*, is defined to be

$$V^* = \begin{cases} \sqrt{\varepsilon} & \text{for } \beta = 0 \\ 1 & \text{for } \beta \in (0, 1.5]. \end{cases} \tag{4.1}$$

This was motivated by the need to have a scaling factor that does not require to be recomputed for each new value of ε and N (see Appendix A). In the papers [5], [6]

and [7] we used the scaling factor

$$V_{old}^* = \max_{\Omega_\varepsilon^N} |V_{FS}|.$$

V_{old}^* yields identical orders of convergence as V^*, but had to be recalculated for each ε when calculating the differences as in Section 4.6.

4.3   Convergence of the method

Before investigating the results of the method we must look at the convergence of the iterative method. In Table 4.1 we see that the number of iterations tends to a fixed value as ε decreases for all N and β.

Thus an ε-uniform amount of computational work is required by (A_ε^N) for the generation of $(U_\varepsilon, V_\varepsilon)$ for various β.

	$\beta = 0.5$						$\beta = 1.0$						$\beta = 1.5$				
$\varepsilon \backslash N$	32	64	128	256	512	$\varepsilon \backslash N$	32	64	128	256	512	$\varepsilon \backslash N$	32	64	128	256	512
2^{-0}	8	10	11	11	11	2^{-0}	12	14	15	16	16	2^{-0}	14	15	17	18	19
2^{-2}	12	12	12	12	11	2^{-2}	13	14	15	16	16	2^{-2}	14	15	17	18	18
2^{-4}	12	12	12	11	11	2^{-4}	13	14	15	15	16	2^{-4}	13	16	17	18	18
2^{-6}	12	12	11	11	10	2^{-6}	13	14	15	15	15	2^{-6}	13	15	18	18	18
2^{-8}	11	11	11	10	10	2^{-8}	12	14	15	15	15	2^{-8}	13	15	17	17	18
2^{-10}	10	10	10	9	9	2^{-10}	12	13	14	14	14	2^{-10}	13	14	16	16	17
2^{-12}	9	9	9	8	8	2^{-12}	11	12	13	13	13	2^{-12}	13	14	15	15	16
2^{-14}	9	8	8	8	8	2^{-14}	11	12	12	12	12	2^{-14}	13	14	15	15	15
2^{-16}	9	8	8	8	8	2^{-16}	11	12	12	11	11	2^{-16}	13	14	15	15	14
2^{-18}	9	8	8	8	8	2^{-18}	11	12	12	11	10	2^{-18}	13	14	15	15	14
2^{-20}	9	8	8	8	8	2^{-20}	11	12	12	11	10	2^{-20}	13	14	15	15	14

Table 4.1: Number of one dimensional linear solver iterations required for convergence for method A_ε^N applied to problem (P_ε) for various values of ε, N and $\beta = 0.5$, 1.0 and 1.5.

4.4   Error analysis based on the finest mesh solution

In this section we estimate, computationally, the maximum pointwise error in the numerical solution and its discrete derivatives, generated by the algorithm (A_ε^N) of the previous section. Since the exact solution in the expression for the computed maximum pointwise error is unknown, we replace it by the solution U_ε^{512} generated by (A_ε^N) on the finest mesh Ω_ε^{512}. Thus, for U_ε and $\frac{1}{V^*}V_\varepsilon$, we define the computed

maximum pointwise errors

$$E_\varepsilon^N(U_\varepsilon) = ||U_\varepsilon - \overline{U_\varepsilon^{512}}||_{\overline{\Omega}_\varepsilon^N} \qquad E_\varepsilon^N(\tfrac{1}{V^*}V_\varepsilon) = \tfrac{1}{V^*}||V_\varepsilon - \overline{V_\varepsilon^{512}}||_{\overline{\Omega}_\varepsilon^N \backslash \Gamma_L}$$

and

$$E^N(U_\varepsilon) = \max_\varepsilon E_\varepsilon^N(U_\varepsilon) \qquad E^N(\tfrac{1}{V^*}V_\varepsilon) = \max_\varepsilon E_\varepsilon^N(\tfrac{1}{V^*}V_\varepsilon).$$

As in the previous chapter, for the sake of brevity we show the errors for three typical values of the angle of the wedge; $\beta = 0.5$, $\beta = 1.0$ and $\beta = 1.5$. Note that similar results are given for the flat plate ($\beta = 0.0$) in [26] and for the value of the angle of the wedge $\beta = 0.6$ in [5].

The values of the computed maximum pointwise errors generated by (A_ε^N) applied to problem (P_ε) for U_ε and $\frac{1}{V^*}V_\varepsilon$ are given in Tables 4.2 and 4.3, respectively, for various values of ε, N and β.

$\varepsilon \backslash N$	$\beta = 0.5$ 32	64	128	256	$\varepsilon \backslash N$	$\beta = 1.0$ 32	64	128	256
2^{-0}	8.09e-04	4.32e-04	2.02e-04	7.06e-05	2^{-0}	4.04e-04	1.90e-04	8.18e-05	2.73e-05
2^{-2}	5.22e-03	2.60e-03	1.15e-03	3.91e-04	2^{-2}	9.75e-04	4.72e-04	2.06e-04	6.94e-05
2^{-4}	9.75e-03	4.72e-03	2.06e-03	6.94e-04	2^{-4}	1.95e-03	8.87e-04	3.75e-04	1.24e-04
2^{-6}	1.16e-02	5.58e-03	2.41e-03	8.09e-04	2^{-6}	3.54e-03	1.84e-03	7.67e-04	2.52e-04
2^{-8}	1.16e-02	5.61e-03	2.45e-03	8.25e-04	2^{-8}	3.41e-03	1.78e-03	8.36e-04	3.36e-04
2^{-10}	1.15e-02	5.61e-03	2.45e-03	8.25e-04	2^{-10}	3.39e-03	1.78e-03	8.36e-04	3.36e-04
2^{-12}	1.14e-02	5.60e-03	2.45e-03	8.25e-04	2^{-12}	3.33e-03	1.78e-03	8.36e-04	3.36e-04
2^{-14}	1.14e-02	5.60e-03	2.45e-03	8.25e-04	2^{-14}	3.28e-03	1.77e-03	8.36e-04	3.36e-04
2^{-16}	1.13e-02	5.60e-03	2.45e-03	8.25e-04	2^{-16}	3.24e-03	1.77e-03	8.36e-04	3.36e-04
2^{-18}	1.13e-02	5.60e-03	2.45e-03	8.25e-04	2^{-18}	3.22e-03	1.77e-03	8.36e-04	3.36e-04
2^{-20}	1.13e-02	5.60e-03	2.45e-03	8.25e-04	2^{-20}	3.21e-03	1.77e-03	8.36e-04	3.36e-04
E^N	1.16e-02	5.61e-03	2.45e-03	8.25e-04	E^N	3.54e-03	1.84e-03	8.36e-04	3.36e-04

$\varepsilon \backslash N$	$\beta = 1.5$ 32	64	128	256
2^{-0}	3.23e-02	1.58e-02	6.92e-03	2.33e-03
2^{-2}	4.23e-02	2.14e-02	9.66e-03	3.32e-03
2^{-4}	5.76e-02	2.73e-02	1.35e-02	4.80e-03
2^{-6}	6.48e-02	3.21e-02	1.93e-02	7.22e-03
2^{-8}	6.73e-02	3.24e-02	1.86e-02	9.21e-03
2^{-10}	6.79e-02	3.24e-02	1.86e-02	9.21e-03
2^{-12}	6.80e-02	3.24e-02	1.86e-02	9.21e-03
2^{-14}	6.81e-02	3.24e-02	1.86e-02	9.21e-03
2^{-16}	6.81e-02	3.24e-02	1.86e-02	9.21e-03
2^{-18}	6.81e-02	3.24e-02	1.86e-02	9.21e-03
2^{-20}	6.81e-02	3.24e-02	1.86e-02	9.21e-03
E^N	6.81e-02	3.24e-02	1.93e-02	9.21e-03

Table 4.2: Computed maximum errors $E_\varepsilon^N(U_\varepsilon)$ generated by (A_ε^N) applied to problem (P_ε) for various values of ε, N and β.

Examining the results in Table 4.2 we see that the computed maximum errors decrease as the number of mesh points, N, increases. The maximum errors increase as ε decreases for $1 \le \varepsilon \le 2^{-10}$ for all N and β. For each N the largest maximum errors, E^N, occur when $2^{-6} \le \varepsilon \le 2^{-10}$. When $\varepsilon \le 2^{-12}$ the errors stabilise to a fixed value for any N or β. This suggests that the method is independent of ε for $\beta = 0.5$,

1.0 and 1.5. The maximum errors strongly suggest that the method is ε–uniform for U_ε for all β considered.

In Table 4.3 we see that the computed maximum errors decrease as the number of mesh points, N, increase for all β. The largest errors E^N for $\frac{1}{V_*}V_\varepsilon$ for all N and β occur when $\varepsilon = 1$ or $\varepsilon = 2^{-2}$. We observe that the computed pointwise maximum errors for $\frac{1}{V_*}V_\varepsilon$ decrease as ε decreases for all β considered. Table 4.3 indicates that maximum errors are independent of ε for all β. This suggests that the method is ε–uniform for $\frac{1}{V_*}V_\varepsilon$ for all β considered.

$\varepsilon\backslash N$	$\beta = 0.5$				$\varepsilon\backslash N$	$\beta = 1.0$			
	32	64	128	256		32	64	128	256
2^{-0}	3.73e-02	1.81e-02	8.15e-03	2.80e-03	2^{-0}	1.23e-02	6.07e-03	2.84e-03	1.06e-03
2^{-2}	4.29e-02	2.02e-02	8.76e-03	2.94e-03	2^{-2}	1.53e-02	7.66e-03	3.64e-03	1.38e-03
2^{-4}	3.80e-02	1.76e-02	7.55e-03	2.52e-03	2^{-4}	1.43e-02	7.32e-03	3.56e-03	1.39e-03
2^{-6}	3.55e-02	1.73e-02	7.39e-03	2.46e-03	2^{-6}	1.18e-02	7.10e-03	3.51e-03	1.39e-03
2^{-8}	2.87e-02	1.36e-02	5.99e-03	2.06e-03	2^{-8}	5.64e-03	3.44e-03	1.94e-03	8.54e-04
2^{-10}	2.60e-02	1.20e-02	5.21e-03	1.76e-03	2^{-10}	2.82e-03	1.72e-03	9.68e-04	4.27e-04
2^{-12}	2.46e-02	1.12e-02	4.83e-03	1.62e-03	2^{-12}	1.41e-03	8.60e-04	4.84e-04	2.13e-04
2^{-14}	2.40e-02	1.09e-02	4.65e-03	1.55e-03	2^{-14}	7.05e-04	4.30e-04	2.42e-04	1.07e-04
2^{-16}	2.37e-02	1.07e-02	4.55e-03	1.52e-03	2^{-16}	3.53e-04	2.15e-04	1.21e-04	5.34e-05
2^{-18}	2.35e-02	1.06e-02	4.51e-03	1.50e-03	2^{-18}	1.76e-04	1.07e-04	6.05e-05	2.67e-05
2^{-20}	2.34e-02	1.05e-02	4.49e-03	1.49e-03	2^{-20}	8.82e-05	5.37e-05	3.02e-05	1.33e-05
E^N	4.29e-02	2.02e-02	8.76e-03	2.94e-03	E^N	1.53e-02	7.66e-03	3.64e-03	1.39e-03

$\varepsilon\backslash N$	$\beta = 1.5$			
	32	64	128	256
2^{-0}	1.25e-01	6.02e-02	2.62e-02	8.81e-03
2^{-2}	1.37e-01	6.76e-02	2.97e-02	1.00e-02
2^{-4}	1.33e-01	6.89e-02	3.10e-02	1.06e-02
2^{-6}	7.79e-02	4.95e-02	2.68e-02	1.06e-02
2^{-8}	9.28e-02	3.71e-02	1.37e-02	4.78e-03
2^{-10}	1.13e-01	4.95e-02	2.00e-02	6.35e-03
2^{-12}	1.23e-01	5.56e-02	2.32e-02	7.57e-03
2^{-14}	1.28e-01	5.87e-02	2.48e-02	8.17e-03
2^{-16}	1.31e-01	6.02e-02	2.56e-02	8.47e-03
2^{-18}	1.32e-01	6.10e-02	2.60e-02	8.63e-03
2^{-20}	1.33e-01	6.14e-02	2.62e-02	8.70e-03
E^N	1.37e-01	6.89e-02	3.10e-02	1.06e-02

Table 4.3: Computed maximum errors $E_\varepsilon^N(\frac{1}{V_*}V_\varepsilon)$ generated by (A_ε^N) applied to problem (P_ε) for various values of ε, N and β.

Graphs of the velocity component U_ε of the solution $\mathbf{U}_\varepsilon$ generated by the direct method (A_ε^N) with N=32, and $\beta = 0.5$, 1.0 and 1.5 for $\varepsilon = 1.0$ and 2^{-12}, are shown in Figures 4-2 and 4-3, respectively.

In Figure 4-2 we see that for $\varepsilon = 1.0$ the graphs of U_ε have no boundary layer for various values of β.
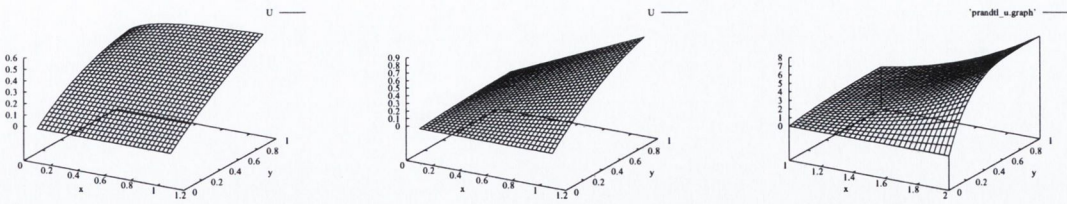
Figure 4-2: Graphs of U_ε for $\varepsilon = 1.0$, $N=32$ and $\beta = 0.5, 1.0, 1.5$.

In Figure 4-3 there is a very visible boundary layer in U_ε along the surface of the wedge for various values of β for $\varepsilon = 2^{-12}$. The velocity component has no non–physical oscillations for all β. The graphs in Figure 4-3 illustrate the importance of the transition point σ. The fine mesh below the transition point contains the boundary layer, which would be neglected by a uniform mesh as shown in Chapter 2.
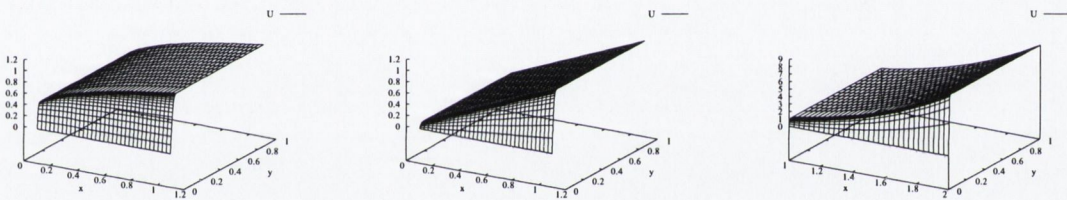
Figure 4-3: Graphs of U_ε for $\varepsilon = 2^{-12}$, $N=32$ and $\beta = 0.5, 1.0, 1.5$.

Graphs of the scaled component $\frac{1}{V^*}V_\varepsilon$ of the solution $\mathbf{U}_\varepsilon$ generated by the direct method $(A_\varepsilon^\mathbf{N})$ with N=32, and $\beta = 0.5$, 1.0 and 1.5 are shown in Figures 4-4 and 4-5 for $\varepsilon = 1.0$ and 2^{-12}, respectively.
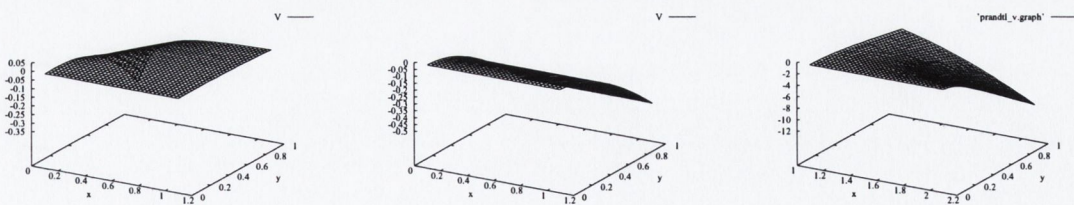
Figure 4-4: Graphs of $\frac{1}{V^*}V_\varepsilon$ for $\varepsilon = 1.0$, $N=32$ and $\beta = 0.5, 1.0, 1.5$.

The graphs in Figures 4-4 and 4-5 show that the scaled velocity component $\frac{1}{V^*}V_\varepsilon$ has no non–physical oscillation for all β and $\varepsilon = 1.0$ and 2^{-12}. Another property

to note is that, unlike the case of the flat plate ($\beta = 0$), we have negative values of V_ε for the values of β considered. $\frac{1}{V^*}V_\varepsilon$ has no visible boundary layer for all β and $\varepsilon = 1.0$ and 2^{-12}.
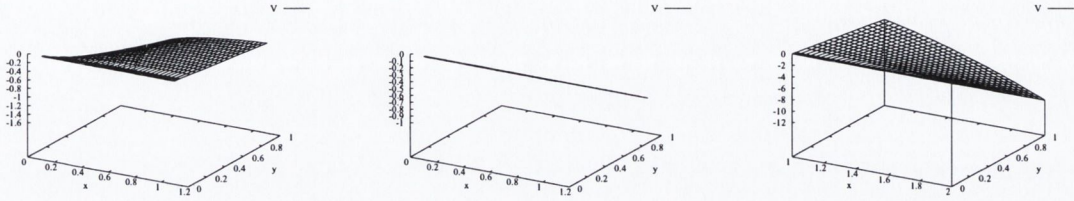
Figure 4-5: Graphs of $\frac{1}{V^*}V_\varepsilon$ for $\varepsilon = 2^{-12}$, $N=32$ and $\beta = 0.5, 1.0, 1.5$.

The computed orders of convergence p_ε^N and p^N for U_ε and $\frac{1}{V^*}V_\varepsilon$ are defined by

$$p_\varepsilon^N(U_\varepsilon) = \log_2 \frac{E_\varepsilon^N(U_\varepsilon)}{E_\varepsilon^{2N}(U_\varepsilon)}, \qquad p^N(U_\varepsilon) = \log_2 \frac{E^N(U_\varepsilon)}{E^{2N}(U_\varepsilon)}$$
$$p_\varepsilon^N(\tfrac{1}{V^*}V_\varepsilon) = \log_2 \frac{E_\varepsilon^N(\frac{1}{V^*}V_\varepsilon)}{E_\varepsilon^{2N}(\frac{1}{V^*}V_\varepsilon)}, \qquad p^N(\tfrac{1}{V^*}V_\varepsilon) = \log_2 \frac{E^N(\frac{1}{V^*}V_\varepsilon)}{E^{2N}(\frac{1}{V^*}V_\varepsilon)}.$$

We take the computed ε–uniform orders of convergence to be

$$p^*(U_\varepsilon) = \min_N p^N(U_\varepsilon), \quad p^*(\tfrac{1}{V^*}V_\varepsilon) = \min_N p^N(\tfrac{1}{V^*}V_\varepsilon).$$

Corresponding to these values of p^* we calculate the quantities

$$C_{p^*}^N(U_\varepsilon) = \frac{E^N(U_\varepsilon)N^{p^*}}{1-2^{-p^*}} \quad C_{p^*}^N(\tfrac{1}{V^*}V_\varepsilon) = \frac{E^N(\frac{1}{V^*}V_\varepsilon)N^{p^*}}{1-2^{-p^*}}$$

and we take the computed ε–uniform error constants to be

$$C_{p^*}^*(U_\varepsilon) = \max_N C_{p^*}^N(U_\varepsilon) \quad C_{p^*}^*(\tfrac{1}{V^*}V_\varepsilon) = \max_N C_{p^*}^N(\tfrac{1}{V^*}V_\varepsilon).$$

The computed orders of convergence and the error constants have analogous expressions for the scaled derivatives of the velocity components.

	$\beta = 0.5$				$\beta = 1.0$				$\beta = 1.5$		
$\varepsilon \backslash N$	32	64	128	$\varepsilon \backslash N$	32	64	128	$\varepsilon \backslash N$	32	64	128
2^{-0}	0.77	0.87	0.87	2^{-0}	0.98	0.99	0.99	2^{-0}	0.90	0.95	0.97
2^{-2}	0.86	0.93	0.96	2^{-2}	0.92	0.96	0.98	2^{-2}	0.93	0.88	0.94
2^{-4}	0.92	0.96	0.98	2^{-4}	1.06	1.03	1.02	2^{-4}	0.97	0.83	0.86
2^{-6}	0.90	0.98	0.99	2^{-6}	1.40	1.06	1.03	2^{-6}	1.14	1.13	1.48
2^{-8}	0.92	0.96	0.98	2^{-8}	1.10	0.97	0.96	2^{-8}	1.14	1.05	1.21
2^{-10}	0.90	0.96	0.98	2^{-10}	1.10	0.97	0.96	2^{-10}	1.14	1.05	1.21
2^{-12}	0.88	0.96	0.98	2^{-12}	1.10	0.97	0.96	2^{-12}	1.14	1.05	1.21
2^{-14}	0.87	0.96	0.98	2^{-14}	1.11	0.97	0.96	2^{-14}	1.14	1.05	1.21
2^{-16}	0.87	0.96	0.98	2^{-16}	1.11	0.97	0.96	2^{-16}	1.14	1.05	1.21
2^{-18}	0.87	0.96	0.98	2^{-18}	1.11	0.97	0.96	2^{-18}	1.14	1.05	1.21
2^{-20}	0.86	0.96	0.98	2^{-20}	1.11	0.97	0.96	2^{-20}	1.14	1.05	1.21
p^N	0.92	0.96	0.98	p^N	1.15	0.97	0.96	p^N_{comp}	1.14	1.05	1.21
$C_{0.92}$	0.31	0.31	0.30	$C_{0.96}$	0.16	0.14	0.14	$C_{1.05}$	7.17	6.72	6.72

Table 4.4: Computed orders of convergence $p_\varepsilon^N(U_\varepsilon)$, $p^N(U_\varepsilon)$ and error constant $C_{p^*}^N$ generated by $(A_\varepsilon^{\mathbf{N}})$ applied to problem (P_ε) for various values of ε, N and β.

	$\beta = 0.5$				$\beta = 1.0$				$\beta = 1.5$		
$\varepsilon \backslash N$	32	64	128	$\varepsilon \backslash N$	32	64	128	$\varepsilon \backslash N$	32	64	128
2^{-0}	0.93	0.91	0.94	2^{-0}	0.90	0.89	0.89	2^{-0}	0.93	0.97	0.98
2^{-2}	0.98	0.98	0.99	2^{-2}	0.88	0.87	0.87	2^{-2}	0.88	0.94	0.97
2^{-4}	1.04	1.00	1.00	2^{-4}	0.84	0.83	0.82	2^{-4}	0.77	0.89	0.95
2^{-6}	0.90	1.01	1.00	2^{-6}	0.38	0.80	0.80	2^{-6}	0.81	0.49	0.61
2^{-8}	1.01	0.95	0.94	2^{-8}	0.49	0.54	0.58	2^{-8}	1.25	1.27	1.03
2^{-10}	1.04	0.98	0.97	2^{-10}	0.49	0.54	0.58	2^{-10}	1.11	1.11	1.11
2^{-12}	1.07	1.00	0.98	2^{-12}	0.49	0.54	0.58	2^{-12}	1.06	1.05	1.05
2^{-14}	1.08	1.01	0.99	2^{-14}	0.49	0.54	0.58	2^{-14}	1.04	1.03	1.02
2^{-16}	1.09	1.01	1.00	2^{-16}	0.49	0.54	0.58	2^{-16}	1.03	1.02	1.01
2^{-18}	1.09	1.02	1.00	2^{-18}	0.49	0.54	0.58	2^{-18}	1.02	1.01	1.01
2^{-20}	1.10	1.02	1.00	2^{-20}	0.49	0.54	0.58	2^{-20}	1.02	1.01	1.01
p^N_{comp}	0.98	0.98	0.99	p^N_{comp}	0.88	0.87	0.85	p^N_{comp}	0.91	0.89	0.94
$C_{0.98}$	1.36	1.36	1.36	$C_{0.85}$	0.36	0.36	0.35	$C_{0.89}$	3.40	3.35	3.35

Table 4.5: Computed orders of convergence $p_\varepsilon^N(\frac{1}{V^*}V_\varepsilon)$, $p^N(\frac{1}{V^*}V_\varepsilon)$ and error constants $C_{p^*}^N$ generated by $(A_\varepsilon^{\mathbf{N}})$ applied to problem (P_ε) for various values of ε, N and β.

The computed orders of convergence p_ε^N and p^N and the constants of convergence $C_{p^*}^N$ for U_ε and $\frac{1}{V^*}V_\varepsilon$ are given in Tables 4.4 and 4.5, respectively, for various values of ε, N and β. The results in Tables 4.2 - 4.5 suggest that $(A_\varepsilon^{\mathbf{N}})$ is an ε–uniform numerical method of order at least 0.9 for U_ε and 0.8 for $\frac{1}{V^*}V_\varepsilon$ for $\beta = 0.5$, 1.0 and 1.5.

Reading from the bottom row of Tables 4.4 and 4.5 we obtain the computed error

bounds for U_ε and $\frac{1}{V^*}V_\varepsilon$

$$\begin{aligned} \beta = 0.5 \quad &\|U_\varepsilon - u_\varepsilon\|_{\Omega_\varepsilon^N} \leq 0.31N^{-0.92} \\ \beta = 1.0 \quad &\|U_\varepsilon - u_\varepsilon\|_{\Omega_\varepsilon^N} \leq 0.16N^{-0.96} \\ \beta = 1.5 \quad &\|U_\varepsilon - u_\varepsilon\|_{\Omega_\varepsilon^N} \leq 7.17N^{-1.05} \end{aligned} \tag{4.2}$$

$$\begin{aligned} \beta = 0.5 \quad &\tfrac{1}{V_*}\|V_\varepsilon - v_\varepsilon\|_{\Omega_\varepsilon^N \setminus \Gamma_L} \leq 1.36N^{-0.91} \\ \beta = 1.0 \quad &\tfrac{1}{V^*}\|V_\varepsilon - v_\varepsilon\|_{\Omega_\varepsilon^N \setminus \Gamma_L} \leq 0.36N^{-0.85} \\ \beta = 1.5 \quad &\tfrac{1}{V^*}\|V_\varepsilon - v_\varepsilon\|_{\Omega_\varepsilon^N \setminus \Gamma_L} \leq 3.40N^{-0.80}. \end{aligned} \tag{4.3}$$

The results shown in this chapter are all for $\Omega = (0.1 + \gamma(\beta), 1.1 + \gamma(\beta)) \times (0,1)$. It is worth noting that as β tends to 1, the effect of the leading edge singularity lessens. Thus, we can shift Ω_ε^N closer to the leading edge. For stagnation flow ($\beta = 1$) we can have $\Omega = (0,1) \times (0,1)$, see Figure 4-9.

Graphs of the computed scaled discrete derivatives $\sqrt{\varepsilon}D_y^- U_\varepsilon$, $D_y^- V_\varepsilon$ and $D_x^- V_\varepsilon$ generated by (A_ε^N) are given in Figures 4-6, 4-7 and 4-8, respectively, for $N = 32$, $\varepsilon = 2^{-12}$ and β=0.5, 1.0 and 1.5. Graphs of $\sqrt{\varepsilon}D_y^- U_\varepsilon$, and $D_y^- V_\varepsilon$ in Figures 4-6 and 4-7 show a region of rapid change along the wedge for various β. Although there was no visible boundary layer for $\frac{1}{V^*}V_\varepsilon$ in Figure 4-5, there is a visible layer for $D_y^- V_\varepsilon$ along the wedge.
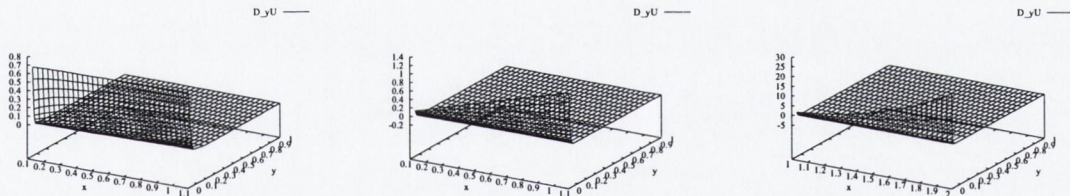
Figure 4-6: Graphs of $\sqrt{\varepsilon}D_y^- U_\varepsilon$ for $\varepsilon = 2^{-12}$, N=32 and $\beta = 0.5, 1.0, 1.5$.
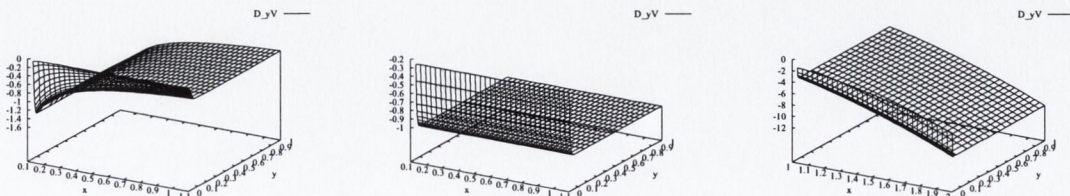
Figure 4-7: Graphs of $D_y^- V_\varepsilon$ for $\varepsilon = 2^{-12}$, N=32 and $\beta = 0.5, 1.0, 1.5$.

Figure 4-8 shows $D_x^- V_\varepsilon$ to be a smooth function for both $\beta = 0.5$ and 1.5.
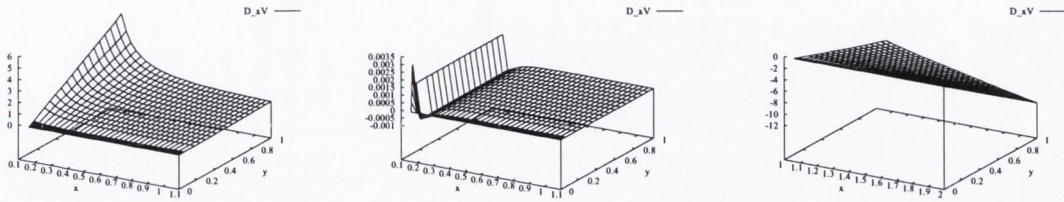
Figure 4-8: Graphs of $\frac{1}{V^*} D_x^- V_\varepsilon$ for $\varepsilon = 2^{-12}$, $N{=}32$ and $\beta = 0.5, 1.0, 1.5$.
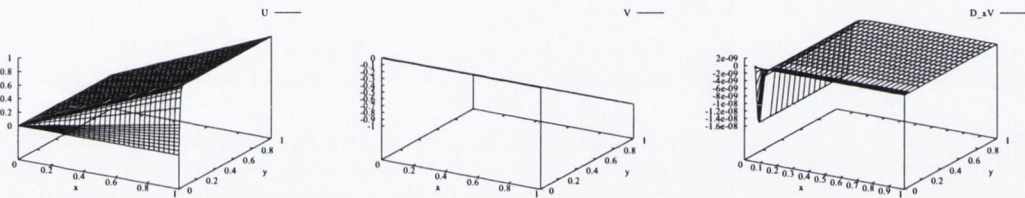
Figure 4-9: Graphs of U_ε, $\frac{1}{V^*} V_\varepsilon$ and $\frac{1}{V^*} D_x^- V_\varepsilon$ for $\varepsilon = 2^{-12}$, $N{=}32$ and $\beta = 1.0$ on $\Omega = (0,1) \times (0,1)$.

In the graph of $\frac{1}{V^*} D_x^- V_\varepsilon$ for $\beta = 1.0$ in Figure 4-8 we see a very non-physical jump along the left hand edge of the region. This is a unique case as $\frac{\partial v_\varepsilon}{\partial x} = 0$ for all x.

$\varepsilon \backslash N$	$\beta = 0.5$				$\varepsilon \backslash N$	$\beta = 1.0$			
	32	64	128	256		32	64	128	256
2^{-0}	1.21e-02	5.98e-03	2.66e-03	9.07e-04	2^{-0}	1.75e-02	8.19e-03	3.51e-03	1.17e-03
2^{-2}	2.10e-02	9.83e-03	4.22e-03	1.44e-03	2^{-2}	3.50e-02	1.65e-02	7.11e-03	2.37e-03
2^{-4}	4.18e-02	1.96e-02	8.43e-03	2.82e-03	2^{-4}	6.67e-02	3.24e-02	1.40e-02	4.70e-03
2^{-6}	6.96e-02	3.90e-02	1.68e-02	5.61e-03	2^{-6}	1.05e-01	6.23e-02	2.78e-02	9.36e-03
2^{-8}	6.66e-02	3.76e-02	1.84e-02	6.80e-03	2^{-8}	1.00e-01	6.00e-02	3.03e-02	1.13e-02
2^{-10}	6.66e-02	3.76e-02	1.84e-02	6.80e-03	2^{-10}	1.00e-01	6.00e-02	3.03e-02	1.13e-02
2^{-12}	6.66e-02	3.76e-02	1.84e-02	6.80e-03	2^{-12}	1.00e-01	6.00e-02	3.03e-02	1.13e-02
2^{-14}	6.66e-02	3.76e-02	1.84e-02	6.80e-03	2^{-14}	1.00e-01	6.00e-02	3.03e-02	1.13e-02
2^{-16}	6.66e-02	3.76e-02	1.84e-02	6.80e-03	2^{-16}	1.00e-01	6.00e-02	3.03e-02	1.13e-02
2^{-18}	6.66e-02	3.76e-02	1.84e-02	6.80e-03	2^{-18}	1.00e-01	6.00e-02	3.03e-02	1.13e-02
2^{-20}	6.66e-02	3.76e-02	1.84e-02	6.80e-03	2^{-20}	1.00e-01	6.00e-02	3.03e-02	1.13e-02
E^{N}	6.96e-02	3.90e-02	1.84e-02	6.80e-03	E^{N}	1.05e-01	6.23e-02	3.03e-02	1.13e-02

$\varepsilon \backslash N$	$\beta = 1.5$			
	32	64	128	256
2^{-0}	1.61e+00	7.77e-01	3.37e-01	1.13e-01
2^{-2}	2.77e+00	1.46e+00	6.47e-01	2.18e-01
2^{-4}	3.83e+00	2.53e+00	1.22e+00	4.22e-01
2^{-6}	3.83e+00	3.14e+00	1.94e+00	8.07e-01
2^{-8}	3.78e+00	3.04e+00	1.82e+00	7.30e-01
2^{-10}	3.78e+00	3.04e+00	1.82e+00	7.30e-01
2^{-12}	3.78e+00	3.04e+00	1.82e+00	7.30e-01
2^{-14}	3.78e+00	3.04e+00	1.82e+00	7.30e-01
2^{-16}	3.78e+00	3.04e+00	1.82e+00	7.30e-01
2^{-18}	3.78e+00	3.04e+00	1.82e+00	7.30e-01
2^{-20}	3.78e+00	3.04e+00	1.82e+00	7.30e-01
E^{N}	3.83e+00	3.14e+00	1.94e+00	8.07e-01

Table 4.6: Computed maximum errors $E_{\varepsilon}^{N}(\sqrt{\varepsilon}D_{y}^{-}U_{\varepsilon})$ generated by $(A_{\varepsilon}^{\mathbf{N}})$ applied to problem (P_{ε}) for various values of ε, N and β.

We also approximate the scaled partial derivatives $\frac{\partial u_{\varepsilon}}{\partial x}$, $\sqrt{\varepsilon}\frac{\partial u_{\varepsilon}}{\partial y}$, $\frac{1}{V^{*}}\frac{\partial v_{\varepsilon}}{\partial x}$ and $\frac{\partial v_{\varepsilon}}{\partial y}$ by the corresponding scaled discrete derivatives $D_{x}^{-}U_{\varepsilon}$, $\sqrt{\varepsilon}D_{y}^{-}U_{\varepsilon}$, $\frac{1}{V^{*}}D_{x}^{-}V_{\varepsilon}$ and $D_{y}^{-}V_{\varepsilon}$. From the definition of the algorithm $(A_{\varepsilon}^{\mathbf{N}})$ we know that $D_{x}^{-}U_{\varepsilon} = -D_{y}^{-}V_{\varepsilon}$. Since the scaled derivatives of the exact solution $\mathbf{u}_{\varepsilon}$ are unknown, we replace them in the expression for the error by the appropriate scaled derivatives of the computed solution $\mathbf{U}_{\varepsilon}^{512}$, generated by method $(A_{\varepsilon}^{\mathbf{N}})$ on the finest available mesh. The resulting computed maximum pointwise errors of the computed scaled discrete derivatives $\sqrt{\varepsilon}D_{y}U_{\varepsilon}$, $D_{y}^{-}V_{\varepsilon}$ and $\frac{1}{V^{*}}D_{x}^{-}V_{\varepsilon}$ are given in the Tables 4.6, 4.7 and 4.8, respectively.

	$\beta = 0.5$					$\beta = 1.0$			
$\varepsilon\backslash N$	32	64	128	256	$\varepsilon\backslash N$	32	64	128	256
2^{-0}	1.07e-01	5.92e-02	2.79e-02	9.73e-03	2^{-0}	1.84e-02	9.17e-03	4.57e-03	1.96e-03
2^{-2}	1.20e-01	6.42e-02	2.96e-02	1.03e-02	2^{-2}	3.35e-02	1.65e-02	7.39e-03	2.73e-03
2^{-4}	1.12e-01	6.05e-02	2.81e-02	9.75e-03	2^{-4}	6.04e-02	3.10e-02	1.39e-02	4.72e-03
2^{-6}	1.35e-01	7.37e-02	3.16e-02	1.05e-02	2^{-6}	8.92e-02	5.65e-02	2.66e-02	9.27e-03
2^{-8}	1.29e-01	7.08e-02	3.47e-02	1.28e-02	2^{-8}	8.55e-02	5.42e-02	2.86e-02	1.10e-02
2^{-10}	1.29e-01	7.08e-02	3.47e-02	1.28e-02	2^{-10}	8.55e-02	5.42e-02	2.86e-02	1.10e-02
2^{-12}	1.29e-01	7.08e-02	3.47e-02	1.28e-02	2^{-12}	8.55e-02	5.42e-02	2.86e-02	1.10e-02
2^{-14}	1.29e-01	7.08e-02	3.47e-02	1.28e-02	2^{-14}	8.55e-02	5.42e-02	2.86e-02	1.10e-02
2^{-16}	1.29e-01	7.08e-02	3.47e-02	1.28e-02	2^{-16}	8.55e-02	5.42e-02	2.86e-02	1.10e-02
2^{-18}	1.29e-01	7.08e-02	3.47e-02	1.28e-02	2^{-18}	8.55e-02	5.42e-02	2.86e-02	1.10e-02
2^{-20}	1.29e-01	7.08e-02	3.47e-02	1.28e-02	2^{-20}	8.55e-02	5.42e-02	2.86e-02	1.10e-02
E^N	1.35e-01	7.37e-02	3.47e-02	1.28e-02	E^N	8.92e-02	5.65e-02	2.86e-02	1.10e-02

	$\beta = 1.5$			
$\varepsilon\backslash N$	32	64	128	256
2^{-0}	1.74e-01	8.13e-02	3.49e-02	1.17e-02
2^{-2}	2.00e-01	1.04e-01	4.68e-02	1.60e-02
2^{-4}	3.18e-01	1.87e-01	8.93e-02	3.13e-02
2^{-6}	3.43e-01	2.48e-01	1.45e-01	5.98e-02
2^{-8}	3.37e-01	2.40e-01	1.35e-01	5.37e-02
2^{-10}	3.37e-01	2.40e-01	1.35e-01	5.37e-02
2^{-12}	3.37e-01	2.40e-01	1.35e-01	5.37e-02
2^{-14}	3.37e-01	2.40e-01	1.35e-01	5.37e-02
2^{-16}	3.37e-01	2.40e-01	1.35e-01	5.37e-02
2^{-18}	3.37e-01	2.40e-01	1.35e-01	5.37e-02
2^{-20}	3.37e-01	2.40e-01	1.35e-01	5.37e-02
E^N	3.43e-01	2.48e-01	1.45e-01	5.98e-02

Table 4.7: Computed maximum errors $E_\varepsilon^N(D_y^- V_\varepsilon)$ generated by $(A_\varepsilon^{\mathbf{N}})$ applied to problem (P_ε) for various values of ε, N and β.

The computed maximum errors in Tables 4.6 and 4.7 for $\sqrt{\varepsilon} D_y^- V_\varepsilon$ and $D_y^- V_\varepsilon$, respectively, stabilise to a fixed value after $\varepsilon = 2^{-10}$. This suggests that the method is independent of ε for $\sqrt{\varepsilon} D_y^- V_\varepsilon$ and $D_y^- V_\varepsilon$ for all N and β. Thus, Tables 4.6 and 4.7 suggest that the method is ε –uniform for $\sqrt{\varepsilon} D_y U_\varepsilon$ and $D_y^- V_\varepsilon$ for $\beta = 0.5$, 1.0 and 1.5. The maximum error occurs when $\varepsilon = 2^{-6}$ and 2^{-8} for all N and β for $\sqrt{\varepsilon} D_y^- U_\varepsilon$ and $D_y^- V_\varepsilon$.

| | $\beta = 0.5$ | | | |
$\varepsilon\backslash N$	32	64	128	256
2^{-0}	1.30e+00	6.99e-01	3.39e-01	1.26e-01
2^{-2}	7.37e-01	4.80e-01	2.70e-01	1.19e-01
2^{-4}	6.36e-01	4.29e-01	2.37e-01	1.01e-01
2^{-6}	5.89e-01	4.07e-01	2.30e-01	9.66e-02
2^{-8}	5.44e-01	3.64e-01	2.03e-01	8.60e-02
2^{-10}	5.24e-01	3.44e-01	1.86e-01	7.71e-02
2^{-12}	5.15e-01	3.35e-01	1.78e-01	7.28e-02
2^{-14}	5.10e-01	3.30e-01	1.73e-01	7.06e-02
2^{-16}	5.08e-01	3.28e-01	1.71e-01	6.96e-02
2^{-18}	5.07e-01	3.26e-01	1.70e-01	6.90e-02
2^{-20}	5.06e-01	3.26e-01	1.70e-01	6.88e-02
E^N	1.30e+00	6.99e-01	3.39e-01	1.26e-01

| | $\beta = 1.0$ | | | |
$\varepsilon\backslash N$	32	64	128	256
2^{-0}	4.68e-02	8.21e-02	1.18e-01	1.07e-01
2^{-2}	4.60e-02	7.98e-02	1.13e-01	1.06e-01
2^{-4}	3.72e-02	6.85e-02	9.92e-02	1.03e-01
2^{-6}	2.67e-02	6.03e-02	9.12e-02	9.78e-02
2^{-8}	1.28e-02	2.98e-02	5.19e-02	6.32e-02
2^{-10}	6.27e-03	1.46e-02	2.54e-02	3.09e-02
2^{-12}	3.10e-03	7.22e-03	1.26e-02	1.53e-02
2^{-14}	1.54e-03	3.59e-03	6.25e-03	7.62e-03
2^{-16}	7.69e-04	1.79e-03	3.12e-03	3.80e-03
2^{-18}	3.84e-04	8.95e-04	1.56e-03	1.90e-03
2^{-20}	1.92e-04	4.47e-04	7.78e-04	9.48e-04
E^N	4.68e-02	8.21e-02	1.18e-01	1.07e-01

| | $\beta = 1.5$ | | | |
$\varepsilon\backslash N$	32	64	128	256
2^{-0}	7.78e-02	7.76e-02	6.83e-02	4.64e-02
2^{-2}	6.26e-02	6.31e-02	5.91e-02	4.44e-02
2^{-4}	5.48e-02	5.63e-02	5.48e-02	4.36e-02
2^{-6}	4.67e-02	4.59e-02	4.96e-02	4.54e-02
2^{-8}	4.14e-02	3.27e-02	2.89e-02	2.41e-02
2^{-10}	3.88e-02	2.62e-02	1.90e-02	1.37e-02
2^{-12}	3.75e-02	2.30e-02	1.42e-02	8.45e-03
2^{-14}	3.68e-02	2.14e-02	1.17e-02	5.86e-03
2^{-16}	3.65e-02	2.06e-02	1.05e-02	4.57e-03
2^{-18}	3.63e-02	2.02e-02	9.90e-03	3.92e-03
2^{-20}	3.63e-02	2.00e-02	9.60e-03	3.60e-03
E^N	7.78e-02	7.76e-02	6.83e-02	4.64e-02

Table 4.8: Computed maximum errors $E_\varepsilon^N(\frac{1}{V^*}D_x^- V_\varepsilon)$ generated by $(A_\varepsilon^{\mathbf{N}})$ applied to problem (P_ε) for various values of ε, N and β.

In Table 4.8 the computed maximum errors decrease as ε decreases for $\frac{1}{V^*}D_x^- V_\varepsilon$. The largest computed maximum error occurs at $\varepsilon = 1$ for all N and β. For $\beta = 0.5$ and 1.5 the computed maximum errors decrease as the number of mesh points, N, increases. For $\beta = 1.0$ the computed maximum errors increase as the number of mesh points, N, increases. For $\beta = 0.5$ we observe that the errors stabilise to a fixed value as ε decreases for some N.

The orders of convergence and the computed error constants for $\sqrt{\varepsilon}D_y^- U_\varepsilon$, $D_y^- V_\varepsilon$ and $\frac{1}{V^*}D_x^- V_\varepsilon$ are given in Tables 4.9, 4.10 and 4.11, respectively, for various values of ε, N and β.

The results in Tables 4.6-4.7 and 4.9-4.10 suggest that $(A_\varepsilon^{\mathbf{N}})$ is an ε-uniform numerical method of order of at least 0.71 for $\sqrt{\varepsilon}D_y^- U_\varepsilon$ and $D_y^- V_\varepsilon$ for $N \geq 64$ and $\beta = 0.5$, $\beta = 1.0$ and $\beta = 1.5$.

$\varepsilon\backslash N$	$\beta=0.5$ 32	64	128	$\varepsilon\backslash N$	$\beta=1.0$ 32	64	128	$\varepsilon\backslash N$	$\beta=1.5$ 32	64	128
2^{-0}	0.88	0.92	0.96	2^{-0}	1.00	1.00	1.00	2^{-0}	0.95	0.99	0.99
2^{-2}	1.00	0.98	0.94	2^{-2}	0.99	1.00	1.00	2^{-2}	0.85	0.95	0.99
2^{-4}	0.99	1.00	0.98	2^{-4}	0.95	0.98	1.00	2^{-4}	0.57	0.85	0.95
2^{-6}	0.50	0.99	1.00	2^{-6}	0.42	0.95	0.98	2^{-6}	0.12	0.36	0.58
2^{-8}	0.63	0.73	0.78	2^{-8}	0.56	0.69	0.76	2^{-8}	0.12	0.43	0.65
2^{-10}	0.63	0.73	0.78	2^{-10}	0.56	0.69	0.76	2^{-10}	0.12	0.43	0.65
2^{-12}	0.63	0.73	0.78	2^{-12}	0.56	0.69	0.76	2^{-12}	0.12	0.43	0.65
2^{-14}	0.63	0.73	0.78	2^{-14}	0.56	0.69	0.76	2^{-14}	0.12	0.43	0.65
2^{-16}	0.63	0.73	0.78	2^{-16}	0.56	0.69	0.76	2^{-16}	0.12	0.43	0.65
2^{-18}	0.63	0.73	0.78	2^{-18}	0.56	0.69	0.76	2^{-18}	0.12	0.43	0.65
2^{-20}	0.63	0.73	0.78	2^{-20}	0.56	0.69	0.76	2^{-20}	0.12	0.43	0.65
p^N	0.50	0.94	0.78	p^N	0.42	0.90	0.76	p^N_{comp}	0.49	0.36	0.58
$C_{0.50}$	0.61	0.61	0.45	$C_{0.42}$	0.81	0.81	0.57	$C_{0.36}$	34.33	31.33	31.33

Table 4.9: Computed orders of convergence $p_\varepsilon^N(\sqrt{\varepsilon}D_y^- U_\varepsilon)$, $p^N(\sqrt{\varepsilon}D_y^- U_\varepsilon)$ and error constants $C_{p^*}^N$ generated by (A_ε^N) applied to problem (P_ε) for various values of ε, N and β.

$\varepsilon\backslash N$	$\beta=0.5$ 32	64	128	$\varepsilon\backslash N$	$\beta=1.0$ 32	64	128	$\varepsilon\backslash N$	$\beta=1.5$ 32	64	128
2^{-0}	0.81	0.90	0.95	2^{-0}	0.97	0.79	0.48	2^{-0}	0.99	1.00	0.99
2^{-2}	0.85	0.92	0.96	2^{-2}	0.95	0.97	0.79	2^{-2}	0.86	0.94	0.97
2^{-4}	0.84	0.91	0.95	2^{-4}	0.87	0.95	0.97	2^{-4}	0.70	0.86	0.94
2^{-6}	0.60	1.00	1.00	2^{-6}	0.30	0.87	0.95	2^{-6}	0.30	0.45	0.58
2^{-8}	0.81	0.73	0.77	2^{-8}	0.47	0.62	0.71	2^{-8}	0.30	0.52	0.66
2^{-10}	0.81	0.73	0.77	2^{-10}	0.47	0.62	0.71	2^{-10}	0.30	0.52	0.66
2^{-12}	0.81	0.73	0.77	2^{-12}	0.47	0.62	0.71	2^{-12}	0.30	0.52	0.66
2^{-14}	0.81	0.73	0.77	2^{-14}	0.47	0.62	0.71	2^{-14}	0.30	0.52	0.66
2^{-16}	0.81	0.73	0.77	2^{-16}	0.47	0.62	0.71	2^{-16}	0.30	0.52	0.66
2^{-18}	0.81	0.73	0.77	2^{-18}	0.47	0.62	0.71	2^{-18}	0.30	0.52	0.66
2^{-20}	0.81	0.73	0.77	2^{-20}	0.47	0.62	0.71	2^{-20}	0.30	0.52	0.66
p^N	0.69	0.94	0.77	p^N	0.30	0.86	0.71	p^N_{comp}	0.54	0.45	0.58
$C_{0.69}$	1.96	1.96	1.64	$C_{0.30}$	0.61	0.61	0.41	$C_{0.45}$	3.12	2.93	2.93

Table 4.10: Computed orders of convergence $p_\varepsilon^N(D_y^- V_\varepsilon)$, $p^N(D_y^- V_\varepsilon)$ and error constant $C_{p^*}^N$ generated by (A_ε^N) applied to problem (P_ε) for various values of ε, N and β.

From the orders of convergence in Table 4.11 for $\frac{1}{V^*}D_x^- V_\varepsilon$ we cannot say definitively that the method (A_ε^N) is ε–uniform for $\frac{1}{V^*}D_x^- V_\varepsilon$ for all β; we must look at each value of β separately. From Table 4.11 the computed order of convergence is at least 0.69 for $\frac{1}{V^*}D_x^- V_\varepsilon$ with $\beta=0.5$. We do not need to consider the case when $\beta=1.0$. For $\beta=1.5$ the stabilising nature of the orders of convergence is at least 0.14. In Table 4.11 for β we see very low orders of convergence for ε between 1.0 and 2^{-10}.

	$\beta = 0.5$				$\beta = 1.0$				$\beta = 1.5$		
$\varepsilon \backslash N$	32	64	128	$\varepsilon \backslash N$	32	64	128	$\varepsilon \backslash N$	32	64	128
2^{-0}	0.75	0.77	0.76	2^{-0}	-0.73	-0.43	-0.07	2^{-0}	-0.03	0.06	0.18
2^{-2}	0.57	0.59	0.66	2^{-2}	-0.70	-0.44	-0.14	2^{-2}	-0.08	-0.02	0.06
2^{-4}	0.52	0.65	0.70	2^{-4}	-0.76	-0.49	-0.29	2^{-4}	-0.14	-0.08	-0.00
2^{-6}	0.46	0.64	0.71	2^{-6}	-1.05	-0.56	-0.33	2^{-6}	-0.13	-0.26	-0.21
2^{-8}	0.53	0.66	0.68	2^{-8}	-1.07	-0.76	-0.53	2^{-8}	0.16	-0.03	-0.11
2^{-10}	0.57	0.72	0.70	2^{-10}	-1.08	-0.76	-0.53	2^{-10}	0.40	0.22	0.06
2^{-12}	0.58	0.74	0.71	2^{-12}	-1.08	-0.76	-0.53	2^{-12}	0.56	0.45	0.27
2^{-14}	0.59	0.76	0.72	2^{-14}	-1.08	-0.76	-0.53	2^{-14}	0.65	0.62	0.49
2^{-16}	0.60	0.77	0.72	2^{-16}	-1.08	-0.76	-0.53	2^{-16}	0.71	0.73	0.66
2^{-18}	0.60	0.77	0.72	2^{-18}	-1.08	-0.76	-0.53	2^{-18}	0.73	0.79	0.78
2^{-20}	0.60	0.77	0.72	2^{-20}	-1.08	-0.76	-0.53	2^{-20}	0.75	0.82	0.85
p_{comp}^N	0.75	0.77	0.76	p_{comp}^N	-0.73	-0.43	-0.07	p_{comp}^N	-0.03	0.06	0.18
$C_{0.75}$	20.26	20.26	19.99	$C_{-0.73}$	-0.01	-0.01	-0.00	$C_{-0.03}$	-2.09	-2.09	-1.96

Table 4.11: Computed orders of convergence $p_\varepsilon^N(\frac{1}{V^*}D_x^-V_\varepsilon)$, $p^N(\frac{1}{V^*}D_x^-V_\varepsilon)$ and error constant $C_{p^*}^N$ generated by (A_ε^N) applied to problem (P_ε) for various values of ε, N and β.

From the data in Tables 4.9 and 4.10 we obtain the computed error bounds for $\sqrt{\varepsilon}D_y^-U_\varepsilon$ and $D_y^-V_\varepsilon$

$$
\begin{aligned}
\beta = 0.5 \quad & \sqrt{\varepsilon}\|D_y^-U_\varepsilon - \tfrac{\partial u_\varepsilon}{\partial y}\|_{\Omega_\varepsilon^N} && \leq 0.61 N^{-0.50} \\
\beta = 1.0 \quad & \sqrt{\varepsilon}\|D_y^-U_\varepsilon - \tfrac{\partial u_\varepsilon}{\partial y}\|_{\Omega_\varepsilon^N} && \leq 0.81 N^{-0.42} \\
\beta = 1.5 \quad & \sqrt{\varepsilon}\|D_y^-U_\varepsilon - \tfrac{\partial u_\varepsilon}{\partial y}\|_{\Omega_\varepsilon^N} && \leq 34.33 N^{-0.36}
\end{aligned}
\tag{4.4}
$$

$$
\begin{aligned}
\beta = 0.5 \quad & \|D_y^-V_\varepsilon - \tfrac{\partial v_\varepsilon}{\partial y}\|_{\Omega_\varepsilon^N} && \leq 1.96 N^{-0.69} \\
\beta = 1.0 \quad & \|D_y^-V_\varepsilon - \tfrac{\partial v_\varepsilon}{\partial y}\|_{\Omega_\varepsilon^N} && \leq 0.61 N^{-0.30} \\
\beta = 1.5 \quad & \|D_y^-V_\varepsilon - \tfrac{\partial v_\varepsilon}{\partial y}\|_{\Omega_\varepsilon^N} && \leq 3.12 N^{-0.45}.
\end{aligned}
\tag{4.5}
$$

4.5 Error analysis based on the computed Falkner–Skan solution

As there is no theory to say that the method will be ε–uniform the error analysis based on the computed Falkner–Skan solution in this section and the results from the previous section will give two independently calculated bounds that suggest that the direct numerical method (A_ε^N) is ε–uniform for all β.

In this section we compute ε–uniform maximum pointwise differences in the approximations generated by the direct numerical method described in Section 4.2.

For this case, we compare the parameter uniform maximum pointwise differences in the approximations generated by the direct numerical method of the previous section, with the corresponding values of $\mathbf{U}_{FS}^{8192}$ generated by the method defined in Chapter 3. The scaled maximum pointwise differences $||U_\varepsilon - \overline{U_{FS}}^{8192}||_{\overline{\Omega}_\varepsilon^N}$ and $\frac{1}{V^*}||V_\varepsilon - \overline{V_{FS}}^{8192}||_{\overline{\Omega}_\varepsilon^N \backslash \Gamma_L}$ for various values of N, ε and β are given in Tables 4.12 and 4.13, respectively.

In Tables 4.12 and 4.13 we see that the computed maximum differences for the velocity components decrease as the number of mesh points, N, increases.

In Table 4.12 the largest maximum differences of $||U_\varepsilon - \overline{U_{FS}}^{8192}||_{\overline{\Omega}_\varepsilon^N}$ occur between $2^{-6} \leq \varepsilon \leq 2^{-10}$ for all N and β. The maximum differences stabilise to a fixed value when $\varepsilon \leq 2^{-10}$ for any N or β.

In Table 4.13 the largest maximum differences of $\frac{1}{V^*}||V_\varepsilon - \overline{V_{FS}}^{8192}||_{\overline{\Omega}_\varepsilon^N \backslash \Gamma_L}$ occur for $\varepsilon \geq 2^{-6}$ for all N and β. We see that the computed pointwise maximum errors for $\frac{1}{V^*}V_\varepsilon$ decrease as ε decreases for all $\varepsilon \leq 2^{-8}$, N and β considered.

Thus, Tables 4.12 and 4.13 indicate that the maximum differences are independent of ε for all β and N.

In a similar fashion to Tables 4.2 and 4.3 of the maximum pointwise errors of velocity components, Tables 4.12 and 4.13 suggest that the method is ε–uniform for U_ε and $\frac{1}{V^*}V_\varepsilon$ for all β considered.

| $\beta = 0.5$ | | | | | | $\beta = 1.0$ | | | | |
$\varepsilon\backslash N$	32	64	128	256	512	$\varepsilon\backslash N$	32	64	128	256	512
2^{-0}	8.93e-04	5.15e-04	2.86e-04	1.55e-04	8.49e-05	2^{-0}	4.15e-04	2.02e-04	9.39e-05	3.95e-05	1.22e-05
2^{-2}	5.61e-03	3.00e-03	1.55e-03	7.85e-04	3.94e-04	2^{-2}	1.02e-03	5.22e-04	2.57e-04	1.20e-04	5.03e-05
2^{-4}	1.04e-02	5.41e-03	2.75e-03	1.38e-03	6.87e-04	2^{-4}	2.06e-03	9.93e-04	4.80e-04	2.30e-04	1.06e-04
2^{-6}	1.24e-02	6.37e-03	3.21e-03	1.61e-03	7.98e-04	2^{-6}	3.77e-03	2.07e-03	9.97e-04	4.82e-04	2.31e-04
2^{-8}	1.24e-02	6.44e-03	3.28e-03	1.65e-03	8.29e-04	2^{-8}	3.77e-03	2.16e-03	1.22e-03	6.79e-04	3.71e-04
2^{-10}	1.23e-02	6.44e-03	3.28e-03	1.65e-03	8.29e-04	2^{-10}	3.74e-03	2.16e-03	1.22e-03	6.79e-04	3.71e-04
2^{-12}	1.22e-02	6.43e-03	3.28e-03	1.65e-03	8.29e-04	2^{-12}	3.71e-03	2.16e-03	1.22e-03	6.79e-04	3.71e-04
2^{-14}	1.22e-02	6.43e-03	3.28e-03	1.65e-03	8.29e-04	2^{-14}	3.69e-03	2.16e-03	1.22e-03	6.79e-04	3.71e-04
2^{-16}	1.22e-02	6.43e-03	3.28e-03	1.65e-03	8.29e-04	2^{-16}	3.68e-03	2.16e-03	1.22e-03	6.79e-04	3.71e-04
2^{-18}	1.21e-02	6.43e-03	3.28e-03	1.65e-03	8.29e-04	2^{-18}	3.68e-03	2.15e-03	1.22e-03	6.79e-04	3.71e-04
2^{-20}	1.21e-02	6.42e-03	3.28e-03	1.65e-03	8.29e-04	2^{-20}	3.67e-03	2.15e-03	1.22e-03	6.79e-04	3.71e-04
E^N	1.24e-02	6.44e-03	3.28e-03	1.65e-03	8.29e-04	E^N	3.77e-03	2.16e-03	1.22e-03	6.79e-04	3.71e-04

| $\beta = 1.5$ | | | | | |
$\varepsilon\backslash N$	32	64	128	256	512
2^{-0}	3.45e-02	1.80e-02	9.18e-03	4.60e-03	2.27e-03
2^{-2}	4.52e-02	2.46e-02	1.30e-02	6.61e-03	3.29e-03
2^{-4}	6.15e-02	3.19e-02	1.85e-02	9.83e-03	5.03e-03
2^{-6}	6.92e-02	3.72e-02	2.50e-02	1.55e-02	8.28e-03
2^{-8}	7.18e-02	3.73e-02	2.51e-02	1.58e-02	9.33e-03
2^{-10}	7.24e-02	3.73e-02	2.51e-02	1.58e-02	9.33e-03
2^{-12}	7.26e-02	3.73e-02	2.51e-02	1.58e-02	9.33e-03
2^{-14}	7.26e-02	3.73e-02	2.51e-02	1.58e-02	9.33e-03
2^{-16}	7.26e-02	3.73e-02	2.51e-02	1.58e-02	9.33e-03
2^{-18}	7.26e-02	3.73e-02	2.51e-02	1.58e-02	9.33e-03
2^{-20}	7.26e-02	3.73e-02	2.51e-02	1.58e-02	9.33e-03
E^N	7.26e-02	3.73e-02	2.51e-02	1.58e-02	9.33e-03

Table 4.12: Computed maximum pointwise difference $||U_\varepsilon - \overline{U_{FS}}^{8192}||_{\overline{\Omega}_\varepsilon^N}$ where U_ε is generated by (A_ε^N) for various values of ε, N and β.

$\beta = 0.5$

$\varepsilon \backslash N$	32	64	128	256	512
2^{-0}	4.09e-02	2.18e-02	1.18e-02	6.45e-03	3.65e-03
2^{-2}	4.62e-02	2.36e-02	1.21e-02	6.30e-03	3.36e-03
2^{-4}	4.06e-02	2.03e-02	1.03e-02	5.27e-03	2.75e-03
2^{-6}	3.80e-02	1.99e-02	9.97e-03	5.04e-03	2.58e-03
2^{-8}	3.10e-02	1.59e-02	8.29e-03	4.35e-03	2.30e-03
2^{-10}	2.78e-02	1.39e-02	7.09e-03	3.64e-03	1.88e-03
2^{-12}	2.63e-02	1.29e-02	6.51e-03	3.30e-03	1.68e-03
2^{-14}	2.55e-02	1.24e-02	6.23e-03	3.13e-03	1.58e-03
2^{-16}	2.52e-02	1.22e-02	6.08e-03	3.05e-03	1.53e-03
2^{-18}	2.50e-02	1.21e-02	6.01e-03	3.01e-03	1.51e-03
2^{-20}	2.49e-02	1.20e-02	5.98e-03	2.99e-03	1.49e-03
E^N	4.62e-02	2.36e-02	1.21e-02	6.45e-03	3.65e-03

$\beta = 1.0$

$\varepsilon \backslash N$	32	64	128	256	512
2^{-0}	1.35e-02	7.27e-03	4.07e-03	2.35e-03	1.34e-03
2^{-2}	1.65e-02	8.91e-03	4.95e-03	2.80e-03	1.59e-03
2^{-4}	1.54e-02	8.40e-03	4.71e-03	2.70e-03	1.55e-03
2^{-6}	1.28e-02	8.10e-03	4.59e-03	2.64e-03	1.52e-03
2^{-8}	6.39e-03	4.20e-03	2.76e-03	1.82e-03	1.18e-03
2^{-10}	3.19e-03	2.10e-03	1.38e-03	9.08e-04	5.88e-04
2^{-12}	1.60e-03	1.05e-03	6.91e-04	4.54e-04	2.94e-04
2^{-14}	7.99e-04	5.25e-04	3.46e-04	2.27e-04	1.47e-04
2^{-16}	3.99e-04	2.63e-04	1.73e-04	1.13e-04	7.35e-05
2^{-18}	2.00e-04	1.31e-04	8.64e-05	5.67e-05	3.68e-05
2^{-20}	9.98e-05	6.56e-05	4.32e-05	2.84e-05	1.84e-05
E^N	1.65e-02	8.91e-03	4.95e-03	2.80e-03	1.59e-03

$\beta = 1.5$

$\varepsilon \backslash N$	32	64	128	256	512
2^{-0}	1.35e-01	7.03e-02	3.63e-02	1.89e-02	1.01e-02
2^{-2}	1.48e-01	7.84e-02	4.06e-02	2.09e-02	1.08e-02
2^{-4}	1.44e-01	8.01e-02	4.22e-02	2.18e-02	1.12e-02
2^{-6}	8.92e-02	6.07e-02	3.81e-02	2.19e-02	1.13e-02
2^{-8}	9.50e-02	3.93e-02	1.91e-02	1.14e-02	6.60e-03
2^{-10}	1.19e-01	5.49e-02	2.55e-02	1.18e-02	5.45e-03
2^{-12}	1.30e-01	6.27e-02	3.03e-02	1.47e-02	7.11e-03
2^{-14}	1.36e-01	6.66e-02	3.27e-02	1.61e-02	7.93e-03
2^{-16}	1.39e-01	6.86e-02	3.39e-02	1.68e-02	8.35e-03
2^{-18}	1.41e-01	6.96e-02	3.45e-02	1.72e-02	8.56e-03
2^{-20}	1.41e-01	7.01e-02	3.48e-02	1.74e-02	8.66e-03
E^N	1.48e-01	8.01e-02	4.22e-02	2.19e-02	1.13e-02

Table 4.13: Computed maximum pointwise difference $\frac{1}{V^*}\|V_\varepsilon - \overline{V_{FS}}^{8192}\|_{\overline{\Omega}_\varepsilon^N \backslash \Gamma_L}$ where V_ε is generated by $(A_\varepsilon^\mathbf{N})$ for various values of ε, N and β.
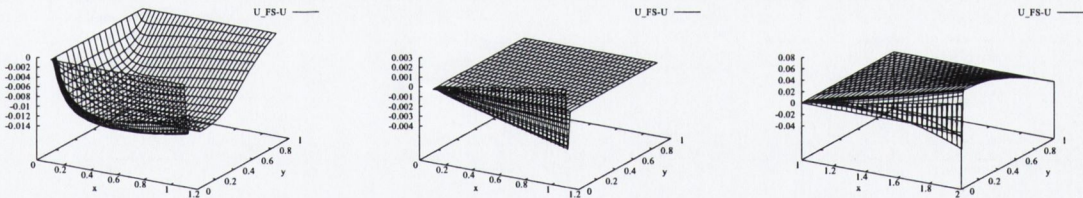
Figure 4-10: Graphs of $U_\varepsilon - U_{FS}^{8192}$ for $\varepsilon = 2^{-12}$, $N{=}32$ and $\beta = 0.5, 1.0, 1.5$.

The graphs of differences $U_\varepsilon - U_{FS}^{8192}$ for $\varepsilon = 2^{-12}$, $N{=}32$ and $\beta = 0.5, 1.0, 1.5$ in Fig. 4-10 show that the largest differences occur in the boundary layer along the surface of the wedge, for all β considered. The graphs of differences $\frac{1}{V^*}(V_\varepsilon - V_{FS}^{8192})$ for $\varepsilon = 2^{-12}$, $N{=}32$ and $\beta = 0.5, 1.0, 1.5$ in Figure 4-11 show that the largest differences are at the farthest point from the surface of the wedge. This is because V_ε is generated by an initial value problem with the initial condition along the wedge.
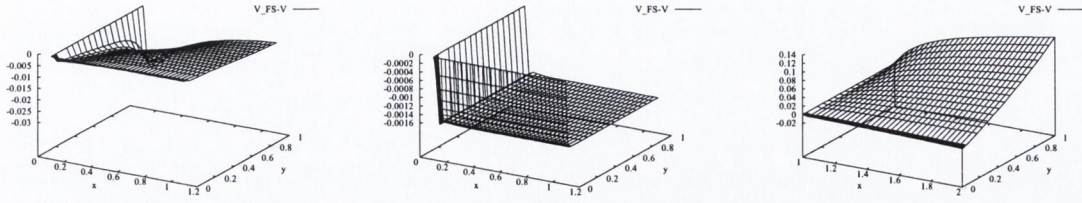
Figure 4-11: Graphs of $\frac{1}{V^*}(V_\varepsilon - V_{FS}^{8192})$ for $\varepsilon = 2^{-12}$, N=32 and $\beta = 0.5, 1.0, 1.5$.

We now estimate the order of convergence of the numerical approximations $\mathbf{U}_\varepsilon$, generated by the direct numerical method $(A_\varepsilon^{\mathbf{N}})$, by introducing the computed order of convergence $p_{\varepsilon,comp}^N$ which is defined by

$$p_{\varepsilon,comp}^N(U_\varepsilon) = \log_2 \frac{||U_\varepsilon^N - U_{FS}^{8192}||_{\Omega_\varepsilon^N}}{||U_\varepsilon^{2N} - U_{FS}^{8192}||_{\Omega_\varepsilon^{2N}}}$$

and p_{comp}^N is defined by

$$p_{comp}^N(U_\varepsilon) = \log_2 \frac{max_\varepsilon ||U_\varepsilon^N - U_{FS}^{8192}||_{\Omega_\varepsilon^N}}{max_\varepsilon ||U_\varepsilon^{2N} - U_{FS}^{8192}||_{\Omega_\varepsilon^{2N}}}.$$

We take the computed ε–uniform order of convergence to be

$$p_{comp}^* = \min_N p_{comp}^N.$$

Corresponding to this value of p_{comp}^* we calculate the quantities

$$C_{p_{comp}^*}^N = \frac{E^N(U_\varepsilon) N^{p_{comp}^*}}{1 - 2^{-p_{comp}^*}}$$

and we take the computed ε–uniform error constant to be

$$C_{p_{comp}^*}^* = \max_N C_{p_{comp}^*}^N.$$

The computed orders of convergence and the error constants have analogous expressions for $\frac{1}{V^*}V_\varepsilon^N$ and the scaled derivatives of the velocity components.
The orders of convergence and the error constants of the scaled velocity components U_ε and $\frac{1}{V^*}V_\varepsilon$ are given in Tables 4.14 and 4.15, respectively.

	$\beta = 0.5$					$\beta = 1.0$					$\beta = 1.5$			
$\varepsilon \backslash N$	32	64	128	256	$\varepsilon \backslash N$	32	64	128	256	$\varepsilon \backslash N$	32	64	128	256
2^{-0}	0.79	0.85	0.88	0.87	2^{-0}	1.04	1.11	1.25	1.69	2^{-0}	0.94	0.97	1.00	1.02
2^{-2}	0.90	0.95	0.98	0.99	2^{-2}	0.97	1.03	1.10	1.25	2^{-2}	0.87	0.93	0.97	1.00
2^{-4}	0.95	0.98	0.99	1.01	2^{-4}	1.05	1.05	1.06	1.12	2^{-4}	0.95	0.79	0.91	0.97
2^{-6}	0.96	0.99	1.00	1.01	2^{-6}	0.87	1.05	1.05	1.06	2^{-6}	0.89	0.57	0.69	0.90
2^{-8}	0.95	0.98	0.99	1.00	2^{-8}	0.80	0.82	0.85	0.87	2^{-8}	0.95	0.57	0.66	0.76
2^{-10}	0.93	0.97	0.99	1.00	2^{-10}	0.79	0.82	0.85	0.87	2^{-10}	0.96	0.57	0.66	0.76
2^{-12}	0.92	0.97	0.99	1.00	2^{-12}	0.78	0.82	0.85	0.87	2^{-12}	0.96	0.57	0.66	0.76
2^{-14}	0.92	0.97	0.99	1.00	2^{-14}	0.78	0.82	0.85	0.87	2^{-14}	0.96	0.57	0.66	0.76
2^{-16}	0.92	0.97	0.99	1.00	2^{-16}	0.77	0.82	0.85	0.87	2^{-16}	0.96	0.57	0.66	0.76
2^{-18}	0.92	0.97	0.99	1.00	2^{-18}	0.77	0.82	0.85	0.87	2^{-18}	0.96	0.57	0.66	0.76
2^{-20}	0.92	0.97	0.99	1.00	2^{-20}	0.77	0.82	0.85	0.87	2^{-20}	0.96	0.57	0.66	0.76
p^N_{comp}	0.95	0.98	0.99	1.00	p^N_{comp}	0.80	0.82	0.85	0.87	p^N_{comp}	0.96	0.57	0.66	0.76
$C_{0.95}$	0.69	0.69	0.67	0.66	$C_{0.80}$	0.14	0.14	0.14	0.14	$C_{0.57}$	1.61	1.23	1.23	1.15

Table 4.14: Computed orders of convergence $p^N_{\varepsilon,comp}$, p^N_{comp} and the error constant $C^N_{p^*_{comp}}$ for $U_\varepsilon - U^{8192}_{FS}$ where U_ε is generated by $(A^{\mathbf{N}}_\varepsilon)$ for various values of ε, N and β.

	$\beta = 0.5$					$\beta = 1.0$					$\beta = 1.5$			
$\varepsilon \backslash N$	32	64	128	256	$\varepsilon \backslash N$	32	64	128	256	$\varepsilon \backslash N$	32	64	128	256
2^{-0}	0.91	0.89	0.87	0.82	2^{-0}	0.89	0.84	0.79	0.81	2^{-0}	0.94	0.95	0.94	0.90
2^{-2}	0.97	0.96	0.94	0.90	2^{-2}	0.89	0.85	0.82	0.82	2^{-2}	0.92	0.95	0.96	0.95
2^{-4}	1.00	0.98	0.97	0.94	2^{-4}	0.87	0.83	0.80	0.80	2^{-4}	0.85	0.92	0.95	0.96
2^{-6}	0.93	0.99	0.98	0.97	2^{-6}	0.66	0.82	0.80	0.80	2^{-6}	0.56	0.67	0.80	0.96
2^{-8}	0.97	0.94	0.93	0.92	2^{-8}	0.60	0.60	0.61	0.63	2^{-8}	1.27	1.04	0.74	0.79
2^{-10}	1.01	0.97	0.96	0.95	2^{-10}	0.60	0.60	0.61	0.63	2^{-10}	1.11	1.11	1.11	1.11
2^{-12}	1.03	0.99	0.98	0.98	2^{-12}	0.60	0.60	0.61	0.63	2^{-12}	1.06	1.05	1.05	1.05
2^{-14}	1.04	1.00	0.99	0.99	2^{-14}	0.60	0.60	0.61	0.63	2^{-14}	1.03	1.03	1.02	1.02
2^{-16}	1.04	1.00	1.00	0.99	2^{-16}	0.60	0.60	0.61	0.63	2^{-16}	1.02	1.02	1.01	1.01
2^{-18}	1.05	1.01	1.00	1.00	2^{-18}	0.60	0.60	0.61	0.63	2^{-18}	1.02	1.01	1.01	1.01
2^{-20}	1.05	1.01	1.00	1.00	2^{-20}	0.60	0.60	0.61	0.63	2^{-20}	1.01	1.01	1.00	1.00
p^N_{comp}	0.97	0.96	0.91	0.82	p^N_{comp}	0.89	0.85	0.82	0.82	p^N_{comp}	0.89	0.92	0.95	0.96
$C_{0.82}$	1.83	1.65	1.50	1.41	$C_{0.82}$	0.65	0.62	0.61	0.61	$C_{0.89}$	6.98	6.98	6.81	6.54

Table 4.15: Computed orders of convergence $p^N_{\varepsilon,comp}$, p^N_{comp} and the error constant $C^N_{p^*_{comp}}$ for $\frac{1}{V^*}(V_\varepsilon - V^{8192}_{FS})$ where V_ε is generated by $(A^{\mathbf{N}}_\varepsilon)$ for various values of ε, N and β.

From Tables 4.14 and 4.15 we see that the order of convergence for the approximations to the scaled velocity components is at least 0.79 for both U_ε and $\frac{1}{V^*}V_\varepsilon$. Tables 4.14-4.15 of the computed orders of convergence for the pointwise differences, and Tables 4.4-4.5 of the computed orders of convergence for the computed maximum errors, exhibit similar behaviour.

Using Tables 4.14-4.15 we obtain the following error bounds

$$\begin{aligned}
\beta = 0.5 \quad & \|U_\varepsilon - U_{FS}^{8192}\|_{\Omega_\varepsilon^N} && \leq 0.69 N^{-0.95} \\
\beta = 1.0 \quad & \|U_\varepsilon - U_{FS}^{8192}\|_{\Omega_\varepsilon^N} && \leq 0.14 N^{-0.80} \\
\beta = 1.5 \quad & \|U_\varepsilon - U_{FS}^{8192}\|_{\Omega_\varepsilon^N} && \leq 1.61 N^{-0.57}
\end{aligned} \tag{4.6}$$

$$\begin{aligned}
\beta = 0.5 \quad & \tfrac{1}{V_*}\|V_\varepsilon - V_{FS}^{8192}\|_{\Omega_\varepsilon^N \setminus \Gamma_L} && \leq 2.05 N^{-0.82} \\
\beta = 1.0 \quad & \tfrac{1}{V_*}\|V_\varepsilon - V_{FS}^{8192}\|_{\Omega_\varepsilon^N \setminus \Gamma_L} && \leq 0.51 N^{-0.81} \\
\beta = 1.5 \quad & \tfrac{1}{V_*}\|V_\varepsilon - V_{FS}^{8192}\|_{\Omega_\varepsilon^N \setminus \Gamma_L} && \leq 2.34 N^{-0.90}.
\end{aligned} \tag{4.7}$$

From Tables 4.12-4.15 and Tables 4.2-4.5 we have shown that for the velocity components the method is ε–uniform for $\beta = 0.5$, 1.0 and 1.5. Further computations, not reported here, show that the errors for the velocity components for $\beta \in [0.0, 1.5]$ have similar behaviour. Therefore the method can be said to be (ε, β)–uniform for the scaled velocity components.

$\beta = 0.5$

$\varepsilon \backslash N$	32	64	128	256	512
2^{-0}	1.32e-02	7.04e-03	3.75e-03	1.99e-03	1.31e-03
2^{-2}	2.27e-02	1.15e-02	5.85e-03	3.10e-03	1.80e-03
2^{-4}	4.51e-02	2.27e-02	1.15e-02	5.85e-03	3.10e-03
2^{-6}	7.78e-02	4.51e-02	2.27e-02	1.15e-02	5.85e-03
2^{-8}	7.78e-02	4.69e-02	2.75e-02	1.58e-02	8.99e-03
2^{-10}	7.78e-02	4.69e-02	2.75e-02	1.58e-02	8.99e-03
2^{-12}	7.78e-02	4.69e-02	2.75e-02	1.58e-02	8.99e-03
2^{-14}	7.78e-02	4.69e-02	2.75e-02	1.58e-02	8.99e-03
2^{-16}	7.78e-02	4.69e-02	2.75e-02	1.58e-02	8.99e-03
2^{-18}	7.78e-02	4.69e-02	2.75e-02	1.58e-02	8.99e-03
2^{-20}	7.78e-02	4.69e-02	2.75e-02	1.58e-02	8.99e-03
E^N	7.78e-02	4.69e-02	2.75e-02	1.58e-02	8.99e-03

$\beta = 1.0$

$\varepsilon \backslash N$	32	64	128	256	512
2^{-0}	1.93e-02	9.92e-03	5.24e-03	2.89e-03	1.72e-03
2^{-2}	3.83e-02	1.95e-02	1.00e-02	5.29e-03	2.91e-03
2^{-4}	7.47e-02	3.80e-02	1.93e-02	9.95e-03	5.25e-03
2^{-6}	1.27e-01	7.47e-02	3.80e-02	1.93e-02	9.95e-03
2^{-8}	1.27e-01	7.76e-02	4.59e-02	2.66e-02	1.52e-02
2^{-10}	1.27e-01	7.76e-02	4.59e-02	2.66e-02	1.52e-02
2^{-12}	1.27e-01	7.76e-02	4.59e-02	2.66e-02	1.52e-02
2^{-14}	1.27e-01	7.76e-02	4.59e-02	2.66e-02	1.52e-02
2^{-16}	1.27e-01	7.76e-02	4.59e-02	2.66e-02	1.52e-02
2^{-18}	1.27e-01	7.76e-02	4.59e-02	2.66e-02	1.52e-02
2^{-20}	1.27e-01	7.76e-02	4.59e-02	2.66e-02	1.52e-02
E^N	1.27e-01	7.76e-02	4.59e-02	2.66e-02	1.52e-02

$\beta = 1.5$

$\varepsilon \backslash N$	32	64	128	256	512
2^{-0}	1.79e+00	9.14e-01	4.67e-01	2.43e-01	1.30e-01
2^{-2}	3.37e+00	1.74e+00	8.89e-01	4.55e-01	2.36e-01
2^{-4}	6.02e+00	3.30e+00	1.71e+00	8.71e-01	4.46e-01
2^{-6}	7.25e+00	4.87e+00	2.99e+00	1.69e+00	8.61e-01
2^{-8}	7.25e+00	4.87e+00	2.99e+00	1.75e+00	1.00e+00
2^{-10}	7.25e+00	4.87e+00	2.99e+00	1.75e+00	1.00e+00
2^{-12}	7.25e+00	4.87e+00	2.99e+00	1.75e+00	1.00e+00
2^{-14}	7.25e+00	4.87e+00	2.99e+00	1.75e+00	1.00e+00
2^{-16}	7.25e+00	4.87e+00	2.99e+00	1.75e+00	1.00e+00
2^{-18}	7.25e+00	4.87e+00	2.99e+00	1.75e+00	1.00e+00
2^{-20}	7.25e+00	4.87e+00	2.99e+00	1.75e+00	1.00e+00
E^N	7.25e+00	4.87e+00	2.99e+00	1.75e+00	1.00e+00

Table 4.16: Computed maximum pointwise scaled difference $\sqrt{\varepsilon}\|D_y^- U_\varepsilon - D_y U_{FS}^{8192}\|_{\overline{\Omega_\varepsilon^N} \setminus \Gamma_B}$ where U_ε is generated by (A_ε^N) for various values of ε, N and β.

In Tables 4.16-4.18 we display the computed maximum pointwise differences of the approximations to the scaled first order derivatives of the velocity components for various values of ε, N and β.
The maximum scaled differences for $\sqrt{\varepsilon} D_y^- U_\varepsilon$ and $D_y^- V_\varepsilon$ in Tables 4.16 and 4.17

stabilise to a fixed value after $\varepsilon = 2^{-10}$, for all values of β and N considered. In a similar fashion to Tables 4.6 and 4.7 of the maximum pointwise errors, Tables 4.16 and 4.17 show that the method is independent of ε for $\sqrt{\varepsilon}D_y^- U_\varepsilon$ and $D_y^- V_\varepsilon$, for all values of β and N considered.

$\beta = 0.5$						$\beta = 1.0$				
$\varepsilon \backslash N$	32	64	128	256	512	$\varepsilon \backslash N$	32	64	128	256	512
2^{-0}	1.12e-01	6.65e-02	3.63e-02	1.88e-02	9.39e-03	2^{-0}	1.97e-02	1.05e-02	5.99e-03	3.76e-03	2.92e-03
2^{-2}	1.27e-01	7.27e-02	3.91e-02	2.03e-02	1.03e-02	2^{-2}	3.79e-02	1.97e-02	1.05e-02	5.99e-03	3.76e-03
2^{-4}	1.19e-01	6.85e-02	3.70e-02	1.93e-02	9.86e-03	2^{-4}	7.25e-02	3.79e-02	1.97e-02	1.05e-02	5.99e-03
2^{-6}	1.46e-01	8.50e-02	4.31e-02	2.20e-02	1.15e-02	2^{-6}	1.19e-01	7.25e-02	3.79e-02	1.97e-02	1.05e-02
2^{-8}	1.46e-01	8.78e-02	5.20e-02	3.01e-02	1.74e-02	2^{-8}	1.19e-01	7.52e-02	4.55e-02	2.68e-02	1.57e-02
2^{-10}	1.46e-01	8.78e-02	5.20e-02	3.01e-02	1.74e-02	2^{-10}	1.19e-01	7.52e-02	4.55e-02	2.68e-02	1.57e-02
2^{-12}	1.46e-01	8.78e-02	5.20e-02	3.01e-02	1.74e-02	2^{-12}	1.19e-01	7.52e-02	4.55e-02	2.68e-02	1.57e-02
2^{-14}	1.46e-01	8.78e-02	5.20e-02	3.01e-02	1.74e-02	2^{-14}	1.19e-01	7.52e-02	4.55e-02	2.68e-02	1.57e-02
2^{-16}	1.46e-01	8.78e-02	5.20e-02	3.01e-02	1.74e-02	2^{-16}	1.19e-01	7.52e-02	4.55e-02	2.68e-02	1.57e-02
2^{-18}	1.46e-01	8.78e-02	5.20e-02	3.01e-02	1.74e-02	2^{-18}	1.19e-01	7.52e-02	4.55e-02	2.68e-02	1.57e-02
2^{-20}	1.46e-01	8.78e-02	5.20e-02	3.01e-02	1.74e-02	2^{-20}	1.19e-01	7.52e-02	4.55e-02	2.68e-02	1.57e-02
E^N	1.46e-01	8.78e-02	5.20e-02	3.01e-02	1.74e-02	E^N	1.19e-01	7.52e-02	4.55e-02	2.68e-02	1.57e-02

$\beta = 1.5$					
$\varepsilon \backslash N$	32	64	128	256	512
2^{-0}	1.85e-01	9.28e-02	4.64e-02	2.32e-02	1.22e-02
2^{-2}	2.43e-01	1.27e-01	6.61e-02	3.49e-02	1.98e-02
2^{-4}	4.46e-01	2.43e-01	1.27e-01	6.61e-02	3.49e-02
2^{-6}	5.51e-01	3.62e-01	2.23e-01	1.27e-01	6.61e-02
2^{-8}	5.51e-01	3.62e-01	2.23e-01	1.32e-01	7.65e-02
2^{-10}	5.51e-01	3.62e-01	2.23e-01	1.32e-01	7.65e-02
2^{-12}	5.51e-01	3.62e-01	2.23e-01	1.32e-01	7.65e-02
2^{-14}	5.51e-01	3.62e-01	2.23e-01	1.32e-01	7.65e-02
2^{-16}	5.51e-01	3.62e-01	2.23e-01	1.32e-01	7.65e-02
2^{-18}	5.51e-01	3.62e-01	2.23e-01	1.32e-01	7.65e-02
2^{-20}	5.51e-01	3.62e-01	2.23e-01	1.32e-01	7.65e-02
E^N	5.51e-01	3.62e-01	2.23e-01	1.32e-01	7.65e-02

Table 4.17: Computed maximum pointwise difference $||D_y^- V_\varepsilon - D_y V_{FS}^{8192}||_{\overline{\Omega_\varepsilon^N \backslash \Gamma_B}}$ where V_ε is generated by (A_ε^N) for various values of ε, N and β.

Table 4.18 shows the maximum scaled difference for $\frac{1}{V^*}D_x^- V_\varepsilon$ for various values of ε, N and β. Table 4.18 shows the maximum pointwise scaled differences decrease as ε decreases. In a similar fashion to Table 4.8 of the maximum errors, the maximum differences occur when $\varepsilon \geq 2^{-6}$ for all β and N.

		$\beta = 0.5$						$\beta = 1.0$			
$\varepsilon\backslash N$	32	64	128	256	512	$\varepsilon\backslash N$	32	64	128	256	512
2^{-0}	4.97e-01	2.86e-01	1.60e-01	8.71e-02	1.77e-01	2^{-0}	2.15e-02	3.74e-02	5.58e-02	6.11e-02	2.63e-02
2^{-2}	6.56e-01	4.56e-01	2.83e-01	1.75e-01	7.59e-02	2^{-2}	3.12e-02	5.46e-02	8.11e-02	9.39e-02	8.40e-02
2^{-4}	8.02e-01	5.76e-01	3.63e-01	2.22e-01	1.07e-01	2^{-4}	3.10e-02	5.78e-02	8.86e-02	1.14e-01	1.24e-01
2^{-6}	8.51e-01	6.27e-01	4.07e-01	2.50e-01	1.30e-01	2^{-6}	2.44e-02	5.58e-02	8.96e-02	1.19e-01	1.37e-01
2^{-8}	8.38e-01	6.00e-01	3.91e-01	2.45e-01	1.36e-01	2^{-8}	1.22e-02	2.89e-02	5.44e-02	8.40e-02	1.12e-01
2^{-10}	8.32e-01	5.84e-01	3.70e-01	2.29e-01	1.27e-01	2^{-10}	6.10e-03	1.45e-02	2.72e-02	4.20e-02	5.58e-02
2^{-12}	8.28e-01	5.76e-01	3.59e-01	2.20e-01	1.23e-01	2^{-12}	3.05e-03	7.23e-03	1.36e-02	2.10e-02	2.79e-02
2^{-14}	8.27e-01	5.72e-01	3.54e-01	2.16e-01	1.20e-01	2^{-14}	1.52e-03	3.61e-03	6.80e-03	1.05e-02	1.40e-02
2^{-16}	8.26e-01	5.70e-01	3.51e-01	2.14e-01	1.19e-01	2^{-16}	7.61e-04	1.81e-03	3.40e-03	5.25e-03	6.98e-03
2^{-18}	8.25e-01	5.69e-01	3.50e-01	2.13e-01	1.19e-01	2^{-18}	3.81e-04	9.03e-04	1.70e-03	2.63e-03	3.49e-03
2^{-20}	8.25e-01	5.68e-01	3.49e-01	2.12e-01	1.18e-01	2^{-20}	1.90e-04	4.52e-04	8.49e-04	1.31e-03	1.74e-03
E^N	8.51e-01	6.27e-01	4.07e-01	2.50e-01	1.77e-01	E^N	3.12e-02	5.78e-02	8.96e-02	1.19e-01	1.37e-01

		$\beta = 1.5$			
$\varepsilon\backslash N$	32	64	128	256	512
2^{-0}	8.31e-01	8.71e-01	8.33e-01	7.36e-01	5.37e-01
2^{-2}	7.26e-01	7.55e-01	7.66e-01	7.40e-01	6.34e-01
2^{-4}	6.59e-01	6.98e-01	7.31e-01	7.37e-01	6.92e-01
2^{-6}	5.75e-01	5.85e-01	6.76e-01	7.62e-01	7.45e-01
2^{-8}	5.19e-01	4.28e-01	4.12e-01	4.35e-01	4.66e-01
2^{-10}	4.91e-01	3.50e-01	2.80e-01	2.56e-01	2.53e-01
2^{-12}	4.77e-01	3.11e-01	2.15e-01	1.67e-01	1.47e-01
2^{-14}	4.70e-01	2.92e-01	1.82e-01	1.23e-01	9.33e-02
2^{-16}	4.67e-01	2.82e-01	1.65e-01	1.00e-01	6.67e-02
2^{-18}	4.65e-01	2.77e-01	1.57e-01	8.92e-02	5.33e-02
2^{-20}	4.64e-01	2.75e-01	1.53e-01	8.36e-02	4.67e-02
E^N	8.31e-01	8.71e-01	8.33e-01	7.62e-01	7.45e-01

Table 4.18: Computed maximum pointwise scaled difference $V^{*-1}\|D_x^- V_\varepsilon - D_x V_{FS}^{8192}\|_{\overline{\Omega_\varepsilon^N}\backslash \Gamma_L \cup X_1}$ where V_ε is generated by (A_ε^N) for various values of ε, N and β.

Graphs of the scaled differences $\sqrt{\varepsilon}(D_y^- U_\varepsilon - D_y U_{FS}^{8192})$, $D_y^- V_\varepsilon - D_y V_{FS}^{8192}$ and $\frac{1}{V^*}(D_x^- V_\varepsilon - D_x V_{FS}^{8192})$ generated by (A_ε^N) are given in Figures 4-12, 4-13 and 4-14.
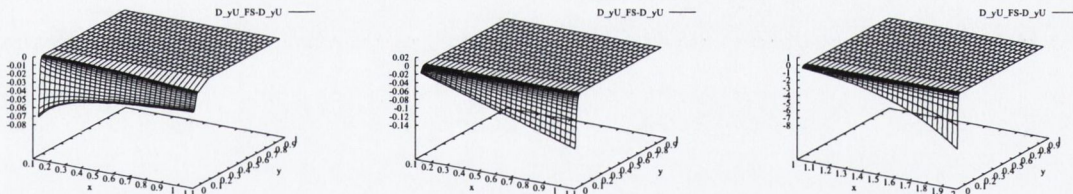
Figure 4-12: Graphs of $\sqrt{\varepsilon}(D_y^- U_\varepsilon - D_y U_{FS}^{8192})$ for $\varepsilon = 2^{-12}$, N=32 and $\beta = 0.5, 1.0, 1.5$.
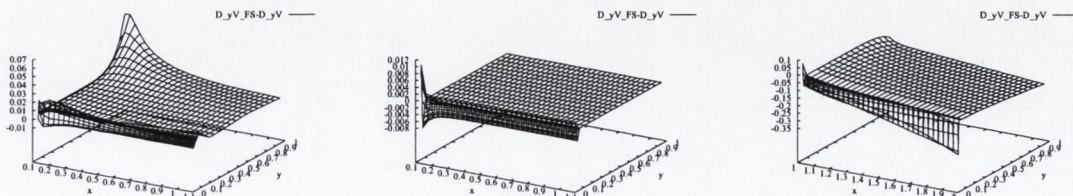
Figure 4-13: Graphs of $D_y^- V_\varepsilon - D_y V_{FS}^{8192}$ for $\varepsilon = 2^{-12}$, N=32 and $\beta = 0.5, 1.0, 1.5$.

Graphs of $\sqrt{\varepsilon}(D_y^- U_\varepsilon - D_y U_{FS}^{8192})$ and $D_y^- V_\varepsilon - D_y V_{FS}^{8192}$ in Figures 4-12 and 4-13 show the largest differences occur in the boundary layer, except for $D_y^- V_\varepsilon - D_y V_{FS}^{8192}$ for $\beta = 0.5$ where the largest difference is at the point furthest away from the wedge.
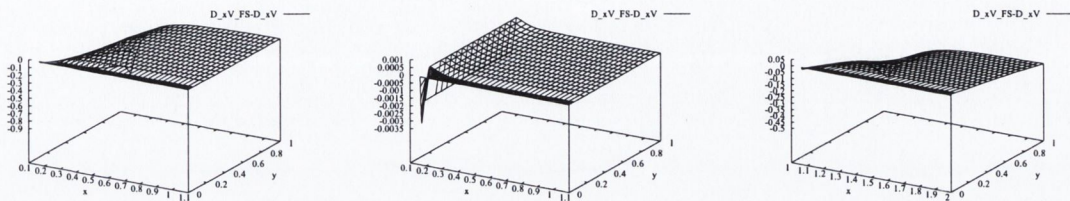
Figure 4-14: Graphs of $\frac{1}{V^*}(D_x^- V_\varepsilon - D_x V_{FS}^{8192})$ for $\varepsilon = 2^{-12}$, $N{=}32$ and $\beta = 0.5, 1.0, 1.5$.

Graphs of $\frac{1}{V^*}(D_x^- V_\varepsilon - D_x V_{FS}^{8192})$ in Figure 4-14 are smooth, with the largest difference occurring at the points farthest from the wedge for $\beta = 0.5$ and 1.5. The graph of $\frac{1}{V^*}(D_x^- V_\varepsilon - D_x V_{FS}^{8192})$ for $\beta = 1.0$ shows a non-physical jump along the left hand edge of Ω_ε^N. This could be due to the leading edge singularity.

In Tables 4.19-4.21 we display the computed orders of convergence for the approximations of the first order scaled derivatives of the velocity components $\sqrt{\varepsilon}D_y^- U_\varepsilon$, $D_y^- V_\varepsilon$ and $\frac{1}{V^*}D_x^- V_\varepsilon$, respectively.

	$\beta = 0.5$					$\beta = 1.0$					$\beta = 1.5$			
$\varepsilon\backslash N$	32	64	128	256	$\varepsilon\backslash N$	32	64	128	256	$\varepsilon\backslash N$	32	64	128	256
2^{-0}	0.91	0.91	0.91	0.60	2^{-0}	0.96	0.92	0.86	0.75	2^{-0}	0.97	0.97	0.95	0.90
2^{-2}	0.98	0.97	0.92	0.78	2^{-2}	0.98	0.96	0.92	0.86	2^{-2}	0.95	0.97	0.97	0.94
2^{-4}	0.99	0.98	0.97	0.92	2^{-4}	0.98	0.97	0.96	0.92	2^{-4}	0.87	0.95	0.97	0.97
2^{-6}	0.79	0.99	0.98	0.97	2^{-6}	0.76	0.98	0.97	0.96	2^{-6}	0.58	0.70	0.83	0.97
2^{-8}	0.73	0.77	0.80	0.81	2^{-8}	0.70	0.76	0.79	0.80	2^{-8}	0.58	0.70	0.77	0.81
2^{-10}	0.73	0.77	0.80	0.81	2^{-10}	0.70	0.76	0.79	0.80	2^{-10}	0.58	0.70	0.77	0.81
2^{-12}	0.73	0.77	0.80	0.81	2^{-12}	0.71	0.76	0.79	0.80	2^{-12}	0.58	0.70	0.77	0.81
2^{-14}	0.73	0.77	0.80	0.81	2^{-14}	0.71	0.76	0.79	0.80	2^{-14}	0.58	0.70	0.77	0.81
2^{-16}	0.73	0.77	0.80	0.81	2^{-16}	0.71	0.76	0.79	0.80	2^{-16}	0.58	0.70	0.77	0.81
2^{-18}	0.73	0.77	0.80	0.81	2^{-18}	0.71	0.76	0.79	0.80	2^{-18}	0.58	0.70	0.77	0.81
2^{-20}	0.73	0.77	0.80	0.81	2^{-20}	0.71	0.76	0.79	0.80	2^{-20}	0.58	0.70	0.77	0.81
p_{comp}^N	0.73	0.77	0.80	0.81	p_{comp}^N	0.71	0.76	0.79	0.80	p_{comp}^N	0.58	0.70	0.77	0.81
$C_{0.73}$	2.46	2.46	2.39	2.28	$C_{0.71}$	3.77	3.77	3.64	3.43	$C_{0.58}$	161.95	161.95	148.36	129.49

Table 4.19: Computed orders of convergence $p_{\varepsilon,comp}^N$, p_{comp}^N and the error constant $C_{p_{comp}^*}^N$ for $\sqrt{\varepsilon}(D_y^- U_\varepsilon - D_y U_{FS}^{8192})$ where U_ε is generated by (A_ε^N) for various values of ε, N and β.

	$\beta = 0.5$					$\beta = 1.0$					$\beta = 1.5$			
$\varepsilon \backslash N$	32	64	128	256	$\varepsilon \backslash N$	32	64	128	256	$\varepsilon \backslash N$	32	64	128	256
2^{-0}	0.75	0.87	0.95	1.00	2^{-0}	0.93	0.87	0.78	0.65	2^{-0}	1.00	1.00	1.00	0.93
2^{-2}	0.81	0.90	0.95	0.97	2^{-2}	0.95	0.93	0.87	0.78	2^{-2}	0.93	0.95	0.92	0.82
2^{-4}	0.79	0.89	0.94	0.97	2^{-4}	0.94	0.95	0.93	0.87	2^{-4}	0.88	0.93	0.95	0.92
2^{-6}	0.78	0.98	0.97	0.94	2^{-6}	0.71	0.94	0.95	0.93	2^{-6}	0.61	0.70	0.81	0.95
2^{-8}	0.74	0.75	0.79	0.80	2^{-8}	0.66	0.72	0.76	0.78	2^{-8}	0.61	0.70	0.76	0.79
2^{-10}	0.74	0.75	0.79	0.80	2^{-10}	0.66	0.72	0.76	0.78	2^{-10}	0.61	0.70	0.76	0.79
2^{-12}	0.74	0.75	0.79	0.80	2^{-12}	0.66	0.72	0.76	0.78	2^{-12}	0.61	0.70	0.76	0.79
2^{-14}	0.74	0.75	0.79	0.80	2^{-14}	0.66	0.72	0.76	0.78	2^{-14}	0.61	0.70	0.76	0.79
2^{-16}	0.74	0.75	0.79	0.80	2^{-16}	0.66	0.72	0.76	0.78	2^{-16}	0.61	0.70	0.76	0.79
2^{-18}	0.74	0.75	0.79	0.80	2^{-18}	0.66	0.72	0.76	0.78	2^{-18}	0.61	0.70	0.76	0.79
2^{-20}	0.74	0.75	0.79	0.80	2^{-20}	0.66	0.72	0.76	0.78	2^{-20}	0.61	0.70	0.76	0.79
p_{comp}^N	0.74	0.75	0.79	0.80	p_{comp}^N	0.66	0.72	0.76	0.78	p_{comp}^N	0.61	0.70	0.76	0.79
$C_{0.74}$	4.70	4.70	4.64	4.48	$C_{0.66}$	3.17	3.17	3.03	2.81	$C_{0.61}$	13.13	13.13	12.34	11.13

Table 4.20: Computed orders of convergence $p_{\varepsilon,comp}^N$, p_{comp}^N and the error constant $C_{p_{comp}^*}^N$ for $D_y^- V_\varepsilon - D_y V_{FS}^{8192}$ where V_ε is generated by $(A_\varepsilon^{\mathbf{N}})$ for various values of ε, N and β.

The results in Tables 4.16-4.17 and 4.19-4.20 suggest that the method is an ε-uniform numerical method with orders of convergence of at least 0.7 for $\sqrt{\varepsilon} D_y^- U_\varepsilon$ and $D_y^- V_\varepsilon$ for $N \geq 64$ for all β.

Tables 4.16-4.20 and Tables 4.6-4.10 strongly indicate that the method is ε-uniform for $\sqrt{\varepsilon} D_y^- U_\varepsilon$ and $D_y^- V_\varepsilon$ for $\beta = 0.5$, 1.0 and 1.5. Further computations, not reported here, show that the errors for $\sqrt{\varepsilon} D_y^- U_\varepsilon$ and $D_y^- V_\varepsilon$ for $\beta \in [0.0, 1.5]$ have similar behaviour. Therefore the method can be said to be (ε, β)–uniform.

	$\beta = 0.5$			
$\varepsilon \backslash N$	32	64	128	256
2^{-0}	0.80	0.83	0.88	-1.02
2^{-2}	0.53	0.69	0.69	1.21
2^{-4}	0.48	0.67	0.70	1.05
2^{-6}	0.44	0.62	0.70	0.94
2^{-8}	0.48	0.62	0.67	0.85
2^{-10}	0.51	0.66	0.70	0.85
2^{-12}	0.52	0.68	0.71	0.84
2^{-14}	0.53	0.69	0.71	0.84
2^{-16}	0.54	0.70	0.72	0.84
2^{-18}	0.54	0.70	0.72	0.84
2^{-20}	0.54	0.70	0.72	0.84
p_{comp}^N	0.44	0.62	0.70	0.50
$C_{0.44}$	14.92	14.92	13.16	10.97

	$\beta = 1.0$			
$\varepsilon \backslash N$	32	64	128	256
2^{-0}	-0.80	-0.58	-0.13	1.22
2^{-2}	-0.81	-0.57	-0.21	0.16
2^{-4}	-0.90	-0.62	-0.36	-0.12
2^{-6}	-1.19	-0.68	-0.41	-0.20
2^{-8}	-1.24	-0.91	-0.63	-0.41
2^{-10}	-1.25	-0.91	-0.63	-0.41
2^{-12}	-1.25	-0.91	-0.63	-0.41
2^{-14}	-1.25	-0.91	-0.63	-0.41
2^{-16}	-1.25	-0.91	-0.63	-0.41
2^{-18}	-1.25	-0.91	-0.63	-0.41
2^{-20}	-1.25	-0.91	-0.63	-0.41
p_{comp}^N	-0.89	-0.63	-0.41	-0.20
$C_{-0.89}$	-0.00	-0.00	-0.00	-0.00

	$\beta = 1.5$			
$\varepsilon \backslash N$	32	64	128	256
2^{-0}	-0.07	0.06	0.18	0.45
2^{-2}	-0.06	-0.02	0.05	0.22
2^{-4}	-0.08	-0.07	-0.01	0.09
2^{-6}	-0.03	-0.21	-0.17	0.03
2^{-8}	0.28	0.06	-0.08	-0.10
2^{-10}	0.49	0.32	0.13	0.02
2^{-12}	0.62	0.54	0.36	0.19
2^{-14}	0.69	0.68	0.57	0.39
2^{-16}	0.73	0.77	0.72	0.59
2^{-18}	0.75	0.82	0.82	0.74
2^{-20}	0.76	0.84	0.87	0.84
p_{comp}^N	-0.07	0.06	0.13	0.03
$C_{-0.07}$	-13.44	-13.44	-12.26	-10.69

Table 4.21: Computed orders of convergence $p_{\varepsilon,comp}^N$, p_{comp}^N and the error constant $C_{p_{comp}^*}^N$ for $\frac{1}{V^*}(D_x^- V_\varepsilon - D_x V_{FS}^{8192})$ in the domain $\overline{\Omega}_\varepsilon^N \backslash (X_1 \bigcup \Gamma_L)$ where V_ε is generated by $(A_\varepsilon^{\mathbf{N}})$ for various values of ε, N and β.

The results in Table 4.21 do not suggest that the numerical method is ε-uniform for $\frac{1}{V^*}(D_x^- V_\varepsilon - D_x V_{FS}^{8192})$ for all β on the domain $\overline{\Omega}_\varepsilon^N \backslash (X_1 \bigcup \Gamma_L)$. Hence we investigate computed orders of convergence for $\frac{1}{V^*}(D_x^- V_\varepsilon - D_x V_{FS}^{8192})$ in the subdomain $\overline{\Omega}_\varepsilon^N \bigcap [x_0 + 0.1, x_N] \times [0, 1]$ in Table 4.22. The results suggest that the method is ε-uniform for $\frac{1}{V^*} D_x^- V_\varepsilon$ in the subdomain.

	$\beta = 0.5$					$\beta = 1.0$					$\beta = 1.5$			
$\varepsilon \backslash N$	32	64	128	256	$\varepsilon \backslash N$	32	64	128	256	$\varepsilon \backslash N$	32	64	128	256
2^{-0}	0.77	0.88	1.01	0.80	2^{-0}	4.17	-0.70	1.05	1.23	2^{-0}	1.06	1.06	1.18	0.80
2^{-2}	0.88	0.93	1.01	0.98	2^{-2}	0.68	1.12	0.25	1.00	2^{-2}	0.98	0.99	1.06	1.04
2^{-4}	0.86	0.92	1.01	1.00	2^{-4}	0.85	0.99	1.19	1.19	2^{-4}	0.97	0.98	1.04	1.02
2^{-6}	0.85	0.93	1.02	1.00	2^{-6}	0.70	1.01	1.17	1.14	2^{-6}	1.01	1.04	1.08	1.02
2^{-8}	0.86	0.92	1.01	0.99	2^{-8}	0.61	0.78	0.97	0.94	2^{-8}	0.96	0.99	1.04	1.04
2^{-10}	0.87	0.93	1.01	1.00	2^{-10}	0.59	0.77	0.97	0.94	2^{-10}	0.94	0.97	1.02	1.02
2^{-12}	0.88	0.93	1.02	1.01	2^{-12}	0.59	0.77	0.97	0.94	2^{-12}	0.93	0.96	1.01	1.01
2^{-14}	0.88	0.93	1.02	1.01	2^{-14}	0.60	0.77	0.97	0.94	2^{-14}	0.92	0.96	1.01	1.00
2^{-16}	0.88	0.93	1.02	1.01	2^{-16}	0.60	0.77	0.97	0.94	2^{-16}	0.92	0.96	1.00	1.00
2^{-18}	0.88	0.93	1.02	1.01	2^{-18}	0.60	0.77	0.97	0.94	2^{-18}	0.92	0.96	1.00	1.00
2^{-20}	0.88	0.93	1.02	1.01	2^{-20}	0.60	0.77	0.97	0.94	2^{-20}	0.92	0.96	1.00	1.00
p_{comp}^{N}	0.85	0.93	1.02	0.86	p_{comp}^{N}	0.76	1.01	1.17	1.14	p_{comp}^{N}	0.92	0.96	1.00	1.00
$C_{0.85}$	17.40	17.40	16.49	14.68	$C_{0.76}$	0.12	0.12	0.10	0.08	$C_{0.92}$	18.33	18.33	17.85	16.85

Table 4.22: Computed orders of convergence $p_{\varepsilon,comp}^{N}$, p_{comp}^{N} and the error constant $C_{p^*}^{N}$ for $\frac{1}{V^*}(D_x^- V_\varepsilon - D_x V_{FS}^{8192})$ in the subdomain $\overline{\Omega}_\varepsilon^{N} \bigcap [x_0 + 0.1, x_N] \times [0,1]$ where V_ε is generated by $(A_\varepsilon^{\mathbf{N}})$ for various values of ε, N and β.

In Appendix D we noted that the introduction of a second transition point

$$\sigma_2 = \min\{0.5\sigma, \frac{\sqrt{\varepsilon}}{8} \ln N\}$$

is beneficial to the computed values of the derivatives of the velocity components. Table 4.23 shows the maximum scaled difference for $\frac{1}{V^*} D_x^- V_\varepsilon$ values of ε, N and β, using the double transition point mesh. Table 4.23 shows the maximum pointwise scaled differences decrease as ε decreases. The maximum differences occur when $\varepsilon = 1$ for all β and N.

In Table 4.24 we display the computed orders of convergence for the approximations of the first order scaled derivative of the y-velocity component, $\frac{1}{V^*} D_x^- V_\varepsilon$, using the double transition point mesh. Comparing the orders of convergence for the approximations of the first order scaled derivative of the y-velocity component generated by one transition point in Table 4.21 and Table 4.24 we see that the numerical method using two transition points yields superior results. While this is not a conclusive proof, it does suggest that a second transition point has merit.

	$\beta = 0.5$						$\beta = 1.5$				
$\varepsilon\backslash N$	32	64	128	256	512	$\varepsilon\backslash N$	32	64	128	256	512
2^{-0}	4.98e-01	2.92e-01	1.64e-01	8.99e-02	1.73e-01	2^{-0}	7.61e-01	7.39e-01	6.56e-01	5.75e-01	4.61e-01
2^{-2}	6.58e-01	4.56e-01	2.83e-01	1.77e-01	7.79e-02	2^{-2}	5.62e-01	5.17e-01	4.34e-01	3.43e-01	2.56e-01
2^{-4}	8.11e-01	5.58e-01	3.42e-01	2.09e-01	1.04e-01	2^{-4}	4.20e-01	4.06e-01	3.37e-01	2.36e-01	1.54e-01
2^{-6}	8.54e-01	5.98e-01	3.64e-01	2.15e-01	1.10e-01	2^{-6}	3.54e-01	3.19e-01	3.08e-01	2.18e-01	1.20e-01
2^{-8}	8.39e-01	5.84e-01	3.61e-01	2.15e-01	1.13e-01	2^{-8}	4.09e-01	2.93e-01	2.40e-01	1.78e-01	1.00e-01
2^{-10}	8.32e-01	5.76e-01	3.55e-01	2.13e-01	1.16e-01	2^{-10}	4.36e-01	2.82e-01	1.94e-01	1.28e-01	6.99e-02
2^{-12}	8.29e-01	5.72e-01	3.52e-01	2.13e-01	1.17e-01	2^{-12}	4.50e-01	2.77e-01	1.72e-01	1.03e-01	5.49e-02
2^{-14}	8.27e-01	5.70e-01	3.50e-01	2.12e-01	1.18e-01	2^{-14}	4.56e-01	2.75e-01	1.60e-01	9.04e-02	4.74e-02
2^{-16}	8.26e-01	5.69e-01	3.49e-01	2.12e-01	1.18e-01	2^{-16}	4.60e-01	2.73e-01	1.55e-01	8.42e-02	4.37e-02
2^{-18}	8.25e-01	5.68e-01	3.49e-01	2.12e-01	1.18e-01	2^{-18}	4.62e-01	2.73e-01	1.52e-01	8.12e-02	4.18e-02
2^{-20}	8.25e-01	5.68e-01	3.49e-01	2.12e-01	1.18e-01	2^{-20}	4.62e-01	2.72e-01	1.50e-01	7.96e-02	4.09e-02
E^N	8.54e-01	5.98e-01	3.64e-01	2.15e-01	1.73e-01	E^N	7.61e-01	7.39e-01	6.56e-01	5.75e-01	4.61e-01

Table 4.23: Computed maximum pointwise scaled difference $V^{*-1}\|D_x^- V_\varepsilon - D_x V_{FS}^{8192}\|_{\overline{\Omega_\varepsilon^N}\backslash\Gamma_L\bigcup X_1}$ where V_ε is generated by $(A_{2\varepsilon}^N)$ for various values of ε, N and β.

	$\beta = 0.5$					$\beta = 1.5$			
$\varepsilon\backslash N$	32	64	128	256	$\varepsilon\backslash N$	32	64	128	256
2^{-0}	0.77	0.83	0.87	-0.94	2^{-0}	0.04	0.17	0.19	0.32
2^{-2}	0.53	0.69	0.68	1.18	2^{-2}	0.12	0.25	0.34	0.42
2^{-4}	0.54	0.71	0.71	1.01	2^{-4}	0.05	0.27	0.51	0.61
2^{-6}	0.51	0.72	0.76	0.97	2^{-6}	0.15	0.05	0.50	0.86
2^{-8}	0.52	0.70	0.75	0.92	2^{-8}	0.48	0.29	0.43	0.82
2^{-10}	0.53	0.70	0.73	0.88	2^{-10}	0.63	0.54	0.61	0.87
2^{-12}	0.53	0.70	0.73	0.86	2^{-12}	0.70	0.69	0.74	0.91
2^{-14}	0.54	0.70	0.72	0.85	2^{-14}	0.73	0.78	0.83	0.93
2^{-16}	0.54	0.70	0.72	0.85	2^{-16}	0.75	0.82	0.88	0.95
2^{-18}	0.54	0.70	0.72	0.84	2^{-18}	0.76	0.85	0.90	0.96
2^{-20}	0.54	0.70	0.72	0.84	2^{-20}	0.76	0.86	0.92	0.96
p_{comp}^N	0.51	0.72	0.76	0.32	p_{comp}^N	0.04	0.17	0.19	0.32
$C_{0.32}$	12.98	11.31	8.57	6.32	$C_{0.04}$	30.45	30.45	27.87	25.16

Table 4.24: Computed orders of convergence $p_{\varepsilon,comp}^N$, p_{comp}^N and the error constant $C_{p_{comp}^*}^N$ for $\frac{1}{V^*}(D_x^- V_\varepsilon - D_x V_{FS}^{8192})$ in the domain $\overline{\Omega}_\varepsilon^N\backslash(X_1\bigcup\Gamma_L)$ where V_ε is generated by $(A_{2\varepsilon}^N)$ for various values of ε, N and β.

Using Tables 4.19-4.20 we obtain the following error bounds

$$
\begin{aligned}
\beta = 0.5 \quad & \sqrt{\varepsilon}\|D_y^- U_\varepsilon - D_y U_{FS}^{8192}\|_{\Omega_\varepsilon^N} && \leq 2.46 N^{-0.73} \\
\beta = 1.0 \quad & \sqrt{\varepsilon}\|D_y^- U_\varepsilon - D_y U_{FS}^{8192}\|_{\Omega_\varepsilon^N} && \leq 3.77 N^{-0.71} \\
\beta = 1.5 \quad & \sqrt{\varepsilon}\|D_y^- U_\varepsilon - D_y U_{FS}^{8192}\|_{\Omega_\varepsilon^N} && \leq 161.95 N^{-0.58}
\end{aligned}
\tag{4.8}
$$

$$
\begin{aligned}
\beta = 0.5 \quad & \|D_y^- V_\varepsilon - D_y V_{FS}^{8192}\|_{\Omega_\varepsilon^N\backslash\Gamma_L} && \leq 4.70 N^{-0.74} \\
\beta = 1.0 \quad & \|D_y^- V_\varepsilon - D_y V_{FS}^{8192}\|_{\Omega_\varepsilon^N\backslash\Gamma_L} && \leq 3.17 N^{-0.66} \\
\beta = 1.5 \quad & \|D_y^- V_\varepsilon - D_y V_{FS}^{8192}\|_{\Omega_\varepsilon^N\backslash\Gamma_L} && \leq 13.13 N^{-0.61}.
\end{aligned}
\tag{4.9}
$$

4.6 Computational error bounds

In this section we use the computed error estimates, obtained in Section 3.6 for the quantities $(U_{\mathrm{B}}^{8192}, V_{\mathrm{B}}^{8192})$ and their scaled discrete derivatives, to estimate the error in the numerical approximations $(U_\varepsilon, \frac{1}{V^*}V_\varepsilon)$ generated by the direct method $(A_\varepsilon^{\mathbf{N}})$. We present an independent estimate of the maximum pointwise errors in the numerical solutions generated by the direct algorithm. The resulting estimates are independent of those obtained in Section 4.4.

First, we use the triangle inequality to obtain

$$
\begin{aligned}
\|U_\varepsilon - u_{\mathrm{W}}\|_{\Omega_\varepsilon^N} &= \|U_\varepsilon - u_{\mathrm{FS}}\|_{\Omega_\varepsilon^N} \\
&\leq \|U_\varepsilon - U_{\mathrm{FS}}^{8192}\|_{\Omega_\varepsilon^N} + \|U_{\mathrm{FS}}^{8192} - u_{\mathrm{FS}}\|_{\Omega_\varepsilon^N} \quad (4.10) \\
\frac{1}{V^*}\|V_\varepsilon - v_{\mathrm{FS}}\|_{\overline{\Omega}_\varepsilon^N \setminus \Gamma_{\mathrm{L}}} &= \frac{1}{V^*}\|V_\varepsilon - v_{\mathrm{FS}}\|_{\overline{\Omega}_\varepsilon^N \setminus \Gamma_{\mathrm{L}}} \\
&\leq \frac{1}{V^*}(\|V_\varepsilon - V_{\mathrm{FS}}^{8192}\|_{\overline{\Omega}_\varepsilon^N \setminus \Gamma_{\mathrm{L}}} + \|V_{\mathrm{FS}}^{8192} - v_{\mathrm{FS}}\|_{\overline{\Omega}_\varepsilon^N}) \quad (4.11)
\end{aligned}
$$

where $\mathbf{U}_\varepsilon = (U_\varepsilon, V_\varepsilon)$ is the solution generated by the direct algorithm $(A_\varepsilon^{\mathbf{N}})$ on the mesh $\Omega_\varepsilon^{\mathbf{N}}$ with $\mathbf{N} = (N, N)$; $\mathbf{u}_{\mathrm{FS}} = (u_{\mathrm{FS}}, v_{\mathrm{FS}})$ is the exact solution of the Prandtl problem constructed from the Falkner Skan formulae (3.3) and (3.4) and $\mathbf{U}_{\mathrm{FS}}^{8192} = (U_{\mathrm{FS}}^{8192}, V_{\mathrm{FS}}^{8192})$ is the computed Falkner Skan solution generated in the previous chapter on a mesh with 8192 intervals. We then observe that the first term on the right–hand side of (4.10) and (4.11) involves the computable quantities $U_\varepsilon, U_{\mathrm{FS}}^{8192}$ and $V_\varepsilon, V_{\mathrm{FS}}^{8192}$, respectively. Furthermore, the second term on each right–hand side of (4.10) and (4.11) involves the scaled pointwise errors $U_{\mathrm{FS}}^{8192} - u_{\mathrm{FS}}$, $\frac{1}{V^*}(V_{\mathrm{FS}}^{8192} - v_{\mathrm{FS}})$, which have already been estimated in Section 3.7 of the previous chapter. This shows that we can estimate the errors in the scaled numerical solutions and their scaled discrete derivatives, generated by the numerical method $(A_\varepsilon^{\mathbf{N}})$ applied to problem (P_ε), even though no theoretical error analysis is available for this numerical method.

We now compare the magnitudes of the two terms on the right–hand side of both (4.10) and (4.11). The first terms are the scaled maximum pointwise differences $\|U_\varepsilon - U_{\mathrm{FS}}^{8192}\|_{\overline{\Omega}_\varepsilon^N}$ and $\frac{1}{V^*}|V_\varepsilon - V_{\mathrm{FS}}^{8192}\|_{\overline{\Omega}_\varepsilon^N \setminus \Gamma_{\mathrm{L}}}$. These quantities are found immediately from the solutions $\mathbf{U}_\varepsilon$ of $(A_\varepsilon^{\mathbf{N}})$ and the solution $\mathbf{U}_{\mathrm{FS}}^{8192}$, respectively, computed in the previous section and chapter. Their numerical bounds are given in Tables 4.14 and 4.15 for various values of ε, N and β. The second terms on the right–hand side of (4.10) and (4.11) are the scaled maximum pointwise errors $\|U_{\mathrm{FS}}^{8192} - u_{\mathrm{FS}}\|_{\Omega_\varepsilon^N}$ and $\frac{1}{V^*}\|V_{\mathrm{FS}}^{8192} - v_{\mathrm{FS}}\|_{\Omega_\varepsilon^N}$ in the computed computed Falkner-Skan solution. The corresponding error bounds (3.31) and (3.33), respectively, show that the second terms are bounded above

by 1.597×10^{-4} and 2.869×10^{-3} for all β.

$$
\begin{aligned}
\|U_\varepsilon - u_{\mathrm{W}}\|_{\Omega_\varepsilon^N} &= \|U_\varepsilon - u_{\mathrm{FS}}\|_{\Omega_\varepsilon^N} \\
&\leq \|U_\varepsilon - U_{\mathrm{FS}}^{8192}\|_{\Omega_\varepsilon^N} + \|U_{\mathrm{FS}}^{8192} - u_{\mathrm{FS}}\|_{\Omega_\varepsilon^N}
\end{aligned}
$$

$$
\begin{aligned}
\beta = 0.5 & \qquad \leq \quad 0.69 N^{-0.95} + 1.597 \times 10^{-4} \\
\beta = 1.0 & \qquad \leq \quad 0.14 N^{-0.80} + 1.597 \times 10^{-4} \\
\beta = 1.5 & \qquad \leq \quad 1.61 N^{-0.57} + 1.597 \times 10^{-4}
\end{aligned}
\tag{4.12}
$$

$$
\begin{aligned}
\tfrac{1}{V^*}\|V_\varepsilon - v_{\mathrm{W}}\|_{\Omega_\varepsilon^N} &= \tfrac{1}{V^*}\|V_\varepsilon - v_{\mathrm{FS}}\|_{\Omega_\varepsilon^N} \\
&\leq \tfrac{1}{V^*}\|V_\varepsilon - V_{\mathrm{FS}}^{8192}\|_{\Omega_\varepsilon^N} + \tfrac{1}{V^*}\|V_{\mathrm{FS}}^{8192} - v_{\mathrm{FS}}\|_{\Omega_\varepsilon^N}
\end{aligned}
$$

$$
\begin{aligned}
\beta = 0.5 & \qquad \leq \quad 2.05 N^{-0.82} + 2.869 \times 10^{-3} \\
\beta = 1.0 & \qquad \leq \quad 0.51 N^{-0.81} + 2.869 \times 10^{-3} \\
\beta = 1.5 & \qquad \leq \quad 2.34 N^{-0.90} + 2.869 \times 10^{-3}
\end{aligned}
\tag{4.13}
$$

The computational error bounds for U_ε and V_ε in (4.12), (4.13), (10.1) and (10.2) give two workable formulas for each velocity component to ensure the error is below a desired value for all ε and β. In a similar manner to the above we calculate computed error bounds for approximations of the scaled first derivatives $\sqrt{\varepsilon} D_y^- U_\varepsilon$ and $D_y^- V_\varepsilon$ by the bounds (3.40), (3.43), (4.8) and (4.9)

$$
\begin{aligned}
\sqrt{\varepsilon}\|D_y^- U_\varepsilon - \partial_y u_{\mathrm{W}}\|_{\Omega_\varepsilon^N \setminus \Gamma_B} &= \sqrt{\varepsilon}\|D_y^- U_\varepsilon - \partial_y u_{\mathrm{FS}}\|_{\Omega_\varepsilon^N \setminus \Gamma_B} \\
&\leq \sqrt{\varepsilon}\|D_y^- U_\varepsilon - D_y U_{\mathrm{FS}}^{8192}\|_{\Omega_\varepsilon^N \setminus \Gamma_B} + \\
&\quad\ \sqrt{\varepsilon}\|D_y U_{\mathrm{FS}}^{8192} - \partial_y u_{\mathrm{FS}}\|_{\Omega_\varepsilon^N \setminus \Gamma_B}
\end{aligned}
$$

$$
\begin{aligned}
\beta = 0.5 & \qquad \leq \quad 2.46 N^{-0.73} + 2.432 \times 10^{-3} \\
\beta = 1.0 & \qquad \leq \quad 3.77 N^{-0.71} + 2.432 \times 10^{-3} \\
\beta = 1.5 & \qquad \leq \quad 161.95 N^{-0.58} + 2.432 \times 10^{-3}
\end{aligned}
\tag{4.14}
$$

$$
\begin{aligned}
\|D_y^- V_\varepsilon - \partial_y v_{\mathrm{W}}\|_{\Omega_\varepsilon^N \setminus \Gamma_B} &= \|D_y^- V_\varepsilon - \partial_y v_{\mathrm{FS}}\|_{\Omega_\varepsilon^N \setminus \Gamma_B} \\
&\leq \|D_y^- V_\varepsilon - D_y V_{\mathrm{FS}}^{8192}\|_{\Omega_\varepsilon^N \setminus \Gamma_B} + \\
&\quad\ \|D_y V_{\mathrm{FS}}^{8192} - \partial_y v_{\mathrm{FS}}\|_{\Omega_\varepsilon^N \setminus \Gamma_B}
\end{aligned}
$$

$$
\begin{aligned}
\beta = 0.5 & \qquad \leq \quad 4.07 N^{-0.74} + 1.794 \times 10^{-3} \\
\beta = 1.0 & \qquad \leq \quad 3.17 N^{-0.66} + 1.794 \times 10^{-3} \\
\beta = 1.5 & \qquad \leq \quad 13.13 N^{-0.61} + 1.794 \times 10^{-3}.
\end{aligned}
\tag{4.15}
$$

It is worth noting that, strictly speaking, the experimental error analysis technique is not known to be applicable to the numerical solutions generated by the algorithm

(A_ε^N) applied to the problem (P_ε), because currently there is no theoretical error analysis known to be available. Nevertheless it is clear from the results in this chapter that the experimental error analysis technique provides a means to estimate the accuracy of the numerical approximations to the unknown continuous solution and its derivatives even when no theoretical error estimates are known.

4.7 Conclusion

In Chapters 3 and 4 we considered the Prandtl boundary layer equations for incompressible laminar flow past a wedge with angle $\beta\pi$, $\beta \in [0.0, 1.5]$. When the Reynolds number is large the solution of this problem has a parabolic boundary layer. We constructed a direct numerical method for computing approximations to the solution of this problem using a piecewise uniform fitted mesh technique appropriate to the parabolic boundary layer. We used the method to approximate the self–similar solution of the Prandtl problem in a finite rectangle excluding the leading edge of the wedge for various values of Re and β. To analyse the efficiency of the numerical method, we constructed and applied a special numerical method related to the computed Falkner–Skan technique to compute reference solutions for the error analysis of the velocity components and their derivatives. By means of extensive numerical experiments we showed that the constructed direct numerical method is ε and β uniform.

Chapter 5

Prandtl flow past a three dimensional semi-infinite yawed wedge – Blasius method

5.1 Introduction

In this chapter and the next we expand the numerical method developed in Chapters 3 and 4 by introducing the velocity component in the z direction. We investigate incompressible laminar flow past a three dimensional semi-infinite yawed wedge W in the domain $D = \mathbf{R}^3 \backslash W$.

In this chapter we use a variant of the semi-analytic approach of Blasius to generate numerical approximations of guaranteed pointwise accuracy to the flow variables and their scaled derivatives. We use the approximate solution, which has known accuracy, to estimate the error to the approximates obtained later by the direct numerical method.

In the following chapter, we construct a direct numerical method to generate numerical approximations of guaranteed accuracy to the flow variables and their scaled derivatives. Although there are at present no theoretical error estimates for the resulting numerical solutions, we determine accuracy by means of extensive numerical experiments and by comparisons with the previously determined semi–analytic approximations. We show that the numerical approximations are pointwise accurate and that they satisfy pointwise error estimates that are uniform with respect to the Reynolds number and the angle of the wedge.
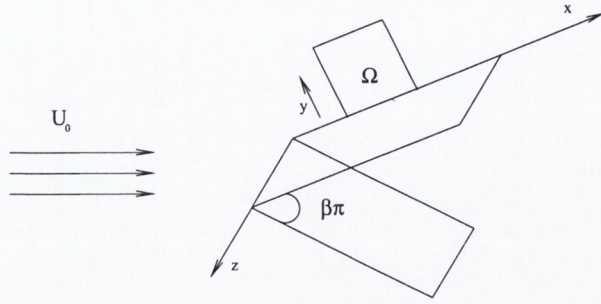
Figure 5-1: Flow past a wedge.

We want to solve the Prandtl problem in a region including the parabolic boundary layer. Since the solution of the problem has another singularity at the leading edge of the wedge [46], we take as the computational domain the finite rectangle $\Omega = (0.1 + \gamma(\beta), 1.1 + \gamma(\beta)) \times (0, 1)$, defined in Chapter 3 on the upper side of the wedge in the x, y plane, which is sufficiently far from the leading edge (see fig. 5-1) that the leading edge singularity does not cause problems for the numerical method. As we intend to solve the Prandtl boundary layer numerically we must compute the approximate solution on a finite domain Ω. The Prandtl boundary layer problem on a finite domain, Ω, is

$$(P_{3W}) \begin{cases} \text{Find } \mathbf{u_{3W}} = (u_{3W}, v_{3W}, w_{3W}) \text{ such that for all } (x, y) \in \Omega \\ \mathbf{u}_{3W} \text{ satisfies the differential equations} \\[2mm] -\frac{1}{Re}\frac{\partial^2 u_{3W}}{\partial^2 y} + u_{3W}\frac{\partial v_{3W}}{\partial x} + v_{3W}\frac{\partial u_{3W}}{\partial y} = U\frac{dU}{dx} \\[2mm] -\frac{1}{Re}\frac{\partial^2 w_{3W}}{\partial^2 y} + u_{3W}\frac{\partial w_{3W}}{\partial x} + v_{3W}\frac{\partial w_{3W}}{\partial y} = 0 \\[2mm] \frac{\partial u_{3W}}{\partial x} + \frac{\partial v_{3W}}{\partial y} = 0 \\[2mm] \text{with boundary conditions} \\ u_{3W} = 0, \quad w_{3W} = 0 \text{ and } v_{3W} = 0 \text{ on } \Gamma_B \\ \mathbf{u}_{3W} = \mathbf{u}_P \ \Gamma_L \bigcup \Gamma_T \end{cases}$$

where $U(x) = x^m$, $m = \frac{\beta}{2-\beta}$ and $\beta\pi$ is the angle of the wedge in radians and u_P is the exact solution of (P_P).

The momentum equation for the x-direction velocity component u_{3W} and the continuity equation for the y-direction velocity component v_{3W} are analogous to the momentum and continuity equations from the problem (P_W) in Chapter 3. The new

momentum equation for the z-direction velocity component w_{3W} is of the same form as the flat plate momentum equation in Chapter 2. Note that for the flat plate ($\beta = 0$) the two momentum equations are identical. Hence the velocity components in the x and z direction are equal: $u_{3W} = w_{3W}$.

Our goal in Chapters 5 and 6 is to construct an (Re, β)–uniform numerical method for solving (P_{3W}), so that the method has error bounds for the solution and its derivatives, independent of Re and β for all $Re \in [1, \infty)$ and all $\beta \in [0.0, 1.5]$.

5.2 Blasius solution

Using the similarity transformation described in [45]

$$\eta = y\sqrt{\frac{(m+1)Re}{2}\frac{U}{x}} \tag{5.1}$$

the velocity components of the Blasius solution $\mathbf{u}_{3B}$ of (P_{3W}) are given by

$$u_{3B}(x,y) = x^m f'(\eta) = U f'(\eta) \tag{5.2}$$

$$v_{3B}(x,y) = -\sqrt{\frac{m+1}{2x}\frac{U}{Re}}\left(f + \frac{m-1}{m+1}\eta f'\right) \tag{5.3}$$

$$w_{3B}(x,y) = g \tag{5.4}$$

where f and g are the solutions of the non–linear ordinary differential equations

$$(P_{3B}) \begin{cases} \text{For } \eta \in (0, \infty) \text{ find } g, \ f \in C^3(0, \infty) \\\\ f''' + ff'' + \beta(1 - f'^2) = 0 \\\\ g'' + fg' = 0 \\\\ \text{with boundary conditions} \\ f(0) = f'(0) = 0, \qquad\qquad \lim_{\eta\to\infty} f'(\eta) = 1. \\ g(0) = 0, \qquad\qquad \lim_{\eta\to\infty} g(\eta) = 1. \end{cases}$$

The problem in (P_{3B}) is known as the computed Blasius equations and in what follows we refer to $\mathbf{u}_{3B}$ as the Blasius solution of (P_{3W}).

The two equations in (P_{3B}) are semi-coupled equations. The first equation is the third order non–linear ordinary differential equation on the semi-infinite domain $(0, \infty)$ for

f, which was dealt with in Chapter 3. The second equation is a second order ordinary differential equation on the semi-infinite domain $(0, \infty)$ for g and f. The problem (P_{3B}) can be solved numerically on any bounded domain I of $(0, \infty)$. In what follows we solve the Blasius problem (P_{3B}) numerically for the functions f, g and their derivatives. We then use the analytic relations (5.2), (5.3) and (5.4) to construct Reynolds uniform analytic approximations with guaranteed accuracy to the solution $\mathbf{u}_{3W}$ of (P_{3W}) for all relevant values of the Reynolds number and angles of the wedge at all points of the domain Ω.

To achieve this it is clear that we need Reynolds uniform pointwise accuracy of $f(\eta)$, $f'(\eta)$, $f''(\eta)$, $g(\eta)$ and $g'(\eta)$ for all $\eta \in (0, \infty)$. We have constructed a method for f and its derivatives in Chapter 3. We now adapt and extend this to include g and g'.

5.3   Singularly perturbed nature of Blasius problem

We have shown the singularly perturbed nature of the first ordinary differential equation of f in Section 3.3. Using similar arguments we show the singularly perturbed nature of the second ordinary differential equation of g and f of (P_{3B}). In the next section we use this observation to motivate the construction of the numerical method for solving (P_{3B}).

We observe that while we need the solution of (P_{3B}) on an infinite interval, in practice we can find numerical solutions only on a finite interval. For this reason we introduce a one-parameter family of problems related to (P_{3B}) on the finite interval $(0, L)$ where the length L of the interval is taken as the parameter of the family. The typical problem in this family is defined for each value of L in the range $1 \leq L \leq \infty$ by

$$g_L''(\eta) + f_L(\eta)g_L'(\eta) = 0 \qquad \eta \in [0, L) \tag{5.5}$$

$$g_L(0) = 0, \qquad g_L(L) = 1 \tag{5.6}$$

When we reformulate (5.5) as a singularly perturbed problem, it turns out that $\frac{1}{L}$ is the singular perturbation parameter and so it is appropriate to introduce the temporary notation $\varepsilon = \frac{1}{L}$. Then the problem (5.5) can be written in the form

$$g_\varepsilon''(\eta) + f_\varepsilon(\eta)g_\varepsilon'(\eta) = 0 \qquad g_\varepsilon(0) = 0 \qquad g_\varepsilon(\frac{1}{\varepsilon}) = 1.$$

Changing variables from η to $\xi = \varepsilon\eta$, which is equivalent to a mapping of the interval $[0, \frac{1}{\varepsilon}]$ to the unit interval $[0, 1]$, and writing $k_\varepsilon(\xi) = g_\varepsilon(\eta)$ and $h(\xi) = f_\varepsilon(\eta)$ we obtain

$$\varepsilon k_\varepsilon''(\xi) + h_\varepsilon(\xi) k_\varepsilon'(\xi) = 0 \quad k_\varepsilon(0) = 0 \quad k_\varepsilon(1) = 1 \qquad (5.7)$$

where $h(0) = 0$ and $h(\xi) = O(\xi)$ for all $\xi \geq \varepsilon$. This is a singularly perturbed problem for k_ε with a boundary layer at $\xi = 0$. In what follows it is natural to refer to L-uniform methods for (5.5). These are defined in an analogous way to ε-uniform methods.

5.4 Robust layer resolving method for Blasius problem

Our strategy for computing L-uniform approximations to the solution of (P_{3B}) is to obtain a numerical solution F_L and G_L for problem (5.5), on the interval $[0, L]$, for an increasing sequence of values of the length L. Since, for each L, we need the values of f_L, f_L', f_L'', g_L and g_L' at all points of the interval $(0, \infty)$, we extend the domain of f_L, f_L' and f_L'' from $[0, L]$ to the semi-infinite interval $[0, \infty)$ by extrapolations defined in 3.7-3.9. We extend the domain of g_L and g_L' from $[0, L]$ to the semi-infinite interval $[0, \infty)$ by defining the following extrapolation

$$g'(\eta) = 0, \text{ for all } \eta \geq L \qquad (5.8)$$
$$g(\eta) = 1, \text{ for all } \eta \geq L. \qquad (5.9)$$

We now describe our numerical method for finding approximations to the solution and its derivatives of problem (P_{3B}). For each fixed N we write $L_N = lnN$ and we divide the interval into the two subintervals $[0, L_N]$ and $[L_N, \infty)$. We construct a uniform mesh

$$\overline{I}_u^N = \{\eta_i \ : \ \eta_i = iN^{-1}nN, 0 \leq i \leq N\}_0^N$$

on the subinterval $[0, L_N]$ and we determine numerical approximations F, D^+F, D^+D^+F, G and D^+G to f_L, f_L', f_L'' g and g', respectively, at the mesh points $\overline{I}_u^N$

using the nonlinear finite difference method

(P_{3B}^N)
$\begin{cases}
\text{Find } F \text{ and } G \text{ on } I_u^N \text{such that, for all } \eta \in I_u^N, \ 2 \le i \le N-1 \\[2ex]
\delta^2(D^-F_i) + F_i(D^+(D^-F_i)) + \beta(1 - (D^-F_i)(D^-F_i)) = 0 \\[2ex]
\delta^2 G_i + F_i(D^+G_i) = 0 \\[2ex]
\text{with boundary conditions} \\
F(0) = D^+F(0) = 0, \qquad\qquad D^0F(\eta_{N-1}) = 1 \\
G(0) = 0, \qquad\qquad G(\eta_N) = 1.
\end{cases}$

In practice, since (P_{3B}^N) is non–linear we need a non–linear solver to compute its solution. Using a variation of the continuation algorithm defined in Section 3.5 with the continuation parameter m

(A_{3B}^N)
$\begin{cases}
\text{For each integer } m, \ 1 \le m \le M \text{ find } F^m \text{ on } I_u^N \\
\text{such that, for all } \eta \in I_u^N, \ 2 \le i \le N-1 \\[2ex]
\delta^2(D^-F_i^m) + F_i^{m-1}(D^+(D^-F_i^m)) + \beta(1 - (D^-F_i^{m-1})(D^-F_i^m)) \\
-(1+\beta)(D^-F_i^m - D^-F_i^{m-1}) = 0 \\[2ex]
\text{with boundary conditions} \\
F(0) = D^+F(0) = 0, \qquad\qquad D^0F(\eta_{N-1}) = 1 \\[2ex]
\text{with an initial guess of } F^0(\eta_i) = \eta_i. \\
\text{Finally, find } G \text{ on } I_u^N \\
\text{such that, for all } \eta \in I_u^N, \ 1 \le i \le N-1 \\[2ex]
\delta^2 G_i + F_i^M(D^+G_i) = 0 \\[2ex]
\text{with boundary conditions} \\
G(0) = 0, \qquad\qquad G(\eta_N) = 1.
\end{cases}$

We assign the value $D^+G(\eta_N) = 0$, so that D^+G is defined at all points of the mesh $\overline{I}_u^N$. We then use piecewise linear interpolation to interpolate from $\overline{I}_u^N$ to each point of the subinterval $[0, L_N]$. We denote the corresponding interpolants by $\overline{G}$ and $\overline{D^+G}$. We extend these functions to the whole of the semi-infinite interval $[0, \infty)$ in

an analogous way to the extensions (5.8) and (5.9) of their continuous counterparts, that is

$$\overline{D^+G}(\eta) = 0, \text{ for all } \eta \in [L_N, \infty) \tag{5.10}$$

$$\overline{G}(\eta) = 1, \text{ for all } \eta \in [L_N, \infty). \tag{5.11}$$

We take the values of G and D^+G, respectively, to be the required numerical approximations to the exact values g and g' of the Blasius solution and its derivatives on the semi-infinite interval $[0, \infty)$.

5.5   Numerical solution of the Blasius problem

As the numerical results for F, D^+F and D^+D^+F have been extensively investigated in Section 3.6, we only need to investigate the numerical results of G and D^+G for various values of β. The definitions of the computed pointwise maximum errors E^N, the pointwise two mesh difference D^N and the two mesh orders of convergence are given in Section 3.6. We choose $\beta = 0.5, \beta = 1.0$ and $\beta = 1.5$ to be consistent with Chapters 3 and 4. For $\beta = 0.5, 1.0$ and 1.5 the computed maximum pointwise error E^N, computed two mesh difference D^N and the computed order of convergence p^N for $\overline{G}$ and $\overline{D^+G}$, are given by Tables 5.1 and 5.2, respectively.

				$\beta = 0.5$				
N	128	256	512	1024	2048	4096	8192	16384
E^N	0.008064	0.004623	0.002589	0.001424	0.000767	0.000402	0.000201	0.000091
D^N	0.003432	0.002032	0.001166	0.000657	0.000365	0.000201	0.000110	0.000059
p^N	0.76	0.80	0.83	0.85	0.86	0.87	0.88	0.89
				$\beta = 1.0$				
E^N	0.008493	0.004860	0.002722	0.001497	0.000806	0.000422	0.000211	0.000096
D^N	0.003632	0.002138	0.001225	0.000690	0.000384	0.000211	0.000115	0.000062
p^N	0.76	0.80	0.83	0.85	0.86	0.87	0.88	0.89
				$\beta = 1.5$				
E^N	0.008745	0.005001	0.002801	0.001540	0.000830	0.000435	0.000217	0.000099
D^N	0.003738	0.002197	0.001260	0.000710	0.000395	0.000217	0.000119	0.000064
p^N	0.77	0.80	0.83	0.85	0.86	0.87	0.88	0.89

Table 5.1: Computed maximum pointwise error E^N, computed two mesh difference D^N and computed order of convergence p^N for $\bar{G}$ on $\overline{T}_u^N$ generated by (A_{3B}^N) with $M = 8nN$ applied to problem (P_{3B}) for various values of N and β.

$\beta = 0.5$							
N	128	256	512	1024	2048	4096	8192	16384
E^N	0.008727	0.004998	0.002799	0.001539	0.000829	0.000434	0.000217	0.000099
D^N	0.003729	0.002199	0.001260	0.000710	0.000395	0.000217	0.000118	0.000064
p^N	0.76	0.80	0.83	0.85	0.86	0.87	0.88	0.89
$\beta = 1.0$							
E^N	0.009891	0.005658	0.003168	0.001742	0.000938	0.000492	0.000246	0.000112
D^N	0.004233	0.002490	0.001427	0.000804	0.000447	0.000246	0.000134	0.000073
p^N	0.77	0.80	0.83	0.85	0.86	0.87	0.88	0.89
$\beta = 1.5$							
E^N	0.010665	0.006098	0.003414	0.001877	0.001011	0.000530	0.000265	0.000120
D^N	0.004567	0.002683	0.001537	0.000866	0.000481	0.000265	0.000144	0.000078
p^N	0.77	0.80	0.83	0.85	0.86	0.87	0.88	0.89

Table 5.2: Computed maximum pointwise error E^N, computed two mesh difference D^N and computed order of convergence p^N for $\overline{D^+G}$ on $\overline{I}_u^N \backslash \{\eta_N\}$ generated by (A_{3B}^N) with $M = 8nN$ applied to problem (P_{3B}) for various values of N and β.

Comparison of the entries in the p^N rows of Tables 5.1 and 5.2 with the Table of theoretical behaviour of the order of convergence defined p^N in Appendix B, suggests strongly that the computed order of L-uniform convergence p^N corresponds to the theoretical behaviour $N^{-1}nN$.

From Tables 5.1 and 5.2 we see that the L-uniform order of convergence on $[0, L_N]$ of the numerical solution G of the exact G_L and of the discrete derivative D^+G to the derivative g'_L, is, in practice, better than 0.8 for all $N \geq 512$ and β.

Graphs of $\overline{G}$ for $N = 8192$ and various values of β on $[0, L_N]$ are given in Figure 5-2. We can see that there is a region of rapid change near $\eta = 0$.
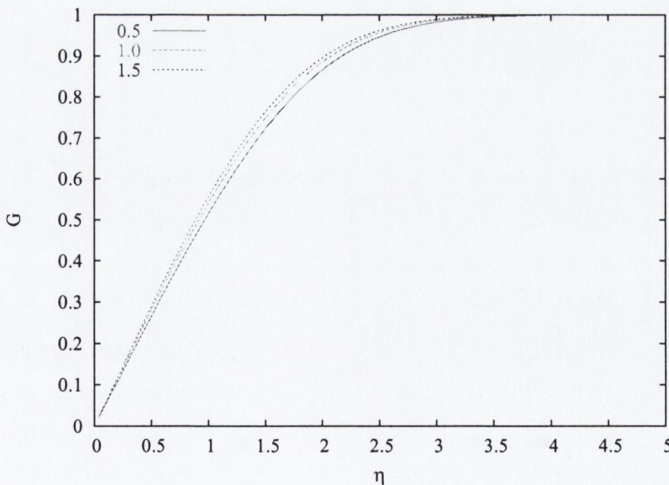
Figure 5-2: Solution $\overline{G}$ generated by method (A_{3B}^N) applied to the problem P_{3B} with $M = 8nN$, $N = 8192$ and various values of β.

Graphs of $\overline{D^+G}$ for $N = 8192$ and various values of β on $[0, L_N]$ are given in Figure 5-3. We see that there is an subtle difference for each value of β.
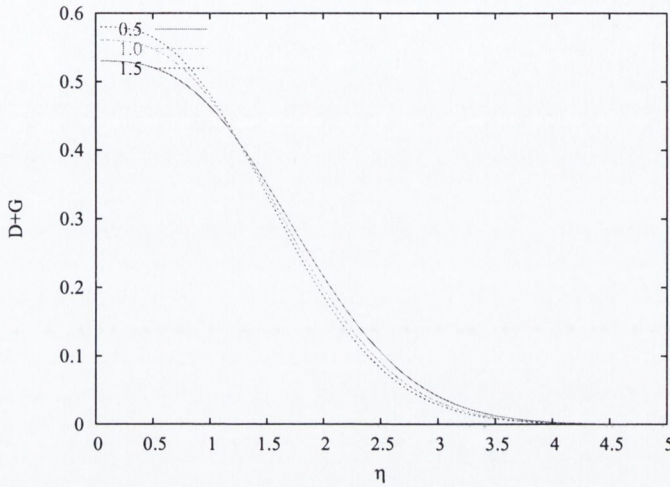
Figure 5-3: Solution $\overline{D^+G}$ generated by method (A_{3B}^N) applied to the problem P_{3B} with $M = 8nN$, $N = 8192$ and various values of β.

5.6   Computed error estimates for Blasius problem

Theoretical estimates in [26] indicate that, for all $N \geq N_0$, the approximations of $\overline{G}$ and $\overline{D^+G}$, respectively, to the exact solution of the computed Blasius problem (P_{3B}) and its derivatives satisfy error bounds of the form

$$||\overline{G} - g||_{[0,\infty)} \leq C_p N^{-p} \tag{5.12}$$

$$||\overline{D^+G} - g||_{[0,\infty)} \leq C_p N^{-p} \tag{5.13}$$

where the error parameters are unknown. The computed two–mesh difference, computed order of convergence, computed global order of convergence and the computed global constant error are defined in Section 3.6.

We now use the experimental techniques to obtain computed parameter uniform global error parameters for the function $\overline{G}$ on the semi-infinite interval $[0, \infty)$ for various β. To determine the two mesh differences $\overline{D}$ and hence the computed order of convergence $\overline{p}^N$ and the constant of convergence $\overline{C}_{\overline{p}^*}^N$ for a pair of meshes with N and 2N points respectively, we have to consider the three subintervals $[0, L_N)$, $[L_N, L_{2N})$ and $[L_{2N}, \infty)$ separately. For $\eta \in [L_N, L_{2N})$ the two mesh difference at η for $\overline{G}$ is $\overline{G}^{2N}(\eta) - 1$ and for $\overline{D^+G}$ is $\overline{D^+G}^{2N}(\eta)$. In the subinterval $[L_{2N}, \infty)$ the two

mesh difference at η for $\overline{G}$ and $\overline{D^+G}$ is zero. The resulting computed global two-mesh difference $\overline{D}$, the computed order of convergence $\overline{p}^N$ and the constant of convergence $\overline{C}_{\overline{p}^*}^N$ for $\overline{G}$, $\overline{D^+G}$ and $\eta\overline{D^+G}$ for various values of N and β are given in Tables 5.3, 5.4 and 5.5.

				$\beta = 0.5$				
N	128	256	512	1024	2048	4096	8192	16384
D^N	0.003432	0.002032	0.001166	0.000657	0.000365	0.000201	0.000110	0.000059
p^N	0.76	0.80	0.83	0.85	0.86	0.87	0.88	0.89
$C_{0.86}^N$	0.499628	0.537599	0.560498	0.573756	0.579885	0.579885	0.574990	0.566100
				$\beta = 1.0$				
D^N	0.003632	0.002138	0.001225	0.000690	0.000384	0.000211	0.000115	0.000062
p^N	0.76	0.80	0.83	0.85	0.86	0.87	0.88	0.89
$C_{0.86}^N$	0.528981	0.566006	0.589314	0.603358	0.609859	0.609859	0.604763	0.595449
				$\beta = 1.5$				
D^N	0.003738	0.002197	0.001260	0.000710	0.000395	0.000217	0.000119	0.000064
p^N	0.77	0.80	0.83	0.85	0.86	0.87	0.88	0.89
$C_{0.86}^N$	0.544352	0.581488	0.606184	0.620732	0.627382	0.627382	0.622128	0.612524

Table 5.3: Computed two mesh difference $\overline{D}^N$, order of convergence $\overline{p}^N$ and the constant of convergence $\overline{C}_{\overline{p}^*}^N$ for $\bar{G}$ on $[0,\infty)$ generated by (A_{3B}^N) with $M = 8nN$ applied to problem (P_{3B}) for various values of N and β.

				$\beta = 0.5$				
N	128	256	512	1024	2048	4096	8192	16384
D^N	0.003729	0.002199	0.001260	0.000710	0.000395	0.000217	0.000118	0.000064
p^N	0.76	0.80	0.83	0.85	0.86	0.87	0.88	0.89
$C_{0.86}^N$	0.543034	0.582001	0.606187	0.620558	0.627033	0.627033	0.621739	0.612148
				$\beta = 1.0$				
D^N	0.004233	0.002490	0.001427	0.000804	0.000447	0.000246	0.000134	0.000073
p^N	0.77	0.80	0.83	0.85	0.86	0.87	0.88	0.89
$C_{0.86}^N$	0.616475	0.658970	0.686236	0.702504	0.709835	0.709835	0.703842	0.692985
				$\beta = 1.5$				
D^N	0.004567	0.002683	0.001537	0.000866	0.000481	0.000265	0.000144	0.000078
p^N	0.77	0.80	0.83	0.85	0.86	0.87	0.88	0.89
$C_{0.86}^N$	0.665188	0.710322	0.739632	0.757142	0.765034	0.765034	0.758581	0.746888

Table 5.4: Computed two mesh difference $\bar{D}^N$, order of convergence $\overline{p}^N$ and the constant of convergence $\overline{C}_{\overline{p}^*}^N$ for $\overline{D^+G}$ on $[0,\infty)$ generated by (A_{3B}^N) with $M = 8nN$ applied to problem (P_{3B}) for various values of N and β.

				$\beta = 0.5$				
N	128	256	512	1024	2048	4096	8192	16384
D^N	0.003274	0.001947	0.001123	0.000634	0.000353	0.000195	0.000106	0.000058
p^N	0.75	0.79	0.82	0.84	0.86	0.87	0.88	0.89
$C_{0.86}^N$	0.474384	0.512433	0.536410	0.550549	0.556825	0.556825	0.552032	0.543206
				$\beta = 1.0$				
D^N	0.003418	0.002030	0.001173	0.000664	0.000370	0.000204	0.000111	0.000060
p^N	0.75	0.79	0.82	0.84	0.86	0.87	0.88	0.89
$C_{0.86}^N$	0.495212	0.533985	0.560548	0.575605	0.582181	0.582181	0.577162	0.567937
				$\beta = 1.5$				
D^N	0.003524	0.002085	0.001204	0.000681	0.000380	0.000209	0.000114	0.000062
p^N	0.76	0.79	0.82	0.84	0.86	0.87	0.88	0.89
$C_{0.86}^N$	0.510290	0.548284	0.574944	0.590122	0.597267	0.597267	0.592041	0.582533

Table 5.5: Computed two mesh difference $\bar{D}^N$, order of convergence $\bar{p}^N$ and the constant of convergence $\overline{C}_{\bar{p}}^N$ for $\overline{\eta D^+ G}$ on $[0, \infty)$ generated by (A_{3B}^N) with $M = 8nN$ applied to problem (P_{3B}) for various values of N and β.

The computed global error can be used to calculate the global error bounds for all values of $N \geq 256$, however in Chapter 6 we only need the value $N = 8192$. For this number of nodes we use Tables 5.3, 5.4 and 5.5 and the experimental technique to obtain the following error bounds for $N \geq 2048$

$$\begin{aligned}
\beta &= 0.5 & ||\overline{G} - g||_{[0,\infty)} &\leq 0.580 N^{-0.86} \\
\beta &= 1.0 & ||\overline{G} - g||_{[0,\infty)} &\leq 0.609 N^{-0.86} \\
\beta &= 1.5 & ||\overline{G} - g||_{[0,\infty)} &\leq 0.627 N^{-0.86}
\end{aligned} \tag{5.14}$$

$$\begin{aligned}
\beta &= 0.5 & ||\overline{D^+ G} - g'||_{[0,\infty)} &\leq 0.627 N^{-0.86} \\
\beta &= 1.0 & ||\overline{D^+ G} - g'||_{[0,\infty)} &\leq 0.710 N^{-0.86} \\
\beta &= 1.5 & ||\overline{D^+ G} - g'||_{[0,\infty)} &\leq 0.765 N^{-0.86}
\end{aligned} \tag{5.15}$$

$$\begin{aligned}
\beta &= 0.5 & ||\eta(\overline{D^+ G} - g')||_{[0,\infty)} &\leq 0.557 N^{-0.86} \\
\beta &= 1.0 & ||\eta(\overline{D^+ G} - g')||_{[0,\infty)} &\leq 0.582 N^{-0.86} \\
\beta &= 1.5 & ||\eta(\overline{D^+ G} - g')||_{[0,\infty)} &\leq 0.597 N^{-0.86}.
\end{aligned} \tag{5.16}$$

5.7 Computed global error estimates for the computed Blasius solution

Using the same techniques employed in Section 3.7, we obtain approximate expressions W_{3B} for the Blasius solution w_{3B} of (P_{3W}) by substituting into the relation (5.4) the approximations $\overline{G}$ and $\overline{D^+ G}$ for g and g', computed by (A_{3W}^N). Thus for each

(x, y) in the rectangle $\overline{\Omega}$ we define

$$W_{3B}(x, y) = \overline{G}(\eta) \tag{5.17}$$

where $\eta \in [0, \infty)$ is given by (5.1).

For the z-component W_{3B} of the velocity we obtain, from (5.17) and (5.14), the following computed error bound for all $N \geq 2048$

$$
\begin{aligned}
\beta = 0.5 \quad \|W_{3B} - w_{3B}\|_{\overline{\Omega}} &= \|\overline{G} - g\|_{[0,\infty)} \\
&\leq 0.580 N^{-0.86} \\
\beta = 1.0 \quad \|W_{3B} - w_{3B}\|_{\overline{\Omega}} &\leq 0.609 N^{-0.86} \\
\beta = 1.5 \quad \|W_{3B} - w_{3B}\|_{\overline{\Omega}} &\leq 0.627 N^{-0.86}.
\end{aligned} \tag{5.18}
$$

In the specific case $N = 8192$ the computed error bounds (5.18) become

$$
\begin{aligned}
\beta = 0.5 \quad \|W_{3B} - w_{3B}\|_{\overline{\Omega}} &\leq 2.543 \times 10^{-4} \\
\beta = 1.0 \quad \|W_{3B} - w_{3B}\|_{\overline{\Omega}} &\leq 2.625 \times 10^{-4} \\
\beta = 1.5 \quad \|W_{3B} - w_{3B}\|_{\overline{\Omega}} &\leq 2.702 \times 10^{-4}.
\end{aligned} \tag{5.19}
$$

In a similar manner to the above we calculate computed error bounds for approximations of the scaled first derivatives by scaled discrete derivatives

$$\partial_y W_{3B} = \frac{\eta}{y} \overline{D^+ G}(\eta) \tag{5.20}$$

$$\partial_x W_{3B} = \frac{m-1}{2x} \eta \overline{D^+ G}(\eta). \tag{5.21}$$

$$\frac{1}{\sqrt{Re}} \|\partial_y W_{3B} - \frac{\partial w_{3B}}{\partial y}\|_{\overline{\Omega}} = \frac{1}{\sqrt{Re}} \sqrt{\frac{(m+1) Re}{2} \frac{U(x)}{x}} \|\overline{D^+ G} - g'\|_{[0,\infty)}. \tag{5.22}$$

For $\partial_y W_{3B}$ we obtain, from (5.20) and (5.15), the following computed error bound for all $N \geq 2048$

$$
\begin{aligned}
\beta = 0.5 \quad \frac{1}{\sqrt{Re}} \|\partial_y W_{3B} - \frac{\partial w_{3B}}{\partial y}\|_{\overline{\Omega}} &\leq \sqrt{\frac{(1.333)}{2} \frac{1.1^{0.333}}{1.1}} (0.627 N^{-0.86}) \\
\beta = 1.0 \quad \frac{1}{\sqrt{Re}} \|\partial_y W_{3B} - \frac{\partial w_{3B}}{\partial y}\|_{\overline{\Omega}} &\leq \sqrt{\frac{(1)}{2} \frac{1.1^1}{1.1}} (0.710 N^{-0.86}) \\
\beta = 1.5 \quad \frac{1}{\sqrt{Re}} \|\partial_y W_{3B} - \frac{\partial w_{3B}}{\partial y}\|_{\overline{\Omega}} &\leq \sqrt{\frac{(4)}{2} \frac{1.1^3}{1.1}} (0.765 N^{-0.86}).
\end{aligned} \tag{5.23}
$$

In the specific case $N = 8192$ the computed error bounds

$$
\begin{aligned}
\beta = 0.5 \quad & \tfrac{1}{\sqrt{Re}} \| \partial_y W_{3B} - \tfrac{\partial w_{3B}}{\partial y} \|_{\overline{\Omega}} \le 1.822 \times 10^{-4} \\
\beta = 1.0 \quad & \tfrac{1}{\sqrt{Re}} \| \partial_y W_{3B} - \tfrac{\partial w_{3B}}{\partial y} \|_{\overline{\Omega}} \le 2.060 \times 10^{-4} \\
\beta = 1.5 \quad & \tfrac{1}{\sqrt{Re}} \| \partial_y W_{3B} - \tfrac{\partial w_{3B}}{\partial y} \|_{\overline{\Omega}} \le 2.223 \times 10^{-4}.
\end{aligned} \tag{5.24}
$$

For $\partial_x W_{3B}$ we obtain, from (5.21) and (5.16), the following computed error bound for all $N \ge 2048$

$$
\| \partial_x W_{3B} - \tfrac{\partial w_{3B}}{\partial x} \|_{\overline{\Omega}} = \tfrac{|m-1|}{2x} \| \eta (\overline{D^+ G} - g') \|_{[0,\infty)} \tag{5.25}
$$

$$
\begin{aligned}
\beta = 0.5 \quad & \| \partial_x W_{3B} - \tfrac{\partial w_{3B}}{\partial x} \|_{\overline{\Omega}} \le \tfrac{0.667}{2(1.1)}(0.557 N^{-0.86}) \\
\beta = 1.0 \quad & \| \partial_x W_{3B} - \tfrac{\partial w_{3B}}{\partial x} \|_{\overline{\Omega}} \le 0 \\
\beta = 1.5 \quad & \| \partial_x W_{3B} - \tfrac{\partial w_{3B}}{\partial x} \|_{\overline{\Omega}} \le \tfrac{3}{2(2.1)}(0.597 N^{-0.86}).
\end{aligned} \tag{5.26}
$$

In the specific case $N = 8192$ the computed error bounds become

$$
\begin{aligned}
\beta = 0.5 \quad & \| \partial_x W_{3B} - \tfrac{\partial w_{3B}}{\partial x} \|_{\overline{\Omega}} \le 7.275 \times 10^{-5} \\
\beta = 1.0 \quad & \| \partial_x W_{3B} - \tfrac{\partial w_{3B}}{\partial x} \|_{\overline{\Omega}} \le 0 \\
\beta = 1.5 \quad & \| \partial_x W_{3B} - \tfrac{\partial w_{3B}}{\partial x} \|_{\overline{\Omega}} \le 1.608 \times 10^{-4}.
\end{aligned} \tag{5.27}
$$

Chapter 6

A Reynolds uniform numerical method for the Prandtl boundary layer problem for flow past a three dimensional yawed wedge

6.1 Introduction

Using the same method as described in Chapter 4, we make use of the computed Blasius similarity solution of the Prandtl problem in Chapter 5 in two ways. Firstly, we use it to provide the required artificial boundary conditions on the boundary of Ω in the direct numerical method for the Prandtl problem.

Secondly, we use the computed Blasius similarity solution as a reference solution for the unknown exact solution in the expression for the error. Since the computed Blasius solution is known to converge (Re, β)–uniformly to the solution of the Prandtl problem, we can compute (Re, β)–uniform error bounds. For this purpose we use the computed Blasius solution for (P_{3B}) when $N=8192$, namely $\mathbf{U}_{3B}^{8192}$, which provides the required accuracy for the velocity components U_{3B}^{8192}, V_{3B}^{8192}, W_{3B}^{8192}, their derivatives $D_x V_{3B}^{8192}$, $D_y V_{3B}^{8192}$, $D_x W_{3B}^{8192}$ and their scaled derivatives $\sqrt{\varepsilon} D_y U_{3B}^{8192}$ and $\sqrt{\varepsilon} D_y W_{3B}^{8192}$. Again, it is convenient to introduce the notation $\varepsilon = \frac{1}{Re}$, to emphasise the singularly

perturbed nature of the problem. The problem (P_{3W}) in Chapter 5 is now written as

$$(P_{3\varepsilon}) \begin{cases} \text{Find } \mathbf{u_{3\varepsilon}} = (u_{3\varepsilon}, v_{3\varepsilon}, w_{3\varepsilon}) \text{ such that for all } (x, y) \in \Omega \\ \mathbf{u}_\varepsilon \text{ satisfies the differential equations} \\[2mm] -\varepsilon \frac{\partial^2 u_{3\varepsilon}}{\partial^2 y} + u_{3\varepsilon} \frac{\partial v_{3\varepsilon}}{\partial x} + v_{3\varepsilon} \frac{\partial u_{3\varepsilon}}{\partial y} = U \frac{dU}{dx} \\[3mm] -\varepsilon \frac{\partial^2 w_{3\varepsilon}}{\partial^2 y} + u_{3\varepsilon} \frac{\partial w_{3\varepsilon}}{\partial x} + v_{3\varepsilon} \frac{\partial w_{3\varepsilon}}{\partial y} = 0 \\[3mm] \frac{\partial u_{3\varepsilon}}{\partial x} + \frac{\partial v_{3\varepsilon}}{\partial y} = 0 \\[4mm] \text{with boundary conditions} \\ u_{3\varepsilon} = 0, \quad w_{3\varepsilon} = 0 \text{ and } v_{3\varepsilon} = 0 \text{ on } \Gamma_B \\ \mathbf{u_{3\varepsilon}} = \mathbf{u}_B \quad \Gamma_L \bigcup \Gamma_T \end{cases}$$

where $(U(x) = x^m, 0)$ is the solution of the reduced problem, $m = \frac{\beta}{2-\beta}$, and $\beta\pi$ is the angle in radians of the wedge.

6.2 Direct Numerical method for the Prandtl Problem

The aim of this section is to construct a direct numerical method to solve the Prandtl problem $(P_{3\varepsilon})$ for all $Re \in [1, \infty)$ and all $\beta \in [0, 1.5]$. We use the same piecewise uniform fitted mesh $\Omega_\varepsilon^{\mathbf{N}} = \Omega_u^{N_x} \times \Omega_\varepsilon^{N_y}$ in the rectangle Ω as defined in Chapter 4.

The problem $(P_{3\varepsilon})$ is discretised by the following non-linear upwind finite differ-

ence method on the piecewise uniform fitted mesh $\Omega_\varepsilon^{\mathbf{N}}$

$(P_{3\varepsilon}^N)$ $\begin{cases} \text{Find } \mathbf{U_{3\varepsilon}} = (U_{3\varepsilon}, V_{3\varepsilon}, W_{3\varepsilon}) \text{ such that for all mesh points } (x_i, y_j) \in \Omega_\varepsilon^{\mathbf{N}} \\ \mathbf{U_{3\varepsilon}} \text{ satisfies the finite mesh difference equations} \\[2mm] -\varepsilon \delta_y^2 U_{3\varepsilon}(x_i, y_j) + U_{3\varepsilon} D_x^- U_{3\varepsilon}(x_i, y_j) + V_{3\varepsilon} D_y^u U_{3\varepsilon}(x_i, y_j) = U \frac{dU}{dx} \\[3mm] -\varepsilon \delta_y^2 W_{3\varepsilon}(x_i, y_j) + U_{3\varepsilon} D_x^- W_{3\varepsilon}(x_i, y_j) + V_{3\varepsilon} D_y^u W_{3\varepsilon}(x_i, y_j) = 0 \\[3mm] D_x^- U_{3\varepsilon}(x_i, y_j) + D_y^- V_{3\varepsilon}(x_i, y_j) = 0 \\[3mm] \text{with boundary conditions} \\ U_{3\varepsilon} = 0, \quad W_{3\varepsilon} = 0 \text{ and } V_{3\varepsilon} = 0 \text{ on } \Gamma_B \\ U_{3\varepsilon} = U_{3B}^{8192} \text{ and } W_{3\varepsilon} = W_{3B}^{8192} \;\; \Gamma_L \bigcup \Gamma_T \end{cases}$

where D_x^-, D_x^+ and D_y^-, D_y^+ are the standard first–order backward and forward finite difference operators, respectively, in the x and y directions and, for any continuous function $V_{3\varepsilon}$ on the domain $\Omega_\varepsilon^{\mathbf{N}}$, $D_y^u U_{3\varepsilon}$ is the upwind finite difference operator. δ_y^2 is the standard second order centered finite difference operator in the y direction.

Since $(P_{3\varepsilon}^{\mathbf{N}})$ is a non–linear finite difference method an iterative method is required for its solution. This is obtained by replacing the system of non–linear equations by

the following sequence of systems of linear equations

$(A_{3\varepsilon}^{\mathbf{N}})$ $\begin{cases} \text{With the boundary condition } \mathbf{U}_{3\varepsilon}^{\mathbf{M}} = \mathbf{U}_{3\mathbf{B}}^{\mathbf{8192}} \text{ on } \Gamma_{\mathrm{L}}, \text{for each } i, 1 \le i \le N, \\ \text{use the initial guess } \mathbf{U}_{3\varepsilon}^{0}|_{X_i} = \mathbf{U}_{3\varepsilon}^{0}|_{X_{i-1}} \text{and for } m = 1, \dots, M \text{ solve the following} \\ \text{two point boundary value problem for } U_{3\varepsilon}^m(x_i, y_j) \\ \\ -\varepsilon\delta_y^2 U_{3\varepsilon}^m(x_i, y_j) + U_{3\varepsilon}^{m-1} D_x^- U_{3\varepsilon}^m(x_i, y_j) + V_{3\varepsilon}^{m-1} D_y^u U_{3\varepsilon}^m(x_i, y_j) = U\frac{dU}{dx} \quad 1 \le j \le N - 1 \\ \\ \text{with the boundary conditions } U_{3\varepsilon}^m = U_{3\mathrm{B}} \text{ on } \Gamma_{\mathrm{B}} \cup \Gamma_{\mathrm{T}}, \\ \text{and the initial guess for } V_{3\varepsilon}^0|_{X_1} = 0. \\ \text{Also, solve the initial value problem for } V_\varepsilon^m(x_i, y_j) \\ \\ D_x^- U_{3\varepsilon}^m(x_i, y_j) + D_y^- V_{3\varepsilon}^m(x_i, y_j) = 0 \\ \\ \text{with initial condition } V_{3\varepsilon}^m = 0 \text{ on } \Gamma_{\mathrm{B}}. \\ \text{Continue to iterate between the equations for } \mathbf{U}_\varepsilon^m \text{ until } m = M, \\ \text{where } M \text{ is such that} \\ \max\left(|U_{3\varepsilon}^M - U_\varepsilon^{M-1}|_{\overline{\Omega}_\varepsilon^N}, \frac{1}{V^*}|V_{3\varepsilon}^M - V_{3\varepsilon}^{M-1}|_{\overline{\Omega}_\varepsilon^N}\right) \le tol. \\ \text{Finally, solve the two point boundary value problem for } W_{3\varepsilon}(x_i, y_j) \\ \\ -\varepsilon\delta_y^2 W_{3\varepsilon}(x_i, y_j) + U_{3\varepsilon}^M D_x^- W_{3\varepsilon}(x_i, y_j) + V_{3\varepsilon}^M D_y^u W_{3\varepsilon}(x_i, y_j) = 0, \quad 1 \le j \le N - 1 \\ \\ \text{with the boundary conditions } W_{3\varepsilon} = W_{3\mathrm{B}} \text{ on } \Gamma_{\mathrm{B}} \cup \Gamma_{\mathrm{T}}. \end{cases}$

V^* is defined in Appendix A. For notational simplicity, we suppress explicit mention of the iteration superscript M, and henceforth we write simply $\mathbf{U}_{3\varepsilon}$ for the solution generated by $(A_{3\varepsilon}^{\mathbf{N}})$. We take $tol = 10^{-6}$ in the computations.

6.3 Error analysis based upon the finest mesh

In this section we estimate, computationally, the maximum pointwise error in the numerical solution and its discrete derivatives generated by the algorithm $(A_{3\varepsilon}^{\mathbf{N}})$ of the previous section. Since the exact solution in the expression for the computed maximum pointwise error is unknown, we replace it by the solution $\mathbf{U}_{3\varepsilon}^{512}$ generated by $(A_{3\varepsilon}^{\mathbf{N}})$ on the finest mesh Ω_ε^{512}. The results for $U_{3\varepsilon}$, $\frac{1}{V^*}V_{3\varepsilon}$ and their derivatives have been extensively investigated in Section 4.4. We need only investigate the results for $W_{3\varepsilon}$ and its derivatives.

For $W_{3\varepsilon}$ we define the computed maximum pointwise errors

$$E_\varepsilon^N(W_{3\varepsilon}) = ||W_{3\varepsilon} - \overline{W_{3\varepsilon}^{512}}||_{\overline{\Omega}_{3\varepsilon}^N}$$

and

$$E^N(W_{3\varepsilon}) = \max_\varepsilon E_\varepsilon^N(W_{3\varepsilon}).$$

As in the previous chapter, we show the errors for only three values of the angle of the wedge $\beta = 0.5$, $\beta = 1.0$ and $\beta = 1.5$. Note that similar results for the flat plate ($\beta = 0.0$) are in [26] and those for the value of $\beta = 0.7$ are in [7].

The values of the computed maximum pointwise errors generated by $(A_{3\varepsilon}^N)$ applied to problem $(P_{3\varepsilon})$ for $W_{3\varepsilon}$ are given in Table 6.1 for various values of ε, N and β. The results in Table 6.1 stabilise to a fixed value for all N and all β considered. The computed maximum error for $W_{3\varepsilon}$ decreases as the number of mesh points increase. For each N the largest computed maximum error occurs when $2^{-6} \leq \varepsilon \leq 2^{-12}$. Table 6.1 strongly suggests that the method is ε-uniform for $W_{3\varepsilon}$ for all β considered.

| $\varepsilon \backslash N$ | $\beta = 0.5$ | | | | $\varepsilon \backslash N$ | $\beta = 1.0$ | | | |
	32	64	128	256		32	64	128	256
2^{-0}	4.28e-03	2.34e-03	1.26e-03	6.68e-04	2^{-0}	4.90e-04	2.57e-04	1.38e-04	7.87e-05
2^{-2}	8.01e-03	4.18e-03	2.19e-03	1.17e-03	2^{-2}	2.83e-03	1.50e-03	8.12e-04	4.60e-04
2^{-4}	7.96e-03	4.13e-03	2.15e-03	1.14e-03	2^{-4}	4.95e-03	2.44e-03	1.17e-03	6.60e-04
2^{-6}	9.91e-03	5.04e-03	2.58e-03	1.35e-03	2^{-6}	1.07e-02	5.36e-03	2.63e-03	1.24e-03
2^{-8}	1.03e-02	5.57e-03	2.99e-03	1.67e-03	2^{-8}	1.11e-02	6.69e-03	3.86e-03	2.15e-03
2^{-10}	1.03e-02	5.57e-03	2.99e-03	1.67e-03	2^{-10}	1.11e-02	6.70e-03	3.86e-03	2.15e-03
2^{-12}	1.03e-02	5.57e-03	2.99e-03	1.67e-03	2^{-12}	1.10e-02	6.70e-03	3.86e-03	2.15e-03
2^{-14}	1.03e-02	5.57e-03	2.99e-03	1.67e-03	2^{-14}	1.09e-02	6.69e-03	3.86e-03	2.15e-03
2^{-16}	1.03e-02	5.57e-03	2.99e-03	1.67e-03	2^{-16}	1.08e-02	6.68e-03	3.86e-03	2.15e-03
2^{-18}	1.03e-02	5.57e-03	2.99e-03	1.67e-03	2^{-18}	1.07e-02	6.68e-03	3.86e-03	2.15e-03
2^{-20}	1.03e-02	5.57e-03	2.99e-03	1.67e-03	2^{-20}	1.07e-02	6.68e-03	3.86e-03	2.15e-03
E^N	1.03e-02	5.57e-03	2.99e-03	1.67e-03	E^N	1.11e-02	6.70e-03	3.86e-03	2.15e-03

| $\varepsilon \backslash N$ | $\beta = 1.5$ | | | |
	32	64	128	256
2^{-0}	5.11e-03	2.52e-03	1.21e-03	5.54e-04
2^{-2}	1.69e-02	8.53e-03	4.23e-03	2.04e-03
2^{-4}	2.75e-02	1.41e-02	7.11e-03	3.51e-03
2^{-6}	3.28e-02	1.97e-02	1.15e-02	6.29e-03
2^{-8}	3.29e-02	1.96e-02	1.15e-02	6.48e-03
2^{-10}	3.30e-02	1.96e-02	1.15e-02	6.48e-03
2^{-12}	3.30e-02	1.97e-02	1.15e-02	6.48e-03
2^{-14}	3.30e-02	1.97e-02	1.15e-02	6.48e-03
2^{-16}	3.30e-02	1.97e-02	1.15e-02	6.48e-03
2^{-18}	3.30e-02	1.97e-02	1.15e-02	6.48e-03
2^{-20}	3.30e-02	1.97e-02	1.15e-02	6.48e-03
E^N	3.30e-02	1.97e-02	1.15e-02	6.48e-03

Table 6.1: Computed maximum errors $E_\varepsilon^N(W_{3\varepsilon})$ generated by $(A_{3\varepsilon}^N)$ applied to problem $(P_{3\varepsilon})$ for various values of ε, N and β.

Graphs of the z velocity component $W_{3\varepsilon}$ of the solution $\mathbf{U}_{3\varepsilon}$ generated by the direct method $(A_{3\varepsilon}^N)$ with N=32, and $\beta = 0.5$, 1.0 and 1.5 for $\varepsilon = 1.0$ and 2^{-12} shown, are in Figures 6-1 and 6-2, respectively.

In Figure 6-1 we see the graphs of $W_{3\varepsilon}$ are smooth for various values of β, with

$\varepsilon = 1.0$.
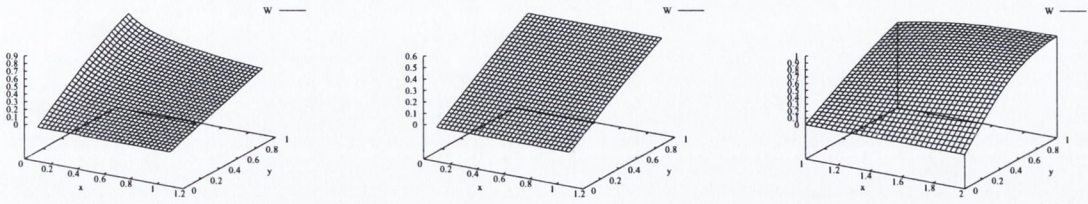
Figure 6-1: Graphs of $W_{3\varepsilon}$ for $\varepsilon = 1.0$, N=32 and $\beta = 0.5, 1.0, 1.5$.
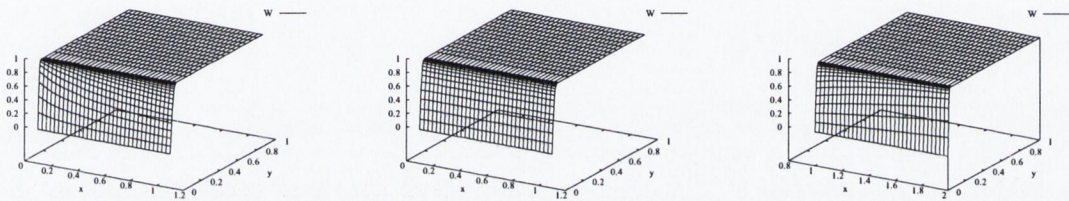
Figure 6-2: Graphs of $W_{3\varepsilon}$ for $\varepsilon = 2^{-12}$, N=32 and $\beta = 0.5, 1.0, 1.5$.

In Figure 6-2 we see the boundary layer along the surface of the wedge for $W_{3\varepsilon}$ for various values of β and $\varepsilon = 2^{-12}$. In both Figures the z velocity component has no non–physical oscillations for all β.

The computed orders of convergence p_ε^N, p^N and the error constants for $W_{3\varepsilon}$ are defined in an analogous manner to the computed orders of convergence and error constants in Section 4.4. The computed orders of convergence p_ε^N and p^N and the constant of convergence $C_{p^*}^N$ for $W_{3\varepsilon}$ are given in Table 6.2 for various values of ε, N and β. The results in Tables 6.1 and 6.2 suggest that $(A_{3\varepsilon}^N)$ is an ε–uniform numerical method of order at least 0.80 for $W_{3\varepsilon}$ for all β.

$\varepsilon\backslash N$	$\beta=0.5$			$\varepsilon\backslash N$	$\beta=1.0$			$\varepsilon\backslash N$	$\beta=1.5$		
	32	64	128		32	64	128		32	64	128
2^{-0}	0.83	0.89	0.94	2^{-0}	0.98	0.99	0.99	2^{-0}	0.99	1.00	1.00
2^{-2}	0.95	0.97	0.99	2^{-2}	0.94	0.97	0.99	2^{-2}	0.96	0.98	0.99
2^{-4}	0.96	0.97	0.98	2^{-4}	0.96	0.98	0.99	2^{-4}	0.94	0.96	0.98
2^{-6}	1.00	1.00	1.00	2^{-6}	0.96	0.98	0.99	2^{-6}	0.46	0.74	0.67
2^{-8}	0.97	0.99	0.96	2^{-8}	0.65	0.72	0.79	2^{-8}	0.47	0.76	0.78
2^{-10}	0.97	0.99	0.96	2^{-10}	0.65	0.72	0.79	2^{-10}	0.48	0.76	0.78
2^{-12}	0.97	0.99	0.96	2^{-12}	0.61	0.72	0.79	2^{-12}	0.48	0.76	0.78
2^{-14}	0.97	0.99	0.96	2^{-14}	0.57	0.72	0.79	2^{-14}	0.48	0.76	0.78
2^{-16}	0.97	0.99	0.96	2^{-16}	0.54	0.71	0.79	2^{-16}	0.48	0.77	0.78
2^{-18}	0.97	0.99	0.96	2^{-18}	0.52	0.71	0.79	2^{-18}	0.48	0.77	0.78
2^{-20}	0.97	0.99	0.96	2^{-20}	0.51	0.71	0.79	2^{-20}	0.48	0.77	0.78
p_{comp}^{N}	0.93	0.91	0.94	p_{comp}^{N}	0.90	0.89	0.89	p_{comp}^{N}	0.93	0.97	0.80
$C_{0.91}$	1.36	1.36	1.36	$C_{0.89}$	0.36	0.36	0.35	$C_{0.80}$	0.97	0.97	0.95

Table 6.2: Computed orders of convergence $p_\varepsilon^N(W_{3\varepsilon})$, $p^N(W_{3\varepsilon})$ and the error constants $C_{p^*}^N$ generated by $(A_{3\varepsilon}^N)$ applied to problem $(P_{3\varepsilon})$ for various values of ε, N and β.

From the data in Table 6.2 we obtain the computed error bounds for $W_{3\varepsilon}$

$$\beta = 0.5 \quad ||W_{3\varepsilon} - w_{3\varepsilon}||_{\Omega_\varepsilon^N} \leq 1.36 N^{-0.91}$$
$$\beta = 1.0 \quad ||W_{3\varepsilon} - w_{3\varepsilon}||_{\Omega_\varepsilon^N} \leq 0.36 N^{-0.89} \tag{6.1}$$
$$\beta = 1.5 \quad ||W_{3\varepsilon} - w_{3\varepsilon}||_{\Omega_\varepsilon^N} \leq 0.97 N^{-0.80}.$$

Graphs of the computed scaled discrete derivatives $\sqrt{\varepsilon}D_y^- W_{3\varepsilon}$ and $D_x^- W_{3\varepsilon}$ generated by $(A_{3\varepsilon}^N)$ are given in Figures 6-3 and 6-4, respectively, for $N = 32$, $\varepsilon = 2^{-12}$ and β=0.5, 1.0 and 1.5. Graphs of $\sqrt{\varepsilon}D_y^- W_{3\varepsilon}$ in Figure 6-3 show a region of rapid change along the wedge for various β. Graphs of $D_x^- W_{3\varepsilon}$ in Figure 6-4 show the region closest to the leading edge to be the most active.
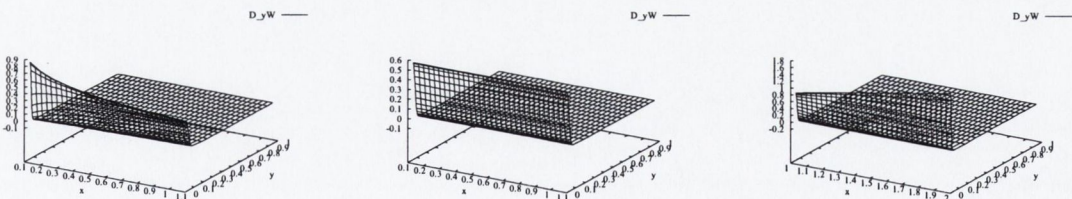
Figure 6-3: Graphs of $\sqrt{\varepsilon}D_y^- W_{3\varepsilon}$ for $\varepsilon = 2^{-12}$, N=32 and $\beta = 0.5, 1.0, 1.5$.
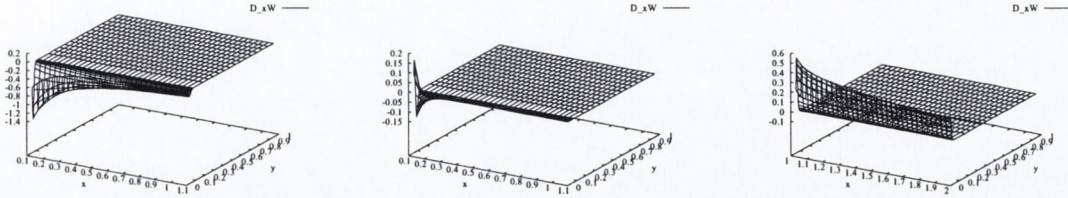
Figure 6-4: Graphs of $D_x^- W_{3\varepsilon}$ for $\varepsilon = 2^{-12}$, $N=32$ and $\beta = 0.5, 1.0, 1.5$.

We approximate the scaled partial derivatives $\frac{\partial w_{3\varepsilon}}{\partial x}$ and $\sqrt{\varepsilon}\frac{\partial w_{3\varepsilon}}{\partial y}$ by the corresponding scaled discrete derivatives $D_x^- W_{3\varepsilon}$ and $\sqrt{\varepsilon}D_y^- W_{3\varepsilon}$. Since the scaled derivatives of the exact solution $w_{3\varepsilon}$ are unknown, we replace them in the expression for the error by the appropriate scaled derivatives of the computed solution $W_{3\varepsilon}^{512}$, generated by method $(A_{3\varepsilon}^N)$ on the finest available mesh. The resulting computed maximum pointwise errors of the computed scaled discrete derivatives $\sqrt{\varepsilon}D_y W_{3\varepsilon}$ and $D_x^- W_{3\varepsilon}$ are given in the Tables 6.3 and 6.4, respectively.

$\beta = 0.5$					$\beta = 1.0$			
$\varepsilon\backslash N$	32	64	128	256	$\varepsilon\backslash N$	32	64	128	256
2^{-0}	1.33e-02	7.92e-03	4.64e-03	2.88e-03	2^{-0}	3.17e-03	1.57e-03	7.36e-04	2.85e-04
2^{-2}	2.55e-02	1.19e-02	5.14e-03	1.85e-03	2^{-2}	9.02e-03	4.26e-03	1.86e-03	8.58e-04
2^{-4}	5.10e-02	2.38e-02	1.02e-02	3.39e-03	2^{-4}	1.81e-02	8.45e-03	3.63e-03	1.35e-03
2^{-6}	1.01e-01	4.76e-02	2.04e-02	6.81e-03	2^{-6}	3.59e-02	1.69e-02	7.24e-03	2.46e-03
2^{-8}	9.96e-02	5.46e-02	2.69e-02	9.93e-03	2^{-8}	3.51e-02	1.95e-02	9.53e-03	3.90e-03
2^{-10}	9.96e-02	5.46e-02	2.69e-02	9.93e-03	2^{-10}	3.51e-02	1.95e-02	9.53e-03	3.90e-03
2^{-12}	9.96e-02	5.46e-02	2.69e-02	9.93e-03	2^{-12}	3.51e-02	1.95e-02	9.53e-03	3.90e-03
2^{-14}	9.96e-02	5.46e-02	2.69e-02	9.93e-03	2^{-14}	3.51e-02	1.95e-02	9.53e-03	3.90e-03
2^{-16}	9.96e-02	5.46e-02	2.69e-02	9.93e-03	2^{-16}	3.51e-02	1.95e-02	9.53e-03	3.90e-03
2^{-18}	9.96e-02	5.46e-02	2.69e-02	9.93e-03	2^{-18}	3.51e-02	1.95e-02	9.53e-03	3.90e-03
2^{-20}	9.96e-02	5.46e-02	2.69e-02	9.93e-03	2^{-20}	3.51e-02	1.95e-02	9.53e-03	3.90e-03
E^N	1.01e-01	5.46e-02	2.69e-02	9.93e-03	E^N	3.59e-02	1.95e-02	9.53e-03	3.90e-03

$\beta = 1.5$				
$\varepsilon\backslash N$	32	64	128	256
2^{-0}	4.07e-02	1.95e-02	8.84e-03	3.54e-03
2^{-2}	6.89e-02	3.40e-02	1.57e-02	6.47e-03
2^{-4}	1.20e-01	5.95e-02	2.78e-02	1.21e-02
2^{-6}	1.47e-01	8.50e-02	4.55e-02	2.44e-02
2^{-8}	1.44e-01	8.33e-02	4.37e-02	2.53e-02
2^{-10}	1.44e-01	8.33e-02	4.37e-02	2.53e-02
2^{-12}	1.44e-01	8.33e-02	4.37e-02	2.53e-02
2^{-14}	1.44e-01	8.33e-02	4.37e-02	2.53e-02
2^{-16}	1.44e-01	8.33e-02	4.37e-02	2.53e-02
2^{-18}	1.44e-01	8.33e-02	4.37e-02	2.53e-02
2^{-20}	1.44e-01	8.33e-02	4.37e-02	2.53e-02
E^N	1.47e-01	8.50e-02	4.55e-02	2.53e-02

Table 6.3: Computed maximum errors $E_\varepsilon^N(\sqrt{\varepsilon}D_y^- W_{3\varepsilon})$ generated by $(A_{3\varepsilon}^N)$ applied to problem $(P_{3\varepsilon})$ for various values of ε, N and β.

$\varepsilon \backslash N$	$\beta = 0.5$			
	32	64	128	256
2^{-0}	1.11e-01	6.44e-02	3.17e-02	1.17e-02
2^{-2}	6.82e-02	3.36e-02	1.39e-02	1.49e-02
2^{-4}	6.57e-02	3.37e-02	1.45e-02	1.86e-02
2^{-6}	6.17e-02	3.22e-02	2.05e-02	2.63e-02
2^{-8}	6.01e-02	3.23e-02	3.13e-02	3.69e-02
2^{-10}	6.01e-02	3.23e-02	3.13e-02	3.69e-02
2^{-12}	6.01e-02	3.23e-02	3.13e-02	3.69e-02
2^{-14}	6.01e-02	3.23e-02	3.13e-02	3.69e-02
2^{-16}	6.01e-02	3.23e-02	3.13e-02	3.69e-02
2^{-18}	6.01e-02	3.23e-02	3.13e-02	3.69e-02
2^{-20}	6.01e-02	3.23e-02	3.13e-02	3.69e-02
E^N	1.11e-01	6.44e-02	3.17e-02	3.69e-02

$\varepsilon \backslash N$	$\beta = 1.0$			
	32	64	128	256
2^{-0}	1.65e-03	2.49e-03	3.66e-03	4.83e-03
2^{-2}	1.78e-02	1.91e-02	1.84e-02	1.58e-02
2^{-4}	3.22e-02	3.09e-02	3.31e-02	2.89e-02
2^{-6}	6.60e-02	5.62e-02	6.19e-02	5.47e-02
2^{-8}	6.81e-02	7.02e-02	8.63e-02	8.78e-02
2^{-10}	6.79e-02	7.02e-02	8.63e-02	8.78e-02
2^{-12}	6.76e-02	7.02e-02	8.63e-02	8.78e-02
2^{-14}	6.74e-02	7.02e-02	8.63e-02	8.78e-02
2^{-16}	6.73e-02	7.02e-02	8.63e-02	8.78e-02
2^{-18}	6.73e-02	7.02e-02	8.63e-02	8.78e-02
2^{-20}	6.72e-02	7.02e-02	8.63e-02	8.78e-02
E^N	6.81e-02	7.02e-02	8.63e-02	8.78e-02

$\varepsilon \backslash N$	$\beta = 1.5$			
	32	64	128	256
2^{-0}	9.58e-03	8.34e-03	8.30e-03	6.43e-03
2^{-2}	3.02e-02	2.27e-02	1.89e-02	1.34e-02
2^{-4}	5.73e-02	4.87e-02	3.92e-02	2.72e-02
2^{-6}	7.27e-02	7.44e-02	7.05e-02	5.44e-02
2^{-8}	7.28e-02	7.44e-02	7.05e-02	5.65e-02
2^{-10}	7.27e-02	7.44e-02	7.05e-02	5.65e-02
2^{-12}	7.27e-02	7.44e-02	7.05e-02	5.65e-02
2^{-14}	7.27e-02	7.44e-02	7.05e-02	5.65e-02
2^{-16}	7.27e-02	7.44e-02	7.05e-02	5.65e-02
2^{-18}	7.27e-02	7.44e-02	7.05e-02	5.65e-02
2^{-20}	7.27e-02	7.44e-02	7.05e-02	5.65e-02
E^N	7.28e-02	7.44e-02	7.05e-02	5.65e-02

Table 6.4: Computed maximum errors $E_\varepsilon^N(D_x^- W_{3\varepsilon})$ generated by $(A_{3\varepsilon}^{\mathbf{N}})$ applied to problem $(P_{3\varepsilon})$ for various values of ε, N and β.

The computed maximum errors in Tables 6.3 and 6.4 for $\sqrt{\varepsilon}D_y^- W_{3\varepsilon}$ and $D_x^- W_{3\varepsilon}$, respectively, stabilise to a fixed value after $\varepsilon = 2^{-10}$ for all β. The computed maximum error for $\sqrt{\varepsilon}D_y^- W_{3\varepsilon}$ decreases as the number of mesh points increase. The results in Table 6.3 suggest that the method is independent of ε for $\sqrt{\varepsilon}D_y W_{3\varepsilon}$ for $\beta = 0.5$, 1.0 and 1.5. The computed maximum error for $D_x^- W_{3\varepsilon}$ decreases as the number of mesh points increase for $N \geq 128$. The orders of convergence and the compound error constants for $\sqrt{\varepsilon}D_y^- W_{3\varepsilon}$ and $D_x^- W_{3\varepsilon}$ are given in Tables 6.5 and 6.6, respectively, for various values of ε, N and β.

$\beta = 0.5$				$\beta = 1.0$				$\beta = 1.5$		
$\varepsilon \backslash N$	32	64	128	$\varepsilon \backslash N$	32	64	128	$\varepsilon \backslash N$	32	64	128
2^{-0}	1.01	0.88	0.91	2^{-0}	0.95	0.95	0.66	2^{-0}	0.98	0.99	1.00
2^{-2}	1.00	1.01	0.95	2^{-2}	0.99	0.98	0.90	2^{-2}	0.94	0.96	0.98
2^{-4}	0.99	1.00	1.01	2^{-4}	1.00	0.99	0.98	2^{-4}	0.91	0.95	0.97
2^{-6}	0.96	0.99	1.00	2^{-6}	1.00	1.00	0.99	2^{-6}	0.61	0.61	0.66
2^{-8}	0.67	0.73	0.77	2^{-8}	0.65	0.73	0.77	2^{-8}	0.61	0.68	0.74
2^{-10}	0.67	0.73	0.77	2^{-10}	0.65	0.73	0.77	2^{-10}	0.61	0.68	0.74
2^{-12}	0.67	0.73	0.77	2^{-12}	0.65	0.73	0.77	2^{-12}	0.61	0.68	0.74
2^{-14}	0.67	0.73	0.77	2^{-14}	0.65	0.73	0.77	2^{-14}	0.60	0.68	0.74
2^{-16}	0.67	0.73	0.77	2^{-16}	0.65	0.73	0.77	2^{-16}	0.60	0.68	0.74
2^{-18}	0.67	0.73	0.77	2^{-18}	0.65	0.73	0.77	2^{-18}	0.60	0.68	0.74
2^{-20}	0.67	0.73	0.77	2^{-20}	0.65	0.73	0.77	2^{-20}	0.60	0.68	0.74
p_{comp}^N	0.91	0.73	0.77	p_{comp}^N	0.95	0.73	0.77	p_{comp}^N	0.66	0.61	0.66
$C_{0.73}$	1.68	1.48	1.48	$C_{0.73}$	0.61	0.53	0.53	$C_{0.61}$	1.47	1.42	1.42

Table 6.5: Computed orders of convergence $p_\varepsilon^N(\sqrt{\varepsilon}D_y^- W_{3\varepsilon})$, $p^N(\sqrt{\varepsilon}D_y^- W_{3\varepsilon})$ and $C_{p^*}^N$ generated by $(A_{3\varepsilon}^N)$ applied to problem $(P_{3\varepsilon})$ for various values of ε, N and β.

$\beta = 0.5$				$\beta = 1.0$				$\beta = 1.5$		
$\varepsilon \backslash N$	32	64	128	$\varepsilon \backslash N$	32	64	128	$\varepsilon \backslash N$	32	64	128
2^{-0}	0.65	0.82	0.92	2^{-0}	-0.43	-0.26	0.05	2^{-0}	0.12	0.14	0.44
2^{-2}	0.81	0.87	0.93	2^{-2}	0.06	0.22	0.37	2^{-2}	0.20	0.31	0.53
2^{-4}	0.78	0.88	0.93	2^{-4}	0.00	0.07	0.30	2^{-4}	0.10	0.32	0.54
2^{-6}	0.75	0.86	0.93	2^{-6}	0.14	-0.01	0.26	2^{-6}	-0.21	-0.04	0.24
2^{-8}	0.74	0.93	0.25	2^{-8}	-0.16	-0.21	0.04	2^{-8}	-0.21	0.03	0.29
2^{-10}	0.74	0.93	0.25	2^{-10}	-0.17	-0.21	0.04	2^{-10}	-0.21	0.03	0.29
2^{-12}	0.74	0.93	0.25	2^{-12}	-0.19	-0.21	0.04	2^{-12}	-0.21	0.03	0.29
2^{-14}	0.74	0.93	0.25	2^{-14}	-0.19	-0.21	0.04	2^{-14}	-0.21	0.03	0.29
2^{-16}	0.74	0.93	0.25	2^{-16}	-0.20	-0.21	0.04	2^{-16}	-0.21	0.03	0.29
2^{-18}	0.74	0.93	0.25	2^{-18}	-0.20	-0.21	0.04	2^{-18}	-0.21	0.03	0.29
2^{-20}	0.74	0.93	0.25	2^{-20}	-0.20	-0.21	0.04	2^{-20}	-0.21	0.03	0.29
p_{comp}^N	0.65	0.82	0.92	p_{comp}^N	0.02	-0.21	0.04	p_{comp}^N	-0.21	-0.04	0.24
$C_{0.65}$	1.55	1.55	1.38	$C_{-0.21}$	-0.11	-0.09	-0.09	$C_{-0.21}$	-0.08	-0.08	-0.07

Table 6.6: Computed orders of convergence $p_\varepsilon^N(D_x^- W_{3\varepsilon})$, $p^N(D_x^- W_{3\varepsilon})$ and $C_{p^*}^N$ generated by $(A_{3\varepsilon}^N)$ applied to problem $(P_{3\varepsilon})$ for various values of ε, N and β.

The results in Tables 6.3 and 6.5 suggest that $(A_{3\varepsilon}^N)$ is an ε-uniform numerical method of order of at least 0.61 for $\sqrt{\varepsilon}D_y^- W_{3\varepsilon}$, for $N \geq 64$ and β. We cannot draw the same conclusion from Tables 6.4 and 6.6 for $D_x^- W_{3\varepsilon}$ as we have negative orders of convergence.

From the data in Table 6.5 we obtain the computed error bounds for $\sqrt{\varepsilon}D_y^- W_{3\varepsilon}$

$$\begin{aligned} \beta = 0.5 \quad & \sqrt{\varepsilon}||D_y^- W_{3\varepsilon} - \tfrac{\partial w_{3\varepsilon}}{\partial y}||_{\Omega_\varepsilon^N} \leq 1.68 N^{-0.73} \\ \beta = 1.0 \quad & \sqrt{\varepsilon}||D_y^- W_{3\varepsilon} - \tfrac{\partial w_{3\varepsilon}}{\partial y}||_{\Omega_\varepsilon^N} \leq 0.61 N^{-0.73} \\ \beta = 1.5 \quad & \sqrt{\varepsilon}||D_y^- W_{3\varepsilon} - \tfrac{\partial w_{3\varepsilon}}{\partial y}||_{\Omega_\varepsilon^N} \leq 1.47 N^{-0.61}. \end{aligned}$$

(6.2)

6.4 Error analysis based upon the computed Blasius solution

In this section we compute ε–uniform maximum pointwise differences in the approximations generated by the direct numerical method described in Section 6.2. For this case we compare the parameter uniform maximum pointwise differences in the approximations generated by the direct numerical method of the previous section with the corresponding values of W_{3B}^{8192} generated by the method defined in Chapter 5. The scaled maximum pointwise difference $||W_{3\varepsilon} - \overline{W_{3B}}^{8192}||_{\overline{\Omega}_\varepsilon^N}$ of N, ε and β are given in Table 6.7.

The results in Table 6.7 stabilise to a fixed value for all N and all β considered. The computed maximum difference for $W_{3\varepsilon}$ decreases as the number of mesh points increase. For each N the largest computed maximum difference occurs when $2^{-6} \leq \varepsilon \leq 2^{-12}$ for all β. The results in Table 6.7 indicate that the method is independent of ε for the z-velocity component for various β. In a similar fashion to Table 6.1 of the pointwise errors of $W_{3\varepsilon}$, Table 6.7 strongly suggests that the method is ε–uniform for $W_{3\varepsilon}$ for all β considered.

$\beta = 0.5$						$\beta = 1.0$				
$\varepsilon \backslash N$	32	64	128	256	512	$\varepsilon \backslash N$	32	64	128	256	512
2^{-0}	4.28e-03	2.34e-03	1.26e-03	6.68e-04	3.60e-04	2^{-0}	4.90e-04	2.57e-04	1.38e-04	7.87e-05	4.88e-05
2^{-2}	8.01e-03	4.18e-03	2.19e-03	1.17e-03	6.58e-04	2^{-2}	2.83e-03	1.50e-03	8.12e-04	4.60e-04	2.83e-04
2^{-4}	7.96e-03	4.13e-03	2.15e-03	1.14e-03	6.33e-04	2^{-4}	4.95e-03	2.44e-03	1.17e-03	6.60e-04	4.03e-04
2^{-6}	9.91e-03	5.04e-03	2.58e-03	1.35e-03	7.32e-04	2^{-6}	1.07e-02	5.36e-03	2.63e-03	1.24e-03	6.62e-04
2^{-8}	1.02e-02	5.54e-03	2.99e-03	1.63e-03	9.10e-04	2^{-8}	1.11e-02	6.72e-03	3.88e-03	2.17e-03	1.16e-03
2^{-10}	1.02e-02	5.54e-03	2.99e-03	1.63e-03	9.10e-04	2^{-10}	1.11e-02	6.72e-03	3.88e-03	2.17e-03	1.16e-03
2^{-12}	1.02e-02	5.54e-03	2.99e-03	1.63e-03	9.10e-04	2^{-12}	1.10e-02	6.72e-03	3.88e-03	2.17e-03	1.16e-03
2^{-14}	1.02e-02	5.54e-03	2.99e-03	1.63e-03	9.10e-04	2^{-14}	1.09e-02	6.71e-03	3.88e-03	2.17e-03	1.16e-03
2^{-16}	1.02e-02	5.54e-03	2.99e-03	1.63e-03	9.10e-04	2^{-16}	1.08e-02	6.71e-03	3.88e-03	2.17e-03	1.16e-03
2^{-18}	1.02e-02	5.54e-03	2.99e-03	1.63e-03	9.10e-04	2^{-18}	1.07e-02	6.70e-03	3.88e-03	2.17e-03	1.16e-03
2^{-20}	1.02e-02	5.54e-03	2.99e-03	1.63e-03	9.10e-04	2^{-20}	1.07e-02	6.70e-03	3.88e-03	2.17e-03	1.16e-03
E^N	1.02e-02	5.54e-03	2.99e-03	1.63e-03	9.10e-04	E^N	1.11e-02	6.72e-03	3.88e-03	2.17e-03	1.16e-03

$\beta = 1.5$					
$\varepsilon \backslash N$	32	64	128	256	512
2^{-0}	5.11e-03	2.52e-03	1.21e-03	5.54e-04	2.43e-04
2^{-2}	1.69e-02	8.53e-03	4.23e-03	2.04e-03	9.42e-04
2^{-4}	2.75e-02	1.41e-02	7.11e-03	3.51e-03	1.68e-03
2^{-6}	3.29e-02	1.97e-02	1.16e-02	6.29e-03	3.10e-03
2^{-8}	3.30e-02	1.97e-02	1.16e-02	6.51e-03	3.57e-03
2^{-10}	3.31e-02	1.97e-02	1.16e-02	6.51e-03	3.57e-03
2^{-12}	3.31e-02	1.97e-02	1.16e-02	6.51e-03	3.57e-03
2^{-14}	3.31e-02	1.97e-02	1.16e-02	6.51e-03	3.57e-03
2^{-16}	3.31e-02	1.97e-02	1.16e-02	6.51e-03	3.57e-03
2^{-18}	3.31e-02	1.97e-02	1.16e-02	6.51e-03	3.57e-03
2^{-20}	3.31e-02	1.97e-02	1.16e-02	6.51e-03	3.57e-03
E^N	3.31e-02	1.97e-02	1.16e-02	6.51e-03	3.57e-03

Table 6.7: Computed maximum pointwise difference $||W_{3\varepsilon} - \overline{W_{3B}}^{8192}||_{\overline{\Omega}_\varepsilon^N}$ where $W_{3\varepsilon}$ is generated by $(A_{3\varepsilon}^N)$ for various values of ε, N and β.
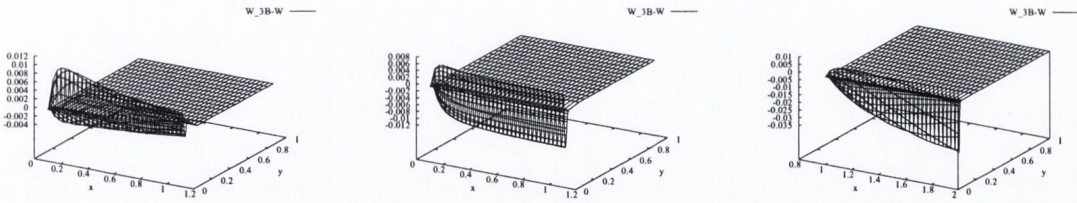
Figure 6-5: Graphs of $W_{3\varepsilon} - W_{3B}^{8192}$ for $\varepsilon = 2^{-12}$, N=32 and $\beta = 0.5, 1.0, 1.5$.

The graphs of differences $W_{3\varepsilon} - W_{3B}^{8192}$ for $\varepsilon = 2^{-12}$, N=32 and $\beta = 0.5, 1.0, 1.5$ in Figure 6-5 show that the largest difference is contained within the boundary layer along the surface of the wedge for all β considered.

We now estimate the order of convergence of the numerical approximation $W_{3\varepsilon}$, generated by the direct numerical method $(A_{3\varepsilon}^N)$, by using the computed order of convergence defined in Section 4.5.

The orders of convergence and the error constants of the velocity component $W_{3\varepsilon}$ are given in Table 6.8.

	$\beta = 0.5$					$\beta = 1.0$					$\beta = 1.5$			
$\varepsilon\backslash N$	32	64	128	256	$\varepsilon\backslash N$	32	64	128	256	$\varepsilon\backslash N$	32	64	128	256
2^{-0}	0.87	0.89	0.91	0.89	2^{-0}	0.93	0.89	0.81	0.69	2^{-0}	1.02	1.06	1.13	1.19
2^{-2}	0.94	0.93	0.90	0.83	2^{-2}	0.91	0.89	0.82	0.70	2^{-2}	0.99	1.01	1.05	1.12
2^{-4}	0.95	0.94	0.91	0.85	2^{-4}	1.02	1.06	0.83	0.71	2^{-4}	0.97	0.98	1.02	1.06
2^{-6}	0.98	0.97	0.94	0.88	2^{-6}	0.99	1.03	1.08	0.91	2^{-6}	0.74	0.77	0.88	1.02
2^{-8}	0.88	0.89	0.88	0.84	2^{-8}	0.73	0.79	0.84	0.91	2^{-8}	0.74	0.77	0.83	0.86
2^{-10}	0.88	0.89	0.88	0.84	2^{-10}	0.73	0.79	0.84	0.91	2^{-10}	0.74	0.77	0.83	0.86
2^{-12}	0.88	0.89	0.88	0.84	2^{-12}	0.71	0.79	0.84	0.91	2^{-12}	0.75	0.77	0.83	0.86
2^{-14}	0.88	0.89	0.88	0.84	2^{-14}	0.69	0.79	0.84	0.91	2^{-14}	0.75	0.77	0.83	0.86
2^{-16}	0.88	0.89	0.88	0.84	2^{-16}	0.68	0.79	0.84	0.91	2^{-16}	0.75	0.77	0.83	0.86
2^{-18}	0.88	0.89	0.88	0.84	2^{-18}	0.68	0.79	0.84	0.91	2^{-18}	0.75	0.77	0.83	0.86
2^{-20}	0.88	0.89	0.88	0.84	2^{-20}	0.67	0.79	0.84	0.91	2^{-20}	0.75	0.77	0.83	0.86
p_{comp}^N	0.88	0.89	0.88	0.84	p_{comp}^N	0.73	0.79	0.84	0.91	p_{comp}^N	0.75	0.77	0.83	0.86
$C_{0.84}$	0.43	0.41	0.40	0.39	$C_{0.73}$	0.35	0.35	0.33	0.31	$C_{0.75}$	1.09	1.09	1.07	1.01

Table 6.8: Computed orders of convergence $p_{\varepsilon,comp}^N$, p_{comp}^N and the error constant $C_{p_{comp}^*}^N$ for $W_{3\varepsilon} - W_{3B}^{8192}$ where $W_{3\varepsilon}$ is generated by $(A_{3\varepsilon}^N)$ for various values of ε, N and β.

From Table 6.8 we see that the order of convergence for the approximations to the scaled velocity component in each case is at least 0.75 for $W_{3\varepsilon}$ for $\beta = 0.5, 1.0$

and 1.5. Using Table 6.8 we obtain the following error bounds

$$
\begin{aligned}
\beta &= 0.5 \quad \|W_{3\varepsilon} - W_{3B}^{8192}\|_{\Omega_\varepsilon^N} \leq 0.43 N^{-0.84} \\
\beta &= 1.0 \quad \|W_{3\varepsilon} - W_{3B}^{8192}\|_{\Omega_\varepsilon^N} \leq 0.35 N^{-0.73} \\
\beta &= 1.5 \quad \|W_{3\varepsilon} - W_{3B}^{8192}\|_{\Omega_\varepsilon^N} \leq 1.09 N^{-0.75}.
\end{aligned}
\tag{6.3}
$$

From Tables 6.7 and 6.8 we have shown that for the z-velocity component the method is ε–uniform for $\beta = 0.5$, 1.0 and 1.5. Further computations, not reported here, show that the errors for the z- velocity component for $\beta \in [0.0, 1.5]$ have similar behaviour, therefore the method can be said to be (ε, β)–uniform for the scaled velocity components.

$\beta = 0.5$

$\varepsilon \backslash N$	32	64	128	256	512
2^{-0}	1.39e-02	7.09e-03	3.81e-03	2.05e-03	1.28e-03
2^{-2}	2.75e-02	1.39e-02	7.09e-03	3.70e-03	2.05e-03
2^{-4}	5.47e-02	2.75e-02	1.39e-02	7.09e-03	3.70e-03
2^{-6}	1.08e-01	5.47e-02	2.75e-02	1.39e-02	7.09e-03
2^{-8}	1.13e-01	6.73e-02	3.99e-02	2.30e-02	1.30e-02
2^{-10}	1.13e-01	6.73e-02	3.99e-02	2.30e-02	1.30e-02
2^{-12}	1.13e-01	6.73e-02	3.99e-02	2.30e-02	1.30e-02
2^{-14}	1.13e-01	6.73e-02	3.99e-02	2.30e-02	1.30e-02
2^{-16}	1.13e-01	6.73e-02	3.99e-02	2.30e-02	1.30e-02
2^{-18}	1.13e-01	6.73e-02	3.99e-02	2.30e-02	1.30e-02
2^{-20}	1.13e-01	6.73e-02	3.99e-02	2.30e-02	1.30e-02
E^N	1.13e-01	6.73e-02	3.99e-02	2.30e-02	1.30e-02

$\beta = 1.0$

$\varepsilon \backslash N$	32	64	128	256	512
2^{-0}	3.55e-03	1.86e-03	1.01e-03	5.90e-04	3.77e-04
2^{-2}	9.82e-03	5.00e-03	2.60e-03	1.42e-03	8.27e-04
2^{-4}	1.95e-02	9.82e-03	5.00e-03	2.60e-03	1.42e-03
2^{-6}	3.84e-02	1.95e-02	9.82e-03	5.00e-03	2.60e-03
2^{-8}	3.98e-02	2.41e-02	1.42e-02	8.20e-03	4.69e-03
2^{-10}	3.98e-02	2.41e-02	1.42e-02	8.20e-03	4.69e-03
2^{-12}	3.98e-02	2.41e-02	1.42e-02	8.20e-03	4.69e-03
2^{-14}	3.98e-02	2.41e-02	1.42e-02	8.20e-03	4.69e-03
2^{-16}	3.98e-02	2.41e-02	1.42e-02	8.20e-03	4.69e-03
2^{-18}	3.98e-02	2.41e-02	1.42e-02	8.20e-03	4.69e-03
2^{-20}	3.98e-02	2.41e-02	1.42e-02	8.20e-03	4.69e-03
E^N	3.98e-02	2.41e-02	1.42e-02	8.20e-03	4.69e-03

$\beta = 1.5$

$\varepsilon \backslash N$	32	64	128	256	512
2^{-0}	4.28e-02	2.15e-02	1.08e-02	5.42e-03	2.72e-03
2^{-2}	7.24e-02	3.72e-02	1.89e-02	9.46e-03	4.70e-03
2^{-4}	1.25e-01	6.60e-02	3.37e-02	1.70e-02	8.52e-03
2^{-6}	1.60e-01	9.63e-02	5.71e-02	3.18e-02	1.60e-02
2^{-8}	1.60e-01	9.63e-02	5.71e-02	3.29e-02	1.86e-02
2^{-10}	1.60e-01	9.63e-02	5.71e-02	3.29e-02	1.86e-02
2^{-12}	1.60e-01	9.63e-02	5.71e-02	3.29e-02	1.86e-02
2^{-14}	1.60e-01	9.63e-02	5.71e-02	3.29e-02	1.86e-02
2^{-16}	1.60e-01	9.63e-02	5.71e-02	3.29e-02	1.86e-02
2^{-18}	1.60e-01	9.63e-02	5.71e-02	3.29e-02	1.86e-02
2^{-20}	1.60e-01	9.63e-02	5.71e-02	3.29e-02	1.86e-02
E^N	1.60e-01	9.63e-02	5.71e-02	3.29e-02	1.86e-02

Table 6.9: Computed maximum pointwise scaled difference $\sqrt{\varepsilon}\|D_y^- W_{3\varepsilon} - D_y W_{3B}^{8192}\|_{\overline{\Omega_\varepsilon^N}/\Gamma_L}$ where $W_{3\varepsilon}$ is generated by $(A_{3\varepsilon}^N)$ for various values of ε, N and β.

In Tables 6.9 and 6.10 we display the computed maximum pointwise differences of the approximations to the scaled first order derivatives of the z-velocity component $\sqrt{\varepsilon}D_y^- W_{3\varepsilon}$ and $D_x^- W_{3\varepsilon}$ for various values of ε, N and β.

In Table 6.9 we see that the computed maximum pointwise differences of $\sqrt{\varepsilon}D_y^- W_{3\varepsilon}$ decrease as the number of mesh points increase. For each N the largest computed maximum difference occurs when $2^{-6} \leq \varepsilon \leq 2^{-12}$ for all β. The maximum differences stabilise to a fixed value as ε decreases for any ε or β. The results in Table 6.9 indicate that the method is independent of ε for $\sqrt{\varepsilon}D_y^- W_{3B}$ for various β. In a similar fashion

to Table 6.3 of the pointwise errors of $\sqrt{\varepsilon}D_y^-W_{3\varepsilon}$, Table 6.9 strongly suggests that the method is ε–uniform for $\sqrt{\varepsilon}D_y^-W_{3\varepsilon}$ for all β considered.

	$\beta = 0.5$						$\beta = 1.0$				
$\varepsilon \backslash N$	32	64	128	256	512	$\varepsilon \backslash N$	32	64	128	256	512
2^{-0}	1.19e-01	7.37e-02	4.28e-02	2.34e-02	1.26e-02	2^{-0}	1.65e-03	2.49e-03	3.66e-03	4.83e-03	5.26e-03
2^{-2}	7.54e-02	4.14e-02	2.16e-02	1.08e-02	5.12e-03	2^{-2}	1.78e-02	1.91e-02	1.84e-02	1.58e-02	1.21e-02
2^{-4}	7.26e-02	4.06e-02	2.11e-02	1.06e-02	5.06e-03	2^{-4}	3.22e-02	3.09e-02	3.31e-02	2.89e-02	2.18e-02
2^{-6}	6.69e-02	3.80e-02	2.01e-02	1.01e-02	7.46e-03	2^{-6}	6.60e-02	5.62e-02	6.19e-02	5.47e-02	4.12e-02
2^{-8}	6.52e-02	3.74e-02	1.97e-02	2.03e-02	1.58e-02	2^{-8}	6.81e-02	7.02e-02	8.63e-02	8.78e-02	7.45e-02
2^{-10}	6.52e-02	3.74e-02	1.97e-02	2.03e-02	1.58e-02	2^{-10}	6.79e-02	7.02e-02	8.63e-02	8.78e-02	7.45e-02
2^{-12}	6.52e-02	3.74e-02	1.97e-02	2.03e-02	1.58e-02	2^{-12}	6.76e-02	7.02e-02	8.63e-02	8.78e-02	7.45e-02
2^{-14}	6.52e-02	3.74e-02	1.97e-02	2.03e-02	1.58e-02	2^{-14}	6.74e-02	7.02e-02	8.63e-02	8.78e-02	7.45e-02
2^{-16}	6.52e-02	3.74e-02	1.97e-02	2.03e-02	1.58e-02	2^{-16}	6.73e-02	7.02e-02	8.63e-02	8.78e-02	7.45e-02
2^{-18}	6.52e-02	3.74e-02	1.97e-02	2.03e-02	1.58e-02	2^{-18}	6.73e-02	7.02e-02	8.63e-02	8.78e-02	7.45e-02
2^{-20}	6.52e-02	3.74e-02	1.97e-02	2.03e-02	1.58e-02	2^{-20}	6.72e-02	7.02e-02	8.63e-02	8.78e-02	7.45e-02
E^N	1.19e-01	7.37e-02	4.28e-02	2.34e-02	1.58e-02	E^N	6.81e-02	7.02e-02	8.63e-02	8.78e-02	7.45e-02

	$\beta = 1.5$				
$\varepsilon \backslash N$	32	64	128	256	512
2^{-0}	1.04e-02	5.34e-03	2.80e-03	1.52e-03	7.88e-04
2^{-2}	2.70e-02	1.43e-02	7.13e-03	3.27e-03	1.28e-03
2^{-4}	1.31e-02	9.59e-03	5.85e-03	3.19e-03	1.81e-03
2^{-6}	1.74e-02	1.61e-02	1.22e-02	7.44e-03	4.08e-03
2^{-8}	1.74e-02	1.61e-02	1.22e-02	7.77e-03	4.82e-03
2^{-10}	1.74e-02	1.61e-02	1.22e-02	7.77e-03	4.82e-03
2^{-12}	1.74e-02	1.61e-02	1.22e-02	7.77e-03	4.82e-03
2^{-14}	1.74e-02	1.61e-02	1.22e-02	7.77e-03	4.82e-03
2^{-16}	1.74e-02	1.61e-02	1.22e-02	7.77e-03	4.82e-03
2^{-18}	1.74e-02	1.61e-02	1.22e-02	7.77e-03	4.82e-03
2^{-20}	1.74e-02	1.61e-02	1.22e-02	7.77e-03	4.82e-03
E^N	2.70e-02	1.61e-02	1.22e-02	7.77e-03	4.82e-03

Table 6.10: Computed maximum pointwise difference $||D_x^-W_{3\varepsilon} - D_xW_{3B}^{8192}||_{\overline{\Omega_\varepsilon^N}}$ where $W_{3\varepsilon}$ is generated by $(A_{3\varepsilon}^N)$ for various values of ε, N and β.

Graphs of the computed pointwise maximum differences of the scaled discrete derivatives $\sqrt{\varepsilon}D_y^-W_{3\varepsilon}$ and $D_x^-W_{3\varepsilon}$ generated by $(A_{3\varepsilon}^N)$ are given in Figures 6-6 and 6-7, respectively, for $N = 32$, $\varepsilon = 2^{-12}$ and β=0.5, 1.0 and 1.5.
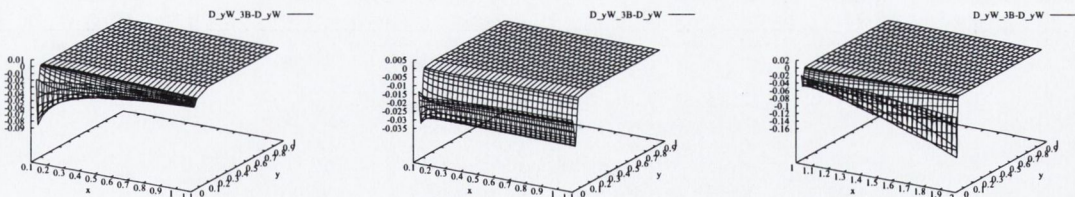
Figure 6-6: Graphs of $\sqrt{\varepsilon}(D_y^-W_{3\varepsilon} - D_yW_{3B}^{8192})$ for $\varepsilon = 2^{-12}$, N=32 and $\beta = 0.5, 1.0, 1.5$.

Graphs of the computed pointwise maximum differences of $\sqrt{\varepsilon}D_y^-W_{3\varepsilon}$ in Figure 6-6 show the largest differences to be along the wedge.
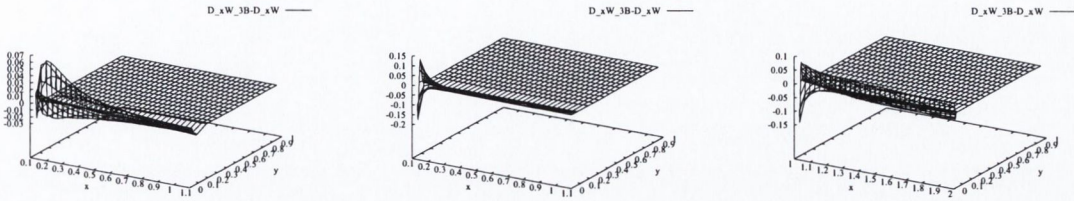
Figure 6-7: Graphs of $D_x^- W_{3\varepsilon} - D_x W_{3B}^{8192}$ for $\varepsilon = 2^{-12}$, $N=32$ and $\beta = 0.5, 1.0, 1.5$.

Graphs of the computed pointwise maximum differences of $D_x^- W_{3\varepsilon}$ in Figure 6-7 show the largest differences to be concentrated at the points in the domain nearest the leading edge.

In Tables 6.11 and 6.12 we display the computed orders of convergence for the approximations of the first order scaled derivatives of the velocity components $\sqrt{\varepsilon} D_y^- W_{3\varepsilon}$ and $D_x^- W_{3\varepsilon}$, respectively. From Table 6.11 we see that the order of convergence for the approximations to the scaled velocity component is at least 0.72 for $\sqrt{\varepsilon} D_y^- W_{3\varepsilon}$ for all β.

	$\beta = 0.5$					$\beta = 1.0$					$\beta = 1.5$			
$\varepsilon \backslash N$	32	64	128	256	$\varepsilon \backslash N$	32	64	128	256	$\varepsilon \backslash N$	32	64	128	256
2^{-0}	0.97	0.89	0.90	0.67	2^{-0}	0.93	0.85	0.74	0.60	2^{-0}	0.99	0.99	1.00	1.00
2^{-2}	0.99	0.97	0.94	0.85	2^{-2}	0.97	0.93	0.84	0.75	2^{-2}	0.96	0.98	0.99	1.01
2^{-4}	0.99	0.99	0.97	0.94	2^{-4}	0.99	0.97	0.93	0.84	2^{-4}	0.93	0.97	0.98	1.00
2^{-6}	0.98	0.99	0.99	0.97	2^{-6}	0.78	0.99	0.97	0.93	2^{-6}	0.73	0.75	0.85	0.99
2^{-8}	0.74	0.75	0.80	0.82	2^{-8}	0.73	0.76	0.79	0.79	2^{-8}	0.73	0.75	0.79	0.83
2^{-10}	0.74	0.75	0.80	0.82	2^{-10}	0.73	0.76	0.79	0.79	2^{-10}	0.73	0.75	0.79	0.83
2^{-12}	0.74	0.75	0.80	0.82	2^{-12}	0.73	0.76	0.79	0.79	2^{-12}	0.73	0.75	0.79	0.83
2^{-14}	0.74	0.75	0.80	0.82	2^{-14}	0.73	0.76	0.79	0.79	2^{-14}	0.73	0.75	0.79	0.83
2^{-16}	0.74	0.75	0.80	0.82	2^{-16}	0.73	0.76	0.79	0.79	2^{-16}	0.73	0.75	0.79	0.83
2^{-18}	0.74	0.75	0.80	0.82	2^{-18}	0.73	0.76	0.79	0.79	2^{-18}	0.73	0.75	0.79	0.83
2^{-20}	0.74	0.75	0.80	0.82	2^{-20}	0.73	0.76	0.79	0.79	2^{-20}	0.73	0.75	0.79	0.83
p_{comp}^N	0.74	0.75	0.80	0.82	p_{comp}^N	0.73	0.76	0.79	0.79	p_{comp}^N	0.73	0.75	0.79	0.83
$C_{0.74}$	3.67	3.67	3.64	3.50	$C_{0.73}$	1.05	1.05	1.02	0.98	$C_{0.73}$	5.09	5.09	5.02	4.81

Table 6.11: Computed orders of convergence $p_{\varepsilon,comp}^N$, p_{comp}^N and the error constant $C_{p_{comp}^*}^N$ for $\sqrt{\varepsilon}(D_y^- W_{3\varepsilon} - D_y W_{3B}^{8192})$ where $W_{3\varepsilon}$ is generated by $(A_{3\varepsilon}^N)$ for various values of ε, N and β.

	$\beta = 0.5$					$\beta = 1.0$					$\beta = 1.5$			
$\varepsilon \backslash N$	32	64	128	256	$\varepsilon \backslash N$	32	64	128	256	$\varepsilon \backslash N$	32	64	128	256
2^{-0}	0.69	0.78	0.87	0.90	2^{-0}	-0.59	-0.56	-0.40	-0.12	2^{-0}	0.96	0.93	0.88	0.95
2^{-2}	0.87	0.94	1.00	1.08	2^{-2}	-0.11	0.05	0.22	0.39	2^{-2}	0.92	1.00	1.12	1.35
2^{-4}	0.84	0.94	1.00	1.07	2^{-4}	0.06	-0.10	0.20	0.41	2^{-4}	0.45	0.71	0.88	0.81
2^{-6}	0.81	0.92	0.99	0.44	2^{-6}	0.23	-0.14	0.18	0.41	2^{-6}	0.12	0.40	0.71	0.87
2^{-8}	0.80	0.92	-0.04	0.36	2^{-8}	-0.04	-0.30	-0.02	0.24	2^{-8}	0.12	0.40	0.65	0.69
2^{-10}	0.80	0.92	-0.04	0.36	2^{-10}	-0.05	-0.30	-0.02	0.24	2^{-10}	0.12	0.40	0.65	0.69
2^{-12}	0.80	0.92	-0.04	0.36	2^{-12}	-0.05	-0.30	-0.02	0.24	2^{-12}	0.12	0.40	0.65	0.69
2^{-14}	0.80	0.92	-0.04	0.36	2^{-14}	-0.06	-0.30	-0.02	0.24	2^{-14}	0.12	0.40	0.65	0.69
2^{-16}	0.80	0.92	-0.04	0.36	2^{-16}	-0.06	-0.30	-0.02	0.24	2^{-16}	0.12	0.40	0.65	0.69
2^{-18}	0.80	0.92	-0.04	0.36	2^{-18}	-0.06	-0.30	-0.02	0.24	2^{-18}	0.12	0.40	0.65	0.69
2^{-20}	0.80	0.92	-0.04	0.36	2^{-20}	-0.06	-0.30	-0.02	0.24	2^{-20}	0.12	0.40	0.65	0.69
p_{comp}^N	0.69	0.78	0.87	0.57	p_{comp}^N	-0.04	-0.30	-0.02	0.24	p_{comp}^N	0.75	0.40	0.65	0.69
$C_{0.57}$	2.60	2.39	2.06	1.67	$C_{-0.30}$	-0.11	-0.09	-0.09	-0.07	$C_{0.40}$	0.45	0.35	0.35	0.29

Table 6.12: Computed orders of convergence $p_{\varepsilon,comp}^N$, p_{comp}^N and the error constant $C_{p_{comp}^*}^N$ for $D_x^- W_{3\varepsilon} - D_x W_{3B}^{8192}$ where $W_{3\varepsilon}$ is generated by $(A_{3\varepsilon}^N)$ for various values of ε, N and β.

Similar to Section 4.5, we investigate the beneficial nature of a second transition point,

$$\sigma_2 = \min\{0.5\sigma, \frac{\sqrt{\varepsilon}}{8} \ln N\},$$

to the computed values of the derivatives of the velocity components.

In Table 6.13 we display the computed orders of convergence for the approximations of the first order scaled derivative of the z-velocity component in the x direction, $D_x^- W_\varepsilon$, for various N, ε and β, using the double transition point mesh. Comparing the orders of convergence for the approximations of the first order scaled derivative of the z-velocity component generated by one transition point in Table 6.12 and Table 6.13 we see that the numerical method using two transition points yields superior results (see Appendix D).

	$\beta = 0.5$					$\beta = 1.5$			
$\varepsilon \backslash N$	32	64	128	256	$\varepsilon \backslash N$	32	64	128	256
2^{-0}	0.69	0.78	0.87	0.90	2^{-0}	0.35	0.17	0.43	0.56
2^{-2}	0.87	0.94	1.00	1.07	2^{-2}	0.91	0.50	0.62	0.75
2^{-4}	0.88	0.94	1.00	1.08	2^{-4}	0.70	0.86	0.95	1.01
2^{-6}	0.66	0.98	0.97	0.89	2^{-6}	0.39	0.80	0.90	0.94
2^{-8}	0.61	0.94	0.52	0.54	2^{-8}	0.35	0.57	0.69	0.75
2^{-10}	0.61	0.94	0.52	0.54	2^{-10}	0.35	0.57	0.69	0.75
2^{-12}	0.61	0.94	0.52	0.54	2^{-12}	0.35	0.57	0.69	0.75
2^{-14}	0.61	0.94	0.52	0.54	2^{-14}	0.35	0.57	0.69	0.75
2^{-16}	0.61	0.94	0.52	0.54	2^{-16}	0.35	0.57	0.69	0.75
2^{-18}	0.61	0.94	0.52	0.54	2^{-18}	0.35	0.57	0.69	0.75
2^{-20}	0.61	0.94	0.52	0.54	2^{-20}	0.35	0.57	0.69	0.75
p_{comp}^N	0.69	0.78	0.87	0.85	p_{comp}^N	0.35	0.57	0.69	0.75
$C_{0.69}$	3.40	3.40	3.18	2.80	$C_{0.35}$	3.03	3.03	2.61	2.07

Table 6.13: Computed orders of convergence $p_{\varepsilon,comp}^N$, p_{comp}^N and the error constant $C_{p_{comp}^\star}^N$ for $D_x^- W_{3\varepsilon} - D_x W_{3B}^{8192}$ where $W_{3\varepsilon}$ is generated by $(A_{3\varepsilon}^{\mathbf{N}})$ for various values of ε, N and β.

From the data in Table 6.11 we obtain the following error bounds for the $\sqrt{\varepsilon} D_y^- W_\varepsilon$

$$
\begin{aligned}
\beta = 0.5 \quad & \sqrt{\varepsilon} \| D_y^- W_\varepsilon - D_y W_{3B}^{8192} \|_{\Omega_\varepsilon^N} \leq 2.93 N^{-0.72} \\
\beta = 1.0 \quad & \sqrt{\varepsilon} \| D_y^- W_\varepsilon - D_y W_{3B}^{8192} \|_{\Omega_\varepsilon^N} \leq 1.05 N^{-0.73} \\
\beta = 1.5 \quad & \sqrt{\varepsilon} \| D_y^- W_\varepsilon - D_y W_{3B}^{8192} \|_{\Omega_\varepsilon^N} \leq 5.09 N^{-0.73}.
\end{aligned}
\tag{6.4}
$$

Further computations, not reported here, show that the errors for $\sqrt{\varepsilon} D_y W_{3\varepsilon}$ for $\beta \in [0.0, 1.5]$ have similar behaviour. Therefore, the method can be said to be (ε, β)-uniform for the scaled velocity component.

6.5 Computational error bounds

Similar to Section 4.6, we use the computed error estimates obtained in Section 7.9 for the quantities W_B^{8192} and its scaled discrete derivatives to estimate the error in the numerical approximations $W_{3\varepsilon}$ generated by the direct method $(A_{3\varepsilon}^{\mathbf{N}})$. The resulting estimates are independent of those obtained in Section 6.3.

First, we use the triangle inequality to obtain

$$
\begin{aligned}
\| W_{3\varepsilon} - w_{3W} \|_{\Omega_\varepsilon^N} &= \| W_{3\varepsilon} - w_{3B} \|_{\Omega_\varepsilon^N} \\
&\leq \| W_{3\varepsilon} - W_{3B}^{8192} \|_{\Omega_\varepsilon^N} + \| W_{3B}^{8192} - w_{3B} \|_{\Omega_\varepsilon^N}
\end{aligned}
\tag{6.5}
$$

where $W_{3\varepsilon}$ is the solution generated by the direct algorithm $(A_{3\varepsilon}^N)$ on the mesh Ω_ε^N. w_{3B} is the exact solution of the Prandtl problem constructed from the Blasius formulae (5.4). W_{3B}^{8192} is the computed Blasius solution generated in the previous chapter on a mesh with 8192 intervals. We then observe that the first term on the right–hand side of (6.5) involves the computable quantities W_ε and W_{3B}^{8192}. Furthermore, the second term on the right–hand side involves the scaled pointwise errors $W_{3B}^{8192} - w_{3B}$, which have already been estimated in Section 7.10 of the previous chapter. This shows that we can estimate the errors in the scaled numerical solutions and their scaled discrete derivatives, generated by the numerical method $(A_{3\varepsilon}^N)$ applied to problem $(P_{3\varepsilon})$, even though no theoretical error analysis is available for this numerical method.

We now compare the magnitudes of the two terms on the right–hand side of (6.5). The first term is the scaled maximum pointwise differences $\|W_\varepsilon - W_{3B}^{8192}\|_{\overline{\Omega}_\varepsilon^N}$. These quantities are found immediately from the solutions $\mathbf{U}_{3\varepsilon}$ of $(A_{3\varepsilon}^N)$ and the solution W_{3B}^{8192}, computed in the previous section and chapter. Their numerical values are given in Table 6.7 for various values of ε, N and β. The second term on the right–hand side of (6.5) is the scaled maximum pointwise errors $\|W_{3B}^{8192} - w_{3B}\|_{\Omega_\varepsilon^N}$ in the computed Blasius solution. The corresponding error bound (5.19), shows that the second term is bounded above by 2.702×10^{-4} for all β.

$$
\begin{aligned}
\|W_{3\varepsilon} - w_{3W}\|_{\Omega_\varepsilon^N} &= \|W_{3\varepsilon} - w_{3B}\|_{\Omega_\varepsilon^N} \\
&\leq \|W_{3\varepsilon} - W_{3B}^{8192}\|_{\Omega_\varepsilon^N} + \|W_{3B}^{8192} - w_{3B}\|_{\Omega_\varepsilon^N} \\
\beta = 0.5 \quad &\leq 1.15N^{-0.84} + 2.702 \times 10^{-4} \\
\beta = 1.0 \quad &\leq 0.51N^{-0.86} + 2.702 \times 10^{-4} \\
\beta = 1.5 \quad &\leq 1.09N^{-0.75} + 2.702 \times 10^{-4}.
\end{aligned}
\tag{6.6}
$$

The computational error bounds for $W_{3\varepsilon}$ in (6.6) and (6.3) give two computational formula such that we can ensure the error is below a desired value for all ε and β. In a similar manner to the above, we calculate computed error bounds for approximations of the scaled first derivative $\sqrt{\varepsilon}D_y^- W_{3\varepsilon}$ by the bounds (5.24) and (6.4)

$$
\begin{aligned}
\sqrt{\varepsilon}\|D_y^- W_{3\varepsilon} - \partial_y w_{3W}\|_{\Omega_\varepsilon^N} &= \sqrt{\varepsilon}\|D_y^- W_{3\varepsilon} - \partial_y w_{3B}\|_{\Omega_\varepsilon^N} \\
&\leq \sqrt{\varepsilon}\|D_y^- W_{3\varepsilon} - D_y W_{3B}^{8192}\|_{\Omega_\varepsilon^N} \\
&\quad + \sqrt{\varepsilon}\|D_y W_{3B}^{8192} - \partial_y w_{3B}\|_{\Omega_\varepsilon^N} \\
\beta = 0.5 \quad &\leq 2.93N^{-0.72} + 2.223 \times 10^{-4} \\
\beta = 1.0 \quad &\leq 1.05N^{-0.73} + 2.223 \times 10^{-4} \\
\beta = 1.5 \quad &\leq 5.09N^{-0.73} + 2.223 \times 10^{-4}.
\end{aligned}
\tag{6.7}
$$

The computational error bounds for $D_y^- W_{3\varepsilon}$ in (6.7) and (6.4) give two computational

formula to suggest the error is below a desired value for all ε and β.

6.6   Conclusion

In Chapters 5 and 6 we considered the Prandtl boundary layer equations for incompressible laminar flow past a three dimensional yawed wedge with angle $\beta\pi$, $\beta \in [0.0, 1.5]$. When the Reynolds number is large the solution of this problem has a parabolic boundary layer. We constructed a direct numerical method for computing approximations to the solution of this problem using a piecewise uniform fitted mesh technique appropriate to the parabolic boundary layer. We used the method to approximate the self–similar solution of the Prandtl problem in a finite rectangle excluding the leading edge of the wedge for various values of Re and β. We constructed and applied a special numerical method, related to the Blasius technique, to compute reference solutions to the problem. These were used to obtain approximate boundary conditions on the artificial boundaries of the computational domain and in the error analysis of the velocity components and their derivatives. Extensive numerical experiments indicated that the constructed direct numerical method is (Re, β)–uniform.

Chapter 7

Prandtl flow past a wedge with heat transfer – Blasius method

7.1 Prandtl Boundary layer equations

In this chapter and the next we use and adapt the numerical methods developed in Chapters 3, 4, 5 and 6 and apply them to the Prandtl boundary layer equations for flow past a semi-infinite wedge with heat transfer. The energy equation is singularly perturbed with respect to the product of the Prandtl and Reynolds number. This introduces a second layer, the thermal boundary layer, which also needs to be resolved (see Figure 7-1).
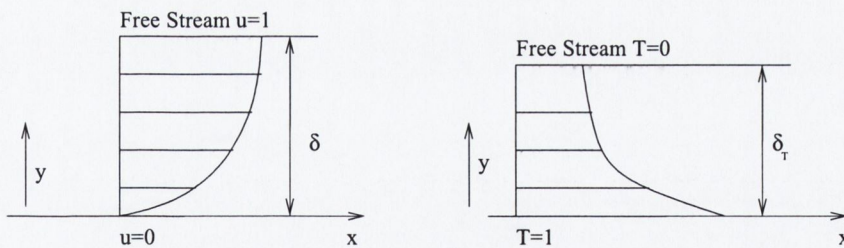
Figure 7-1: Boundary layer and thermal boundary layer.

In Figure 7-1 δ denotes the width of the boundary layer. δ_T denotes the width of the thermal boundary layer. For large Prandtl numbers, $Pr > 1$, the width of the thermal layer is less than the width of the boundary layer, $\frac{1}{\sqrt[3]{Pr}}\delta \sim \delta_T$ for small β. For small Prandtl numbers, $Pr < 1$, the width of the thermal layer is greater than the width of the boundary layer, $\frac{1}{\sqrt{Pr}}\delta \sim \delta_T$ for small β (see [18]).

We use a variant of the semi-analytic approach of Blasius to generate numerical ap-

proximations of guaranteed accuracy to the flow variables and their scaled derivatives. In the next chapter, we construct a direct numerical method to generate numerical approximations of guaranteed accuracy to the flow variables and their scaled derivatives. We show that the numerical approximations are pointwise accurate and that they satisfy pointwise error estimates that are uniform with respect to the Reynolds number, the Prandtl number, the heat transfer parameter and the angle of the wedge. Incompressible flow past a wedge with heat transfer on a finite domain is governed by the non-dimensional equations ([18])

$$(P_T) \begin{cases} \text{Find } \mathbf{u}_T = (u_T, v_T) \text{ and } t_T \text{ such that for all } (x,y) \in \Omega \\ \mathbf{u}_T \text{ and } t_T \text{ satisfies the differential equations} \\ \\ -\frac{1}{Re}\frac{\partial^2 u_T(x,y)}{\partial y^2} + \mathbf{u}_T(x,y).\nabla \mathbf{u}_T(x,y) = U(x)\frac{dU(x)}{dx} \\ \\ \nabla \mathbf{u}_T(x,y) = 0 \\ \\ -\frac{1}{Re}\frac{1}{Pr}\frac{\partial^2 t_T(x,y)}{\partial y^2} + u_T(x,y)\left(\frac{\partial t_T(x,y)}{\partial x} + \frac{n}{x}t_T(x,y)\right) + v_T\frac{\partial t_T(x,y)}{\partial y} = 0 \\ \\ \text{with the boundary conditions} \\ \\ \mathbf{u}_T = 0 \text{ and } t_T = 1 \text{ on } \Gamma_B \\ \mathbf{u}_T = \mathbf{u}_P \text{ and } t_T = t_P \text{ on } \Gamma_L \bigcup \Gamma_T \end{cases}$$

where $(U(x) = x^m, 0)$ is the solution of the reduced problem, $m = \frac{\beta}{2-\beta}$ and $\beta\pi$ is the angle in radians of the wedge. u_p and t_p are the exact solution to (P_P) and n is the heat transfer parameter. When $n = 0$ we have a constant wall temperature. When $n = \frac{(1-m)}{2}$ we have a constant heat flux (see [46]). In all of the numerical computations in this and the next chapter we use the specific range of values

$$Re \in [1, \infty) \quad Pr \in [0.1, 10000] \text{ and } \beta \in [0.0, 0.3]$$

for constant wall temperature, $n = 0$ and for constant heat flux, $n = \frac{1-m}{2}$.

Our goal in Chapters 7 and 8 is to model the flow for all Reynolds numbers, Re, angles of the wedge, β and all Prandtl numbers, Pr for walls of constant temperature and constant heat flux for which the flow remains laminar and no separation occurs on the wedge.

7.2   Blasius solution

Using the similarity transformation described in [18]

$$\eta = y\sqrt{\frac{(m + 1.0)U(x)Re}{2x}} \qquad (7.1)$$

the velocity components of the Blasius solution $\mathbf{u}_B$ and temperature component of the Blasius' solution t_{TB} of (P_T) are given in terms of f and θ by

$$u_{TB}(x, y) = U f'(\eta) \qquad (7.2)$$

$$v_{TB}(x, y) = -\sqrt{\frac{(m + 1)\varepsilon U}{2x}}(f + \frac{1 - m}{m + 1}\eta f'(\eta)) \qquad (7.3)$$

$$t_{TB}(x, y) = \theta(\eta) \qquad (7.4)$$

where f and θ are the solutions of the coupled non–linear problem

$$(P_{TB}) \begin{cases} \text{Find } f \in C^3([0, \infty)) \text{ such that for all } \eta \in [0, \infty) \\ f'''(\eta) + f(\eta)f''(\eta) + \beta(1 - f'^2(\eta)) = 0 \\ \theta''(\eta) + Prf(\eta)\theta'(\eta) - (2 - \beta)nPrf'\theta = 0 \\ \\ f(0) = 0, \ \ \theta(0) = 1, \ \ f'(0) = 0, \ \ \lim_{\eta \to \infty} f'(\eta) = 1 \ \ \lim_{\eta \to \infty} \theta(\eta) = 0. \end{cases}$$

The problem in (P_{TB}) is known as the Blasius problem and in what follows we refer to $\mathbf{u}_{TB}$ and t_{TB} as the Blasius solution of (P_T).

The two equations in (P_{TB}) are semi-coupled equations. The first equation is a third order non–linear ordinary differential equation on the semi-infinite domain $(0, \infty)$ for f which was dealt with in Chapter 3. The second equation is a second order ordinary differential equation on the semi-infinite domain $(0, \infty)$ for θ and f.

Note that the case for $n = 0$ and $Pr = 1$ and all $\beta \in [0, 1.5]$ of the Blasius problem was dealt with in Chapter 5 for f and for $\theta = 1 - g$ and their derivatives.

The problem (P_{TB}) can be solved numerically on any bounded domain I of $(0, \infty)$. In what follows we solve the Blasius problem (P_{TB}) numerically for the functions f and θ and their derivatives. We then use the analytic relations (7.2), (7.3) and (7.4) to construct Reynolds uniform analytic approximations with guaranteed accuracy to the solution $\mathbf{u}_T$ and t_T of (P_T) for all relevant values of the Reynolds number, the Prandtl number, the heat parameter and angles of the wedge at all points of the domain Ω.

To achieve this it is clear that we need Reynolds uniform pointwise accuracy of $f(\eta)$,

$f'(\eta)$, $f''(\eta)$, $\theta(\eta)$ and $\theta'(\eta)$ for all $\eta \in (0, \infty)$. We have constructed a method for f and its derivatives in Chapter 5. We now adapt and extend this to include θ and θ'.

7.3 Singularly perturbed nature of Blasius problem

We have shown the singularly perturbed nature of the ordinary differential equation of f in Section 3.3. Using similar arguments we will show the singularly perturbed nature of the ordinary differential equation for θ and f of (P_{TB}). In the next section we use this observation to motivate the construction of the numerical method for solving (P_{TB}).

We observe that while we need the solution of (P_{TB}) on an infinite interval, in practice we can find numerical solutions only on a finite interval. For this reason we introduce a one-parameter family of problems related to (P_{TB}) on the finite interval $(0, L)$ where the length L of the interval is taken as the parameter of the family. The typical problem in this family is defined for each value of L in the range $1 \leq L \leq \infty$ by

$$\theta_L''(\eta) + Pr f_L(\eta)\theta_L'(\eta) - (2 - \beta)nPr f_L'(\eta)\theta_L(\eta) = 0 \tag{7.5}$$

$$\theta_L(0) = 0, \qquad \theta_L(L) = 1. \tag{7.6}$$

When we reformulate (7.5) as a singularly perturbed problem, transpires that $\frac{1}{L}$ is the singular perturbation parameter and so it is appropriate to introduce the temporary notation $\varepsilon = \frac{1}{L}$. Then the problem (7.5) can be written in the form

$$\theta_\varepsilon''(\eta) + Pr f_\varepsilon(\eta)\theta_\varepsilon'(\eta) - (2 - \beta)nPr f_\varepsilon'(\eta)\theta_\varepsilon(\eta) = 0, \quad \theta_\varepsilon(0) = 0, \quad \theta_\varepsilon(\frac{1}{\varepsilon}) = 1.$$

Changing variables from η to $\xi = \varepsilon\eta$ which is equivalent to a mapping of the interval $[0, \frac{1}{\varepsilon}]$ to the unit interval $[0, 1]$, and writing $\vartheta_\varepsilon(\xi) = \theta_\varepsilon(\eta)$ and $h(\xi) = f_\varepsilon(\eta)$ we obtain

$$\frac{1}{Pr}\varepsilon\vartheta_\varepsilon''(\xi) + f_\varepsilon(\xi)\vartheta_\varepsilon'(\xi) - (2 - \beta)nf_\varepsilon'(\xi)\vartheta_\varepsilon(\xi) = 0 \qquad \vartheta_\varepsilon(0) = 0 \quad \vartheta_\varepsilon(1) = 1 \quad (7.7)$$

where $h(0) = 0$ and $h(\xi) = O(\xi)$ for all $\xi \geq \varepsilon$. This is a singularly perturbed problem for ϑ_ε with a boundary layer at $\xi = 0$. The singularly perturbed parameters are ε and Pr. In what follows it is natural to refer to L-uniform methods for (7.5).

7.4 Robust layer resolving method for Blasius problem

Our strategy for computing L-uniform approximations to the solution of (P_{TB}) is to obtain a numerical solution F_L and Θ_L, on the interval $[0, L]$, for an increasing sequence of values of the length L. Since, for each L, we need the values of f_L, f'_L, f''_L, θ_L and θ'_L at all points of the interval $(0, \infty)$, we extend the domain of f_L, f'_L and f''_L from $[0, L]$ to the semi-infinite interval $[0, \infty)$ by extrapolations (3.7)-(3.9). We extend the domain of θ_L and θ'_L from $[0, L]$ to the semi-infinite interval $[0, \infty)$ by defining the following extrapolation

$$\theta'(\eta) = 0, \text{ for all } \eta \geq L \tag{7.8}$$

$$\theta(\eta) = 0, \text{ for all } \eta \geq L. \tag{7.9}$$

We now describe our numerical method for finding approximations to the solution and its derivatives of problem (P_{TB}). For each fixed N we write $L_N = \ln N$ and we divide the interval into the two subintervals $[0, L_N]$ and $[L_N, \infty)$. We construct a uniform mesh

$$\overline{I}_u^N = \{\eta_i \ : \ \eta_i = C_{Pr} i N^{-1} \ln N, 0 \leq i \leq N\}_0^N$$

on the subinterval $[0, L_N]$. For values of $Pr > 1$, $N \geq 2048$ is sufficiently large to resolve the boundary layer. For values of $Pr < 1$ we need to extend the domain with respect to $\sqrt{Pr}$. We do this by defining

$$C_{Pr} = \begin{cases} \frac{1}{\sqrt{Pr}} & Pr < 1 \\ 1 & Pr \geq 1. \end{cases}$$

We determine numerical approximations F, D^+F, D^+D^+F, Θ and $D^+\Theta$ to f_L, f'_L, f''_L, θ and θ', respectively, at the mesh points $\overline{I}_u^N$.

Using a variation of the continuation algorithm defined in Section 7.8 we have

(A_{TB}^N) $\begin{cases} \text{For each integer } m, \ 1 \leq m \leq M \text{ find } F^m \text{ on } I_u^N \\ \text{such that, for all } \eta \in I_u^N, \ 2 \leq i \leq N-1 \\[2ex] \delta^2(D^- F_i^m) + F_i^{1-m}(D^+(D^- F_i^m)) + \beta(1 - (D^- F_i^{1-m})(D^- F_i^m)) \\ -(1+\beta)(D^- F_i^m - D^- F_i^{1-m}) = 0 \\[2ex] \text{with boundary conditions} \\ F(0) = D^+ F(0) = 0, \qquad\qquad D^0 F(\eta_{N-1}) = 1 \\[2ex] \text{with an initial guess of } F^0(\eta_i) = \eta_i. \\[2ex] \text{Finally, find } \Theta \text{ on } I_u^N \\ \text{such that, for all } \eta \in I_u^N, \ 1 \leq i \leq N-1 \\[2ex] \delta^2 \Theta_i + Pr F_i^M D^+ \Theta_i - (2-\beta)nPrD^+F^M \Theta_i = 0 \\[2ex] \text{with boundary conditions} \\ \Theta(0) = 0, \qquad\qquad \Theta(\eta_N) = 1 \end{cases}$

We assign the value $D^+\Theta(\eta_N) = 0$, so that $D^+\Theta$ is defined at all points of the mesh $\overline{I}_u^N$. We then use piecewise linear interpolation to interpolate from $\overline{I}_u^N$ to each point of the subinterval $[0, L_N]$. We denote the corresponding interpolants by $\overline{\Theta}$ and $\overline{D^+\Theta}$. We extend these functions to the whole of the semi-infinite interval $[0, \infty)$ in an analogous way to the extensions (7.8) and (7.9) of their continuous counterparts, that is

$$\overline{D^+\Theta}(\eta) = 0, \text{ for all } \eta \in [L_N, \infty) \tag{7.10}$$

$$\overline{\Theta}(\eta) = 0, \text{ for all } \eta \in [L_N, \infty). \tag{7.11}$$

We take the values of Θ and $D^+\Theta$, respectively, to be the required numerical approximations to the exact values θ and θ' of the Blasius solution and its derivatives on the semi-infinite interval $[0, \infty)$.

7.5 Numerical solution of the Blasius problem

As the numerical results for F, D^+F and D^+D^+F have been extensively investigate in Section 3.6, we only need to investigate the numerical results for Θ and $D^+\Theta$ for various values of Pr, β and n. The definitions of the computed pointwise maximum errors,the pointwise two mesh difference and the two mesh orders of convergence are given in Section 3.6. For the sake of brevity we only look at the constant heat flux when $n = \frac{1-m}{2}$ and for $Pr = 0.2$, 512 and $10,000$ for $\beta = 0.3$. The computed maximum pointwise error E^N, computed two mesh difference D^N and the computed order of convergence p^N for $\overline{\Theta}$ and $\overline{D^+\Theta}$, are given in Tables 7.6 and 7.7, respectively. The main conclusion to be drawn from the numerical results in these tables is that the method (P_{TB}^N), in conjunction with the algorithm (A_{TB}^N), is, in practice a robust layer-resolving method for problem (7.5) for all values of Pr, β and n in that it is L-uniform and that the L-uniform order of convergence on $[0, L_N]$ of the numerical solution Θ of the exact Θ_L and of the discrete derivative $D^+\Theta$ to the derivative θ'_L, is, in practice, better than 0.79 for all $N \geq 2048$ and Pr for $\beta = 0.3$ and $n = \frac{1-m}{2}$.

N	128	256	512	1024	2048	4096	8192	16384
				$Pr = 0.2$				
E^N	0.009213	0.005232	0.002921	0.001603	0.000863	0.000452	0.000226	0.000103
D^N	0.003981	0.002311	0.001317	0.000740	0.000411	0.000226	0.000123	0.000067
p^N	0.78	0.81	0.83	0.85	0.86	0.87	0.88	0.89
				$Pr = 512$				
E^N	0.065058	0.037326	0.020828	0.011457	0.006171	0.003234	0.001617	0.000735
D^N	0.027983	0.016101	0.009371	0.005244	0.002934	0.001616	0.000882	0.000478
p^N	0.80	0.78	0.84	0.84	0.86	0.87	0.88	0.89
				$Pr = 10000$				
E^N	0.183302	0.102446	0.056976	0.031214	0.016807	0.008806	0.004406	0.002004
D^N	0.081218	0.043540	0.025174	0.014177	0.007972	0.004378	0.002401	0.001301
p^N	0.90	0.79	0.83	0.83	0.86	0.87	0.88	0.89

Table 7.1: Computed maximum pointwise error E^N, computed two mesh difference $\overline{D}^N$ and the order of convergence $\overline{p}^N$ for $\overline{\Theta}$ on $\overline{I}_u^N$ generated by (A_{TB}^N) with $M = 8 \ln N$ applied to problem (P_{TB}) for various values of N and Pr with $\beta = 0.3$ and $n = \frac{1-m}{2}$.

				$Pr = 0.2$				
N	128	256	512	1024	2048	4096	8192	16384
E^N	0.011134	0.006502	0.003688	0.002042	0.001105	0.000580	0.000291	0.000132
D^N	0.004722	0.002845	0.001656	0.000941	0.000526	0.000290	0.000158	0.000086
p^N	0.73	0.78	0.82	0.84	0.86	0.87	0.88	0.89
				$Pr = 512$				
E^N	0.793622	0.525761	0.319183	0.183472	0.101298	0.053796	0.027100	0.012368
D^N	0.303333	0.218680	0.139630	0.083386	0.047859	0.026793	0.014756	0.008034
p^N	0.47	0.65	0.74	0.80	0.84	0.86	0.88	0.89
				$Pr = 10000$				
E^N	2.640333	2.676810	1.942980	1.218800	0.704148	0.383096	0.195500	0.089844
D^N	0.632685	0.965106	0.799971	0.538230	0.328013	0.189495	0.106121	0.058302
p^N	-0.61	0.27	0.57	0.71	0.79	0.84	0.86	0.88

Table 7.2: Computed maximum pointwise error E^N, computed two mesh difference $\overline{D}^N$ and the order of convergence $\overline{p}^N$ for $\overline{D^+\Theta}$ on $\overline{I}_u^N \backslash \{\eta_N\}$ generated by (A_{TB}^N) with $M = 8nN$ applied to problem (P_{TB}) for various values of N and Pr with $\beta = 0.3$ and $n = \frac{1-m}{2}$.

Comparison of the entries for the order of convergence p^N in Tables 7.6 and 7.7 with the Table of theoretical behavior for $N^{-1}nN$, and $2N^{-1}(\ln \frac{N}{2})$ of the order of convergence defined p^N in Appendix B, suggests that the computed order of L-uniform convergence p^N for $\overline{\Theta}$ corresponds to the theoretical behavior $N^{-1}\ln N$ and $\overline{D^+\Theta}$ corresponds to the theoretical behavior $2N^{-1}\ln \frac{N}{2}$ for $N \geq 2048$ for all Pr considered.

7.6 Computed error estimates for Blasius problem

Theoretical estimates in [26] indicate that, for all $N \geq N_0$, the approximations of $\overline{\Theta}$ and $\overline{D^+\Theta}$, respectively, to the exact solution of the Blasius problem (P_{TB}) and its derivatives satisfy error bounds of the form

$$||\overline{\Theta} - \theta||_{[0,\infty)} \leq C_p N^{-p} \tag{7.12}$$

$$||\overline{D^+\Theta} - \theta'||_{[0,\infty)} \leq C_p N^{-p} \tag{7.13}$$

where the error parameters are unknown. The computed two–mesh difference, computed order of convergence, computed global order of convergence and the computed global constant error are defined in Section 3.6. We now use these experimental techniques to obtain computed parameter uniform global error parameters for the function $\overline{\Theta}$ on the semi-infinite interval $[0, \infty)$ for various Pr for $\beta = 0.3$ and $n = \frac{1-m}{2}$. To determine the two mesh differences $\overline{D}$ and hence the computed order of convergence

$\overline{p}^N$ and the constant of convergence $\overline{C}_{\overline{p}^*}^N$ for a pair of meshes with N and 2N points, respectively, we have to consider the 3 subintervals $[0, L_N)$, $[L_N, L_{2N})$ and $[L_{2N}, \infty)$ separately. For $\eta \in [L_N, L_{2N})$ the two mesh difference at η for $\overline{\Theta}$ is $\overline{\Theta}^{2N}(\eta)$ and for $\overline{D^+\Theta}$ is $\overline{D^+\Theta}^{2N}(\eta)$. In the subinterval $[L_{2N}, \infty)$ the two mesh difference at η for $\overline{\Theta}$ and $\overline{D^+\Theta}$ is zero. The resulting computed global two-mesh difference $\overline{D}$, the computed order of convergence $\overline{p}^N$ and the constant of convergence $\overline{C}_{\overline{p}^*}^N$ for $\overline{\Theta}$, $\overline{D^+\Theta}$ and $\eta\overline{D^+\Theta}$ are given in Tables 7.8, 7.9 and 7.10 for various values of N and Pr for $\beta = 0.3$ and $n = \frac{m-1}{2}$.

N	128	256	512	1024	2048	4096	8192	16384
				$Pr = 0.2$				
D^N	0.003981	0.002311	0.001317	0.000740	0.000411	0.000226	0.000123	0.000067
p^N	0.78	0.81	0.83	0.85	0.86	0.87	0.88	0.89
$C_{0.86}^N$	0.582252	0.614857	0.637175	0.651015	0.657630	0.657630	0.652279	0.642531
				$Pr = 512$				
D^N	0.027983	0.016101	0.009371	0.005244	0.002934	0.001616	0.000882	0.000478
p^N	0.80	0.78	0.84	0.84	0.86	0.87	0.88	0.89
$C_{0.86}^N$	4.056749	4.239105	4.480440	4.553639	4.626976	4.626976	4.585773	4.511894
				$Pr = 10000$				
D^N	0.081218	0.043540	0.025174	0.014177	0.007972	0.004378	0.002401	0.001301
p^N	0.90	0.79	0.83	0.83	0.86	0.87	0.88	0.89
$C_{0.86}^N$	11.95620	11.67087	12.28674	12.59916	12.90103	12.90103	12.88301	12.71298

Table 7.3: Computed two mesh difference $\overline{D}^N$, the order of convergence $\overline{p}^N$ and computed global error constant $\overline{C}_{\overline{p}^*}^N$ for $\overline{\Theta}$ on $[0, \infty)$ generated by (A_{TB}^N) with $M = 8nN$ applied to problem (P_{TB}) for various values of N and Pr with $\beta = 0.3$ and $n = \frac{1-m}{2}$.

N	128	256	512	1024	2048	4096	8192	16384
				$Pr = 0.2$				
D^N	0.004722	0.002845	0.001656	0.000941	0.000526	0.000290	0.000158	0.000086
p^N	0.73	0.78	0.82	0.84	0.86	0.87	0.88	0.89
$C_{0.86}^N$	0.677075	0.739432	0.779930	0.803307	0.813477	0.813477	0.805625	0.791697
				$Pr = 512$				
D^N	0.303333	0.218680	0.139630	0.083386	0.047859	0.026793	0.014756	0.008034
p^N	0.47	0.65	0.74	0.80	0.84	0.86	0.88	0.89
$C_{0.84}^N$	39.982911	51.487505	58.723431	62.641831	64.220045	64.220045	63.175418	61.443988
				$Pr = 10000$				
D^N	0.632685	0.965106	0.799971	0.538230	0.328013	0.189495	0.106121	0.058302
p^N	-0.61	0.27	0.57	0.71	0.79	0.84	0.86	0.88
$C_{0.79}^N$	69.762694	184.206073	264.299411	307.810267	324.712684	324.712684	314.770500	299.341216

Table 7.4: Computed two mesh difference $\overline{D}^N$, the order of convergence $\overline{p}^N$ and computed global error constant $\overline{C}_{\overline{p}^*}^N$ for $\overline{D^+\Theta}$ on $[0, \infty)$ generated by (A_{TB}^N) with $M = 8nN$ applied to problem (P_{TB}) for various values of N and Pr with $\beta = 0.3$ and $n = \frac{1-m}{2}$.

N	128	256	512	1024	2048	4096	8192	16384
				$Pr = 0.2$				
D^N	0.003865	0.002314	0.001345	0.000763	0.000426	0.000235	0.000128	0.000070
p^N	0.74	0.78	0.82	0.84	0.86	0.87	0.88	0.89
$C_{0.86}^N$	0.556262	0.604012	0.636861	0.654869	0.663397	0.663397	0.657177	0.646107
				$Pr = 512$				
D^N	0.016925	0.012540	0.007870	0.004650	0.002665	0.001482	0.000816	0.000444
p^N	0.43	0.67	0.76	0.80	0.85	0.86	0.88	0.89
$C_{0.85}^N$	2.320194	3.091701	3.489808	3.708389	3.823173	3.823173	3.783681	3.702956
				$Pr = 10000$				
D^N	0.029011	0.019389	0.016228	0.011377	0.006808	0.003907	0.002176	0.001194
p^N	0.58	0.26	0.51	0.74	0.80	0.84	0.87	0.88
$C_{0.80}^N$	3.320610	3.866961	5.639537	6.889689	7.184060	7.184060	6.971925	6.664989

Table 7.5: Computed two mesh difference $\overline{D}^N$, the order of convergence $\overline{p}^N$ and computed global error constant $\overline{C}_{\overline{p}^*}^N$ for $\overline{\eta D^+ \Theta}$ on $[0, \infty)$ generated by (A_{TB}^N) with $M = 8nN$ applied to problem (P_{TB}) for various values of N and Pr with $\beta = 0.3$ and $n = \frac{1-m}{2}$.

The computed global error can be used to calculate the global error bounds for all values of $N \geq 256$, however in the next chapter we only need the value $N = 8192$. For this number of nodes we use Tables 7.8, 7.9 and 7.10 and the experimental technique to obtain the following error bounds for $N \geq 2048$

$$
\begin{aligned}
Pr &= 0.2 & ||\overline{\Theta} - \theta||_{[0,\infty)} &\leq 0.657 N^{-0.86} \\
Pr &= 512 & ||\overline{\Theta} - \theta||_{[0,\infty)} &\leq 4.626 N^{-0.86} \\
Pr &= 10000 & ||\overline{\Theta} - \theta||_{[0,\infty)} &\leq 12.90 N^{-0.86}
\end{aligned}
\tag{7.14}
$$

$$
\begin{aligned}
Pr &= 0.2 & ||\overline{D^+\Theta} - \theta'||_{[0,\infty)} &\leq 0.627 N^{-0.86} \\
Pr &= 512 & ||\overline{D^+\Theta} - \theta'||_{[0,\infty)} &\leq 0.710 N^{-0.84} \\
Pr &= 10000 & ||\overline{D^+\Theta} - \theta'||_{[0,\infty)} &\leq 324.71 N^{-0.79}
\end{aligned}
\tag{7.15}
$$

$$
\begin{aligned}
Pr &= 0.2 & ||\eta(\overline{D^+\Theta} - \theta')||_{[0,\infty)} &\leq 0.663 N^{-0.86} \\
Pr &= 512 & ||\eta(\overline{D^+\Theta} - \theta')||_{[0,\infty)} &\leq 3.823 N^{-0.85} \\
Pr &= 10000 & ||\eta(\overline{D^+\Theta} - \theta')||_{[0,\infty)} &\leq 7.184 N^{-0.80}.
\end{aligned}
\tag{7.16}
$$

7.7 Computed global error estimates for Blasius solution

We now obtain approximate expressions T_{TB} for the Blasius solution t_{TB} of (P_T) by substituting into the relation (7.4) the approximations $\overline{\Theta}$ and $\overline{D^+\Theta}$ for θ and θ',

computed by (A_T^N). Thus for each (x, y) in the rectangle $\overline{\Omega}$ we define

$$T_{TB}(x, y) = \overline{\Theta}(\eta) \tag{7.17}$$

where $\eta \in [0, \infty)$ is given by (7.1).

The following theoretical bounds hold for the approximation T_T to the temperature t_T

$$\|T_{TB} - t_{TB}\|_{\overline{\Omega}} \leq C_{p_1} N^{-p_1} \quad p_1 > 0 \tag{7.18}$$

where T_{TB} is the computed Blasius solution of the Prandtl problem on $\overline{\Omega}$ given by (7.17) and t_{TB} is the exact solution of (P_T). Here N_0 and the error parameters p_1, p_2, C_{p_1} and C_{p_2} are independent of N and M.

For the heat component t_{TB} we obtain, from (7.17), and (7.32), the following computed error bound for all $N \geq 2048$

$$
\begin{aligned}
Pr = 0.2 \quad \|T_{TB} - t_{TB}\|_{\overline{\Omega}} &= \|\overline{\Theta} - \theta\|_{[0,\infty)} \\
&\leq 0.657 N^{-0.86} \\
Pr = 512 \quad \|T_{TB} - t_{TB}\|_{\overline{\Omega}} &\leq 4.627 N^{-0.86} \\
Pr = 10000 \quad \|T_{TB} - t_{TB}\|_{\overline{\Omega}} &\leq 12.90 N^{-0.86}.
\end{aligned} \tag{7.19}
$$

In the specific case $N = 8192$ the computed error bounds (7.37) become

$$
\begin{aligned}
Pr = 0.2 \quad \|T_{TB} - t_{TB}\|_{\overline{\Omega}} &\leq 2.832 \times 10^{-4} \\
Pr = 512 \quad \|T_{TB} - t_{TB}\|_{\overline{\Omega}} &\leq 1.995 \times 10^{-3} \\
Pr = 10000 \quad \|T_{TB} - t_{TB}\|_{\overline{\Omega}} &\leq 5.560 \times 10^{-3}.
\end{aligned} \tag{7.20}
$$

In a similar manner to the above we calculate computed error bounds for approximations of the scaled first derivatives by scaled discrete derivatives

$$\partial_y T_{TB} = \frac{\eta}{y} \overline{D^+ \Theta}(\eta) \tag{7.21}$$

$$\partial_x T_{TB} = \frac{1 - m}{2x} \eta \overline{D^+ \Theta}(\eta). \tag{7.22}$$

In terms of these quantities the computed global error bounds for the scaled discrete derivative of the temperature components are

$$T_y^* \frac{1}{\sqrt{Re}} \|\partial_y T_{TB} - \frac{\partial t_{TB}}{\partial y}\|_{\overline{\Omega}} = T_y^* \frac{1}{\sqrt{Re}} \sqrt{\frac{(m+1) Re}{2} \frac{U(x)}{x}} \|\overline{D^+ \Theta} - \theta'\|_{[0,\infty)} \tag{7.23}$$

where T_y^* is defined to be

$$T_y^* = \begin{cases} \frac{1}{\sqrt[3]{\epsilon_{Pr}}} & \text{for } Pr \geq 1 \\ \frac{1}{\sqrt{\epsilon_{Pr}}} & \text{for } Pr < 1. \end{cases} \qquad (7.24)$$

The choice of scaling factor T_y^* is motivated by the width of the thermal boundary [46].

For $\partial_y T_{TB}$ we obtain, from (7.39), and (7.33), the following computed error bound for all $N \geq 2048$

$$\begin{array}{lll}
Pr = 0.2 & \frac{1}{\sqrt{0.2}}\frac{1}{\sqrt{Re}}||\partial_y T_{TB} - \frac{\partial t_{TB}}{\partial y}||_{\overline{\Omega}} & \leq \frac{1}{\sqrt{0.2}}\sqrt{\frac{(1.1764)}{2}\frac{1.1^{0.1746}}{1.1}}(0.813N^{-0.86}) \\
Pr = 512 & \frac{1}{\sqrt[3]{512}}\frac{1}{\sqrt{Re}}||\partial_y T_{TB} - \frac{\partial t_{TB}}{\partial y}||_{\overline{\Omega}} & \leq \frac{1}{\sqrt[3]{512}}\sqrt{\frac{(1.1764)}{2}\frac{1.1^{0.1746}}{1.1}}(64.22N^{-0.81}) \\
Pr = 10000 & \frac{1}{\sqrt[3]{10000}}\frac{1}{\sqrt{Re}}||\partial_y T_{TB} - \frac{\partial t_{TB}}{\partial y}||_{\overline{\Omega}} & \leq \frac{1}{\sqrt[3]{10000}}\sqrt{\frac{(1.1764)}{2}\frac{1.1^{0.1746}}{1.1}}(324.71N^{-0.79}).
\end{array} \qquad (7.25)$$

In the specific case $N = 8192$ the computed error bounds hold:

$$\begin{array}{lll}
Pr = 0.2 & \frac{1}{\sqrt{Re}}||\partial_y T_{TB} - \frac{\partial t_{TB}}{\partial y}||_{\overline{\Omega}} & \leq 5.778 \times 10^{-4} \\
Pr = 512 & \frac{1}{\sqrt{Re}}||\partial_y T_{TB} - \frac{\partial t_{TB}}{\partial y}||_{\overline{\Omega}} & \leq 4.004 \times 10^{-3} \\
Pr = 10000 & \frac{1}{\sqrt{Re}}||\partial_y T_{TB} - \frac{\partial t_{TB}}{\partial y}||_{\overline{\Omega}} & \leq 9.002 \times 10^{-3}.
\end{array} \qquad (7.26)$$

For $\partial_x T_{TB}$ we obtain, from (7.40), and (7.34), the following computed error bound for all $N \geq 2048$

$$||\partial_x T_{TB} - \frac{\partial t_{TB}}{\partial x}||_{\overline{\Omega}} = \frac{(m-1)}{2x}||\eta(\overline{D^+\Theta} - \theta')||_{[0,\infty)} \qquad (7.27)$$

$$\begin{array}{lll}
Pr = 0.2 & ||\partial_x T_{TB} - \frac{\partial t_{TB}}{\partial x}||_{\overline{\Omega}} & \leq \frac{0.823}{2(1.1)}(0.654N^{-0.86}) \\
Pr = 512 & ||\partial_x T_{TB} - \frac{\partial t_{TB}}{\partial x}||_{\overline{\Omega}} & \leq \frac{0.823}{2(1.1)}(0.3.70N^{-0.85}) \\
Pr = 10000 & ||\partial_x T_{TB} - \frac{\partial t_{TB}}{\partial x}||_{\overline{\Omega}} & \leq \frac{0.823}{2(1.1)}(7.18N^{-0.80}).
\end{array} \qquad (7.28)$$

In the specific case $N = 8192$ the computed error bounds

$$\begin{array}{lll}
Pr = 0.2 & ||\partial_x T_{TB} - \frac{\partial t_{TB}}{\partial x}||_{\overline{\Omega}} & \leq 6.063 \times 10^{-5} \\
Pr = 512 & ||\partial_x T_{TB} - \frac{\partial t_{TB}}{\partial x}||_{\overline{\Omega}} & \leq 3.754 \times 10^{-4} \\
Pr = 10000 & ||\partial_x T_{TB} - \frac{\partial t_{TB}}{\partial x}||_{\overline{\Omega}} & \leq 1.143 \times 10^{-3}.
\end{array} \qquad (7.29)$$

7.8 Numerical solution of the Blasius problem

As the numerical results for F, D^+F and D^+D^+F have been extensively investigate in section 3.6, we only need to investigate the numerical results of Θ and $D^+\Theta$ for

various values of β. The definitions of the computed pointwise maximum errors, the pointwise two mesh difference and the two mesh orders of convergence are given in section 3.6. We choose $\beta = 0.5, \beta = 1.0$, and $\beta = 1.5$ to be consistent with chapters 3 and 4. For $\beta = 0.5, 1.0$ and 1.5 the computed maximum pointwise error E^N, computed two mesh difference D^N and the computed order of convergence p^N for $\overline{\Theta}$ and $\overline{D^+\Theta}$, are given by Tables 7.6 and 7.7, respectively. The main conclusion to be drawn from the numerical results in these Tables is that method (P_{TB}^N), in conjunction with algorithm (A_{TB}^N), is, in practice a robust layer-resolving method for problem 7.5 for all values of β in the sense that it is L-uniform and that the L-uniform order of convergence on $[0, L_N]$ of the numerical solution Θ of the exact Θ_L and of the discrete derivative $D^+\Theta$ to the derivative θ'_L, is, in practice, better than 0.8 for all $N \geq 512$ and β.

N	128	256	512	1024	2048	4096	8192	16384
				$\beta = 0.5$				
E^N	0.008064	0.004623	0.002589	0.001424	0.000767	0.000402	0.000201	0.000091
D^N	0.003432	0.002032	0.001166	0.000657	0.000365	0.000201	0.000110	0.000059
p^N	0.76	0.80	0.83	0.85	0.86	0.87	0.88	0.89
				$\beta = 1.0$				
E^N	0.008493	0.004860	0.002722	0.001497	0.000806	0.000422	0.000211	0.000096
D^N	0.003632	0.002138	0.001225	0.000690	0.000384	0.000211	0.000115	0.000062
p^N	0.76	0.80	0.83	0.85	0.86	0.87	0.88	0.89
				$\beta = 1.5$				
E^N	0.008745	0.005001	0.002801	0.001540	0.000830	0.000435	0.000217	0.000099
D^N	0.003738	0.002197	0.001260	0.000710	0.000395	0.000217	0.000119	0.000064
p^N	0.77	0.80	0.83	0.85	0.86	0.87	0.88	0.89

Table 7.6: Computed maximum pointwise error E^N for $\bar{\Theta}$ on $\overline{I}_u^N$ generated by (A_{TB}^N) with $M = 8lnN$ applied to problem (P_{TB}) for various values of N and β.

N	128	256	512	1024	2048	4096	8192	16384
				$\beta = 0.5$				
E^N	0.008727	0.004998	0.002799	0.001539	0.000829	0.000434	0.000217	0.000099
D^N	0.003729	0.002199	0.001260	0.000710	0.000395	0.000217	0.000118	0.000064
p^N	0.76	0.80	0.83	0.85	0.86	0.87	0.88	0.89
				$\beta = 1.0$				
E^N	0.009891	0.005658	0.003168	0.001742	0.000938	0.000492	0.000246	0.000112
D^N	0.004233	0.002490	0.001427	0.000804	0.000447	0.000246	0.000134	0.000073
p^N	0.77	0.80	0.83	0.85	0.86	0.87	0.88	0.89
				$\beta = 1.5$				
E^N	0.010665	0.006098	0.003414	0.001877	0.001011	0.000530	0.000265	0.000120
D^N	0.004567	0.002683	0.001537	0.000866	0.000481	0.000265	0.000144	0.000078
p^N	0.77	0.80	0.83	0.85	0.86	0.87	0.88	0.89

Table 7.7: Computed maximum pointwise error E^N for $\overline{D^+\Theta}$ on $\overline{I}_u^N \backslash \{\eta_N\}$ generated by (A_{TB}^N) with $M = 8lnN$ applied to problem (P_{TB}) for various values of N and β.

Comparison of the entries in the last rows of Tables 7.6 and 7.7 with the Table of theoretical behavior for $N^{-1}lnN$, and $N^{-1}(lnN)^2$ of the order of convergence defined p^N in Appendix ?? suggest strongly that the computed order of L-uniform convergence p^N corresponds to the theoretical behavior $N^{-1}lnN$.

Graphs of $\overline{\Theta}$ for $N = 8192$ and various values of β on $[0, L_N]$ are given in Figure 7-2. We can see that there is a region of rapid change near $\eta = 0$.

Figure 7-2: Solution $\overline{\Theta}$ generated by method (A_{TB}^N) applied to the problem P_{TB} with $M = 8lnN$, $N = 8192$ and various values of β.

Graphs of $\overline{D^+\Theta}$ for $N = 8192$ and various values of β on $[0, L_N]$ are given in Figure 7-3.

Figure 7-3: Solution $\overline{D^+\Theta}$ generated by method (A_{TB}^N) applied to the problem P_{TB} with $M = 8lnN$, $N = 8192$ and various values of β.

7.9 Computed error estimates for Blasius problem

Theoretical estimates indicate that, for all $N \geq N_0$, the approximations of $\overline{\Theta}$ and $\overline{D^+\Theta}$, respectively, to the exact solution of the Blasius problem (P_{TB}) and its derivatives satisfy error bounds of the form

$$||\overline{\Theta} - \theta||_{[0,\infty)} \leq C_p N^{-p} \tag{7.30}$$

$$||\overline{D^+\Theta} - \theta'||_{[0,\infty)} \leq C_p N^{-p} \tag{7.31}$$

where the error parameters are unknown. The computed two–mesh difference, computed order of convergence,computed global order of convergence and the computed global constant error are defined in section 3.6

We now use the experimental techniques to obtain computed parameter uniform global error parameters for the function $\overline{\Theta}$ on the semi-infinite interval $[0,\infty)$ for various β. To determine the two mesh differences $\overline{D}$ and hence the computed order of convergence $\overline{p}^N$ and the constant of convergence $\overline{C}_{\overline{p}^*}^N$ for a pair of meshes with N and 2N points respectively, we have to consider the 3 subintervals $[0, L_N), [L_N, L_{2N})$ and $[L_{2N}, \infty)$ separately. For $\eta \in [L_N, L_{2N})$ the two mesh difference at η for $\overline{\Theta}$ is $\overline{\Theta}^{2N}(\eta)$ and for $\overline{D^+\Theta}$ is $\overline{D^+\Theta}^{2N}(\eta)$. In the subinterval $[L_{2N}, \infty)$ at η for $\overline{\Theta}$ and $\overline{D^+\Theta}$ it is zero. The resulting computed global two-mesh difference $\overline{D}$, the computed order of convergence $\overline{p}^N$ and the constant of convergence $\overline{C}_{\overline{p}^*}^N$ for $\overline{\Theta}$, $\overline{D^+\Theta}$ and $\eta\overline{D^+\Theta}$ for various values of N and β are given in Tables 7.8, 7.9 and 7.10.

				$\beta = 0.5$				
N	128	256	512	1024	2048	4096	8192	16384
D^N	0.003432	0.002032	0.001166	0.000657	0.000365	0.000201	0.000110	0.000059
p^N	0.76	0.80	0.83	0.85	0.86	0.87	0.88	0.89
$C_{0.86}^N$	0.499628	0.537599	0.560498	0.573756	0.579885	0.579885	0.574990	0.566100
				$\beta = 1.0$				
D^N	0.003632	0.002138	0.001225	0.000690	0.000384	0.000211	0.000115	0.000062
p^N	0.76	0.80	0.83	0.85	0.86	0.87	0.88	0.89
$C_{0.86}^N$	0.528981	0.566006	0.589314	0.603358	0.609859	0.609859	0.604763	0.595449
				$\beta = 1.5$				
D^N	0.003738	0.002197	0.001260	0.000710	0.000395	0.000217	0.000119	0.000064
p^N	0.77	0.80	0.83	0.85	0.86	0.87	0.88	0.89
$C_{0.86}^N$	0.544352	0.581488	0.606184	0.620732	0.627382	0.627382	0.622128	0.612524

Table 7.8: Computed two mesh difference $\overline{D}^N$ and the order of convergence $\overline{p}^N$ for $\overline{\Theta}$ on $[0,\infty)$ generated by (A_{TB}^N) with $M = 8 \ln N$ applied to problem (P_{TB}) for various values of N and β.

				$\beta = 0.50$				
N	128	256	512	1024	2048	4096	8192	16384
D^N	0.003729	0.002199	0.001260	0.000710	0.000395	0.000217	0.000118	0.000064
p^N	0.76	0.80	0.83	0.85	0.86	0.87	0.88	0.89
$C_{0.86}^N$	0.543034	0.582001	0.606187	0.620558	0.627033	0.627033	0.621739	0.612148
				$\beta = 1.00$				
D^N	0.004233	0.002490	0.001427	0.000804	0.000447	0.000246	0.000134	0.000073
p^N	0.77	0.80	0.83	0.85	0.86	0.87	0.88	0.89
$C_{0.86}^N$	0.616475	0.658970	0.686236	0.702504	0.709835	0.709835	0.703842	0.692985
				$\beta = 1.50$				
D^N	0.004567	0.002683	0.001537	0.000866	0.000481	0.000265	0.000144	0.000078
p^N	0.77	0.80	0.83	0.85	0.86	0.87	0.88	0.89
$C_{0.86}^N$	0.665188	0.710322	0.739632	0.757142	0.765034	0.765034	0.758581	0.746888

Table 7.9: Computed two mesh difference $\bar{D}^N$ and the order of convergence $\bar{p}^N$ for $\overline{D^+\Theta}$ on $[0, \infty)$ generated by (A_{TB}^N) with $M = 8lnN$ applied to problem (P_{TB}) for various values of N and β.

				$\beta = 0.50$				
N	128	256	512	1024	2048	4096	8192	16384
D^N	0.003274	0.001947	0.001123	0.000634	0.000353	0.000195	0.000106	0.000058
p^N	0.75	0.79	0.82	0.84	0.86	0.87	0.88	0.89
$C_{0.86}^N$	0.474384	0.512433	0.536410	0.550549	0.556825	0.556825	0.552032	0.543206
				$\beta = 1.00$				
D^N	0.003418	0.002030	0.001173	0.000664	0.000370	0.000204	0.000111	0.000060
p^N	0.75	0.79	0.82	0.84	0.86	0.87	0.88	0.89
$C_{0.86}^N$	0.495212	0.533985	0.560548	0.575605	0.582181	0.582181	0.577162	0.567937
				$\beta = 1.50$				
D^N	0.003524	0.002085	0.001204	0.000681	0.000380	0.000209	0.000114	0.000062
p^N	0.76	0.79	0.82	0.84	0.86	0.87	0.88	0.89
$C_{0.86}^N$	0.510290	0.548284	0.574944	0.590122	0.597267	0.597267	0.592041	0.582533

Table 7.10: Computed two mesh difference $\bar{D}^N$ and the order of convergence $\bar{p}^N$ for $\overline{\eta D^+\Theta}$ on $[0, \infty)$ generated by (A_{TB}^N) with $M = 8lnN$ applied to problem (P_{TB}) for various values of N and β.

The computed global error can be used to calculate the global error bounds for all values of $N \geq 256$, but in the next chapter we only need the value $N = 8192$. For this number of nodes we use the Tables 7.8, 7.9 and 7.10 and the experimental technique to obtain the following error bounds for $N \geq 2048$

$$\begin{aligned}
\beta = 0.5 \quad & ||\overline{\Theta} - \theta||_{[0,\infty)} \leq 0.580 N^{-0.86} \\
\beta = 1.0 \quad & ||\overline{\Theta} - \theta||_{[0,\infty)} \leq 0.609 N^{-0.86} \\
\beta = 1.5 \quad & ||\overline{\Theta} - \theta||_{[0,\infty)} \leq 0.627 N^{-0.86}
\end{aligned}$$
(7.32)

$$\beta = 0.5 \quad ||\overline{D^+\Theta} - \theta'||_{[0,\infty)} \leq 0.627N^{-0.86}$$
$$\beta = 1.0 \quad ||\overline{D^+\Theta} - \theta'||_{[0,\infty)} \leq 0.710N^{-0.86} \tag{7.33}$$
$$\beta = 1.5 \quad ||\overline{D^+\Theta} - \theta'||_{[0,\infty)} \leq 0.765N^{-0.86}$$

$$\beta = 0.5 \quad ||\eta(\overline{D^+\Theta} - \theta')||_{[0,\infty)} \leq 0.557N^{-0.86}$$
$$\beta = 1.0 \quad ||\eta(\overline{D^+\Theta} - \theta')||_{[0,\infty)} \leq 0.582N^{-0.86} \tag{7.34}$$
$$\beta = 1.5 \quad ||\eta(\overline{D^+\Theta} - \theta')||_{[0,\infty)} \leq 0.597N^{-0.86}$$

7.10 Computed global error estimates for Blasius solution

We now obtain approximate expressions T_{TB} for the Blasius solution t_{TB} of (P_T) by substituting into the relation (7.4) the approximations $\overline{\Theta}$ and $\overline{D^+\Theta}$ for g and g', computed by (A_T^N). Thus for each (x, y) in the rectangle $\overline{\Omega}$ we define

$$T_{TB}(x, y) = \overline{\Theta}(\eta) \tag{7.35}$$

where $\eta \in [0, \infty)$ is given by (7.1).

Preliminary analytical investigations also indicate that for all $N \geq N_0$ and some unknown constants p_1, and C_{p_1}, the following theoretical bounds hold for the approximation T_T to the scaled velocity t_T

$$||T_{TB} - t_{TB}||_{\overline{\Omega}} \leq C_{p_1} N^{-p_1} \quad p_1 > 0 \tag{7.36}$$

where T_{TB} is the computed Blasius solution of the Prandtl problem on $\overline{\Omega}$ given by (7.17) and t_{TB} is the exact solution of (P_T). Here N_0 and the error parameters p_1, p_2, C_{p_1} and C_{p_2} are independent of N and M.

In what follows, we use the experimental techniques to determine realistic error bounds of the form (7.36).

For the heat component t_{TB} we obtain from (7.17), and (7.32) the following computed error bound for all $N \geq 2048$

$$\beta = 0.5 \quad ||T_{TB} - t_{TB}||_{\overline{\Omega}} = ||\overline{\Theta} - g||_{[0,\infty)}$$
$$\leq 0.580N^{-0.86}$$
$$\beta = 1.0 \quad ||T_{TB} - t_{TB}||_{\overline{\Omega}} \leq 0.609N^{-0.86} \tag{7.37}$$
$$\beta = 1.5 \quad ||T_{TB} - t_{TB}||_{\overline{\Omega}} \leq 0.627N^{-0.86}$$

In the specific case $N = 8192$ the computed error bounds 5.18 become

$$
\begin{aligned}
\beta = 0.5 \quad &\|T_{TB} - t_{TB}\|_{\overline{\Omega}} \leq 2.543e - 04 \\
\beta = 1.0 \quad &\|T_{TB} - t_{TB}\|_{\overline{\Omega}} \leq 2.625e - 04 \\
\beta = 1.5 \quad &\|T_{TB} - t_{TB}\|_{\overline{\Omega}} \leq 2.702e - 04
\end{aligned} \tag{7.38}
$$

In a similar manner to the above we calculate computed error bounds for approximations of the scaled first derivatives by scaled discrete derivatives

$$
\partial_y T_{TB} = \frac{\eta}{y} \overline{D^+ \Theta}(\eta) \tag{7.39}
$$

$$
\partial_x T_{TB} = \frac{m-1}{2x} \eta \overline{D^+ \Theta}(\eta). \tag{7.40}
$$

In terms of these quantities the computed global error bounds for the scaled discrete derivative of the velocity components.

$$
\frac{1}{\sqrt{Re}} \| \partial_y T_{TB} - \frac{\partial t_{TB}}{\partial y} \|_{\overline{\Omega}} = \frac{1}{\sqrt{Re}} \sqrt{\frac{(m+1)Re\,U(x)}{2}\frac{}{x}} \| \overline{D^+ \Theta} - g' \|_{[0,\infty)} \tag{7.41}
$$

For $\partial_y T_{TB}$ we obtain, from (7.39), and (7.33) the following computed error bound for all $N \geq 2048$

$$
\begin{aligned}
\beta = 0.5 \quad &\frac{1}{\sqrt{Re}} \| \partial_y T_{TB} - \frac{\partial t_{TB}}{\partial y} \|_{\overline{\Omega}} \leq \sqrt{\frac{(1.333)}{2} \frac{1.1^{0.333}}{1.1}}(0.627 N^{-0.86}) \\
\beta = 1.0 \quad &\frac{1}{\sqrt{Re}} \| \partial_y T_{TB} - \frac{\partial t_{TB}}{\partial y} \|_{\overline{\Omega}} \leq \sqrt{\frac{(1)}{2} \frac{1.1^1}{1.1}}(0.710 N^{-0.86}) \\
\beta = 1.5 \quad &\frac{1}{\sqrt{Re}} \| \partial_y T_{TB} - \frac{\partial t_{TB}}{\partial y} \|_{\overline{\Omega}} \leq \sqrt{\frac{(4)}{2} \frac{1.1^3}{1.1}}(0.765 N^{-0.86})
\end{aligned} \tag{7.42}
$$

In the specific case $N = 8192$ the computed error bounds

$$
\begin{aligned}
\beta = 0.5 \quad &\frac{1}{\sqrt{Re}} \| \partial_y T_{TB} - \frac{\partial t_{TB}}{\partial y} \|_{\overline{\Omega}} \leq 1.822e - 04 \\
\beta = 1.0 \quad &\frac{1}{\sqrt{Re}} \| \partial_y T_{TB} - \frac{\partial t_{TB}}{\partial y} \|_{\overline{\Omega}} \leq 2.060e - 04 \\
\beta = 1.5 \quad &\frac{1}{\sqrt{Re}} \| \partial_y T_{TB} - \frac{\partial t_{TB}}{\partial y} \|_{\overline{\Omega}} \leq 2.223e - 04.
\end{aligned} \tag{7.43}
$$

For $\partial_x T_{TB}$ we obtain, from (7.40), and (7.34) the following computed error bound for all $N \geq 2048$

$$
\|\partial_x T_{TB} - \frac{\partial t_{TB}}{\partial x}\|_{\overline{\Omega}} = \frac{(m-1)}{2x} \|\eta(\overline{D^+ \Theta} - g')\|_{[0,\infty)} \tag{7.44}
$$

$$
\begin{aligned}
\beta = 0.5 \quad &\|\partial_x T_{TB} - \frac{\partial t_{TB}}{\partial x}\|_{\overline{\Omega}} \leq \frac{0.667}{2(1.1)}(0.557 N^{-0.86}) \\
\beta = 1.0 \quad &\|\partial_x T_{TB} - \frac{\partial t_{TB}}{\partial x}\|_{\overline{\Omega}} \leq 0 \\
\beta = 1.5 \quad &\|\partial_x T_{TB} - \frac{\partial t_{TB}}{\partial x}\|_{\overline{\Omega}} \leq \frac{3}{2(2.1)}(0.597 N^{-0.86})
\end{aligned} \tag{7.45}
$$

Chapter 8

A Reynolds and Prandtl uniform numerical method for the Prandtl boundary layer problem for flow past a wedge with heat transfer

8.1 Introduction

Adapting the parameter–uniform methods described in Chapters 4 and 6 we construct a Reynolds and Prandtl uniform numerical method for the Prandtl boundary layer problem for flow past a wedge with heat transfer. The momentum equation and energy equation are parabolic and singularly perturbed. In the case of the momentum equation the parameter is the reciprocal of the Reynolds number Re. In the case of the energy equation the parameter is the reciprocal of the product of the Reynolds number and Prandtl number Pr. For convenience we use the notation $\varepsilon = \frac{1}{Re}$ and $\varepsilon_{Pr} = \frac{1}{Pr}$.

The Prandtl boundary layer problem (P_T) in Chapter 7 is rewritten as

$(P_{T\varepsilon})$
$$
\begin{cases}
\text{Find } \mathbf{u_{T\varepsilon}} = (u_{T\varepsilon}, v_{T\varepsilon}) \text{ and } t_{T\varepsilon} \text{ such that for all } (x,y) \in \Omega \\[4pt]
\mathbf{u_{T\varepsilon}} \text{ and } t_{T\varepsilon} \text{ satisfy the differential equations} \\[10pt]
-\varepsilon \frac{\partial^2 u_{T\varepsilon}}{\partial^2 y} + u_{T\varepsilon}\frac{\partial v_{T\varepsilon}}{\partial x} + v_{T\varepsilon}\frac{\partial u_{T\varepsilon}}{\partial y} = U\frac{dU}{dx} \\[10pt]
-\varepsilon\varepsilon_{Pr}\frac{\partial^2 t_{T\varepsilon}}{\partial^2 y} + u_{T\varepsilon}\left(\frac{\partial t_{T\varepsilon}}{\partial x} + \frac{n}{x}t_{T\varepsilon}\right) + v_{T\varepsilon}\frac{\partial t_{T\varepsilon}}{\partial y} = 0 \\[10pt]
\frac{\partial u_{T\varepsilon}}{\partial x} + \frac{\partial v_{T\varepsilon}}{\partial y} = 0 \\[10pt]
\text{with boundary conditions} \\[4pt]
u_{T\varepsilon} = 0, \quad t_{T\varepsilon} = 1 \text{ and } v_{T\varepsilon} = 0 \text{ on } \Gamma_B \\[4pt]
\mathbf{u_{T\varepsilon}} = \mathbf{u}_{TB}^{8192} \text{ and } t_{T\varepsilon} = t_{TB}^{8192} \quad \text{on } \Gamma_L \bigcup \Gamma_T
\end{cases}
$$

where $U(x) = x^m$, $m = \frac{\beta}{2-\beta}$ and $\beta\pi$ is the angle of the wedge in radians. n is the heat transfer parameter.

We make use of the computed Blasius similarity solution of the Prandtl problem, calculated in Chapter 7, in two ways. Firstly, we use it to provide the required artificial boundary conditions on the boundary of Ω in the direct numerical method for the Prandtl problem discussed in the next section. Secondly, we use it as a reference solution for the unknown exact solution in the expression for the error. Since the computed Blasius solution is known to converge (Re, Pr, β, n)–uniformly to the solution of the Prandtl problem, we can compute (Re, Pr, β, n)–uniform error bounds. For this purpose we use the computed Blasius solution for (P_{TB}) when $N{=}8192$, namely $\mathbf{U}_{TB}^{8192}$ and T_{TB}^{8192}, which provides the required accuracy for the velocity components U_{TB}^{8192} and V_{TB}^{8192}, their derivatives $D_x V_B^{8192}$, $D_y V_{TB}^{8192}$, their scaled derivatives $\sqrt{\varepsilon}D_y U_{TB}^{8192}$, the temperature component T_{TB}^{8192} and its derivative $D_x T_B^{8192}$ and its scaled derivative $T_y^* \sqrt{\varepsilon}D_y T_B^{8192}$.

Our goal is to construct an (Re, Pr, β, n)–uniform numerical method for solving $(P_{T\varepsilon})$, in the sense that the method has error bounds, for the solutions and their derivatives, independent of Re, Pr and β, for all $Re \in [1,\infty)$, $Pr \in [0.1, 10000]$ and all $\beta \in [0, 0.3]$, for constant heat flux and walls of constant temperature.

8.2 Direct Numerical method for the Prandtl Problem

The aim of this section is to construct a direct numerical method to solve the Prandtl problem $(P_{T\varepsilon})$ for all $Re \in [1, \infty)$, $Pr \in [0.1, 10000]$ and $\beta \in [0, 0.3]$ for constant heat flux, $n = \frac{m-1}{2}$, and walls of constant temperature, $n = 0$. We require a compound piecewise–uniform fitted mesh $\Omega_\varepsilon^{\mathbf{N}}$ in the rectangle Ω, where $\mathbf{N}=(N_x, N_y)$. We define the mesh as the tensor product $\Omega_\varepsilon^{\mathbf{N}} = \Omega_u^{N_x} \times \Omega_\varepsilon^{N_y}$, where the one–dimensional mesh in the x direction is the uniform mesh $\Omega_u^{N_x} = \{x_i : x_i = 0.1 + iN_x^{-1}, 0 \leq i \leq N_x\}$ and the mesh in the y-direction is the compound piecewise–uniform fitted mesh

$$\Omega_\varepsilon^{N_y} = \{y_j : y_j = \sigma_2 j \frac{4}{N_y}, 0 \leq j \leq \frac{N_y}{4}; y_j = \sigma_2 + (\sigma - \sigma_2)(j - \frac{N_y}{4})\frac{4}{N_y}, \frac{N_y}{4} \leq j \leq \frac{N_y}{2};$$
$$y_j = \sigma + (1 - \sigma)(j - \frac{N_y}{2})\frac{2}{N_y}, \frac{N_y}{2} \leq j \leq N_y\}.$$

It is important to note that the transition points σ and σ_2 are chosen so that there are fine meshes in the boundary layers whenever they are required. The appropriate choices for $Pr \geq 1$ are

$$\sigma = \min\{\frac{1}{2}, 1.2\sqrt{\varepsilon} ln N_y\} \tag{8.1}$$

$$\sigma_2 = \min\{\frac{1}{2}\sigma, 1.2\sqrt{\varepsilon}\sqrt[3]{\varepsilon_{Pr}} ln N_y\}. \tag{8.2}$$

and for $Pr < 1$ are

$$\sigma = \min\{\frac{1}{2}, 1.2\sqrt{\varepsilon_{Pr}}\sqrt{\varepsilon} ln N_y\} \tag{8.3}$$

$$\sigma_2 = \min\{\frac{1}{2}\sigma, 1.2\sqrt{\varepsilon} ln N_y\}. \tag{8.4}$$

The factor $\sqrt{\varepsilon}$ may be motivated from asymptotic analysis [18]. The factors $\sqrt[3]{\varepsilon_{Pr}}$ and $\sqrt{\varepsilon_{Pr}}$ may be motivated from *a priori* estimates of the thermal layer or from asymptotic analysis. For simplicity we take $N_x = N_y = N$.

The problem $(P_{T\varepsilon})$ is discretised by the following non-linear upwind finite difference

method, on the piecewise uniform fitted mesh Ω_ε^N

$(P_{T\varepsilon}^N)$ $\begin{cases} \text{Find } \mathbf{U_{T\varepsilon}} = (U_{T\varepsilon}, V_{T\varepsilon}) \text{ and } T_{T\varepsilon} \text{ such that for all mesh points } (x_i, y_j) \in \Omega_\varepsilon^N, \\ \mathbf{U_{T\varepsilon}} \text{ and } T_{T\varepsilon} \text{ satisfy the finite mesh difference equations} \\[4pt] -\varepsilon\delta_y^2 U_{T\varepsilon}(x_i, y_j) + U_{T\varepsilon} D_x^- U_{T\varepsilon}(x_i, y_j) + V_{T\varepsilon} D_y^u U_{T\varepsilon}(x_i, y_j) = U\frac{dU}{dx} \\[6pt] -\varepsilon\varepsilon_{Pr}\delta_y^2 T_{T\varepsilon}(x_i, y_j) + U_{T\varepsilon}(D_x^- T_{T\varepsilon}(x_i, y_j) + \frac{n}{x}T_{T\varepsilon}) + V_{T\varepsilon} D_y^u T_{T\varepsilon}(x_i, y_j) = 0 \\[6pt] D_x^- U_{T\varepsilon}(x_i, y_j) + D_y^- V_{T\varepsilon}(x_i, y_j) = 0 \\[6pt] \text{with boundary conditions} \\ U_{T\varepsilon} = 0, \quad T_{T\varepsilon} = 1 \text{ and } V_{T\varepsilon} = 0 \text{ on } \Gamma_B \\ U_{T\varepsilon} = U_{TB}^{8192} \text{ and } T_{T\varepsilon} = T_{TB}^{8192} \quad \Gamma_L \bigcup \Gamma_T. \end{cases}$

Since $(P_{T\varepsilon}^N)$ is a non–linear finite difference method an iterative method is required for its solution. This is obtained by replacing the system of non–linear equations by

the following sequence of systems of linear equations

$(A_{T\varepsilon}^{\mathbf{N}})$ $\left\{\begin{array}{l}\end{array}\right.$

With the boundary condition $\mathbf{U}_{T\varepsilon}^{\mathbf{M}} = \mathbf{U}_{TB}^{\mathbf{8192}}$ on Γ_L, for each $i, 1 \le i \le N$,
use the initial guess $\mathbf{U}_{T\varepsilon}^{0}|_{X_i} = \mathbf{U}_{T\varepsilon}^{M_{i-1}}|_{X_{i-1}}$ and for $m = 1, \ldots, M$
solve the following two point boundary value problem for $U_{T\varepsilon}^{m}(x_i, y_j)$

$$-\varepsilon \delta_y^2 U_{T\varepsilon}^{m}(x_i, y_j) + U_{T\varepsilon}^{m-1} D_x^- U_{T\varepsilon}^{m}(x_i, y_j) + V_{T\varepsilon}^{m-1} D_y^u U_{T\varepsilon}^{m}(x_i, y_j) = U \frac{dU}{dx} \quad 1 \le j \le N-1$$

with the boundary conditions $U_{T\varepsilon}^{m} = U_{TB}$ on $\Gamma_B \cup \Gamma_T$,
and the initial guess for $V_{T\varepsilon}^{0}|_{X_1} = 0$.
Also solve the initial value problem for $V_{T\varepsilon}^{m}(x_i, y_j)$

$$D_x^- U_{T\varepsilon}^{m}(x_i, y_j) + D_y^- V_{T\varepsilon}^{m}(x_i, y_j) = 0$$

with initial condition $V_{T\varepsilon}^{m} = 0$ on Γ_B.
Continue to iterate between the equations for $\mathbf{U}_{T\varepsilon}^{m}$ until $m = M$,
where M is such that
$\max\left(|U_{T\varepsilon}^{M} - U_{T\varepsilon}^{M-1}|_{\overline{\Omega}_\varepsilon^N}, \frac{1}{V^*}|V_{T\varepsilon}^{M} - V_{T\varepsilon}^{M-1}|_{\overline{\Omega}_\varepsilon^N}\right) \le tol.$
Finally, solve the two point boundary value problem for $T_{T\varepsilon}(x_i, y_j)$

$$-\varepsilon \varepsilon_{Pr} \delta_y^2 T_{T\varepsilon}(x_i, y_j) + U_{T\varepsilon}^{M}(D_x^- T_{T\varepsilon}(x_i, y_j) + \frac{n}{x} T_{T\varepsilon}(x_i, y_j)) + V_{T\varepsilon}^{M} D_y^u T_{T\varepsilon}(x_i, y_j) = 0,$$
$$1 \le j \le N-1$$

with the boundary conditions $T_{T\varepsilon} = T_B$ on $\Gamma_B \cup \Gamma_T \cup \Gamma_L$.

For notational simplicity, we suppress explicit mention of the iteration superscript M_i, and henceforth we write simply $\mathbf{U}_\varepsilon$ and T_ε for the solution generated by $(A_\varepsilon^{\mathbf{N}})$. We take $tol = 10^{-6}$ in the computations.

8.3 Error analysis based upon the finest mesh

In this section we estimate, computationally, the maximum pointwise error in the numerical solution and its discrete derivatives generated by the algorithm $(A_{T\varepsilon}^{\mathbf{N}})$ of the previous section. Since the exact solution in the expression for the computed maximum pointwise error is unknown, we replace it by the solution $\mathbf{U}_{T\varepsilon}^{512}$ and $T_{T\varepsilon}^{512}$ generated by $(A_{T\varepsilon}^{\mathbf{N}})$ on the finest mesh Ω_ε^{512}. The results for $U_{T\varepsilon}$, $\frac{1}{V^*}V_{T\varepsilon}$ and their derivatives are similar to the results in Chapter 4 (also see Appendix D). We need

only investigate the results for $T_{T\varepsilon}$ and its derivatives.

For $T_{T\varepsilon}$ we define the computed maximum pointwise errors

$$E_\varepsilon^N(T_{T\varepsilon}) = ||T_{T\varepsilon} - \overline{T_{T\varepsilon}^{512}}||_{\overline{\Omega}_{T\varepsilon}^N}$$

and

$$E^N(T_{T\varepsilon}) = \max_\varepsilon E_\varepsilon^N(T_{T\varepsilon}).$$

As in the previous chapter, we show the errors for only three values of the Prandtl number $Pr = 0.2$, 512 and 10000 with $\beta = 0.3$ for constant heat flux $n = \frac{1-m}{2}$. The values of the computed maximum pointwise errors generated by $(A_{T\varepsilon}^\mathbf{N})$ applied to problem $(P_{T\varepsilon})$ for $T_{T\varepsilon}$ are given in Tables 8.1 for various values of ε, N and Pr, with $\beta = 0.3$ and constant heat flux $n = \frac{1-m}{2}$. The results in Table 8.1 stabilise to a fixed value for all N and all Pr considered. The computed maximum error for $T_{T\varepsilon}$ decreases as the number of mesh points increase. For each N the largest computed maximum error occurs when $2^{-2} \leq \varepsilon \leq 2^{-10}$. Table 8.1 strongly suggests that the method is ε–uniform for $T_{T\varepsilon}$, for all Pr considered, with $\beta = 0.3$ and $n = \frac{1-m}{2}$.

$\varepsilon \backslash N$	$Pr = 0.2$				$\varepsilon \backslash N$	$Pr = 512$			
	32	64	128	256		32	64	128	256
2^{-0}	9.99e-04	5.07e-04	2.35e-04	8.17e-05	2^{-0}	1.57e-02	7.00e-03	2.93e-03	9.68e-04
2^{-2}	2.95e-03	1.50e-03	6.83e-04	2.35e-04	2^{-2}	3.51e-02	1.53e-02	6.34e-03	2.08e-03
2^{-4}	2.82e-03	1.43e-03	6.47e-04	2.21e-04	2^{-4}	3.64e-02	1.84e-02	8.55e-03	3.02e-03
2^{-6}	2.37e-03	1.11e-03	4.86e-04	1.64e-04	2^{-6}	3.66e-02	1.86e-02	8.62e-03	3.04e-03
2^{-8}	3.95e-03	1.18e-03	4.76e-04	1.59e-04	2^{-8}	3.64e-02	1.85e-02	8.66e-03	3.07e-03
2^{-10}	4.48e-03	1.61e-03	6.03e-04	2.09e-04	2^{-10}	3.64e-02	1.85e-02	8.65e-03	3.06e-03
2^{-12}	4.48e-03	1.61e-03	6.03e-04	2.09e-04	2^{-12}	3.64e-02	1.85e-02	8.65e-03	3.06e-03
2^{-14}	4.48e-03	1.61e-03	6.03e-04	2.09e-04	2^{-14}	3.64e-02	1.85e-02	8.65e-03	3.06e-03
2^{-16}	4.48e-03	1.61e-03	6.03e-04	2.09e-04	2^{-16}	3.64e-02	1.85e-02	8.65e-03	3.06e-03
2^{-18}	4.48e-03	1.61e-03	6.03e-04	2.09e-04	2^{-18}	3.64e-02	1.85e-02	8.65e-03	3.06e-03
2^{-20}	4.48e-03	1.61e-03	6.03e-04	2.09e-04	2^{-20}	3.64e-02	1.85e-02	8.65e-03	3.06e-03
E^N	4.48e-03	1.61e-03	6.83e-04	2.35e-04	E^N	3.66e-02	1.86e-02	8.66e-03	3.07e-03

$\varepsilon \backslash N$	$Pr = 10000$			
	32	64	128	256
2^{-0}	3.62e-02	1.90e-02	8.59e-03	2.80e-03
2^{-2}	3.69e-02	1.88e-02	8.72e-03	3.06e-03
2^{-4}	3.92e-02	1.96e-02	9.06e-03	3.18e-03
2^{-6}	4.02e-02	2.02e-02	9.29e-03	3.25e-03
2^{-8}	4.06e-02	2.07e-02	9.59e-03	3.37e-03
2^{-10}	4.06e-02	2.06e-02	9.56e-03	3.36e-03
2^{-12}	4.06e-02	2.06e-02	9.56e-03	3.36e-03
2^{-14}	4.06e-02	2.06e-02	9.56e-03	3.36e-03
2^{-16}	4.06e-02	2.06e-02	9.56e-03	3.36e-03
2^{-18}	4.06e-02	2.06e-02	9.56e-03	3.36e-03
2^{-20}	4.06e-02	2.06e-02	9.56e-03	3.36e-03
E^N	4.06e-02	2.07e-02	9.59e-03	3.37e-03

Table 8.1: Computed maximum errors $E_\varepsilon^N(T_{T\varepsilon})$ generated by $(A_{T\varepsilon}^\mathbf{N})$ applied to problem $(P_{T\varepsilon})$ for various values of ε, Pr and N with $\beta = 0.3$ and $n = \frac{1-m}{2}$.

Graphs of the temperature component $T_{T\varepsilon}$ of the solution $\mathbf{U}_{\mathbf{T}\varepsilon}$ generated by the direct method $(A_{T\varepsilon}^\mathbf{N})$ with $N = 32$, $\beta = 0.3$ and $Pr = 0.2$, 512 and 10000 for $\varepsilon = 1.0$ and 2^{-12} are shown in Figures 8-1 and 8-2, respectively.

In Figure 8-1 we see the graphs of $T_{T\varepsilon}$ are smooth for various values of Pr, for $\varepsilon = 1.0$, $\beta = 0.3$ and $n = \frac{1-m}{2}$.
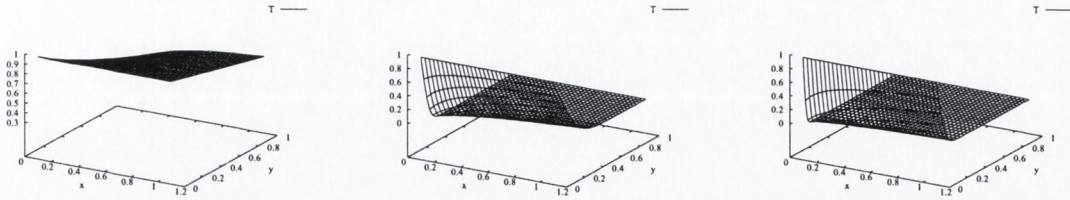
Figure 8-1: Graphs of $T_{T\varepsilon}$ for $\varepsilon = 1.0$, N=32, $\beta = 0.3$ and $Pr = 0.2, 512, 10000$.

In Figure 8-1 we see a region of rapid change along the wedge for $Pr = 512$ and 10000, with $\beta = 0.3$ and $\varepsilon = 1$.
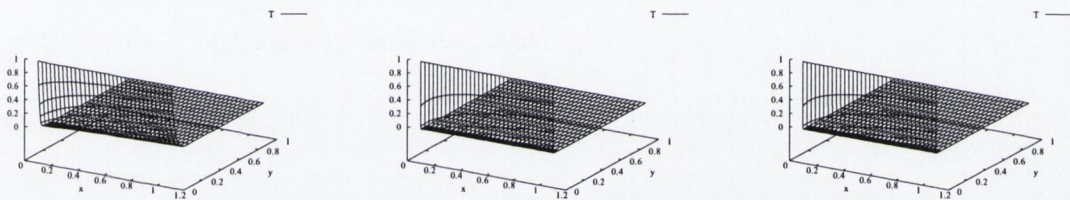
Figure 8-2: Graphs of $T_{T\varepsilon}$ for $\varepsilon = 2^{-12}$, N=32, $\beta = 0.3$ and $Pr = 0.2, 512, 10000$.

In Figure 8-2 we see the boundary layer along the surface of the wedge for $T_{T\varepsilon}$ for various values of Pr, with $\beta = 0.3$ and $\varepsilon = 2^{-12}$. In both Figures the temperature component has no non–physical oscillations for all Pr.

The computed orders of convergence p_{ε}^N, p^N and the error constants for $T_{T\varepsilon}$ are defined in an analogous manner to the computed orders of convergence and error constants in Section 4.4. The computed orders of convergence p_{ε}^N and p^N and the constant of convergence $C_{p^*}^N$ for $T_{T\varepsilon}$ are given in Table 8.2 for various values of ε, N and Pr, with $\beta = 0.3$ and $n = \frac{1-m}{2}$. The results in Tables 8.1 and 8.2 suggest that $(A_{T\varepsilon}^N)$ is an ε–uniform numerical method of order at least 0.72 for $T_{T\varepsilon}$ for all Pr with $\beta = 0.3$ and $n = \frac{1-m}{2}$.

$\varepsilon\backslash N$	Pr = 0.2			$\varepsilon\backslash N$	Pr = 512			$\varepsilon\backslash N$	Pr = 10000		
	32	64	128		32	64	128		32	64	128
2^{-0}	0.80	0.88	0.92	2^{-0}	1.10	1.05	1.02	2^{-0}	0.88	0.71	1.05
2^{-2}	0.81	0.88	0.93	2^{-2}	1.18	1.08	1.03	2^{-2}	1.06	0.70	0.87
2^{-4}	0.84	0.90	0.94	2^{-4}	1.05	0.70	0.87	2^{-4}	1.07	0.72	0.88
2^{-6}	1.08	0.96	0.97	2^{-6}	1.03	0.70	0.87	2^{-6}	1.05	0.74	0.88
2^{-8}	1.94	1.30	1.00	2^{-8}	1.02	0.68	0.86	2^{-8}	1.02	0.72	0.87
2^{-10}	1.43	1.79	1.35	2^{-10}	1.02	0.68	0.86	2^{-10}	1.02	0.72	0.87
2^{-12}	1.43	1.79	1.35	2^{-12}	1.02	0.68	0.86	2^{-12}	1.02	0.72	0.87
2^{-14}	1.43	1.79	1.35	2^{-14}	1.02	0.68	0.86	2^{-14}	1.02	0.72	0.87
2^{-16}	1.43	1.79	1.35	2^{-16}	1.02	0.68	0.86	2^{-16}	1.02	0.72	0.87
2^{-18}	1.43	1.79	1.35	2^{-18}	1.02	0.68	0.86	2^{-18}	1.02	0.72	0.87
2^{-20}	1.43	1.79	1.35	2^{-20}	1.02	0.68	0.86	2^{-20}	1.02	0.72	0.87
p_{comp}^N	0.96	0.95	0.94	p_{comp}^N	0.72	2.77	1.03	p_{comp}^N	1.17	2.73	1.03
$C_{0.94}$	1.11	1.09	1.09	$C_{0.72}$	1.34	1.17	1.06	$C_{1.03}$	1.34	1.14	1.06

Table 8.2: Computed orders of convergence $p_\varepsilon^N(T_{T\varepsilon})$, $p^N(T_{T\varepsilon})$ and the error constants $C_{p^*}^N$ generated by $(A_{T\varepsilon}^N)$ applied to problem $(P_{T\varepsilon})$ for various values of ε, Pr and N with $\beta = 0.3$ and $n = \frac{1-m}{2}$.

From the data in Table 8.2 we obtain the computed error bounds for $T_{T\varepsilon}$

$$
\begin{aligned}
Pr &= 0.2 & ||T_{T\varepsilon} - t_{T\varepsilon}||_{\Omega_\varepsilon^N} &\leq 1.11 N^{-0.94} \\
Pr &= 512 & ||T_{T\varepsilon} - t_{T\varepsilon}||_{\Omega_\varepsilon^N} &\leq 1.34 N^{-0.72} \\
Pr &= 10000 & ||T_{T\varepsilon} - t_{T\varepsilon}||_{\Omega_\varepsilon^N} &\leq 1.36 N^{-1.03}.
\end{aligned}
\tag{8.5}
$$

Graphs of the computed scaled discrete derivatives $T_y^* \sqrt{\varepsilon} D_y^- T_{T\varepsilon}$ and $D_x^- T_{T\varepsilon}$, generated by $(A_{T\varepsilon}^N)$, are given in Figures 8-3, and 8-4, respectively, for $N = 32$, $\varepsilon = 2^{-12}$, $\beta = 0.3$ and $Pr = 0.2$, 512 and 10000. Graphs of $\sqrt{\varepsilon} D_y^- T_{T\varepsilon}$, in Figure 8-3, show a region of rapid change along the wedge for all Pr. Graphs of $D_x^- T_{T\varepsilon}$ in Figure 8-4 show the region closest to the leading edge to be the most active.
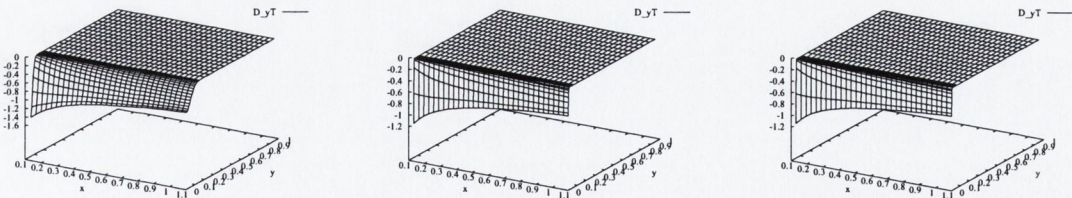
Figure 8-3: Graphs of $T_y^* \sqrt{\varepsilon} D_y^- T_{T\varepsilon}$ for $\varepsilon = 2^{-12}$, $N=32$, $\beta = 0.3$ and $Pr = 0.2, 512, 10000$.
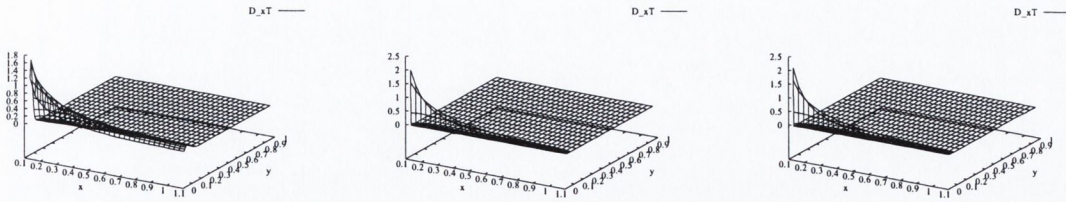
Figure 8-4: Graphs of $D_x^- T_{T\varepsilon}$ for $\varepsilon = 2^{-12}$, N=32, $\beta = 0.3$ and $Pr = 0.2, 512, 10000$.

We approximate the scaled partial derivatives $\frac{\partial t_{T\varepsilon}}{\partial x}$ and $\sqrt{\varepsilon}\frac{\partial t_{T\varepsilon}}{\partial y}$, by the corresponding scaled discrete derivatives $D_x^- T_{T\varepsilon}$ and $\sqrt{\varepsilon}D_y^- T_{T\varepsilon}$. Since the scaled derivatives of the exact solution $t_{T\varepsilon}$ are unknown, we replace them in the expression for the error by the appropriate scaled derivatives of the computed solution $T_{T\varepsilon}^{512}$, generated by method $(A_{T\varepsilon}^N)$ on the finest available mesh. The resulting computed maximum pointwise errors of the computed scaled discrete derivatives $T_y^* \sqrt{\varepsilon} D_y T_{T\varepsilon}$ and $D_x^- T_{T\varepsilon}$ are given in the Tables 8.3 and 8.4, respectively.

$\varepsilon\backslash N$	$Pr = 0.2$				$\varepsilon\backslash N$	$Pr = 512$			
---	32	64	128	256	---	32	64	128	256
2^{-0}	1.28e-02	6.04e-03	2.75e-03	1.23e-03	2^{-0}	1.82e-01	8.63e-02	3.85e-02	1.43e-02
2^{-2}	2.55e-02	1.19e-02	5.20e-03	1.91e-03	2^{-2}	3.18e-01	1.69e-01	7.20e-02	2.43e-02
2^{-4}	5.09e-02	2.38e-02	1.02e-02	3.50e-03	2^{-4}	3.04e-01	1.84e-01	9.51e-02	3.56e-02
2^{-6}	1.01e-01	4.74e-02	2.03e-02	6.84e-03	2^{-6}	3.04e-01	1.84e-01	9.51e-02	3.56e-02
2^{-8}	1.97e-01	9.43e-02	4.07e-02	1.36e-02	2^{-8}	3.04e-01	1.84e-01	9.51e-02	3.56e-02
2^{-10}	1.95e-01	1.08e-01	5.36e-02	1.98e-02	2^{-10}	3.04e-01	1.84e-01	9.51e-02	3.56e-02
2^{-12}	1.95e-01	1.08e-01	5.36e-02	1.98e-02	2^{-12}	3.04e-01	1.84e-01	9.51e-02	3.56e-02
2^{-14}	1.95e-01	1.08e-01	5.36e-02	1.98e-02	2^{-14}	3.04e-01	1.84e-01	9.51e-02	3.56e-02
2^{-16}	1.95e-01	1.08e-01	5.36e-02	1.98e-02	2^{-16}	3.04e-01	1.84e-01	9.51e-02	3.56e-02
2^{-18}	1.95e-01	1.08e-01	5.36e-02	1.98e-02	2^{-18}	3.04e-01	1.84e-01	9.51e-02	3.56e-02
2^{-20}	1.95e-01	1.08e-01	5.36e-02	1.98e-02	2^{-20}	3.04e-01	1.84e-01	9.51e-02	3.56e-02
E^N	1.97e-01	1.08e-01	5.36e-02	1.98e-02	E^N	3.18e-01	1.84e-01	9.51e-02	3.56e-02

$\varepsilon\backslash N$	$Pr = 10000$			
---	32	64	128	256
2^{-0}	3.15e-01	2.00e-01	9.25e-02	3.16e-02
2^{-2}	3.08e-01	1.83e-01	9.45e-02	3.92e-02
2^{-4}	3.08e-01	1.83e-01	9.45e-02	3.92e-02
2^{-6}	3.08e-01	1.83e-01	9.45e-02	3.92e-02
2^{-8}	3.08e-01	1.83e-01	9.45e-02	3.92e-02
2^{-10}	3.08e-01	1.83e-01	9.45e-02	3.92e-02
2^{-12}	3.08e-01	1.83e-01	9.45e-02	3.92e-02
2^{-14}	3.08e-01	1.83e-01	9.45e-02	3.92e-02
2^{-16}	3.08e-01	1.83e-01	9.45e-02	3.92e-02
2^{-18}	3.08e-01	1.83e-01	9.45e-02	3.92e-02
2^{-20}	3.08e-01	1.83e-01	9.45e-02	3.92e-02
E^N	3.15e-01	2.00e-01	9.45e-02	3.92e-02

Table 8.3: Computed maximum errors $E_\varepsilon^N(T_y^* \sqrt{\varepsilon} D_y^- T_{T\varepsilon})$ generated by $(A_{T\varepsilon}^N)$ applied to problem $(P_{T\varepsilon})$ for various values of ε, Pr and N with $\beta = 0.3$ and $n = \frac{1-m}{2}$.

$\varepsilon\backslash N$	Pr = 0.2				$\varepsilon\backslash N$	Pr = 512			
	32	64	128	256		32	64	128	256
2^{-0}	1.39e-01	9.22e-02	4.84e-02	1.82e-02	2^{-0}	2.13e-01	1.49e-01	7.92e-02	2.99e-02
2^{-2}	1.23e-01	6.57e-02	2.90e-02	9.84e-03	2^{-2}	3.05e-01	2.32e-01	1.30e-01	5.08e-02
2^{-4}	1.20e-01	6.88e-02	3.13e-02	1.08e-02	2^{-4}	3.14e-01	2.68e-01	1.65e-01	7.44e-02
2^{-6}	1.11e-01	7.36e-02	3.93e-02	1.60e-02	2^{-6}	3.08e-01	2.63e-01	1.64e-01	7.44e-02
2^{-8}	6.15e-02	6.31e-02	5.12e-02	2.62e-02	2^{-8}	2.98e-01	2.48e-01	1.60e-01	7.41e-02
2^{-10}	6.13e-02	5.19e-02	5.48e-02	3.76e-02	2^{-10}	2.98e-01	2.48e-01	1.60e-01	7.41e-02
2^{-12}	6.13e-02	5.19e-02	5.48e-02	3.76e-02	2^{-12}	2.98e-01	2.48e-01	1.60e-01	7.41e-02
2^{-14}	6.13e-02	5.19e-02	5.48e-02	3.76e-02	2^{-14}	2.98e-01	2.48e-01	1.60e-01	7.41e-02
2^{-16}	6.13e-02	5.19e-02	5.48e-02	3.76e-02	2^{-16}	2.98e-01	2.48e-01	1.60e-01	7.41e-02
2^{-18}	6.13e-02	5.19e-02	5.48e-02	3.76e-02	2^{-18}	2.98e-01	2.48e-01	1.60e-01	7.41e-02
2^{-20}	6.13e-02	5.19e-02	5.48e-02	3.76e-02	2^{-20}	2.98e-01	2.48e-01	1.60e-01	7.41e-02
E^N	1.39e-01	9.22e-02	5.48e-02	3.76e-02	E^N	3.14e-01	2.68e-01	1.65e-01	7.44e-02

$\varepsilon\backslash N$	Pr = 10000			
	32	64	128	256
2^{-0}	2.99e-01	2.73e-01	1.63e-01	6.54e-02
2^{-2}	3.21e-01	2.77e-01	1.68e-01	8.85e-02
2^{-4}	3.24e-01	2.85e-01	1.73e-01	9.02e-02
2^{-6}	3.19e-01	2.96e-01	1.83e-01	9.35e-02
2^{-8}	2.98e-01	2.94e-01	1.94e-01	1.00e-01
2^{-10}	2.98e-01	2.94e-01	1.93e-01	9.97e-02
2^{-12}	2.98e-01	2.94e-01	1.93e-01	9.97e-02
2^{-14}	2.98e-01	2.94e-01	1.93e-01	9.97e-02
2^{-16}	2.98e-01	2.94e-01	1.93e-01	9.97e-02
2^{-18}	2.98e-01	2.94e-01	1.93e-01	9.97e-02
2^{-20}	2.98e-01	2.94e-01	1.93e-01	9.97e-02
E^N	3.24e-01	2.96e-01	1.94e-01	1.00e-01

Table 8.4: Computed maximum errors $E_\varepsilon^N(D_x^- T_{T\varepsilon})$ generated by $(A_{T\varepsilon}^N)$ applied to problem $(P_{T\varepsilon})$ for various values of ε, Pr and N with $\beta = 0.3$ and $n = \frac{1-m}{2}$.

The computed maximum errors in Tables 8.3 and 8.4 for $T_y^* \sqrt{\varepsilon} D_y^- T_{T\varepsilon}$ and $D_x^- T_{T\varepsilon}$, respectively, stabilise to a fixed value after $\varepsilon = 2^{-10}$ for all Pr and N for $\beta = 0.3$ and $n = \frac{1-m}{2}$. The computed maximum error for $T_y^* \sqrt{\varepsilon} D_y^- T_{T\varepsilon}$ decreases as the number of mesh points increase. Table 8.3 suggests that the method is independent of ε for $T_y^* \sqrt{\varepsilon} D_y T_{T\varepsilon}$ for $Pr = 0.2$, 512, 10000 and $\beta = 0.3$ and $n = \frac{1-m}{2}$. The computed maximum error for $D_x^- T_{T\varepsilon}$ decreases as the number of mesh points increase for $N \geq 128$.

The orders of convergence and the compound error constants for $T_y^* \sqrt{\varepsilon} D_y^- T_{T\varepsilon}$ and $D_x^- T_{T\varepsilon}$, are given in Tables 8.5 and 8.6, respectively, for various values of ε, Pr and N with $\beta = 0.3$ and $n = \frac{1-m}{2}$.

	$Pr = 0.2$				$Pr = 512$				$Pr = 10000$		
$\varepsilon \backslash N$	32	64	128	$\varepsilon \backslash N$	32	64	128	$\varepsilon \backslash N$	32	64	128
2^{-0}	0.97	0.88	0.63	2^{-0}	1.00	0.99	0.77	2^{-0}	0.32	0.68	1.04
2^{-2}	0.99	0.97	0.88	2^{-2}	0.91	1.00	0.99	2^{-2}	0.46	0.58	0.69
2^{-4}	1.00	0.99	0.97	2^{-4}	0.46	0.63	0.77	2^{-4}	0.46	0.58	0.69
2^{-6}	0.98	1.00	0.99	2^{-6}	0.46	0.63	0.77	2^{-6}	0.46	0.58	0.69
2^{-8}	0.94	0.98	1.00	2^{-8}	0.46	0.63	0.77	2^{-8}	0.46	0.58	0.69
2^{-10}	0.64	0.72	0.77	2^{-10}	0.46	0.63	0.77	2^{-10}	0.46	0.58	0.69
2^{-12}	0.64	0.72	0.77	2^{-12}	0.46	0.63	0.77	2^{-12}	0.46	0.58	0.69
2^{-14}	0.64	0.72	0.77	2^{-14}	0.46	0.63	0.77	2^{-14}	0.46	0.58	0.69
2^{-16}	0.64	0.72	0.77	2^{-16}	0.46	0.63	0.77	2^{-16}	0.46	0.58	0.69
2^{-18}	0.64	0.72	0.77	2^{-18}	0.46	0.63	0.77	2^{-18}	0.46	0.58	0.69
2^{-20}	0.64	0.72	0.77	2^{-20}	0.46	0.63	0.77	2^{-20}	0.46	0.58	0.69
p^N_{comp}	0.89	0.72	0.77	p^N_{comp}	0.91	0.67	0.77	p^N_{comp}	0.32	0.68	0.73
$C_{0.72}$	3.20	2.85	2.85	$C_{0.67}$	4.99	4.20	4.20	$C_{0.32}$	1.98	1.98	1.54

Table 8.5: Computed orders of convergence $p^N_\varepsilon(T^*_y \sqrt{\varepsilon} D^-_y T_{T\varepsilon})$, $p^N(T^*_y \sqrt{\varepsilon} D^-_y T_{T\varepsilon})$ and $C^N_{p^*}$ generated by $(A^N_{T\varepsilon})$ applied to problem $(P_{T\varepsilon})$ for various values of ε, Pr and N with $\beta = 0.3$ and $n = \frac{1-m}{2}$.

	$Pr = 0.2$				$Pr = 512$				$Pr = 10000$		
$\varepsilon \backslash N$	32	64	128	$\varepsilon \backslash N$	32	64	128	$\varepsilon \backslash N$	32	64	128
2^{-0}	0.53	0.73	0.85	2^{-0}	0.49	0.72	0.82	2^{-0}	0.34	0.72	0.72
2^{-2}	0.79	0.94	0.96	2^{-2}	0.38	0.65	0.78	2^{-2}	0.35	0.71	0.38
2^{-4}	0.69	0.90	0.96	2^{-4}	0.38	0.66	0.63	2^{-4}	0.32	0.71	0.40
2^{-6}	0.39	0.66	0.74	2^{-6}	0.38	0.64	0.62	2^{-6}	0.23	0.68	0.43
2^{-8}	-0.01	-0.13	0.42	2^{-8}	0.41	0.60	0.58	2^{-8}	0.15	0.57	0.41
2^{-10}	0.43	-0.34	0.01	2^{-10}	0.41	0.59	0.58	2^{-10}	0.15	0.58	0.41
2^{-12}	0.43	-0.34	0.01	2^{-12}	0.41	0.59	0.58	2^{-12}	0.15	0.58	0.41
2^{-14}	0.43	-0.34	0.01	2^{-14}	0.41	0.59	0.58	2^{-14}	0.15	0.58	0.41
2^{-16}	0.43	-0.34	0.01	2^{-16}	0.41	0.59	0.58	2^{-16}	0.15	0.58	0.41
2^{-18}	0.43	-0.34	0.01	2^{-18}	0.41	0.59	0.58	2^{-18}	0.15	0.58	0.41
2^{-20}	0.43	-0.34	0.01	2^{-20}	0.41	0.59	0.58	2^{-20}	0.15	0.58	0.41
p^N_{comp}	0.53	0.51	0.01	p^N_{comp}	0.38	0.66	0.63	p^N_{comp}	0.27	0.60	0.41
$C_{0.01}$	8.60	6.01	4.26	$C_{0.38}$	3.84	3.84	3.17	$C_{0.27}$	3.63	3.63	2.88

Table 8.6: Computed orders of convergence $p^N_\varepsilon(D^-_x T_{T\varepsilon})$, $p^N(D^-_x T_{T\varepsilon})$ and $C^N_{p^*}$ generated by $(A^N_{T\varepsilon})$ applied to problem $(P_{T\varepsilon})$ for various values of ε, Pr and N with $\beta = 0.3$ and $n = \frac{1-m}{2}$.

The results in Tables 8.3 and 8.5 suggest that $(A^N_{T\varepsilon})$ is an ε-uniform numerical method of order of at least 0.67 for $T^*_y \sqrt{\varepsilon} D^-_y T_{T\varepsilon}$ for all Pr for $N \geq 64$ and $\beta = 0.3$. We cannot draw the same conclusion from Tables 8.4 and 8.6 for $D^-_x T_{T\varepsilon}$ as we have negative orders of convergence for $Pr < 1$.

From the data in Table 8.5 we obtain the computed error bounds for $T_y^* \sqrt{\varepsilon} D_y^- T_{T\varepsilon}$

$$
\begin{array}{ll}
Pr = 0.2 & T_y^* \sqrt{\varepsilon} ||D_y^- T_{T\varepsilon} - \frac{\partial t_{T\varepsilon}}{\partial y}||_{\Omega_\varepsilon^N} \leq 3.20 N^{-0.72} \\
Pr = 512 & T_y^* \sqrt{\varepsilon} ||D_y^- T_{T\varepsilon} - \frac{\partial t_{T\varepsilon}}{\partial y}||_{\Omega_\varepsilon^N} \leq 4.99 N^{-0.67} \\
Pr = 10000 & T_y^* \sqrt{\varepsilon} ||D_y^- T_{T\varepsilon} - \frac{\partial t_{T\varepsilon}}{\partial y}||_{\Omega_\varepsilon^N} \leq 1.98 N^{-0.32}.
\end{array}
\tag{8.6}
$$

8.4 Error analysis based upon the Blasius solution

In this section we compute ε–uniform maximum pointwise differences in the approximations generated by the direct numerical method described in Section 8.2. For this case we compare the parameter uniform maximum pointwise differences in the approximations generated by the direct numerical method of the previous section with the corresponding values of T_{TB}^{8192} generated be the method defined in Chapter 7. The scaled maximum pointwise difference $||T_{T\varepsilon} - \overline{T_{TB}}^{8192}||_{\overline{\Omega}_\varepsilon^N}$ of N, ε and Pr for $\beta = 0.3$ and $n = \frac{1-m}{2}$ are given in Table 8.7.

The results in Table 8.7 stabilise to a fixed value for all N and all Pr considered with $\beta = 0.3$. The computed maximum difference for $T_{T\varepsilon}$ decreases as the number of mesh points increase. For each N the largest computed maximum difference occurs when $2^{-6} \leq \varepsilon \leq 2^{-12}$ for $\beta = 0.3$ and all Pr. The results in Table 8.7 indicate that the method is independent of ε for the temperature component for various Pr. In a similar fashion to Table 8.1 of the pointwise errors of $T_{T\varepsilon}$, Table 8.7 strongly suggests that the method is ε–uniform for $T_{T\varepsilon}$ for $\beta = 0.3$ and all Pr considered.

$\varepsilon\backslash N$	$Pr = 0.2$					$\varepsilon\backslash N$	$Pr = 512$				
	32	64	128	256	512		32	64	128	256	512
2^{-0}	1.12e-03	6.25e-04	3.60e-04	2.07e-04	1.26e-04	2^{-0}	1.54e-02	6.70e-03	2.73e-03	9.49e-04	1.12e-03
2^{-2}	3.26e-03	1.82e-03	1.00e-03	5.54e-04	3.21e-04	2^{-2}	3.59e-02	1.61e-02	7.09e-03	2.86e-03	9.10e-04
2^{-4}	3.14e-03	1.76e-03	9.67e-04	5.42e-04	3.25e-04	2^{-4}	3.89e-02	2.11e-02	1.12e-02	5.63e-03	2.55e-03
2^{-6}	2.63e-03	1.37e-03	7.46e-04	4.24e-04	2.64e-04	2^{-6}	3.91e-02	2.12e-02	1.13e-02	5.66e-03	2.56e-03
2^{-8}	4.10e-03	1.26e-03	6.04e-04	2.88e-04	1.73e-04	2^{-8}	3.89e-02	2.12e-02	1.13e-02	5.70e-03	2.58e-03
2^{-10}	4.42e-03	2.05e-03	1.03e-03	5.83e-04	3.28e-04	2^{-10}	3.89e-02	2.12e-02	1.13e-02	5.71e-03	2.59e-03
2^{-12}	4.42e-03	2.05e-03	1.03e-03	5.83e-04	3.28e-04	2^{-12}	3.89e-02	2.12e-02	1.13e-02	5.71e-03	2.59e-03
2^{-14}	4.42e-03	2.05e-03	1.03e-03	5.83e-04	3.28e-04	2^{-14}	3.89e-02	2.12e-02	1.13e-02	5.71e-03	2.59e-03
2^{-16}	4.42e-03	2.05e-03	1.03e-03	5.83e-04	3.28e-04	2^{-16}	3.89e-02	2.12e-02	1.13e-02	5.71e-03	2.59e-03
2^{-18}	4.42e-03	2.05e-03	1.03e-03	5.83e-04	3.28e-04	2^{-18}	3.89e-02	2.12e-02	1.13e-02	5.71e-03	2.59e-03
2^{-20}	4.42e-03	2.05e-03	1.03e-03	5.83e-04	3.28e-04	2^{-20}	3.89e-02	2.12e-02	1.13e-02	5.71e-03	2.59e-03
E^N	4.42e-03	2.05e-03	1.03e-03	5.83e-04	3.28e-04	E^N	3.91e-02	2.12e-02	1.13e-02	5.71e-03	2.59e-03

$\varepsilon\backslash N$	$Pr = 10000$				
	32	64	128	256	512
2^{-0}	3.58e-02	1.85e-02	8.17e-03	2.66e-03	2.80e-03
2^{-2}	3.80e-02	1.98e-02	9.72e-03	4.12e-03	2.10e-03
2^{-4}	4.01e-02	2.05e-02	1.00e-02	4.21e-03	1.98e-03
2^{-6}	4.12e-02	2.12e-02	1.03e-02	4.34e-03	1.92e-03
2^{-8}	4.15e-02	2.17e-02	1.07e-02	4.56e-03	1.83e-03
2^{-10}	4.15e-02	2.17e-02	1.07e-02	4.58e-03	1.80e-03
2^{-12}	4.15e-02	2.17e-02	1.07e-02	4.58e-03	1.80e-03
2^{-14}	4.15e-02	2.17e-02	1.07e-02	4.58e-03	1.80e-03
2^{-16}	4.15e-02	2.17e-02	1.07e-02	4.58e-03	1.80e-03
2^{-18}	4.15e-02	2.17e-02	1.07e-02	4.58e-03	1.80e-03
2^{-20}	4.15e-02	2.17e-02	1.07e-02	4.58e-03	1.80e-03
E^N	4.15e-02	2.17e-02	1.07e-02	4.58e-03	2.80e-03

Table 8.7: Computed maximum pointwise difference $||T_{T\varepsilon} - \overline{T_{TB}}^{8192}||_{\overline{\Omega}_\varepsilon^N}$ where $T_{T\varepsilon}$ is generated by $(A_{T\varepsilon}^N)$ for various values of ε, Pr and N with $\beta = 0.3$ and $n = \frac{1-m}{2}$.
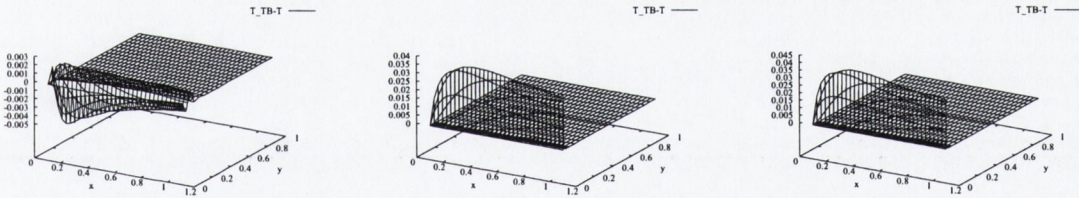
Figure 8-5: Graphs of $T_{T\varepsilon} - T_{TB}^{8192}$ for $\varepsilon = 2^{-12}$, $N{=}32$, $\beta = 0.3$ and $Pr = 0.2, 512, 10000$.

The graphs of differences $T_{T\varepsilon} - T_{TB}^{8192}$ for $\varepsilon = 2^{-12}$, $N{=}32$, $\beta = 0.3$ and $Pr = 0.2, 512, 10000$ in Figure 8-5 show that the largest difference is contained within the boundary layer along the surface of the wedge for all Pr considered and $\beta = 0.3$.

We now estimate the order of convergence of the numerical approximation $T_{T\varepsilon}$, generated by the direct numerical method $(A_{T\varepsilon}^N)$, by using the computed order of convergence defined in Section 4.5. The orders of convergence and the error constants of the temperature component $T_{T\varepsilon}$ are given in Table 8.8.

	$Pr = 0.2$					$Pr = 512$					$Pr = 10000$			
$\varepsilon \backslash N$	32	64	128	256	$\varepsilon \backslash N$	32	64	128	256	$\varepsilon \backslash N$	32	64	128	256
2^{-0}	0.84	0.80	0.79	0.71	2^{-0}	1.20	1.30	1.53	-0.24	2^{-0}	0.95	1.18	1.62	-0.07
2^{-2}	0.85	0.86	0.86	0.79	2^{-2}	1.16	1.18	1.31	1.65	2^{-2}	0.94	1.03	1.24	0.98
2^{-4}	0.84	0.86	0.83	0.74	2^{-4}	0.88	0.92	0.99	1.14	2^{-4}	0.97	1.04	1.25	1.09
2^{-6}	0.95	0.87	0.81	0.68	2^{-6}	0.88	0.92	0.99	1.14	2^{-6}	0.96	1.04	1.25	1.18
2^{-8}	1.71	1.06	1.07	0.74	2^{-8}	0.87	0.91	0.99	1.14	2^{-8}	0.94	1.02	1.23	1.32
2^{-10}	1.11	0.99	0.82	0.83	2^{-10}	0.87	0.91	0.99	1.14	2^{-10}	0.94	1.02	1.22	1.34
2^{-12}	1.11	0.99	0.82	0.83	2^{-12}	0.87	0.91	0.99	1.14	2^{-12}	0.94	1.02	1.22	1.34
2^{-14}	1.11	0.99	0.82	0.83	2^{-14}	0.87	0.91	0.99	1.14	2^{-14}	0.94	1.02	1.22	1.34
2^{-16}	1.11	0.99	0.82	0.83	2^{-16}	0.87	0.91	0.99	1.14	2^{-16}	0.94	1.02	1.22	1.34
2^{-18}	1.11	0.99	0.82	0.83	2^{-18}	0.87	0.91	0.99	1.14	2^{-18}	0.94	1.02	1.22	1.34
2^{-20}	1.11	0.99	0.82	0.83	2^{-20}	0.87	0.91	0.99	1.14	2^{-20}	0.94	1.02	1.22	1.34
p_{comp}^{N}	1.11	0.99	0.82	0.83	p_{comp}^{N}	0.88	0.91	0.99	1.14	p_{comp}^{N}	0.94	1.02	1.22	0.71
$C_{0.82}$	0.17	0.14	0.13	0.13	$C_{0.88}$	1.81	1.81	1.77	1.65	$C_{0.71}$	1.25	1.07	0.86	0.60

Table 8.8: Computed orders of convergence $p_{\varepsilon,comp}^{N}$, p_{comp}^{N} and the error constant $C_{p_{comp}^{*}}^{N}$ for $T_{T\varepsilon} - T_{TB}^{8192}$ where $T_{T\varepsilon}$ is generated by $(A_{T\varepsilon}^{N})$ for various values of ε, Pr and N with $\beta = 0.3$ and $n = \frac{1-m}{2}$.

From Table 8.8 we see the order of convergence for the approximations to the temperature component in each case is at least 0.71 for $T_{T\varepsilon}$ for $Pr = 0.2$, 512, 10000 with $\beta = 0.3$ and $n = \frac{1-m}{2}$. Using Table 8.8 we obtain the following error bounds

$$
\begin{aligned}
Pr &= 0.2 & ||T_{T\varepsilon} - T_{TB}^{8192}||_{\Omega_{\varepsilon}^{N}} &\leq 0.17 N^{-0.82} \\
Pr &= 512 & ||T_{T\varepsilon} - T_{TB}^{8192}||_{\Omega_{\varepsilon}^{N}} &\leq 1.81 N^{-0.88} \\
Pr &= 10000 & ||T_{T\varepsilon} - T_{TB}^{8192}||_{\Omega_{\varepsilon}^{N}} &\leq 1.25 N^{-0.73}.
\end{aligned} \tag{8.7}
$$

From Tables 8.7 and 8.8 we have shown that for the temperature component the method is ε-uniform for $Pr = 0.2$, 512 and 10000 with $\beta = 0.3$ and $n = \frac{1-m}{2}$. Further computations, not reported here, show that the errors for the temperature component for $Pr \in [0.1, 10000]$ and $\beta \in [0.0, 0.3]$ for constant heat flux and constant wall temperature have similar behaviour; therefore the method can be said to be $(\varepsilon, Pr, \beta, n)$-uniform for the scaled temperature component.

Pr = 0.2

$\varepsilon\backslash N$	32	64	128	256	512
2^{-0}	1.40e-02	7.26e-03	3.97e-03	2.47e-03	2.02e-03
2^{-2}	2.76e-02	1.40e-02	7.26e-03	3.97e-03	2.47e-03
2^{-4}	5.47e-02	2.76e-02	1.40e-02	7.26e-03	3.97e-03
2^{-6}	1.08e-01	5.47e-02	2.76e-02	1.40e-02	7.26e-03
2^{-8}	2.11e-01	1.08e-01	5.47e-02	2.76e-02	1.40e-02
2^{-10}	2.21e-01	1.33e-01	7.93e-02	4.56e-02	2.58e-02
2^{-12}	2.21e-01	1.33e-01	7.93e-02	4.56e-02	2.58e-02
2^{-14}	2.21e-01	1.33e-01	7.93e-02	4.56e-02	2.58e-02
2^{-16}	2.21e-01	1.33e-01	7.93e-02	4.56e-02	2.58e-02
2^{-18}	2.21e-01	1.33e-01	7.93e-02	4.56e-02	2.58e-02
2^{-20}	2.21e-01	1.33e-01	7.93e-02	4.56e-02	2.58e-02
E^N	2.21e-01	1.33e-01	7.93e-02	4.56e-02	2.58e-02

Pr = 512

$\varepsilon\backslash N$	32	64	128	256	512
2^{-0}	1.95e-01	9.97e-02	5.19e-02	2.77e-02	1.77e-02
2^{-2}	3.37e-01	1.95e-01	9.97e-02	5.19e-02	2.77e-02
2^{-4}	3.36e-01	2.33e-01	1.44e-01	8.41e-02	4.88e-02
2^{-6}	3.36e-01	2.33e-01	1.44e-01	8.41e-02	4.88e-02
2^{-8}	3.36e-01	2.33e-01	1.44e-01	8.41e-02	4.88e-02
2^{-10}	3.36e-01	2.33e-01	1.44e-01	8.41e-02	4.88e-02
2^{-12}	3.36e-01	2.33e-01	1.44e-01	8.41e-02	4.88e-02
2^{-14}	3.36e-01	2.33e-01	1.44e-01	8.41e-02	4.88e-02
2^{-16}	3.36e-01	2.33e-01	1.44e-01	8.41e-02	4.88e-02
2^{-18}	3.36e-01	2.33e-01	1.44e-01	8.41e-02	4.88e-02
2^{-20}	3.36e-01	2.33e-01	1.44e-01	8.41e-02	4.88e-02
E^N	3.37e-01	2.33e-01	1.44e-01	8.41e-02	4.88e-02

Pr = 10000

$\varepsilon\backslash N$	32	64	128	256	512
2^{-0}	3.41e-01	2.39e-01	1.40e-01	7.48e-02	4.74e-02
2^{-2}	3.41e-01	2.39e-01	1.50e-01	9.13e-02	5.57e-02
2^{-4}	3.41e-01	2.39e-01	1.50e-01	9.13e-02	5.57e-02
2^{-6}	3.41e-01	2.39e-01	1.50e-01	9.13e-02	5.57e-02
2^{-8}	3.41e-01	2.39e-01	1.50e-01	9.13e-02	5.57e-02
2^{-10}	3.41e-01	2.39e-01	1.50e-01	9.13e-02	5.57e-02
2^{-12}	3.41e-01	2.39e-01	1.50e-01	9.13e-02	5.57e-02
2^{-14}	3.41e-01	2.39e-01	1.50e-01	9.13e-02	5.57e-02
2^{-16}	3.41e-01	2.39e-01	1.50e-01	9.13e-02	5.57e-02
2^{-18}	3.41e-01	2.39e-01	1.50e-01	9.13e-02	5.57e-02
2^{-20}	3.41e-01	2.39e-01	1.50e-01	9.13e-02	5.57e-02
E^N	3.41e-01	2.39e-01	1.50e-01	9.13e-02	5.57e-02

Table 8.9: Computed maximum pointwise scaled difference $T_y^*\sqrt{\varepsilon}\|D_y^- T_{T\varepsilon} - D_y T_{TB}^{8192}\|_{\overline{\Omega_\varepsilon^N}/\Gamma_L}$ where $T_{T\varepsilon}$ is generated by $(A_{T\varepsilon}^{\mathbf{N}})$ for various values of ε, Pr and N with $\beta = 0.3$ and $n = \frac{1-m}{2}$.

In Tables 8.9 and 8.10 we display the computed maximum pointwise differences of the approximations to the scaled first order derivatives of the temperature component $T_y^*\sqrt{\varepsilon}D_y^- T_{T\varepsilon}$ and $D_x^- T_{T\varepsilon}$ for various values of ε, N and Pr and $\beta = 0.3$.

In Table 8.9 we see that the computed maximum pointwise differences of $T_y^*\sqrt{\varepsilon}D_y^- T_{T\varepsilon}$ decrease as the number of mesh points increase. For each N the largest computed maximum difference occurs when $2^{-6} \leq \varepsilon \leq 2^{-12}$ for all Pr with $\beta = 0.3$ and $n = \frac{1-m}{2}$. The maximum differences stabilise to a fixed value as ε decreases for any ε and Pr. The results in Table 8.9 indicate that the method is independent of ε for $T_y^*\sqrt{\varepsilon}D_y^- T_{TB}$ for various Pr. In a similar fashion to Table 8.3 of the pointwise errors of $T_y^*\sqrt{\varepsilon}D_y^- T_{T\varepsilon}$, Table 8.9 strongly suggests that the method is ε–uniform for $T_y^*\sqrt{\varepsilon}D_y^- T_{T\varepsilon}$ for all Pr considered.

$\varepsilon\backslash N$	Pr = 0.2					$\varepsilon\backslash N$	Pr = 512				
	32	64	128	256	512		32	64	128	256	512
2^{-0}	1.48e-01	1.05e-01	6.44e-02	3.62e-02	1.99e-02	2^{-0}	2.21e-01	1.59e-01	8.81e-02	4.07e-02	2.38e-02
2^{-2}	1.32e-01	7.48e-02	3.80e-02	1.90e-02	9.23e-03	2^{-2}	3.17e-01	2.54e-01	1.58e-01	8.25e-02	3.96e-02
2^{-4}	1.27e-01	7.78e-02	3.98e-02	1.91e-02	9.01e-03	2^{-4}	3.32e-01	3.04e-01	2.15e-01	1.38e-01	8.06e-02
2^{-6}	1.19e-01	8.31e-02	4.96e-02	2.79e-02	1.52e-02	2^{-6}	3.26e-01	3.00e-01	2.15e-01	1.38e-01	8.06e-02
2^{-8}	6.64e-02	7.34e-02	6.49e-02	4.63e-02	2.95e-02	2^{-8}	3.16e-01	2.84e-01	2.10e-01	1.38e-01	8.06e-02
2^{-10}	6.57e-02	6.29e-02	7.22e-02	7.00e-02	5.54e-02	2^{-10}	3.16e-01	2.84e-01	2.10e-01	1.38e-01	8.05e-02
2^{-12}	6.57e-02	6.29e-02	7.22e-02	7.00e-02	5.54e-02	2^{-12}	3.16e-01	2.84e-01	2.10e-01	1.38e-01	8.05e-02
2^{-14}	6.57e-02	6.29e-02	7.22e-02	7.00e-02	5.54e-02	2^{-14}	3.16e-01	2.84e-01	2.10e-01	1.38e-01	8.05e-02
2^{-16}	6.57e-02	6.29e-02	7.22e-02	7.00e-02	5.54e-02	2^{-16}	3.16e-01	2.84e-01	2.10e-01	1.38e-01	8.05e-02
2^{-18}	6.57e-02	6.29e-02	7.22e-02	7.00e-02	5.54e-02	2^{-18}	3.16e-01	2.84e-01	2.10e-01	1.38e-01	8.05e-02
2^{-20}	6.57e-02	6.29e-02	7.22e-02	7.00e-02	5.54e-02	2^{-20}	3.16e-01	2.84e-01	2.10e-01	1.38e-01	8.05e-02
E^N	1.48e-01	1.05e-01	7.22e-02	7.00e-02	5.54e-02	E^N	3.32e-01	3.04e-01	2.15e-01	1.38e-01	8.06e-02

$\varepsilon\backslash N$	Pr = 10000				
	32	64	128	256	512
2^{-0}	3.06e-01	2.85e-01	1.84e-01	9.48e-02	7.13e-02
2^{-2}	3.37e-01	2.98e-01	2.02e-01	1.22e-01	7.21e-02
2^{-4}	3.45e-01	3.07e-01	2.08e-01	1.25e-01	7.26e-02
2^{-6}	3.41e-01	3.18e-01	2.19e-01	1.30e-01	7.37e-02
2^{-8}	3.20e-01	3.18e-01	2.33e-01	1.41e-01	7.59e-02
2^{-10}	3.20e-01	3.18e-01	2.33e-01	1.41e-01	7.67e-02
2^{-12}	3.20e-01	3.18e-01	2.33e-01	1.41e-01	7.67e-02
2^{-14}	3.20e-01	3.18e-01	2.33e-01	1.41e-01	7.67e-02
2^{-16}	3.20e-01	3.18e-01	2.33e-01	1.41e-01	7.67e-02
2^{-18}	3.20e-01	3.18e-01	2.33e-01	1.41e-01	7.67e-02
2^{-20}	3.20e-01	3.18e-01	2.33e-01	1.41e-01	7.67e-02
E^N	3.45e-01	3.18e-01	2.33e-01	1.41e-01	7.67e-02

Table 8.10: Computed maximum pointwise difference $||D_x^- T_{T\varepsilon} - D_x T_{TB}^{8192}||_{\overline{\Omega_\varepsilon^N}}$ where $T_{T\varepsilon}$ is generated by $(A_{T\varepsilon}^N)$ for various values of ε, Pr and N with $\beta = 0.3$ and $n = \frac{1-m}{2}$.

Graphs of the computed pointwise maximum differences of the scaled discrete derivatives $T_y^* \sqrt{\varepsilon} D_y^- T_{T\varepsilon}$ and $D_x^- T_{T\varepsilon}$ generated by $(A_{T\varepsilon}^N)$ are given in Figures 8-6, and 8-7 respectively for $N = 32$, $\varepsilon = 2^{-12}$, $\beta = 0.3$ and $Pr=0.2$, 512 and 10000.
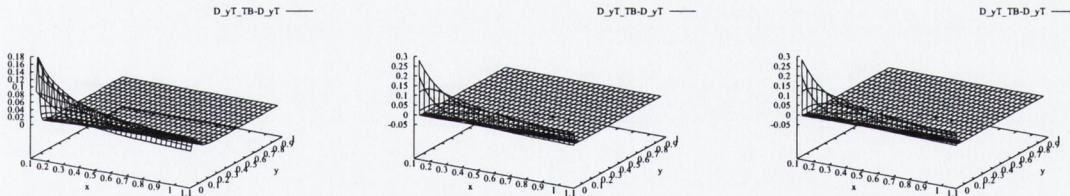

Figure 8-6: Graphs of $T_y^* \sqrt{\varepsilon}(D_y^- T_{T\varepsilon} - D_y T_{TB}^{8192})$ for $\varepsilon = 2^{-12}$, $N=32$, $\beta = 0.3$ and $Pr = 0.2, 512, 10000$.

Graphs of the computed pointwise maximum differences of $T_y^* \sqrt{\varepsilon} D_y^- T_{T\varepsilon}$ in Figure 8-6 show the largest differences to be along the wedge.
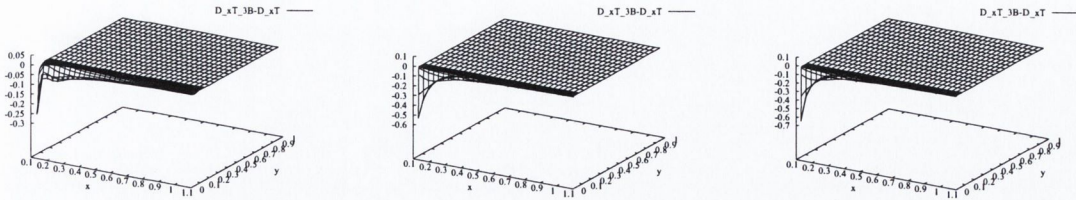
Figure 8-7: Graphs of $D_x^- T_{T\varepsilon} - D_x T_{TB}^{8192}$ for $\varepsilon = 2^{-12}$, $N=32$, $\beta = 0.3$ and $Pr = 0.2, 512, 10000$.

Graphs of the computed pointwise maximum differences of $D_x^- T_{T\varepsilon}$ in Figure 8-7 show the largest differences to be concentrated at the points in the domain nearest the leading edge.

In Tables 8.11 and 8.12 we display the computed orders of convergence for the approximations of the first order scaled derivatives of the temperature component $T_y^* \sqrt{\varepsilon} D_y^- T_{T\varepsilon}$ and $D_x^- T_{T\varepsilon}$, respectively. From Table 8.11 we see the order of convergence for the approximations to the scaled temperature component is at least 0.72 for $T_y^* \sqrt{\varepsilon} D_y^- T_{T\varepsilon}$ for all Pr.

	$Pr = 0.2$					$Pr = 512$					$Pr = 10000$			
$\varepsilon\backslash N$	32	64	128	256	$\varepsilon\backslash N$	32	64	128	256	$\varepsilon\backslash N$	32	64	128	256
2^{-0}	0.95	0.87	0.68	0.29	2^{-0}	0.97	0.94	0.90	0.65	2^{-0}	0.51	0.77	0.90	0.66
2^{-2}	0.98	0.95	0.87	0.68	2^{-2}	0.79	0.97	0.94	0.90	2^{-2}	0.51	0.67	0.71	0.71
2^{-4}	0.99	0.98	0.95	0.87	2^{-4}	0.53	0.69	0.77	0.78	2^{-4}	0.51	0.67	0.71	0.71
2^{-6}	0.99	0.99	0.98	0.95	2^{-6}	0.53	0.69	0.77	0.78	2^{-6}	0.51	0.67	0.71	0.71
2^{-8}	0.96	0.99	0.99	0.98	2^{-8}	0.53	0.69	0.77	0.78	2^{-8}	0.51	0.67	0.71	0.71
2^{-10}	0.73	0.75	0.80	0.82	2^{-10}	0.53	0.69	0.77	0.78	2^{-10}	0.51	0.67	0.71	0.71
2^{-12}	0.73	0.75	0.80	0.82	2^{-12}	0.53	0.69	0.77	0.78	2^{-12}	0.51	0.67	0.71	0.71
2^{-14}	0.73	0.75	0.80	0.82	2^{-14}	0.53	0.69	0.77	0.78	2^{-14}	0.51	0.67	0.71	0.71
2^{-16}	0.73	0.75	0.80	0.82	2^{-16}	0.53	0.69	0.77	0.78	2^{-16}	0.51	0.67	0.71	0.71
2^{-18}	0.73	0.75	0.80	0.82	2^{-18}	0.53	0.69	0.77	0.78	2^{-18}	0.51	0.67	0.71	0.71
2^{-20}	0.73	0.75	0.80	0.82	2^{-20}	0.53	0.69	0.77	0.78	2^{-20}	0.51	0.67	0.71	0.71
p_{comp}^N	0.73	0.75	0.80	0.82	p_{comp}^N	0.53	0.69	0.77	0.78	p_{comp}^N	0.51	0.67	0.71	0.71
$C_{0.73}$	6.92	6.92	6.82	6.48	$C_{0.53}$	6.94	6.94	6.21	5.26	$C_{0.51}$	6.75	6.75	6.05	5.28

Table 8.11: Computed orders of convergence $p_{\varepsilon,comp}^N$, p_{comp}^N and the error constant $C_{p_{comp}^*}^N$ for $T_y^* \sqrt{\varepsilon}(D_y^- T_{T\varepsilon} - D_y T_{TB}^{8192})$ where $T_{T\varepsilon}$ is generated by $(A_{T\varepsilon}^N)$ for various values of ε, Pr and N with $\beta = 0.3$ and $n = \frac{1-m}{2}$.

$Pr = 0.2$

$\varepsilon\backslash N$	32	64	128	256
2^{-0}	0.49	0.71	0.83	0.86
2^{-2}	0.81	0.97	1.00	1.04
2^{-4}	0.71	0.97	1.06	1.08
2^{-6}	0.51	0.75	0.83	0.88
2^{-8}	-0.14	0.18	0.49	0.65
2^{-10}	0.06	-0.20	0.04	0.34
2^{-12}	0.06	-0.20	0.04	0.34
2^{-14}	0.06	-0.20	0.04	0.34
2^{-16}	0.06	-0.20	0.04	0.34
2^{-18}	0.06	-0.20	0.04	0.34
2^{-20}	0.06	-0.20	0.04	0.34
p^N_{comp}	0.49	0.54	0.04	0.34
$C_{0.04}$	5.63	4.14	2.93	2.93

$Pr = 512$

$\varepsilon\backslash N$	32	64	128	256
2^{-0}	0.47	0.85	1.11	0.77
2^{-2}	0.32	0.69	0.94	1.06
2^{-4}	0.13	0.50	0.64	0.77
2^{-6}	0.12	0.48	0.64	0.77
2^{-8}	0.16	0.44	0.61	0.77
2^{-10}	0.16	0.44	0.61	0.77
2^{-12}	0.16	0.44	0.61	0.77
2^{-14}	0.16	0.44	0.61	0.77
2^{-16}	0.16	0.44	0.61	0.77
2^{-18}	0.16	0.44	0.61	0.77
2^{-20}	0.16	0.44	0.61	0.77
p^N_{comp}	0.13	0.50	0.64	0.77
$C_{0.13}$	6.15	6.15	4.75	3.32

$Pr = 10000$

$\varepsilon\backslash N$	32	64	128	256
2^{-0}	0.11	0.63	0.96	0.41
2^{-2}	0.18	0.56	0.72	0.76
2^{-4}	0.17	0.56	0.74	0.78
2^{-6}	0.10	0.54	0.75	0.82
2^{-8}	0.01	0.45	0.73	0.89
2^{-10}	0.01	0.45	0.72	0.88
2^{-12}	0.01	0.45	0.72	0.88
2^{-14}	0.01	0.45	0.72	0.88
2^{-16}	0.01	0.45	0.72	0.88
2^{-18}	0.01	0.45	0.72	0.88
2^{-20}	0.01	0.45	0.72	0.88
p^N_{comp}	0.12	0.45	0.72	0.88
$C_{0.12}$	6.68	6.68	5.31	3.48

Table 8.12: Computed orders of convergence $p^N_{\varepsilon,comp}$, p^N_{comp} and the error constant $C^N_{p^*_{comp}}$ for $D^-_x T_{T\varepsilon} - D_x T^{8192}_{TB}$ where $T_{T\varepsilon}$ is generated by $(A^N_{T\varepsilon})$ for various values of ε, Pr and N with $\beta = 0.3$ and $n = \frac{1-m}{2}$.

In Table 8.13 we display the computed orders of convergence for the approximations of the first order scaled derivative of the y-velocity component in the x direction, $\frac{1}{V^*} D^-_x V_\varepsilon$, for various values of ε, Pr and N with $\beta = 0.3$ and $n = \frac{1-m}{2}$. As Pr increase the orders of convergence become more stable. This behaviour is discussed briefly in Appendix D.

	$Pr = 0.2$					$Pr = 512$			
$\varepsilon \backslash N$	32	64	128	256	$\varepsilon \backslash N$	32	64	128	256
2^{-0}	0.68	0.86	0.81	-0.73	2^{-0}	0.68	0.86	0.81	-0.73
2^{-2}	0.68	0.55	0.05	-0.62	2^{-2}	0.68	0.55	0.05	-0.62
2^{-4}	0.35	0.41	0.02	-0.22	2^{-4}	0.51	0.88	0.57	-0.47
2^{-6}	0.25	0.20	0.18	-0.08	2^{-6}	0.54	0.86	0.93	0.65
2^{-8}	-0.14	0.31	0.24	0.26	2^{-8}	0.43	0.76	0.90	0.97
2^{-10}	0.38	-0.13	0.07	0.25	2^{-10}	0.41	0.70	0.84	0.94
2^{-12}	0.67	0.60	0.42	0.25	2^{-12}	0.40	0.67	0.79	0.93
2^{-14}	0.54	0.73	0.80	0.89	2^{-14}	0.40	0.65	0.77	0.90
2^{-16}	0.46	0.73	0.80	0.88	2^{-16}	0.40	0.65	0.76	0.87
2^{-18}	0.43	0.68	0.81	0.87	2^{-18}	0.39	0.64	0.75	0.86
2^{-20}	0.41	0.66	0.78	0.89	2^{-20}	0.39	0.64	0.75	0.85
p_{comp}^N	0.41	0.49	0.07	0.25	p_{comp}^N	0.47	0.64	0.75	-0.01
$C_{0.07}$	23.22	18.32	13.72	13.72	$C_{-0.01}$	-83.92	-59.85	-37.94	-22.33

	$Pr = 10000$			
$\varepsilon \backslash N$	32	64	128	256
2^{-0}	0.67	0.82	0.81	-0.73
2^{-2}	0.02	0.56	0.87	-0.26
2^{-4}	0.33	0.59	0.78	1.00
2^{-6}	0.63	0.64	0.66	0.89
2^{-8}	0.49	0.66	0.66	0.79
2^{-10}	0.44	0.65	0.70	0.82
2^{-12}	0.42	0.64	0.73	0.83
2^{-14}	0.41	0.64	0.74	0.84
2^{-16}	0.40	0.64	0.74	0.84
2^{-18}	0.40	0.64	0.74	0.85
2^{-20}	0.39	0.64	0.75	0.85
p_{comp}^N	0.53	0.65	0.67	0.36
$C_{0.36}$	14.91	13.20	10.78	8.66

Table 8.13: Computed orders of convergence $p_{\varepsilon,comp}^N$, p_{comp}^N and the error constant $C_{p_{comp}^*}^N$ for $\frac{1}{V^*}(D_x^- V_\varepsilon - D_x V_{FS}^{8192})$ in the domain $\overline{\Omega}_\varepsilon^N \backslash (X_1 \bigcup \Gamma_L)$ where V_ε is generated by $(A_{T\varepsilon}^N)$ for various values of ε, Pr and N with $\beta = 0.3$ and $n = \frac{1-m}{2}$.

From the data in Table 8.11 we obtain the following error bounds for the $T_y^* \sqrt{\varepsilon} D_y^- T_\varepsilon$

$$
\begin{aligned}
Pr &= 0.2 & T_y^* \sqrt{\varepsilon} \| D_y^- T_\varepsilon - D_y T_{TB}^{8192} \|_{\Omega_\varepsilon^N} &\leq 6.92 N^{-0.73} \\
Pr &= 512 & T_y^* \sqrt{\varepsilon} \| D_y^- T_\varepsilon - D_y T_{TB}^{8192} \|_{\Omega_\varepsilon^N} &\leq 6.94 N^{-0.53} \\
Pr &= 10000 & T_y^* \sqrt{\varepsilon} \| D_y^- T_\varepsilon - D_y T_{TB}^{8192} \|_{\Omega_\varepsilon^N} &\leq 6.75 N^{-0.51}.
\end{aligned} \tag{8.8}
$$

Further computations, not reported here, show that the errors for $T_y^* \sqrt{\varepsilon} D_y T_{T\varepsilon}$ for $Pr \in [0.1, 10000]$ and $\beta \in [0.0, 0.3]$ for constant heat flux, $n = \frac{1-m}{2}$ and a constant wall temperature $n = 0$ have similar behaviour therefore the method can be said to be $(\varepsilon, Pr, \beta, n)$–uniform for the scaled temperature component.

8.5   Computational error bounds

Similar to Section 6.5, we use the computed error estimates, obtained in Section 7.6, for the quantities T_{B}^{8192} and its scaled discrete derivatives to estimate the error in the numerical approximations $T_{T\varepsilon}$ generated by the direct method $(A_{T\varepsilon}^{\mathbf{N}})$. The resulting estimates are independent of those obtained in Section 8.3.

First, we use the triangle inequality to obtain

$$
\begin{aligned}
\|T_{T\varepsilon} - t_{TT}\|_{\Omega_\varepsilon^N} &= \|T_{T\varepsilon} - t_{\mathrm{TB}}\|_{\Omega_\varepsilon^N} \\
&\le \|T_{T\varepsilon} - T_{\mathrm{TB}}^{8192}\|_{\Omega_\varepsilon^N} + \|T_{\mathrm{TB}}^{8192} - t_{\mathrm{TB}}\|_{\Omega_\varepsilon^N}
\end{aligned}
\tag{8.9}
$$

where $T_{T\varepsilon}$ is the solution generated by the direct algorithm $(A_{T\varepsilon}^{\mathbf{N}})$ on the mesh $\Omega_\varepsilon^{\mathbf{N}}$. t_{TB} is the exact solution of the Prandtl problem constructed from the Blasius formula (7.4). T_{TB}^{8192} is the computed Blasius solution generated in the previous chapter on a mesh with 8192 intervals. We then observe that the first term on the right–hand side of (8.9) involves the computable quantities $T_{T\varepsilon}$ and T_{TB}^{8192}. Furthermore, the second term on the right–hand side involves the scaled pointwise errors $T_{\mathrm{TB}}^{8192} - t_{\mathrm{TB}}$, which have already been estimated in Section 7.10 of the previous chapter. This shows that we can estimate the errors in the scaled numerical solutions and their scaled discrete derivatives, generated by the numerical method $(A_{T\varepsilon}^{\mathbf{N}})$ applied to problem $(P_{T\varepsilon})$, even though no theoretical error analysis is available for this numerical method.

We now compare the magnitude of the terms on the right–hand side of (8.9). The first term is the scaled maximum pointwise difference $\|T_\varepsilon - T_{\mathrm{TB}}^{8192}\|_{\overline{\Omega}_\varepsilon^N}$. This quantity is found immediately from the solutions $T_{T\varepsilon}$ of $(A_{T\varepsilon}^{\mathbf{N}})$ and the solution T_{TB}^{8192}, computed in Chapter 7. Their numerical values are given in Table 8.7 for various values of ε, N and Pr for $\beta = 0.3$ and $n = \frac{1-m}{2}$. The second term on the right–hand side of (8.9) is the scaled maximum pointwise error $\|T_{\mathrm{TB}}^{8192} - t_{\mathrm{TB}}\|_{\Omega_\varepsilon^N}$ in the computed Blasius solution. The corresponding error bound (7.38), shows that the second term is bounded above by 5.560×10^{-3} for all Pr and β.

$$
\begin{aligned}
\|T_{T\varepsilon} - t_{TT}\|_{\Omega_\varepsilon^N} &= \|T_{T\varepsilon} - t_{\mathrm{TB}}\|_{\Omega_\varepsilon^N} \\
&\le \|T_{T\varepsilon} - T_{\mathrm{TB}}^{8192}\|_{\Omega_\varepsilon^N} + \|T_{\mathrm{TB}}^{8192} - t_{\mathrm{TB}}\|_{\Omega_\varepsilon^N} \\
Pr = 0.2 \qquad &\le 1.15 N^{-0.104} + 5.560 \times 10^{-3} \\
Pr = 512 \qquad &\le 0.51 N^{-0.106} + 5.560 \times 10^{-3} \\
Pr = 10000 \qquad &\le 1.09 N^{-0.75} + 5.560 \times 10^{-3}.
\end{aligned}
\tag{8.10}
$$

The computational error bounds for $T_{T\varepsilon}$ in (8.10) and (8.7) give two computational formulae such that we can ensure the error is below a desired value for all ε, Pr and

$\beta \in [0,3]$. In a similar manner to the above we calculate computed error bounds for approximations of the scaled first derivative $T_y^* \sqrt{\varepsilon} D_y^- T_{T\varepsilon}$ by the bounds (7.43) and (8.8)

$$
\begin{aligned}
T_y^* \sqrt{\varepsilon} \|D_y^- T_{T\varepsilon} - \partial_y t_{TT}\|_{\Omega_\varepsilon^N} &= T_y^* \sqrt{\varepsilon} \|D_y^- T_{T\varepsilon} - \partial_y t_{TB}\|_{\Omega_\varepsilon^N} \\
&\leq T_y^* \sqrt{\varepsilon} \|D_y^- T_{T\varepsilon} - D_y T_{TB}^{8192}\|_{\Omega_\varepsilon^N} \\
&\quad + T_y^* \sqrt{\varepsilon} \|D_y T_{TB}^{8192} - \partial_y t_{TB}\|_{\Omega_\varepsilon^N}
\end{aligned}
$$

$$
\begin{aligned}
Pr &= 0.2 &\leq 6.92 N^{-0.73} + 9.002 \times 10^{-3} \\
Pr &= 512 &\leq 6.94 N^{-0.53} + 9.002 \times 10^{-3} \\
Pr &= 10000 &\leq 6.75 N^{-0.51} + 9.002 \times 10^{-3}.
\end{aligned}
$$

(8.11)

The computational error bounds for $D_y^- T_{T\varepsilon}$ in (8.11) and (8.8) give two computational formula such that we can ensure the error is below a desired value for all ε, Pr and β, for constant heat flux and walls of constant temperature.

8.6 Conclusion

In Chapters 7 and 8 we considered the Prandtl boundary layer equations for incompressible laminar flow past a wedge with angle $\beta\pi$, $\beta \in [0, 0.3]$ with heat transfer. When the Reynolds number and Prandtl number are large the solution of this problem has two parabolic boundary layers. We constructed a direct numerical method for computing approximations to the solution of this problem using a compound piecewise uniform fitted mesh technique appropriate to the parabolic boundary layers. We used the method to approximate the self–similar solution of the Prandtl problem in a finite rectangle excluding the leading edge of the wedge for various values of Re, Pr, β and n. We constructed and applied a special numerical method related to the Blasius technique, to compute reference solutions to the problem. These were used to obtain approximate boundary conditions on the artificial boundaries of the computational domain and in the error analysis of the velocity components, their derivatives, the temperature component and its derivatives. Extensive numerical experiments indicated that the constructed direct numerical method is (Re, Pr, β, n)–uniform.

Chapter 9

Prandtl flow past a wedge with mass transfer – Blasius' method.

9.1 Prandtl Boundary layer equations

In this chapter and the next, we use and adapt the numerical methods developed in Chapters 3 and 4 and apply it to the Prandtl boundary layer equation for flow past a semi-infinite wedge with mass transfer. The introduction of mass transfer adds another layer of complexity to the equation.

In the present chapter we use a variant of the semi-analytic approach of Blasius' to generate numerical approximations of guaranteed accuracy to the flow variables and their scaled derivatives.

In the next chapter, we construct a direct numerical method for solving the problem. We show that the numerical approximations are pointwise accurate and that they satisfy pointwise error estimates that are uniform with respect to the Reynolds number, the mass transfer parameter and the angle of the wedge.

We choose the computational domain to be the finite rectangle $\Omega = (0.6, 1.6) \times (0, 1)$ on the upper side of the wedge, sufficiently far from the leading edge (see Fig. 9-1) such that the leading edge singularity and mass transfer singularity do not cause excessive problems for the numerical method.
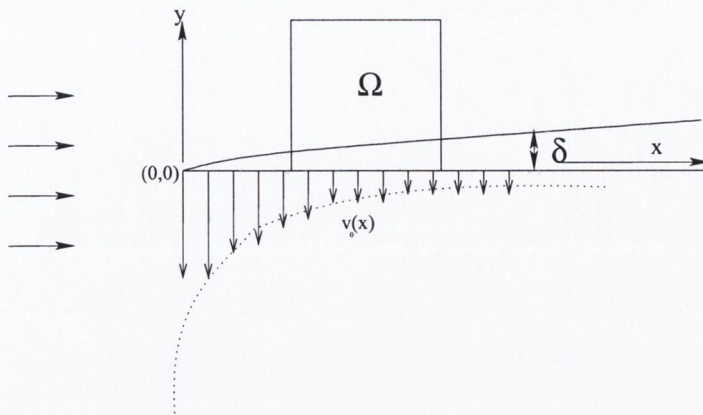
Figure 9-1: Flow past a plate with suction/blowing.

In Figure 9-1 we see the constant flow to the left hand side of the plate. Along the plate δ denotes the width of the boundary layer and $v_0(x)$ denotes the mass transfer. As we intend to solve the Prandtl boundary layer numerically we must compute the approximate solution on a finite domain Ω. The Prandtl boundary layer problem on a finite domain, Ω, is

$$(P_M) \begin{cases} \text{Find } \mathbf{u_M} = (u_M, v_M) \text{ such that for all } (x, y) \in \Omega \\ \mathbf{u}_M \text{ satisfies the differential equation} \\[2mm] -\frac{1}{Re}\frac{\partial^2 u_M}{\partial^2 y} + \mathbf{u}_M.\nabla u_M = U(x)\frac{dU(x)}{dx} \\[2mm] \nabla.\mathbf{u_M} = 0 \\[2mm] \text{with boundary conditions} \\ u_M = 0 \text{ and } v_M = v_0(x) \text{ on } \Gamma_B \\ \mathbf{u_M} = \mathbf{u}_P \text{ on } \Gamma_L \bigcup \Gamma_T \end{cases}$$

where $U(x) = x^m$ is the solution of the reduced problem, $m = \frac{\beta}{2-\beta}$ and $\beta\pi$ is the angle in radians of the wedge. u_P is the exact solution of (P_P). $v_0(x)$ is the velocity normal to the plate at which mass is transferred through its surface (see equation (9.4) in Section 9.2). The case for no mass transfer, $v_0(x) = 0$, was dealt with in Chapters 3 and 4 and it was used as the starting point for this and the next chapter. Our goal in Chapters 9 and 10 is to model the flow for all Reynolds numbers $Re \in [1, \infty)$, all mass transfer $v_i \in [-0.6, 7.07]$ and angles of the wedge, $\beta \in [0.0, 1.0]$, for which the flow remains laminar and no separation occurs on the wedge.

9.2 Blasius' solution

Using the similarity transformation described in [1]

$$\eta = y\sqrt{\frac{(m+1)Re}{2}\frac{U}{x}} \tag{9.1}$$

the velocity components of the Blasius solution $\mathbf{u}_{MB}$ of (P_M) are given by

$$u_{MB}(x,y) = u_1 x^m f'(\eta) = U f'(\eta) \tag{9.2}$$

$$v_{MB}(x,y) = -\sqrt{\frac{m+1}{2x}\frac{U}{Re}}\left(f + \frac{m-1}{m+1}\eta f'\right) \tag{9.3}$$

where f is the solution of the non-linear ordinary differential equation

$$(P_{MB})\begin{cases} \text{For } \eta \in (0,\infty) \text{ find } f \in C^3(0,\infty) \\[2mm] f''' + ff'' + \beta(1 - f'^2) = 0 \\[2mm] \text{with boundary conditions} \\ f(0) = v_i \quad f'(0) = 0, \qquad\qquad f'(\infty) = 1. \end{cases}$$

The Blasius problem (P_{MB}) is solved numerically for the function f, and the relations are used to construct the Blasius solution $\mathbf{u_{MB}}$ of P_M. From [43] we have

$$v_0(x) = -v_i\sqrt{\frac{m+1}{2x}\frac{U}{Re}} \tag{9.4}$$

where v_i is the mass transfer parameter. Negative values of v_i correspond to injection, positive values correspond to suction. Technically v_i can have $(-\infty, \infty)$, but in practice when $v_i \leq -0.87$ the boundary layer is blown away from the surface. In addition to this there is an upper limit of 7.07 [46]. The Blasius equation with no mass transfer, $v_i = 0$, was dealt with in Chapter 3.

Note that the Blasius problem for flow past a flat plate with mass transfer was investigated in [28] and [29].

It is clear that we need Reynolds uniform pointwise accuracy of $f(\eta)$, $f'(\eta)$ and $f''(\eta)$ for all $\eta \in (0,\infty)$. Therefore we construct a new numerical method, which enables us to generate such (Re, β, v_i)-uniform approximations.

Problem (P_{MB}) is dealt with in exactly the same way as problem (P_{FS}) was in Chapter 3. The arguments used in Section 3.3 can be applied to the equation in (P_{MB}) to show the singularly perturbed nature of the equation. The extrapolations (3.7)-(3.9) for f of (P_{FS}) are identical for f of (P_{MB}).

9.3 Robust layer resolving method for Blasius' problem

We now describe our numerical method for finding approximations to the solution and its derivatives of problem (P_{MB}). For each fixed N we write $L_N = lnN$ and we divide the interval into the two subintervals $[0, L_N]$ and $[L_N, \infty)$. We construct a uniform mesh

$$\overline{I}_u^N = \{\eta_i : \eta_i = iN^{-1}nN, 0 \le i \le N\}_0^N$$

on the subinterval $[0, L_N]$ and we determine numerical approximations F, D^+F and D^+D^+F to f_L, f'_L and f''_L, respectively, at the mesh points $\overline{I}_u^N$, using a variation of the continuation algorithm defined in Section 3.4 with the continuation parameter m

$$(A_{MB}^N) \begin{cases} \text{For each integer } m, \ 1 \le m \le M \text{ find } F^m \text{ on } I_u^N \\ \text{such that, for all } \eta \in I_u^N, \ 2 \le i \le N - 1 \\ \\ \delta^2(D^-F_i^m) + F_i^{m-1}(D^+(D^-F_i^m)) + \beta(1 - (D^-F_i^{m-1})(D^-F_i^m)) \\ -(1 + \beta)(D^-F_i^m - D^-F_i^{m-1}) = 0 \\ \\ \text{with boundary conditions} \\ F(0) = v_i \quad D^+F(0) = 0, \qquad\qquad D^0F(x_{N-1}) = 1 \\ \\ \text{and the initial guess } F^0(\eta_i) = \eta_i. \end{cases}$$

To avoid cumbersome notation we suppress explicit mention for N and M and we denote the final output of (A_{MB}^N) simply by F.

We assign the values $D^+F(\eta_N) = 1$ and $D^+D^+F(\eta_N) = D^+D^+F(\eta_{N-1}) = 0$ so that F, D^+F and D^+D^+F are defined at all points of the mesh $\overline{I}_u^N$. We then use piecewise linear interpolation to interpolate from $\overline{I}_u^N$ to each point of the subinterval $[0, L_N]$. We denote the corresponding interpolants by $\overline{F}$, $\overline{D^+F}$ and $\overline{D^+D^+F}$. We extend these functions to the whole of the semi-infinite interval $[0, \infty)$ using the extensions (3.13)-(3.15). We take the values of F, D^+F and D^+D^+F, respectively, to be the

required numerical approximations to the exact values f, f' and f'' of the Blasius solution and its derivatives on the semi-infinite interval $[0, \infty)$.

9.4 Computed error estimates for Blasius' problem

For the sake of brevity we show the errors for only three values of the mass transfer parameter, $v_i = -0.6$, $v_i = 2.0$ and $v_i = 7.0$ and one value of the angle of the wedge, $\beta = 0.8$.

We use the experimental formula defined in Section 3.6 to obtain computed parameter uniform global error parameters for the function $\overline{F}$. The computed two mesh differences $\overline{D}^N$, order of convergence $\overline{p}^N$ and the constant of convergence C_{p*}^N for F, D^+F and D^+D^+F, are given in 9.1, 9.2 and 9.3, respectively, for various values of N, v_i and $\beta = 0.8$.

N	128	256	512	1024	2048	4096	8192	16384
				$v_i = -0.6$				
D^N	0.006577	0.003837	0.002186	0.001227	0.000681	0.000374	0.000204	0.000110
p^N	0.78	0.81	0.83	0.85	0.86	0.87	0.88	0.89
$C_{0.86}^N$	0.963702	1.022864	1.060187	1.082739	1.093094	1.093094	1.084394	1.068444
				$v_i = 2.0$				
D^N	0.012923	0.007518	0.004289	0.002411	0.001338	0.000736	0.000401	0.000217
p^N	0.78	0.81	0.83	0.85	0.86	0.87	0.88	0.89
$C_{0.86}^N$	1.889530	1.999248	2.074426	2.120231	2.141152	2.141152	2.123747	2.091972
				$v_i = 7.0$				
D^N	0.015586	0.009089	0.005193	0.002921	0.001623	0.000892	0.000487	0.000264
p^N	0.78	0.81	0.83	0.85	0.86	0.87	0.88	0.89
$C_{0.86}^N$	2.275442	2.412786	2.506442	2.563224	2.589045	2.589045	2.567705	2.528843

Table 9.1: Computed two mesh difference $\overline{D}^N$, order of convergence $\overline{p}^N$ and the constant of convergence C_{p*}^N for $\overline{F}$ on $[0, \infty)$ generated by (A_{MB}^N) with $M = 8 \ln N$ applied to problem (P_{MB}) for various values of N and v_i with $\beta = 0.8$.

Comparison of the entries in the p^N rows of Tables 9.1, 9.2 and 9.3 with the Table of theoretical behavior for $N^{-1}nN$ of the order of convergence defined p^N in Appendix B suggests strongly that the computed order of L-uniform convergence p^N corresponds to the theoretical behavior $N^{-1}nN$.

Graphs of $\overline{F}$ for $N = 8192$ and various values of v_i and $\beta = 0.8$ on $[0, L_N]$ are given in Figure 9-2. Graphs of $\overline{D^+F}$ and $\overline{D^+D^+F}$ for $N = 8192$ and various values of v_i and $\beta = 0.8$ on $[0, L_N]$ are given in Figures 9-3 and 9-4, respectively. In Figures 9-3 and 9-4 we can make out the significant effect of the mass transfer parameter on the

derivatives of F.
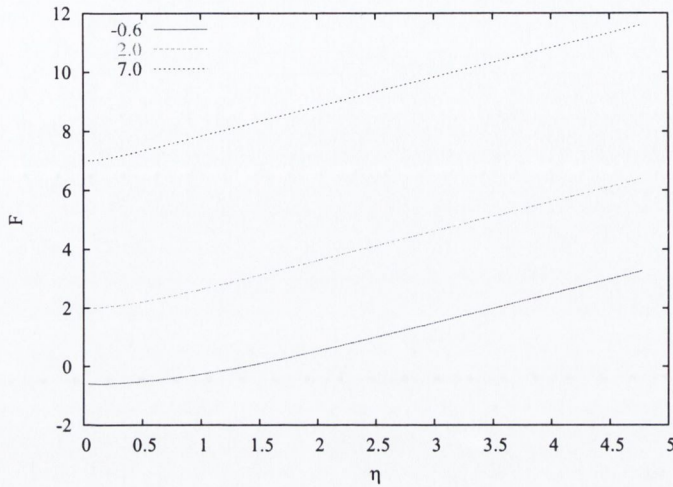
Figure 9-2: Solution $\overline{F}$ generated by method (A_{MB}^N) applied to the problem P_B with $M = 8nN$, $N = 8192$ $v_i = -0.6$, 2.0, 7.0 and $\beta = 0.8$.

				$v_i = -0.6$				
N	128	256	512	1024	2048	4096	8192	16384
D^N	0.001119	0.000650	0.000371	0.000208	0.000116	0.000064	0.000035	0.000019
p^N	0.78	0.81	0.83	0.85	0.86	0.87	0.88	0.89
$C_{0.86}^N$	0.163584	0.172656	0.179109	0.183045	0.184855	0.184855	0.183344	0.180593
				$v_i = 2.0$				
D^N	0.004741	0.002854	0.001647	0.000934	0.000522	0.000288	0.000157	0.000085
p^N	0.73	0.79	0.82	0.84	0.86	0.87	0.88	0.89
$C_{0.86}^N$	0.682728	0.745563	0.780566	0.803133	0.813238	0.813238	0.805734	0.792213
				$v_i = 7.0$				
D^N	0.017325	0.010473	0.006348	0.003693	0.002082	0.001153	0.000632	0.000343
p^N	0.73	0.72	0.78	0.83	0.85	0.87	0.88	0.89
$C_{0.85}^N$	2.426312	2.647697	2.897198	3.042078	3.096208	3.096208	3.065201	3.003570

Table 9.2: Computed two mesh difference $\overline{D}^N$, order of convergence $\overline{p}^N$ and the constant of convergence $C_{p^*}^N$ for $\overline{D^+F}$ on $[0, \infty)$ generated by (A_{MB}^N) with $M = 8nN$ applied to problem (P_{MB}) for various values of N and v_i with $\beta = 0.8$.
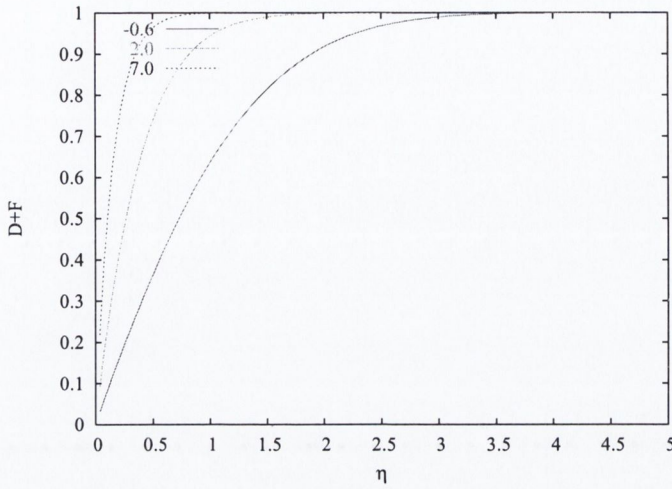
Figure 9-3: Solution $\overline{D^+F}$ generated by method (A_{MB}^N) applied to the problem P_{MB} with $M = 8nN$, $N = 8192$ $v_i = -0.6$, 2.0, 7.0 and $\beta = 0.8$.

				$v_i = -0.6$				
N	128	256	512	1024	2048	4096	8192	16384
D^N	0.003399	0.001977	0.001127	0.000633	0.000351	0.000193	0.000105	0.000057
p^N	0.78	0.81	0.83	0.85	0.86	0.87	0.88	0.89
$C_{0.86}^N$	0.497502	0.526218	0.545499	0.557475	0.562921	0.562921	0.558385	0.550102
				$v_i = 2.0$				
D^N	0.066178	0.042376	0.025598	0.014869	0.008412	0.004674	0.002564	0.001393
p^N	0.64	0.73	0.78	0.82	0.85	0.87	0.88	0.89
$C_{0.85}^N$	9.110601	10.499888	11.415405	11.934206	12.152152	12.152152	11.996945	11.731630
				$v_i = 7.0$				
D^N	0.394216	0.309139	0.212181	0.133040	0.078668	0.044812	0.024922	0.013644
p^N	0.35	0.54	0.67	0.76	0.81	0.85	0.87	0.88
$C_{0.81}^N$	47.070052	64.799507	78.078509	85.944035	89.215246	89.215246	87.103873	83.713079

Table 9.3: Computed two mesh difference $\overline{D}^N$, order of convergence $\overline{p}^N$ and the constant of convergence $C_{p^*}^N$ for $\overline{D^+D^+F}$ on $[0, \infty)$ generated by (A_{MB}^N) with $M = 8nN$ applied to problem (P_{MB}) for various values of N and v_i with $\beta = 0.8$.
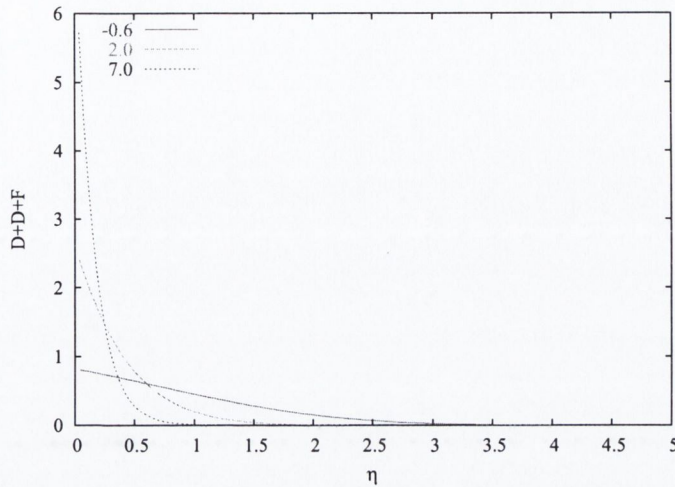
Figure 9-4: Solution $\overline{D^+D^+F}$ generated by method (A_{MB}^N) applied to the problem P_{MB} with $M = 8nN$, $N = 8192$, $v_i = -0.6$, 2.0, 7.0 and $\beta = 0.8$.

We use the tables and the experimental technique to obtain the following error bounds for $N \geq 2048$

$$
\begin{array}{ll}
v_i = -0.6 & ||\overline{F} - f||_{[0,\infty)} \leq 1.093 N^{-0.86} \\
v_i = 2.0 & ||\overline{F} - f||_{[0,\infty)} \leq 2.14 N^{-0.86} \\
v_i = 7.0 & ||\overline{F} - f||_{[0,\infty)} \leq 2.60 N^{-0.86}
\end{array} \tag{9.5}
$$

$$
\begin{array}{ll}
v_i = -0.6 & ||\overline{D^+F} - f'||_{[0,\infty)} \leq 0.185 N^{-0.86} \\
v_i = 2.0 & ||\overline{D^+F} - f'||_{[0,\infty)} \leq 0.81 N^{-0.86} \\
v_i = 7.0 & ||\overline{D^+F} - f'||_{[0,\infty)} \leq 3.09 N^{-0.86}
\end{array} \tag{9.6}
$$

$$
\begin{array}{ll}
v_i = -0.6 & ||\overline{D^+D^+F} - f''||_{[0,\infty)} \leq 0.563 N^{-0.86} \\
v_i = 2.0 & ||\overline{D^+D^+F} - f''||_{[0,\infty)} \leq 12.15 N^{-0.85} \\
v_i = 7.0 & ||\overline{D^+D^+F} - f''||_{[0,\infty)} \leq 89.21 N^{-0.83}.
\end{array} \tag{9.7}
$$

We observe from (9.2) and (9.3) that u_{MB}, v_{MB}, ∇u_{MB} and ∇v_{MB} involve the expression $\eta f''$ and $\beta f' + \frac{m-1}{m+1}\eta f''$. Therefore, we compute the global error bounds for $\eta \overline{D^+D^+F}$ and $\beta \overline{D^+F} + \frac{m-1}{m+1}\eta \overline{D^+D^+F}$, respectively, using the techniques described at the beginning of the section and the data in Tables 9.4-9.5.

				$v_i = -0.6$				
N	128	256	512	1024	2048	4096	8192	16384
D^N	0.001674	0.000978	0.000559	0.000315	0.000175	0.000096	0.000052	0.000028
p^N	0.78	0.81	0.83	0.85	0.86	0.87	0.88	0.89
$C^N_{0.86}$	0.244230	0.259398	0.269625	0.275873	0.278688	0.278688	0.276383	0.272183
				$v_i = 2.0$				
N	128	256	512	1024	2048	4096	8192	16384
D^N	0.002511	0.001486	0.000854	0.000483	0.000269	0.000148	0.000081	0.000044
p^N	0.76	0.80	0.82	0.84	0.86	0.87	0.88	0.89
$C^N_{0.86}$	0.363896	0.390904	0.408126	0.418704	0.423729	0.423729	0.420034	0.413296
				$v_i = 7.0$				
D^N	0.010764	0.006873	0.004041	0.002317	0.001305	0.000722	0.000395	0.000214
p^N	0.65	0.77	0.80	0.83	0.85	0.87	0.88	0.89
$C^N_{0.85}$	1.520247	1.754820	1.865228	1.933840	1.968400	1.968400	1.948069	1.911340

Table 9.4: Computed two mesh difference $\overline{D}^N$, order of convergence $\overline{p}^N$ and the constant of convergence C^N_{p*} for $\beta\overline{D^+F} + \frac{m-1}{m+1}\eta\overline{D^+D^+F}$ on $[0,\infty)$ generated by (A^N_{MB}) with $M = 8nN$ applied to problem (P_{MB}) for various values of N and v_i with $\beta = 0.8$.

				$v_i = -0.6$				
N	128	256	512	1024	2048	4096	8192	16384
D^N	0.005204	0.003067	0.001759	0.000992	0.000552	0.000304	0.000166	0.000090
p^N	0.76	0.80	0.83	0.85	0.86	0.87	0.88	0.89
$C^N_{0.86}$	0.756593	0.810087	0.844375	0.864705	0.874095	0.874095	0.866600	0.853054
				$v_i = 2.0$				
D^N	0.008157	0.004930	0.002881	0.001648	0.000924	0.000510	0.000279	0.000151
p^N	0.73	0.78	0.81	0.83	0.86	0.87	0.88	0.89
$C^N_{0.86}$	1.164691	1.274857	1.349271	1.397907	1.420003	1.420003	1.406448	1.381610
				$v_i = 7.0$				
D^N	0.018083	0.012805	0.007827	0.004684	0.002683	0.001499	0.000825	0.000449
p^N	0.50	0.71	0.74	0.80	0.84	0.86	0.88	0.89
$C^N_{0.84}$	2.415191	3.061948	3.350791	3.590001	3.682037	3.682037	3.628263	3.533041

Table 9.5: Computed two mesh difference $\overline{D}^N$, order of convergence $\overline{p}^N$ and the constant of convergence C^N_{p*} for $\eta\overline{D^+D^+F}$ on $[0,\infty)$ generated by (A^N_{MB}) with $M = 8nN$ applied to problem (P_{MB}) for various values of N and v_i with $\beta = 0.8$

The resulting computed global error bounds from Tables 9.4-9.5, which hold for all $N \geq 2048$, are

$$
\begin{aligned}
v_i &= -0.6 & \left\|\beta\overline{D^+F} + \tfrac{m-1}{m+1}\eta\overline{D^+D^+F} - \beta f' + \tfrac{m-1}{m+1}\eta f''\right\|_{[0,\infty)} &\leq 0.279 N^{-0.86} \\
v_i &= 2.0 & \left\|\beta\overline{D^+F} + \tfrac{m-1}{m+1}\eta\overline{D^+D^+F} - \beta f' + \tfrac{m-1}{m+1}\eta f''\right\|_{[0,\infty)} &\leq 0.423 N^{-0.86} \quad (9.8) \\
v_i &= 7.0 & \left\|\beta\overline{D^+F} + \tfrac{m-1}{m+1}\eta\overline{D^+D^+F} - \beta f' + \tfrac{m-1}{m+1}\eta f''\right\|_{[0,\infty)} &\leq 1.938 N^{-0.86}
\end{aligned}
$$

$$v_i = -0.6 \quad \|\eta(\overline{D^+D^+F} - f'')\|_{[0,\infty)} \leq 0.874N^{-0.86}$$
$$v_i = 2.0 \quad \|\eta(\overline{D^+D^+F} - f'')\|_{[0,\infty)} \leq 1.42N^{-0.86} \quad (9.9)$$
$$v_i = 7.0 \quad \|\eta(\overline{D^+D^+F} - f'')\|_{[0,\infty)} \leq 3.68N^{-0.84}.$$

9.5 Computed global error estimates for Blasius' solution

In a similar manner to Section 3.7 we obtain approximate expressions $\mathbf{U}_{MB} = (U_{MB}, V_{MB})$ for the Blasius solution u_{MB} of (P_W) by substituting into the relations (9.2) and (9.3) the approximations $\overline{F}$ and $\overline{D^+F}$ for f and f', computed by (A_{MB}^N). Thus for each (x, y) in the rectangle $\overline{\Omega}$ we define

$$U_{MB}(x, y) = x^m \overline{D^+F}(\eta) = U(x)\overline{D^+F}(\eta) \quad (9.10)$$

$$V_{MB}(x, y) = -\sqrt{\frac{m+1}{2x}\frac{U(x)}{Re}} \left(\overline{F}(\eta) + \frac{m-1}{m+1}\eta\overline{D^+F}(\eta) \right) \quad (9.11)$$

where $\eta \in [0, \infty)$ is given by (9.1).

For the x-component U_{MB} of the velocity we obtain from (9.10) and (9.6) the following computed error bound for all $N \geq 2048$

$$v_i = -0.6 \quad \|U_{MB} - u_{MB}\|_{\overline{\Omega}} \leq U(1.6)(0.185N^{-0.86})$$
$$v_i = 2.0 \quad \|U_{MB} - u_{MB}\|_{\overline{\Omega}} \leq U(1.6)(0.81N^{-0.86})$$
$$v_i = 7.0 \quad \|U_{MB} - u_{MB}\|_{\overline{\Omega}} \leq U(1.6)(3.09N^{-0.86}).$$

In the specific case of $N = 8192$ we have

$$v_i = -0.6 \quad \|U_{MB} - u_{MB}\|_{\overline{\Omega}} \leq 1.091 \times 10^{-4}$$
$$v_i = 2.0 \quad \|U_{MB} - u_{MB}\|_{\overline{\Omega}} \leq 4.776 \times 10^{-4} \quad (9.12)$$
$$v_i = 7.0 \quad \|U_{MB} - u_{MB}\|_{\overline{\Omega}} \leq 1.822 \times 10^{-3}.$$

Similarly, for the y-component $\frac{1}{V_*}V_{MB}$ of the velocity we obtain

$$\frac{1}{V_*}\|V_{MB} - v_{MB}\|_{\overline{\Omega}} = \frac{1}{V_*}\sqrt{\frac{m+1}{2x}\frac{U(x)}{Re}} \left(\|\overline{F}(\eta) + \frac{m-1}{m+1}\eta\overline{D^+F}(\eta) - (f(\eta) + \frac{m-1}{m+1}\eta f')\| \right)$$
$$\leq \sqrt{\frac{m+1}{2x}U(x)}(\|\overline{F}(\eta) - f(\eta)\|)$$
$$+ U(x)\frac{|m-1|}{2x}y\|\overline{D^+F}(\eta) - f'\| \quad (9.13)$$

$$v_i = -0.6 \quad ||V_{MB} - v_{MB}||_{\overline{\Omega}} \leq \sqrt{\frac{1.6667}{2(1.6)}U(1.6))}(1.093N^{-0.86}) + U(1.6)\frac{0.3333}{2(1.6)}(0.185N^{-0.86})$$

$$v_i = 2.0 \quad ||V_{MB} - v_{MB}||_{\overline{\Omega}} \leq \sqrt{\frac{1.6667}{2(1.6)}U(1.6))}(2.14N^{-0.86}) + U(1.6)\frac{0.3333}{2(1.6)}(0.81N^{-0.86})$$

$$v_i = 7.0 \quad ||V_{MB} - v_{MB}||_{\overline{\Omega}} \leq \sqrt{\frac{1.6667}{2(1.6)}U(1.6))}(2.06N^{-0.86}) + U(1.6)\frac{0.3333)}{2(1.6)}(3.09N^{-0.86}).$$

In the specific case of $N = 8192$ we have

$$v_i = -0.6 \quad ||V_{MB} - v_{MB}||_{\overline{\Omega}} \leq 4.090 \times 10^{-4}$$
$$v_i = 2.0 \quad ||V_{MB} - v_{MB}||_{\overline{\Omega}} \leq 8.283 \times 10^{-4} \tag{9.14}$$
$$v_i = 7.0 \quad ||V_{MB} - v_{MB}||_{\overline{\Omega}} \leq 1.136 \times 10^{-3}.$$

In a similar manner to the above, we calculate computed error bounds for approximations of the scaled first derivatives by scaled discrete derivatives

$$\partial_y U_{MB} = \frac{\eta}{y}U(x)\overline{D^+D^+}F(\eta) \tag{9.15}$$

$$\partial_y V_{MB} = -\frac{\eta}{y}\left(\sqrt{\frac{(m+1)U(x)}{2xRe}}\left(\beta\overline{D^+}F + \frac{m-1}{m+1}\eta\overline{D^+D^+}F\right)\right) \tag{9.16}$$

$$\partial_x U_{MB} = -\partial_y V_{MB} \tag{9.17}$$

$$\partial_x V_{MB} = \frac{m-1.0}{2x}\left(V_{MB} - \sqrt{\frac{(m+1)U(x)}{(2xRe)}}\left(\eta\overline{D^+}F + \eta\frac{m-1.0}{m+1.0}\left(\overline{D^+}F + \eta\overline{D^+D^+}F\right)\right)\right). \tag{9.18}$$

In terms of these quantities, the computed global error bounds for the scaled discrete derivatives of the velocity components for all $N \geq 2048$ are

$$\frac{1}{\sqrt{Re}}||\partial_y U_{MB} - \frac{\partial u_{MB}}{\partial y}||_{\overline{\Omega}} = \frac{1}{\sqrt{Re}}\sqrt{\frac{(m+1)Re\,U(x)}{2}}\frac{U(x)}{x}||\overline{D^+D^+}F - f''||_{[0,\infty)} \tag{9.19}$$

$$v_i = -0.6 \quad \frac{1}{\sqrt{Re}}||\partial_y U_{MB} - \frac{\partial u_{MB}}{\partial y}||_{\overline{\Omega}} \leq \sqrt{\frac{(1.6667)}{2}\frac{U(1.6)}{1.6}}U(1.6)(0.279N^{-0.86})$$

$$v_i = 2.0 \quad \frac{1}{\sqrt{Re}}||\partial_y U_{MB} - \frac{\partial u_{MB}}{\partial y}||_{\overline{\Omega}} \leq \sqrt{\frac{(1.6667)}{2}\frac{U(1.6)}{1.6}}U(1.6)(12.15N^{-0.86})$$

$$v_i = 7.0 \quad \frac{1}{\sqrt{Re}}||\partial_y U_{MB} - \frac{\partial u_{MB}}{\partial y}||_{\overline{\Omega}} \leq \sqrt{\frac{(1.6667)}{2}\frac{U(1.6)}{1.6}}U(1.6)(89.21N^{-0.86}). \tag{9.20}$$

In the specific case of $N = 8192$ we have

$$v_i = 0.5 \quad \frac{1}{\sqrt{Re}}||\partial_y U_{MB} - \frac{\partial u_{MB}}{\partial y}||_{\overline{\Omega}} \leq 3.078 \times 10^{-4}$$
$$v_i = 2.0 \quad \frac{1}{\sqrt{Re}}||\partial_y U_{MB} - \frac{\partial u_{MB}}{\partial y}||_{\overline{\Omega}} \leq 7.493 \times 10^{-3} \tag{9.21}$$
$$v_i = 7.0 \quad \frac{1}{\sqrt{Re}}||\partial_y U_{MB} - \frac{\partial u_{MB}}{\partial y}||_{\overline{\Omega}} \leq 5.502 \times 10^{-2}$$

$$\left\|\partial_y V_{MB} - \frac{\partial v_{MB}}{\partial y}\right\|_{\overline{\Omega}} = \sqrt{\frac{(m+1)Re}{2}\frac{U(x)}{x}}(\sqrt{\frac{(m+1)U(x)}{2xRe}}\|\beta\overline{D^+F} + \frac{m-1}{m+1}\eta\overline{D^+D^+F} - \beta f' - \frac{m-1}{m+1}\eta f''\|_{[0,\infty)}) \tag{9.22}$$

$$\begin{aligned} v_i = -0.6 \quad & \left\|\partial_y V_{MB} - \frac{\partial v_{MB}}{\partial y}\right\|_{\overline{\Omega}} \leq \frac{1.667 U(1.6)}{3.2}(0.279N^{-0.86}) \\ v_i = 2.0 \quad & \left\|\partial_y V_{MB} - \frac{\partial v_{MB}}{\partial y}\right\|_{\overline{\Omega}} \leq \frac{1.667 U(1.6)}{3.2}(0.423N^{-0.86}) \\ v_i = 7.0 \quad & \left\|\partial_y V_{MB} - \frac{\partial v_{MB}}{\partial y}\right\|_{\overline{\Omega}} \leq \frac{1.667 U(1.6)}{3.2}(1.968N^{-0.86}). \end{aligned} \tag{9.23}$$

In the specific case of $N = 8192$ we have

$$\begin{aligned} v_i = -0.6 \quad & \left\|\partial_y V_{MB} - \frac{\partial v_{MB}}{\partial y}\right\|_{\overline{\Omega}} \leq 7.196 \times 10^{-5} \\ v_i = 2.0 \quad & \left\|\partial_y V_{MB} - \frac{\partial v_{MB}}{\partial y}\right\|_{\overline{\Omega}} \leq 2.609 \times 10^{-4} \\ v_i = 7.0 \quad & \left\|\partial_y V_{MB} - \frac{\partial v_{MB}}{\partial y}\right\|_{\overline{\Omega}} \leq 1.214 \times 10^{-3}. \end{aligned} \tag{9.24}$$

For $\frac{1}{V_*} D_x V_{MB}$ of the velocity we obtain from (9.18), (9.5), (9.6) and (9.9) the following computed error bound for all $N \geq 2048$

$$\begin{aligned} \frac{1}{V_*}\left\|\partial_x V_{MB} - \frac{\partial v_{MB}}{\partial x}\right\|_{\overline{\Omega}} &= \frac{m-1.0}{2x}(\|V_{MB} - \sqrt{\frac{(m+1)U(x)}{(2xRe)}}(\eta\overline{D^+}F + \eta\frac{m-1.0}{m+1.0}(\overline{D^+}F + \eta\overline{D^+D^+F})) \\ & \quad -v_{MB} + \sqrt{\frac{(m+1)U(x)}{(2xRe)}}(\eta f' + \eta\frac{m-1.0}{m+1.0}(f' + \eta f''))\|) \\ &\leq \frac{m-1.0}{2x}(\|V_{MB} - v_{MB}\|_{\overline{\Omega}} \\ & \quad +\frac{m+1}{2x}U(x)\beta\|\overline{D^+F} - f'\|_{[0,\infty)} \\ & \quad +\frac{m-1}{m+1}\|\eta\overline{D^+D^+F} - \eta f''\|_{[0,\infty)}) \end{aligned} \tag{9.25}$$

$$\begin{aligned} v_i = -0.6 \quad & \frac{1}{V_*}\left\|\partial_x V_{MB} - \frac{\partial v_{MB}}{\partial x}\right\|_{\overline{\Omega}} \leq \frac{m-1.0}{2x}(\sqrt{\frac{1.6667}{2(1.6)}}U(1.6))(1.093N^{-0.86}) \\ & \qquad +U(1.6)\frac{0.3333}{2(1.6)}(0.185N^{-0.86}) \\ & \qquad +\frac{m+1}{2x}U(x)\beta(0.185N^{-0.86}) \\ & \qquad +\frac{m-1}{m+1}(0.874N^{-0.86}) \\ v_i = 2.0 \quad & \frac{1}{V_*}\left\|\partial_x V_{MB} - \frac{\partial v_{MB}}{\partial x}\right\|_{\overline{\Omega}} \leq \frac{|m-1.0|}{2x}(\sqrt{\frac{1.6667}{2(1.6)}}U(1.6))(2.14N^{-0.86}) \\ & \qquad +U(1.6)\frac{0.3333}{2(1.6)}(0.81N^{-0.86}) \\ & \qquad +\frac{m+1}{2x}U(x)\beta(0.81N^{-0.86}) \\ & \qquad +\frac{|m-1|}{m+1}(1.42N^{-0.86}) \\ v_i = 7.0 \quad & \frac{1}{V_*}\left\|\partial_x V_{MB} - \frac{\partial v_{MB}}{\partial x}\right\|_{\overline{\Omega}} \leq \frac{|m-1.0|}{2x}(\sqrt{\frac{1.6667}{2(1.6)}}U(1.6))(2.06N^{-0.86}) \\ & \qquad +U(1.6)\frac{0.3333)}{2(1.6)}(3.09N^{-0.86}) \\ & \qquad +\frac{m+1}{2x}U(x)\beta(3.09N^{-0.86}) \\ & \qquad +\frac{|m-1|}{m+1}(3.68N^{-0.86}). \end{aligned} \tag{9.26}$$

In the specific case of $N = 8192$ we have

$$
\begin{aligned}
v_i &= -0.6 & \frac{1}{V_*} \| \partial_x V_{MB} - \frac{\partial v_{MB}}{\partial x} \|_{\overline{\Omega}} &\leq 5.282 \times 10^{-5} \\
v_i &= 2.0 & \frac{1}{V_*} \| \partial_x V_{MB} - \frac{\partial v_{MB}}{\partial x} \|_{\overline{\Omega}} &\leq 1.097 \times 10^{-4} \\
v_i &= 7.0 & \frac{1}{V_*} \| \partial_x V_{MB} - \frac{\partial v_{MB}}{\partial x} \|_{\overline{\Omega}} &\leq 1.703 \times 10^{-4}.
\end{aligned}
\tag{9.27}
$$

Chapter 10

A Reynolds–uniform numerical method for the Prandtl boundary layer problem for flow past a wedge with mass transfer

10.1 Introduction

In this chapter, we make use of the Blasius similarity solution of the Prandtl problem calculated in Chapter 9 in two ways. Firstly, we use it to provide the unknown boundary conditions that are required on the boundary of Ω in the direct numerical method for Prandtl problem for flow past a wedge with mass transfer. Secondly, we use the reference solution for the unknown exact solution in the expression for the error. It is convenient to introduce the notation $\varepsilon = \frac{1}{Re}$, to emphasise the singularly

perturbed nature of the problem.

$$(P_{M\varepsilon}) \begin{cases} \text{Find } \mathbf{u_{M\varepsilon}} = (u_{M\varepsilon}, v_{M\varepsilon}) \text{ such that for all } (x,y) \in D \\ \mathbf{u}_{M\varepsilon} \text{ satisfies the differential equation} \\ \\ -\varepsilon \frac{\partial^2 \mathbf{u}_{M\varepsilon}}{\partial^2 y} + \mathbf{u}_{M\varepsilon}.\nabla u_{M\varepsilon} = U(x)\frac{dU(x)}{dx} \\ \\ \nabla.\mathbf{u}_{M\varepsilon} = 0 \\ \\ \text{with boundary conditions} \\ u_{M\varepsilon} = 0 \text{ and } v_0(x) \text{ on } \Gamma_B \\ \mathbf{u}_{M\varepsilon} = \mathbf{u}_{MB} \text{ on } \Gamma_T \bigcup \Gamma_L \end{cases}$$

where $U(x) = x^m$ is the solution of the reduced problem, $m = \frac{\beta}{2-\beta}$ and $\beta\pi$ is the angle in radians of the wedge and $v_0(x)$ is the velocity normal to the wedge at which mass is transferred through its surface (see eqn (9.4) in Section 9.2).

While the mass transfer parameter, v_i, is not a singularly perturbed parameter, it influences the width of the boundary layer in a more subversive way.

10.2 Nonlinear direct finite difference method

In this section, we begin to construct a robust numerical method to solve the Prandtl problem $(P_{M\varepsilon})$ for all admissible values of Reynolds numbers Re and $v_i \in [-0.6, 7.07]$.

We define the rectangular mesh (as in Chapter 4) on the rectangle Ω to be the tensor product of two one–dimensional meshes $\Omega_\varepsilon^{\mathbf{N}} = \Omega_\varepsilon^{N_x} \times \Omega_{M\varepsilon}^{N_y}$, where $\mathbf{N} = (N_x, N_y)$. The mesh in the x-direction is the uniform mesh

$$\Omega_u^{N_x} = \{x_i : x_i = 0.6 + iN_x^{-1}, 0 \leq i \leq N_x\}.$$

The mesh in the y-direction is the compound piecewise–uniform fitted mesh

$$\Omega_{M\varepsilon}^{N_y} = \{y_j : y_j = \sigma_2 j \frac{4}{N_y}, 0 \leq j \leq \frac{N_y}{4}; y_j = \sigma_2 + (\sigma - \sigma_2)(j - \frac{N_y}{4})\frac{4}{N_y}, \frac{N_y}{4} \leq j \leq \frac{N_y}{2};$$
$$y_j = \sigma + (1 - \sigma)(j - \frac{N_y}{2})\frac{2}{N_y}, \frac{N_y}{2} \leq j \leq N_y\}.$$

It is important to note the position of the boundary layer in order to define appropriate transition points σ and σ_2 from the coarse to the fine mesh, so that there are

two fine meshes in the boundary layer. The appropriate choices in this case are

$$\sigma = \min\{\frac{1}{2}, C\sqrt{\varepsilon}lnN_y\},$$

and

$$\sigma_2 = \min\{\frac{\sigma}{2}, C_2\sqrt{\varepsilon}lnN_y\}.$$

The factor $\sqrt{\varepsilon}$ may be motivated from asymptotic analysis [46]. The motivation for a second transition point stems from Chapter 8 and Appendix D in which we saw the benefit of a secondary transition point. The choice of C and C_2 is motivated by the mass transfer parameter v_i

$$C = \begin{cases} 2 & \text{for } v_i \in [-0.6, -0.3) \\ 1 & \text{for } v_i \in [-0.3, 2.0) \\ \frac{2}{v_i} & \text{for } v_i \in [2.0, 7.07] \end{cases}$$

$$C_2 = \begin{cases} \frac{1}{4} & \text{for } v_i \in [-0.6, -0.3) \\ \frac{1}{8} & \text{for } v_i \in [-0.3, 2.0) \\ \frac{1}{4v_i} & \text{for } v_i \in [2.0, 7.07]. \end{cases}$$

For simplicity we take $N_x = N_y = N$. Using the above piecewise uniform fitted mesh Ω_ε^N, the problem $(P_{M\varepsilon})$ is discretised by a nonlinear system of upwind finite difference equations for the approximation velocity components $\mathbf{U_{M\varepsilon}} = (U_{M\varepsilon}, V_{M\varepsilon})$.

10.3 Iterative direct finite difference method

Since the problem $(P_{M\varepsilon}^N)$ is a nonlinear system, an iterative method is required for its solution. This is obtained by replacing the system of nonlinear equations with a sequence of systems of linear equations; this is an adaptation of the method used in [26]. The systems of linearized equations are

$$(A_{M\varepsilon}^{\mathbf{N}}) \begin{cases} \text{With the boundary condition } \mathbf{U}_{M\varepsilon}^{\mathbf{M}} = \mathbf{U}_{\mathbf{MB}}^{\mathbf{8192}} \text{ on } \Gamma_L, \\ \text{for each } i, 1 \le i \le N, \text{ use the initial guess } \mathbf{U}_{M\varepsilon}^0|_{X_i} = \mathbf{U}_\varepsilon^0|_{X_{i-1}} \\ \text{and for } m = 1, \dots, M, \text{ solve the following} \\ \text{two point boundary value problem for } U_{M\varepsilon}^m(x_i, y_j) \\ \\ (-\varepsilon\delta_y^2 + \mathbf{U}_{M\varepsilon}^{m-1} \cdot \mathbf{D}^-)U_{M\varepsilon}^m(x_i, y_j) = 0, \quad 1 \le j \le N - 1 \\ \\ \text{with the boundary conditions } U_{M\varepsilon}^m = U_{MB} \text{ on } \Gamma_B \cup \Gamma_T, \\ \text{and the initial guess for } V_{M\varepsilon}^0|_{X_1} = 0. \\ \text{Also, solve the initial value problem for } V_{M\varepsilon}^m(x_i, y_j) \\ \\ (\mathbf{D}^- \cdot \mathbf{U}_{M\varepsilon}^m)(x_i, y_j) = 0, \\ \\ \text{with initial condition } V_{M\varepsilon}^m = v_0(x_i) \text{ on } \Gamma_B. \\ \text{Continue to iterate between the equations for } \mathbf{U}_{M\varepsilon}^m \text{ until } m = M, \\ \text{where } M \text{ is such that} \\ \\ \max\left(|U_{M\varepsilon}^M - U_{M\varepsilon}^{M-1}|_{\overline{\Omega}_\varepsilon^N}, \tfrac{1}{V^*}|V_{M\varepsilon}^M - V_{M\varepsilon}^{M-1}|_{\overline{\Omega}_\varepsilon^N}\right) \le tol. \end{cases}$$

For notational simplicity, we suppress explicit mention of the iteration superscript M henceforth, and we write simply $\mathbf{U}_{M\varepsilon}$ for the solution generated by $(A_{M\varepsilon}^{\mathbf{N}})$. We take $tol = 10^{-6}$ in the computations. V^* is defined in Appendix C.

10.4 Error analysis based on the finest mesh solution

In this section we estimate, computationally, the maximum pointwise error in the numerical solution and its discrete derivatives generated by the algorithm $(A_{M\varepsilon}^{\mathbf{N}})$ of the previous section. Since the exact solution in the expression for the computed maximum pointwise error is unknown, we replace it by the solution $U_{M\varepsilon}^{512}$ generated by $(A_{M\varepsilon}^{\mathbf{N}})$ on the finest mesh Ω_ε^{512}. Thus, for $U_{M\varepsilon}$ and $\frac{1}{V^*}V_{M\varepsilon}$, we define the computed maximum pointwise errors

$$E_\varepsilon^N(U_{M\varepsilon}) = ||U_{M\varepsilon} - \overline{U_{M\varepsilon}^{512}}||_{\overline{\Omega}_\varepsilon^N} \qquad E_\varepsilon^N(\tfrac{1}{V^*}V_{M\varepsilon}) = \tfrac{1}{V^*}||V_{M\varepsilon} - \overline{V_{M\varepsilon}^{512}}||_{\overline{\Omega}_\varepsilon^N \setminus \Gamma_L}$$

and

$$E^N(U_{M\varepsilon}) = \max_\varepsilon E_\varepsilon^N(U_{M\varepsilon}) \qquad E^N(\tfrac{1}{V^*}V_{M\varepsilon}) = \max_\varepsilon E_\varepsilon^N(\tfrac{1}{V^*}V_{M\varepsilon}).$$

As in the previous chapter, for the sake of brevity we show the errors for three typical values of mass transfer parameter $v_i = -0.6$, 2.0 and 7.0 for $\beta = 0.8$. Note that the results for the flat plate ($\beta = 0.0$) for $v_i \in [-0.3, 0.3]$ are discussed in [6].

The values of the computed maximum pointwise errors generated by $(A_{M\varepsilon}^{\mathbf{N}})$ applied to problem $(P_{M\varepsilon})$ for $U_{M\varepsilon}$ and $\frac{1}{V^*}V_{M\varepsilon}$ are given in Tables 10.1 and 10.2 respectively for various values of ε, N, v_i and $\beta = 0.8$.

In Table 10.1 we observe that the errors stabilise to a fixed value after 2^{-10} for $\beta = 0.8$, all N and all v_i considered. We see that the computed maximum errors decrease as the number of mesh points, N, increases. For each N the largest maximum errors, E^N, occur when $2^{-8} \le \varepsilon \le 2^{-10}$. This suggests that the method is independent of ε for $U_{M\varepsilon}$ for $\beta = 0.8$ and $v_i = -0.6$, 2.0 and 7.0. The maximum errors strongly suggest that the method is ε–uniform for $U_{M\varepsilon}$ for $\beta = 0.8$ and all v_i considered.

$\varepsilon \backslash N$	$v_i = -0.6$				$\varepsilon \backslash N$	$v_i = 2.0$			
	32	64	128	256		32	64	128	256
2^{-0}	1.34e-04	6.40e-05	2.77e-05	9.28e-06	2^{-0}	6.75e-03	3.20e-03	1.38e-03	4.63e-04
2^{-2}	2.92e-04	1.47e-04	6.52e-05	2.20e-05	2^{-2}	2.06e-02	9.61e-03	4.17e-03	1.40e-03
2^{-4}	1.34e-03	6.11e-04	2.63e-04	8.81e-05	2^{-4}	4.62e-02	2.11e-02	8.58e-03	2.69e-03
2^{-6}	4.11e-03	1.88e-03	7.89e-04	2.56e-04	2^{-6}	6.72e-02	3.93e-02	1.71e-02	5.48e-03
2^{-8}	4.85e-03	2.62e-03	1.26e-03	4.60e-04	2^{-8}	6.52e-02	3.75e-02	1.82e-02	6.46e-03
2^{-10}	4.76e-03	2.52e-03	1.17e-03	4.23e-04	2^{-10}	6.52e-02	3.75e-02	1.82e-02	6.46e-03
2^{-12}	4.73e-03	2.52e-03	1.17e-03	4.23e-04	2^{-12}	6.52e-02	3.75e-02	1.82e-02	6.46e-03
2^{-14}	4.71e-03	2.52e-03	1.17e-03	4.23e-04	2^{-14}	6.52e-02	3.75e-02	1.82e-02	6.46e-03
2^{-16}	4.70e-03	2.52e-03	1.17e-03	4.23e-04	2^{-16}	6.52e-02	3.75e-02	1.82e-02	6.46e-03
2^{-18}	4.69e-03	2.52e-03	1.17e-03	4.23e-04	2^{-18}	6.52e-02	3.75e-02	1.82e-02	6.46e-03
2^{-20}	4.69e-03	2.52e-03	1.17e-03	4.23e-04	2^{-20}	6.52e-02	3.75e-02	1.82e-02	6.46e-03
2^{-22}	4.68e-03	2.52e-03	1.17e-03	4.23e-04	2^{-22}	6.52e-02	3.75e-02	1.82e-02	6.46e-03
2^{-24}	4.68e-03	2.52e-03	1.17e-03	4.23e-04	2^{-24}	6.52e-02	3.75e-02	1.82e-02	6.46e-03
E^N	4.85e-03	2.62e-03	1.26e-03	4.60e-04	E^N	6.72e-02	3.93e-02	1.82e-02	6.46e-03

$\varepsilon \backslash N$	$v_i = 7.0$			
	32	64	128	256
2^{-0}	4.64e-02	2.14e-02	8.77e-03	2.79e-03
2^{-2}	9.03e-02	4.65e-02	1.98e-02	6.43e-03
2^{-4}	8.82e-02	4.95e-02	2.41e-02	8.76e-03
2^{-6}	8.99e-02	5.00e-02	2.43e-02	8.80e-03
2^{-8}	9.05e-02	5.03e-02	2.43e-02	8.82e-03
2^{-10}	8.97e-02	5.03e-02	2.44e-02	8.83e-03
2^{-12}	8.77e-02	5.01e-02	2.44e-02	8.83e-03
2^{-14}	8.54e-02	4.96e-02	2.43e-02	8.83e-03
2^{-16}	8.36e-02	4.92e-02	2.42e-02	8.81e-03
2^{-18}	8.25e-02	4.89e-02	2.41e-02	8.80e-03
2^{-20}	8.19e-02	4.86e-02	2.41e-02	8.79e-03
2^{-22}	8.16e-02	4.85e-02	2.40e-02	8.78e-03
2^{-24}	8.14e-02	4.85e-02	2.40e-02	8.77e-03
E^N	9.05e-02	5.03e-02	2.44e-02	8.83e-03

Table 10.1: Computed maximum errors $E_\varepsilon^N(U_{M\varepsilon})$ generated by $(A_{M\varepsilon}^{\mathbf{N}})$ applied to problem $(P_{M\varepsilon})$ for various values of ε, N, v_i and $\beta = 0.8$.

In Table 10.2 we see that the computed maximum errors decrease as the number of mesh points, N, increase for all v_i. The largest errors E^N for $\frac{1}{V^*}V_\varepsilon$ for all N and

β occur when $\varepsilon \geq 2^{-4}$. We observe that the computed pointwise maximum errors for $\frac{1}{V^*}V_\varepsilon$ decrease and tend to a fixed value as ε decreases, for $\beta = 0.8$ and all v_i considered. Table 10.2 indicates that maximum errors are independent of ε for all v_i and β. This suggests that the method is ε–uniform for $\frac{1}{V^*}V_\varepsilon$ for all v_i and β considered.

$\varepsilon \backslash N$	$v_i = -0.6$				$\varepsilon \backslash N$	$v_i = 2.0$			
	32	64	128	256		32	64	128	256
2^{-0}	7.70e-03	3.66e-03	1.61e-03	5.43e-04	2^{-0}	5.01e-02	3.96e-02	2.59e-02	1.27e-02
2^{-2}	1.24e-02	5.79e-03	2.48e-03	8.28e-04	2^{-2}	6.53e-02	4.89e-02	3.09e-02	1.51e-02
2^{-4}	1.37e-02	6.62e-03	2.83e-03	9.42e-04	2^{-4}	5.13e-02	3.47e-02	2.11e-02	1.05e-02
2^{-6}	1.27e-02	5.48e-03	2.27e-03	7.49e-04	2^{-6}	2.96e-02	2.28e-02	1.35e-02	6.20e-03
2^{-8}	8.38e-03	4.21e-03	1.90e-03	6.53e-04	2^{-8}	1.44e-02	1.11e-02	6.87e-03	3.24e-03
2^{-10}	4.96e-03	2.44e-03	1.08e-03	3.70e-04	2^{-10}	7.22e-03	5.53e-03	3.43e-03	1.62e-03
2^{-12}	3.37e-03	1.62e-03	7.15e-04	2.42e-04	2^{-12}	3.61e-03	2.77e-03	1.72e-03	8.11e-04
2^{-14}	2.59e-03	1.22e-03	5.32e-04	1.79e-04	2^{-14}	1.80e-03	1.38e-03	8.59e-04	4.10e-04
2^{-16}	2.20e-03	1.03e-03	4.42e-04	1.48e-04	2^{-16}	1.80e-03	8.18e-04	4.29e-04	2.05e-04
2^{-18}	2.00e-03	9.26e-04	3.97e-04	1.32e-04	2^{-18}	1.80e-03	8.22e-04	3.48e-04	1.15e-04
2^{-20}	1.90e-03	8.77e-04	3.74e-04	1.25e-04	2^{-20}	1.80e-03	8.25e-04	3.50e-04	1.16e-04
2^{-22}	1.86e-03	8.52e-04	3.63e-04	1.21e-04	2^{-22}	1.80e-03	8.26e-04	3.51e-04	1.16e-04
2^{-24}	1.83e-03	8.40e-04	3.57e-04	1.19e-04	2^{-24}	1.81e-03	8.27e-04	3.51e-04	1.17e-04
E^N	1.37e-02	6.62e-03	2.83e-03	9.42e-04	E^N	6.53e-02	4.89e-02	3.09e-02	1.51e-02

$\varepsilon \backslash N$	$v_i = 7.0$			
	32	64	128	256
2^{-0}	2.27e-01	1.70e-01	1.08e-01	5.23e-02
2^{-2}	2.02e-01	1.62e-01	9.84e-02	4.28e-02
2^{-4}	9.90e-02	8.48e-02	5.69e-02	2.63e-02
2^{-6}	4.93e-02	4.24e-02	2.84e-02	1.32e-02
2^{-8}	2.44e-02	2.12e-02	1.42e-02	6.59e-03
2^{-10}	1.21e-02	1.06e-02	7.11e-03	3.30e-03
2^{-12}	5.99e-03	5.28e-03	3.56e-03	1.65e-03
2^{-14}	2.98e-03	2.64e-03	1.78e-03	8.25e-04
2^{-16}	1.83e-03	1.32e-03	8.89e-04	4.12e-04
2^{-18}	1.82e-03	8.31e-04	4.44e-04	2.06e-04
2^{-20}	1.82e-03	8.30e-04	3.52e-04	1.17e-04
2^{-22}	1.81e-03	8.29e-04	3.52e-04	1.17e-04
2^{-24}	1.81e-03	8.28e-04	3.52e-04	1.17e-04
E^N	2.27e-01	1.70e-01	1.08e-01	5.23e-02

Table 10.2: Computed maximum errors $E_\varepsilon^N(\frac{1}{V^*}V_{M\varepsilon})$ generated by $(A_{M\varepsilon}^N)$ applied to problem $(P_{M\varepsilon})$ for various values of ε, N, v_i and $\beta = 0.8$.

Graphs of the velocity component $U_{M\varepsilon}$ of the solution $\mathbf{U}_{M\varepsilon}$ generated by the direct method $(A_{M\varepsilon}^N)$ with $N = 32$, $\beta = 0.8$ and $v_i = -0.6$, 2.0 and 7.0 for $\varepsilon = 1.0$ and 2^{-12} are shown in Figures 10-1 and 10-2, respectively.

In Figure 10-1 we see that, for $\varepsilon = 1.0$, the graphs of $U_{M\varepsilon}$ are smooth for various values of v_i. The effect of the mass transfer parameter on $U_{M\varepsilon}$ is apparent in Figure 10-1.
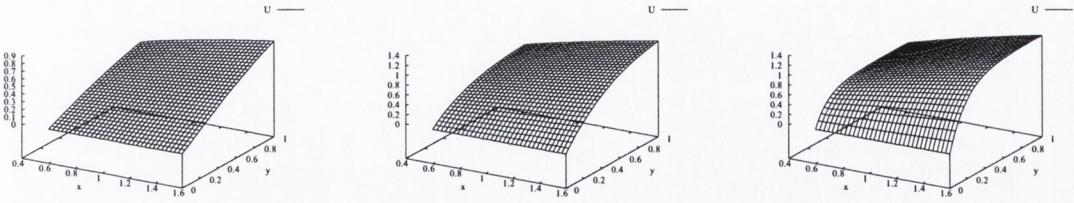
Figure 10-1: Graphs of $U_{M\varepsilon}$ for $\varepsilon = 1.0$, $N{=}32$, $\beta = 0.8$ and $v_i = -0.6, 2.0, 7.0$.

The graphs in Figure 10-2 show a boundary layer along the surface of the wedge for $U_{M\varepsilon}$ for various values of v_i for $\varepsilon = 2^{-12}$ and $\beta = 0.8$.
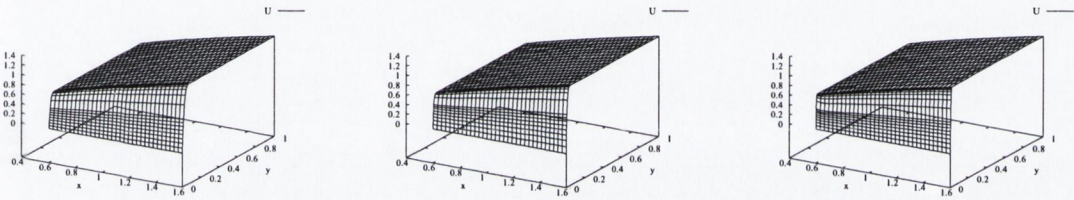
Figure 10-2: Graphs of $U_{M\varepsilon}$ for $\varepsilon = 2^{-12}$, $N{=}32$, $\beta = 0.8$ and $v_i = -0.6, 2.0, 7.0$.

Graphs of the scaled component $\frac{1}{V^*}V_{M\varepsilon}$ of the solution $\mathbf{U_{M\varepsilon}}$ generated by the direct method $(A^{\mathbf{N}}_{M\varepsilon})$ with $N = 32$, $v_i = -0.6$, 2.0 and 7.0 and $\beta = 0.8$ are shown in Figures 10-3 and 10-4 for $\varepsilon = 1.0$ and 2^{-12}, respectively.
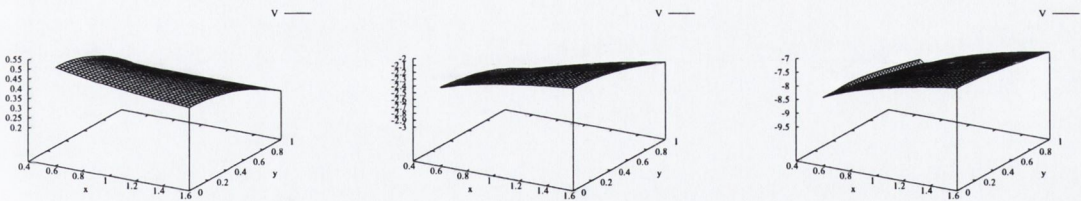
Figure 10-3: Graphs of $\frac{1}{V^*}V_{M\varepsilon}$ for $\varepsilon = 1.0$, $N{=}32$, $\beta = 0.8$ and $v_i = -0.6, 2.0, 7.0$.

The graphs in Figures 10-3 and 10-4 show that the scaled velocity component $\frac{1}{V^*}V_{M\varepsilon}$ has no non–physical oscillations for all v_i and $\varepsilon = 1.0$ and 2^{-12}. The graphs show that $\frac{1}{V^*}V_{M\varepsilon}$ is negative for $v_i = 2.0$ and 7.0 and $\frac{1}{V^*}V_{M\varepsilon}$ is positive for $v_i = -0.6$ and $\varepsilon = 1.0$. $\frac{1}{V^*}V_{M\varepsilon}$ has no visible boundary layer for all v_i and $\varepsilon = 1.0$ and 2^{-12}.
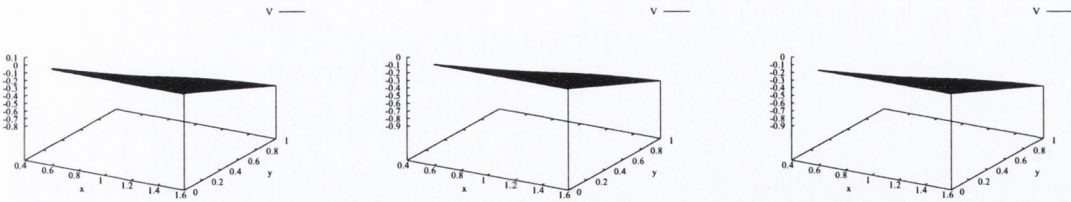
Figure 10-4: Graphs of $\frac{1}{V_*}V_{M\varepsilon}$ for $\varepsilon = 2^{-12}$, $N=32$, $\beta = 0.8$ and $v_i = -0.6, 2.0, 7.0$.

The computed orders of convergence p_ε^N and p^N and the constant of convergence $C_{p^*}^N$ for $U_{M\varepsilon}$ and $\frac{1}{V_*}V_{M\varepsilon}$ are given in Tables 10.3 and 10.4, respectively, for various values of ε, N, v_i and $\beta = 0.8$.

	$v_i = -0.6$				$v_i = 2.0$				$v_i = 7.0$		
$\varepsilon\backslash N$	32	64	128	$\varepsilon\backslash N$	32	64	128	$\varepsilon\backslash N$	32	64	128
2^{-0}	0.96	0.98	0.99	2^{-0}	0.96	0.98	0.99	2^{-0}	1.00	1.07	1.09
2^{-2}	0.82	0.92	0.96	2^{-2}	1.01	0.97	0.99	2^{-2}	0.60	0.98	1.05
2^{-4}	1.07	0.99	0.99	2^{-4}	0.96	1.07	1.13	2^{-4}	0.47	0.77	0.75
2^{-6}	1.01	0.97	1.05	2^{-6}	0.21	0.91	1.03	2^{-6}	0.50	0.78	0.76
2^{-8}	1.18	1.10	0.65	2^{-8}	0.34	0.77	0.80	2^{-8}	0.50	0.79	0.76
2^{-10}	1.18	1.15	0.72	2^{-10}	0.34	0.77	0.80	2^{-10}	0.47	0.79	0.76
2^{-12}	1.18	1.15	0.72	2^{-12}	0.34	0.77	0.80	2^{-12}	0.41	0.77	0.76
2^{-14}	1.19	1.15	0.72	2^{-14}	0.34	0.77	0.80	2^{-14}	0.35	0.76	0.75
2^{-16}	1.19	1.15	0.72	2^{-16}	0.34	0.77	0.80	2^{-16}	0.31	0.74	0.75
2^{-18}	1.19	1.15	0.72	2^{-18}	0.34	0.77	0.80	2^{-18}	0.29	0.74	0.74
2^{-20}	1.19	1.15	0.72	2^{-20}	0.34	0.77	0.80	2^{-20}	0.28	0.73	0.74
2^{-22}	1.19	1.15	0.72	2^{-22}	0.34	0.77	0.80	2^{-22}	0.27	0.73	0.74
2^{-24}	1.19	1.15	0.72	2^{-24}	0.34	0.77	0.80	2^{-24}	0.27	0.73	0.74
p_{comp}^N	1.19	1.10	0.65	p_{comp}^N	0.21	0.91	0.80	p_{comp}^N	0.60	0.81	0.76
$C_{0.65}$	0.09	0.06	0.05	$C_{0.80}$	0.92	1.38	1.29	$C_{0.76}$	1.36	1.52	1.46

Table 10.3: Computed orders of convergence $p_\varepsilon^N(U_{M\varepsilon})$, $p^N(U_{M\varepsilon})$ and error constant $C_{p^*}^N$ generated by $(A_{M\varepsilon}^{\mathbf{N}})$ applied to problem $(P_{M\varepsilon})$ for various values of ε, N, v_i and $\beta = 0.8$.

	$v_i = -0.6$				$v_i = 2.0$				$v_i = 7.0$		
$\varepsilon\backslash N$	32	64	128	$\varepsilon\backslash N$	32	64	128	$\varepsilon\backslash N$	32	64	128
2^{-0}	1.00	0.94	0.98	2^{-0}	0.39	0.51	0.60	2^{-0}	0.45	0.56	0.62
2^{-2}	1.00	1.00	0.99	2^{-2}	0.37	0.53	0.61	2^{-2}	0.27	0.57	0.72
2^{-4}	0.90	1.00	1.00	2^{-4}	0.42	0.54	0.54	2^{-4}	0.21	0.39	0.55
2^{-6}	1.17	1.07	1.03	2^{-6}	-0.03	0.48	0.62	2^{-6}	0.20	0.39	0.55
2^{-8}	0.84	0.90	0.94	2^{-8}	0.08	0.39	0.54	2^{-8}	0.19	0.39	0.55
2^{-10}	0.90	0.92	0.95	2^{-10}	0.08	0.39	0.54	2^{-10}	0.17	0.38	0.55
2^{-12}	0.94	0.94	0.96	2^{-12}	0.08	0.39	0.54	2^{-12}	0.16	0.38	0.55
2^{-14}	0.98	0.97	0.98	2^{-14}	0.36	0.38	0.53	2^{-14}	0.15	0.38	0.55
2^{-16}	1.01	0.99	0.99	2^{-16}	1.05	0.68	0.53	2^{-16}	0.36	0.38	0.55
2^{-18}	1.02	1.00	1.00	2^{-18}	1.05	1.03	1.02	2^{-18}	1.05	0.67	0.55
2^{-20}	1.03	1.01	1.00	2^{-20}	1.04	1.02	1.01	2^{-20}	1.05	1.02	1.01
2^{-22}	1.04	1.01	1.01	2^{-22}	1.04	1.02	1.01	2^{-22}	1.04	1.02	1.01
2^{-24}	1.04	1.02	1.01	2^{-24}	1.04	1.02	1.01	2^{-24}	1.04	1.02	1.01
p_{comp}^N	0.93	1.00	1.00	p_{comp}^N	0.37	0.53	0.61	p_{comp}^N	0.45	0.56	0.62
$C_{1.00}$	0.47	0.49	0.49	$C_{0.53}$	0.88	0.99	0.99	$C_{0.56}$	3.54	3.84	3.84

Table 10.4: Computed orders of convergence $p_\varepsilon^N(\frac{1}{V^*}V_{M\varepsilon})$, $p^N(\frac{1}{V^*}V_{M\varepsilon})$ and error constants $C_{p^*}^N$ generated by $(A_{M\varepsilon}^{\mathbf{N}})$ applied to problem $(P_{M\varepsilon})$ for various values of ε, N, v_i and $\beta = 0.8$.

The results in Tables 10.1-10.4 suggest that $(A_{M\varepsilon}^N)$ is an ε–uniform numerical method of order at least 0.65 for $U_{M\varepsilon}$ and 0.53 for $\frac{1}{V^*}V_{M\varepsilon}$ for $N \geq 64$, $v_i = -0.6, 2.0$ and 7.0 and $\beta = 0.8$.

From the data in Tables 10.1-10.4 we obtain the computed error bounds for $U_{M\varepsilon}$ and $\frac{1}{V^*}V_{M\varepsilon}$ for $N \geq 64$ and $\beta = 0.8$

$$
\begin{aligned}
v_i = -0.6 \quad &||U_{M\varepsilon} - u_{M\varepsilon}||_{\Omega_\varepsilon^N} \leq 0.09N^{-0.65} \\
v_i = 2.0 \quad &||U_{M\varepsilon} - u_{M\varepsilon}||_{\Omega_\varepsilon^N} \leq 1.38N^{-0.80} \\
v_i = 7.0 \quad &||U_{M\varepsilon} - u_{M\varepsilon}||_{\Omega_\varepsilon^N} \leq 1.52N^{-0.76}
\end{aligned}
\tag{10.1}
$$

$$
\begin{aligned}
v_i = -0.6 \quad &\tfrac{1}{V^*}||V_{M\varepsilon} - v_{M\varepsilon}||_{\Omega_\varepsilon^N\backslash\Gamma_L} \leq 0.49N^{-1.00} \\
v_i = 2.0 \quad &\tfrac{1}{V^*}||V_{M\varepsilon} - v_{M\varepsilon}||_{\Omega_\varepsilon^N\backslash\Gamma_L} \leq 0.99N^{-0.53} \\
v_i = 7.0 \quad &\tfrac{1}{V^*}||V_{M\varepsilon} - v_{M\varepsilon}||_{\Omega_\varepsilon^N\backslash\Gamma_L} \leq 3.84N^{-0.56}.
\end{aligned}
\tag{10.2}
$$

Graphs of the computed scaled discrete derivatives $\sqrt{\varepsilon}D_y^- U_{M\varepsilon}$, $D_y^- V_{M\varepsilon}$ and $D_x^- V_{M\varepsilon}$ generated by $(A_{M\varepsilon}^{\mathbf{N}})$ are given in Figures 10-5, 10-6 and 10-7, respectively, for $N = 32$, $\varepsilon = 2^{-12}$, $v_i = -0.6$, 2.0 and 7.0 and $\beta=0.8$. Graphs of $\sqrt{\varepsilon}D_y^- U_{M\varepsilon}$ and $D_y^- V_{M\varepsilon}$ in Figures 10-5 and 10-6 show a region of rapid change along the wedge for various v_i.
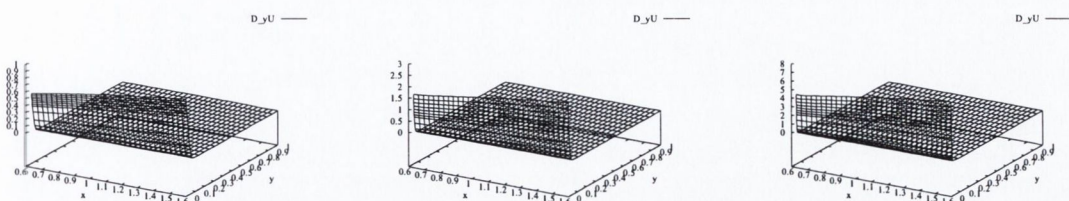
Figure 10-5: Graphs of $\sqrt{\varepsilon}D_y^- U_{M\varepsilon}$ for $\varepsilon = 2^{-12}$, $N=32$, $v_i = -0.6$, 2.0 and 7.0 and $\beta = 0.8$.

In Figure 10-6, for graphs of $D_y^- V_{M\varepsilon}$ we see for $v_i = 2.0$ and 7.0 that there is a significant amount of activity at the points closest to the leading edge.
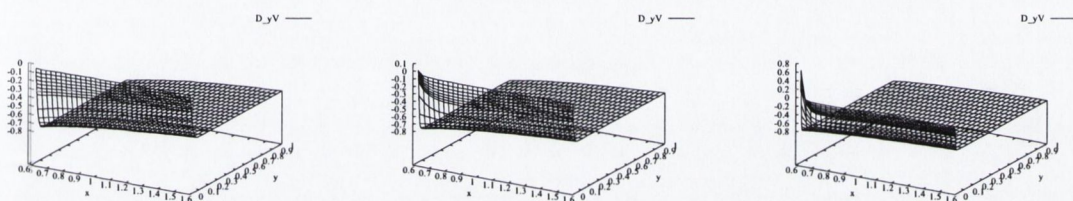
Figure 10-6: Graphs of $D_y^- V_{M\varepsilon}$ for $\varepsilon = 2^{-12}$, $N=32$, $v_i = -0.6$, 2.0 and 7.0 and $\beta = 0.8$.

Looking at the graphs of $\frac{1}{V^*}D_x^- V_{M\varepsilon}$ in Figure 10-7, we note there is a non-physical jump along the left hand boundary.
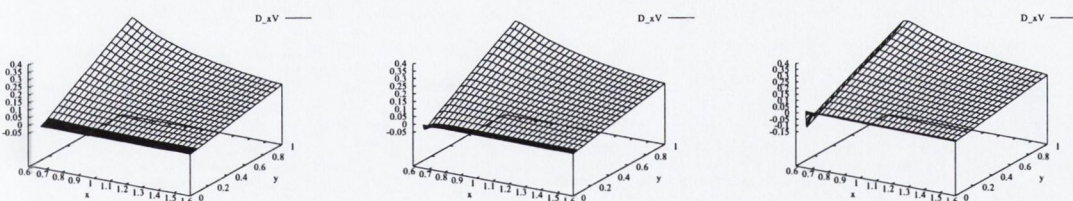
Figure 10-7: Graphs of $\frac{1}{V^*}D_x^- V_{M\varepsilon}$ for $\varepsilon = 2^{-12}$, $N=32$, $v_i = -0.6$, 2.0 and 7.0 and $\beta = 0.8$.

The computed maximum pointwise errors of the computed scaled discrete derivatives $\sqrt{\varepsilon}D_y U_{M\varepsilon}$, $D_y^- V_{M\varepsilon}$ and $\frac{1}{V^*}D_x^- V_{M\varepsilon}$ are given in the Tables 10.5, 10.6 and 10.7, respectively.

$\varepsilon \backslash N$	$v_i = -0.6$				$\varepsilon \backslash N$	$v_i = 2.0$			
	32	64	128	256		32	64	128	256
2^{-0}	5.78e-03	2.70e-03	1.16e-03	3.89e-04	2^{-0}	5.48e-02	2.65e-02	1.19e-02	5.27e-03
2^{-2}	1.13e-02	5.26e-03	2.25e-03	7.51e-04	2^{-2}	8.82e-02	5.13e-02	2.27e-02	7.87e-03
2^{-4}	2.53e-02	1.06e-02	4.56e-03	1.52e-03	2^{-4}	1.72e-01	7.82e-02	3.24e-02	1.14e-02
2^{-6}	6.84e-02	3.08e-02	1.31e-02	4.84e-03	2^{-6}	2.61e-01	1.59e-01	7.52e-02	3.21e-02
2^{-8}	9.42e-02	5.46e-02	3.02e-02	1.50e-02	2^{-8}	2.62e-01	1.61e-01	8.82e-02	4.50e-02
2^{-10}	9.43e-02	5.46e-02	3.02e-02	1.58e-02	2^{-10}	2.62e-01	1.61e-01	8.82e-02	4.50e-02
2^{-12}	9.43e-02	5.46e-02	3.02e-02	1.58e-02	2^{-12}	2.62e-01	1.61e-01	8.82e-02	4.50e-02
2^{-14}	9.43e-02	5.46e-02	3.02e-02	1.58e-02	2^{-14}	2.62e-01	1.61e-01	8.82e-02	4.50e-02
2^{-16}	9.43e-02	5.46e-02	3.02e-02	1.58e-02	2^{-16}	2.62e-01	1.61e-01	8.82e-02	4.50e-02
2^{-18}	9.43e-02	5.46e-02	3.02e-02	1.58e-02	2^{-18}	2.62e-01	1.61e-01	8.82e-02	4.50e-02
2^{-20}	9.43e-02	5.46e-02	3.02e-02	1.58e-02	2^{-20}	2.62e-01	1.61e-01	8.82e-02	4.50e-02
2^{-22}	9.43e-02	5.46e-02	3.02e-02	1.58e-02	2^{-22}	2.62e-01	1.61e-01	8.82e-02	4.50e-02
2^{-24}	9.43e-02	5.46e-02	3.02e-02	1.58e-02	2^{-24}	2.62e-01	1.61e-01	8.82e-02	4.50e-02
E^N	9.43e-02	5.46e-02	3.02e-02	1.58e-02	E^N	2.62e-01	1.61e-01	8.82e-02	4.50e-02

$\varepsilon \backslash N$	$v_i = 7.0$			
	32	64	128	256
2^{-0}	3.39e-01	1.55e-01	6.44e-02	3.12e-02
2^{-2}	6.19e-01	3.38e-01	1.59e-01	7.05e-02
2^{-4}	6.19e-01	3.88e-01	2.21e-01	1.20e-01
2^{-6}	6.14e-01	3.87e-01	2.21e-01	1.20e-01
2^{-8}	6.12e-01	3.86e-01	2.20e-01	1.20e-01
2^{-10}	6.15e-01	3.86e-01	2.20e-01	1.20e-01
2^{-12}	6.21e-01	3.86e-01	2.20e-01	1.20e-01
2^{-14}	6.28e-01	3.88e-01	2.20e-01	1.20e-01
2^{-16}	6.33e-01	3.89e-01	2.21e-01	1.20e-01
2^{-18}	6.36e-01	3.90e-01	2.21e-01	1.20e-01
2^{-20}	6.38e-01	3.91e-01	2.21e-01	1.20e-01
2^{-22}	6.39e-01	3.91e-01	2.21e-01	1.20e-01
2^{-24}	6.40e-01	3.91e-01	2.21e-01	1.20e-01
E^N	6.40e-01	3.91e-01	2.21e-01	1.20e-01

Table 10.5: Computed maximum errors $E_\varepsilon^N(\sqrt{\varepsilon}D_y^- U_{M\varepsilon})$ generated by $(A_{M\varepsilon}^{\mathbf{N}})$ applied to problem $(P_{M\varepsilon})$ for various values of ε, N, v_i and $\beta = 0.8$.

| | $v_i = -0.6$ | | | | | $v_i = 2.0$ | | | |
$\varepsilon \backslash N$	32	64	128	256	$\varepsilon \backslash N$	32	64	128	256
2^{-0}	7.12e-03	3.55e-03	1.85e-03	1.14e-03	2^{-0}	1.02e-01	7.64e-02	4.99e-02	2.56e-02
2^{-2}	1.37e-02	6.51e-03	3.60e-03	2.20e-03	2^{-2}	1.96e-01	1.57e-01	1.04e-01	5.44e-02
2^{-4}	2.30e-02	1.27e-02	7.06e-03	4.22e-03	2^{-4}	2.71e-01	1.78e-01	1.23e-01	7.11e-02
2^{-6}	6.01e-02	2.69e-02	1.10e-02	5.43e-03	2^{-6}	3.08e-01	2.32e-01	1.26e-01	7.12e-02
2^{-8}	7.94e-02	4.62e-02	2.50e-02	1.20e-02	2^{-8}	3.04e-01	2.26e-01	1.33e-01	7.13e-02
2^{-10}	7.94e-02	4.62e-02	2.50e-02	1.26e-02	2^{-10}	3.04e-01	2.26e-01	1.33e-01	7.13e-02
2^{-12}	7.94e-02	4.62e-02	2.50e-02	1.26e-02	2^{-12}	3.04e-01	2.26e-01	1.33e-01	7.13e-02
2^{-14}	7.94e-02	4.62e-02	2.50e-02	1.26e-02	2^{-14}	3.04e-01	2.26e-01	1.33e-01	7.18e-02
2^{-16}	7.94e-02	4.62e-02	2.50e-02	1.26e-02	2^{-16}	3.04e-01	2.26e-01	1.33e-01	7.18e-02
2^{-18}	7.94e-02	4.62e-02	2.50e-02	1.26e-02	2^{-18}	3.04e-01	2.26e-01	1.33e-01	7.18e-02
2^{-20}	7.94e-02	4.62e-02	2.50e-02	1.26e-02	2^{-20}	3.04e-01	2.26e-01	1.33e-01	7.18e-02
2^{-22}	7.94e-02	4.62e-02	2.50e-02	1.26e-02	2^{-22}	3.04e-01	2.26e-01	1.33e-01	7.18e-02
2^{-24}	7.94e-02	4.62e-02	2.50e-02	1.26e-02	2^{-24}	3.04e-01	2.26e-01	1.33e-01	7.18e-02
E^N	7.94e-02	4.62e-02	2.50e-02	1.26e-02	E^N	3.08e-01	2.32e-01	1.33e-01	7.18e-02

| | $v_i = 7.0$ | | | |
$\varepsilon \backslash N$	32	64	128	256
2^{-0}	6.95e-01	5.20e-01	3.35e-01	1.81e-01
2^{-2}	1.17e+00	9.69e-01	5.92e-01	2.50e-01
2^{-4}	1.15e+00	1.03e+00	7.03e-01	3.27e-01
2^{-6}	1.15e+00	1.03e+00	7.04e-01	3.28e-01
2^{-8}	1.15e+00	1.03e+00	7.04e-01	3.28e-01
2^{-10}	1.14e+00	1.03e+00	7.04e-01	3.28e-01
2^{-12}	1.14e+00	1.03e+00	7.04e-01	3.29e-01
2^{-14}	1.14e+00	1.03e+00	7.04e-01	3.29e-01
2^{-16}	1.14e+00	1.03e+00	7.04e-01	3.29e-01
2^{-18}	1.14e+00	1.03e+00	7.04e-01	3.29e-01
2^{-20}	1.14e+00	1.03e+00	7.04e-01	3.29e-01
2^{-22}	1.14e+00	1.03e+00	7.04e-01	3.29e-01
2^{-24}	1.14e+00	1.03e+00	7.04e-01	3.29e-01
E^N	1.17e+00	1.03e+00	7.04e-01	3.29e-01

Table 10.6: Computed maximum errors $E_\varepsilon^N(D_y^- V_{M\varepsilon})$ generated by $(A_{M\varepsilon}^{\mathbf{N}})$ applied to problem $(P_{M\varepsilon})$ for various values of ε, N, v_i and $\beta = 0.8$.

The computed maximum errors in Tables 10.5 and 10.6 for $\sqrt{\varepsilon} D_y^- V_{M\varepsilon}$ and $D_y^- V_{M\varepsilon}$, respectively, stabilise to a fixed value after $\varepsilon = 2^{-10}$ for all v_i considered. We see that the computed maximum errors decrease as the number of mesh points, N, increases. The largest computed maximum error occurs between $\varepsilon = 2^{-2}$ and $\varepsilon = 2^{-8}$ for all N, $\sqrt{\varepsilon} D_y^- U_{M\varepsilon}$ and $D_y^- V_{M\varepsilon}$ for all v_i and $\beta = 0.8$. Tables 10.5 and 10.6 suggest that the method is ε–uniform for $\sqrt{\varepsilon} D_y^- U_{M\varepsilon}$ and $D_y^- V_{M\varepsilon}$ for $\beta = 0.8$ and all v_i considered.

	$v_i = -0.6$					$v_i = 2.0$			
$\varepsilon \backslash N$	32	64	128	256	$\varepsilon \backslash N$	32	64	128	256
2^{-0}	6.74e-02	1.04e-01	1.38e-01	1.50e-01	2^{-0}	1.32e+00	1.63e+00	1.80e+00	1.66e+00
2^{-2}	7.85e-02	1.33e-01	1.88e-01	2.28e-01	2^{-2}	1.22e+00	1.72e+00	2.03e+00	2.01e+00
2^{-4}	7.36e-02	1.46e-01	2.03e-01	2.40e-01	2^{-4}	6.72e-01	8.64e-01	1.17e+00	1.35e+00
2^{-6}	2.88e-02	7.28e-02	1.20e-01	1.60e-01	2^{-6}	3.22e-01	4.10e-01	5.48e-01	6.59e-01
2^{-8}	1.10e-02	3.59e-02	6.01e-02	7.74e-02	2^{-8}	1.59e-01	2.05e-01	2.72e-01	3.27e-01
2^{-10}	7.01e-03	1.79e-02	3.00e-02	3.87e-02	2^{-10}	7.95e-02	1.03e-01	1.36e-01	1.63e-01
2^{-12}	5.75e-03	8.93e-03	1.50e-02	1.94e-02	2^{-12}	3.98e-02	5.14e-02	6.79e-02	8.17e-02
2^{-14}	5.23e-03	4.47e-03	7.47e-03	9.71e-03	2^{-14}	1.99e-02	2.57e-02	3.39e-02	4.22e-02
2^{-16}	5.02e-03	2.35e-03	3.74e-03	4.88e-03	2^{-16}	9.94e-03	1.28e-02	1.70e-02	2.11e-02
2^{-18}	4.93e-03	2.35e-03	1.87e-03	2.47e-03	2^{-18}	4.97e-03	6.42e-03	8.48e-03	1.06e-02
2^{-20}	4.89e-03	2.40e-03	1.11e-03	1.26e-03	2^{-20}	4.55e-03	3.21e-03	4.24e-03	5.32e-03
2^{-22}	4.87e-03	2.43e-03	1.14e-03	6.56e-04	2^{-22}	4.69e-03	2.07e-03	2.12e-03	2.68e-03
2^{-24}	4.86e-03	2.46e-03	1.16e-03	4.06e-04	2^{-24}	4.76e-03	2.13e-03	1.06e-03	1.37e-03
E^N	7.85e-02	1.46e-01	2.03e-01	2.40e-01	E^N	1.32e+00	1.72e+00	2.03e+00	2.01e+00

	$v_i = 7.0$			
$\varepsilon \backslash N$	32	64	128	256
2^{-0}	5.29e+00	6.80e+00	7.47e+00	6.91e+00
2^{-2}	4.23e+00	5.66e+00	5.48e+00	3.93e+00
2^{-4}	2.08e+00	2.96e+00	3.03e+00	2.04e+00
2^{-6}	1.03e+00	1.48e+00	1.51e+00	1.04e+00
2^{-8}	5.15e-01	7.40e-01	7.58e-01	5.19e-01
2^{-10}	2.59e-01	3.70e-01	3.79e-01	2.60e-01
2^{-12}	1.30e-01	1.85e-01	1.90e-01	1.31e-01
2^{-14}	6.54e-02	9.27e-02	9.48e-02	6.53e-02
2^{-16}	3.28e-02	4.64e-02	4.74e-02	3.27e-02
2^{-18}	1.64e-02	2.32e-02	2.37e-02	1.64e-02
2^{-20}	8.21e-03	1.16e-02	1.18e-02	8.21e-03
2^{-22}	4.82e-03	5.80e-03	5.92e-03	4.13e-03
2^{-24}	4.83e-03	2.90e-03	2.96e-03	2.09e-03
E^N	5.29e+00	6.80e+00	7.47e+00	6.91e+00

Table 10.7: Computed maximum errors $E_\varepsilon^N(\frac{1}{V^*}D_x^- V_{M\varepsilon})$ generated by $(A_{M\varepsilon}^{\mathbf{N}})$ applied to problem $(P_{M\varepsilon})$ for various values of ε, N, v_i and $\beta = 0.8$.

In Table 10.7 the computed maximum errors decrease as ε decreases for $\frac{1}{V^*}D_x^- V_{M\varepsilon}$. The largest computed maximum error occurs at $\varepsilon \geq 2^{-4}$ for all N, v_i and $\beta = 0.8$. The computed maximum errors do not decrease as the number of mesh points increase. From Table 10.7 we cannot say that the method is ε for $\frac{1}{V^*}D_x^- V_{M\varepsilon}$.

The orders of convergence and the compound error constants for $\sqrt{\varepsilon}D_y^- U_{M\varepsilon}$, $D_y^- V_{M\varepsilon}$ and $\frac{1}{V^*}D_x^- V_{M\varepsilon}$ are given in Tables 10.8, 10.9 and 10.10, respectively, for various values of ε, N, v_i and $\beta = 0.8$.

The results in Tables 10.5 and 10.8 suggest that $(A_{M\varepsilon}^{\mathbf{N}})$ is an ε-uniform numerical method of order at least 0.14 for $\sqrt{\varepsilon}D_y^- U_{M\varepsilon}$ for all v_i, N and $\beta = 0.8$.

The results in Tables 10.6 and 10.9 suggest that $(A_{M\varepsilon}^{\mathbf{N}})$ is an ε-uniform numerical method of order at least 0.19 for $D_y^- V_{M\varepsilon}$ for all v_i, N and $\beta = 0.8$.

	$v_i = -0.6$				$v_i = 2.0$				$v_i = 7.0$		
$\varepsilon\backslash N$	32	64	128	$\varepsilon\backslash N$	32	64	128	$\varepsilon\backslash N$	32	64	128
2^{-0}	0.99	1.00	0.99	2^{-0}	0.93	0.99	0.58	2^{-0}	0.50	1.26	0.80
2^{-2}	1.00	1.00	1.00	2^{-2}	0.55	0.93	0.99	2^{-2}	0.63	0.21	1.11
2^{-4}	1.27	1.00	1.00	2^{-4}	0.52	1.19	1.30	2^{-4}	0.45	0.10	0.37
2^{-6}	0.59	1.13	1.24	2^{-6}	0.31	0.43	0.93	2^{-6}	0.43	0.10	0.37
2^{-8}	0.43	0.14	0.82	2^{-8}	0.50	0.23	0.45	2^{-8}	0.43	0.09	0.37
2^{-10}	0.43	0.15	0.74	2^{-10}	0.50	0.23	0.45	2^{-10}	0.45	0.09	0.37
2^{-12}	0.43	0.15	0.74	2^{-12}	0.50	0.23	0.45	2^{-12}	0.48	0.10	0.37
2^{-14}	0.43	0.15	0.74	2^{-14}	0.50	0.23	0.45	2^{-14}	0.50	0.11	0.37
2^{-16}	0.43	0.15	0.74	2^{-16}	0.50	0.23	0.45	2^{-16}	0.52	0.11	0.37
2^{-18}	0.43	0.15	0.74	2^{-18}	0.50	0.23	0.45	2^{-18}	0.53	0.12	0.37
2^{-20}	0.43	0.15	0.74	2^{-20}	0.50	0.23	0.45	2^{-20}	0.53	0.12	0.37
2^{-22}	0.43	0.15	0.74	2^{-22}	0.50	0.23	0.45	2^{-22}	0.53	0.12	0.37
2^{-24}	0.43	0.15	0.74	2^{-24}	0.50	0.23	0.45	2^{-24}	0.53	0.12	0.37
p^N_{comp}	0.43	0.14	0.74	p^N_{comp}	0.31	0.42	0.45	p^N_{comp}	0.63	0.18	0.37
$C_{0.14}$	0.68	0.56	0.56	$C_{0.42}$	1.74	1.87	1.87	$C_{0.18}$	4.32	3.16	3.16

Table 10.8: Computed orders of convergence $p^N_\varepsilon(\sqrt{\varepsilon}D_y^- U_{M\varepsilon})$, $p^N(\sqrt{\varepsilon}D_y^- U_{M\varepsilon})$ and error constants $C^N_{p^*}$ generated by $(A^N_{M\varepsilon})$ applied to problem $(P_{M\varepsilon})$ for various values of ε, N, v_i and $\beta = 0.8$.

	$v_i = -0.6$				$v_i = 2.0$				$v_i = 7.0$		
$\varepsilon\backslash N$	32	64	128	$\varepsilon\backslash N$	32	64	128	$\varepsilon\backslash N$	32	64	128
2^{-0}	0.98	0.39	0.31	2^{-0}	0.42	0.50	0.56	2^{-0}	0.47	0.56	0.50
2^{-2}	0.98	0.39	0.35	2^{-2}	0.23	0.48	0.54	2^{-2}	0.25	0.61	0.79
2^{-4}	0.91	0.39	0.40	2^{-4}	0.45	0.38	0.35	2^{-4}	0.17	0.40	0.59
2^{-6}	0.60	1.19	0.82	2^{-6}	0.13	0.57	0.39	2^{-6}	0.17	0.40	0.59
2^{-8}	0.42	0.19	0.87	2^{-8}	0.27	0.42	0.39	2^{-8}	0.17	0.40	0.59
2^{-10}	0.42	0.19	0.80	2^{-10}	0.27	0.42	0.39	2^{-10}	0.17	0.40	0.59
2^{-12}	0.42	0.19	0.80	2^{-12}	0.27	0.42	0.39	2^{-12}	0.16	0.40	0.59
2^{-14}	0.42	0.19	0.80	2^{-14}	0.27	0.42	0.38	2^{-14}	0.16	0.40	0.59
2^{-16}	0.42	0.19	0.80	2^{-16}	0.27	0.42	0.38	2^{-16}	0.16	0.40	0.59
2^{-18}	0.42	0.19	0.80	2^{-18}	0.27	0.42	0.38	2^{-18}	0.16	0.40	0.59
2^{-20}	0.42	0.19	0.80	2^{-20}	0.27	0.42	0.38	2^{-20}	0.16	0.40	0.59
2^{-22}	0.42	0.19	0.80	2^{-22}	0.27	0.42	0.38	2^{-22}	0.16	0.40	0.59
2^{-24}	0.42	0.19	0.80	2^{-24}	0.27	0.42	0.38	2^{-24}	0.16	0.40	0.59
p^N_{comp}	0.42	0.19	0.80	p^N_{comp}	0.21	0.56	0.38	p^N_{comp}	0.25	0.42	0.59
$C_{0.19}$	0.52	0.45	0.45	$C_{0.38}$	2.60	2.93	2.58	$C_{0.42}$	13.24	14.92	14.92

Table 10.9: Computed orders of convergence $p^N_\varepsilon(D_y^- V_{M\varepsilon})$, $p^N(D_y^- V_{M\varepsilon})$ and error constant $C^N_{p^*}$ generated by $(A^N_{M\varepsilon})$ applied to problem $(P_{M\varepsilon})$ for various values of ε, N, v_i and $\beta = 0.8$.

From the orders of convergence in Table 10.10 for $\frac{1}{V^*}D_x^- V_{M\varepsilon}$ we cannot say that the method $(A^N_{M\varepsilon})$ is ε-uniform for $\frac{1}{V^*}D_x^- V_{M\varepsilon}$ for all v_i as the errors increase as N increases.

	$v_i = -0.6$				$v_i = 1.0$				$v_i = 7.0$		
$\varepsilon \backslash N$	32	64	128	$\varepsilon \backslash N$	32	64	128	$\varepsilon \backslash N$	32	64	128
2^{-0}	-0.50	-0.40	-0.45	2^{-0}	-0.30	-0.23	-0.15	2^{-0}	-0.31	-0.19	-0.16
2^{-2}	-0.65	-0.52	-0.48	2^{-2}	-0.56	-0.31	-0.23	2^{-2}	-0.39	-0.03	0.11
2^{-4}	-0.88	-0.48	-0.44	2^{-4}	-0.53	-0.55	-0.48	2^{-4}	-0.45	-0.12	0.12
2^{-6}	-1.18	-0.73	-0.61	2^{-6}	-0.70	-0.58	-0.52	2^{-6}	-0.45	-0.12	0.10
2^{-8}	-1.43	-0.75	-0.58	2^{-8}	-0.70	-0.58	-0.51	2^{-8}	-0.45	-0.13	0.10
2^{-10}	-1.43	-0.75	-0.58	2^{-10}	-0.70	-0.58	-0.51	2^{-10}	-0.44	-0.12	0.10
2^{-12}	-1.24	-0.76	-0.58	2^{-12}	-0.70	-0.58	-0.51	2^{-12}	-0.44	-0.12	0.09
2^{-14}	-0.39	-0.76	-0.57	2^{-14}	-0.70	-0.58	-0.56	2^{-14}	-0.43	-0.12	0.09
2^{-16}	0.55	-0.77	-0.57	2^{-16}	-0.70	-0.59	-0.55	2^{-16}	-0.43	-0.12	0.09
2^{-18}	1.07	-0.35	-0.56	2^{-18}	-0.70	-0.59	-0.55	2^{-18}	-0.43	-0.13	0.09
2^{-20}	1.05	0.61	-0.55	2^{-20}	0.09	-0.60	-0.55	2^{-20}	-0.43	-0.13	0.09
2^{-22}	1.01	0.85	0.19	2^{-22}	1.12	-0.61	-0.54	2^{-22}	-0.43	-0.14	0.09
2^{-24}	0.99	0.84	0.91	2^{-24}	1.12	0.37	-0.53	2^{-24}	0.43	-0.16	0.09
p_{comp}^N	-0.81	-0.48	-0.44	p_{comp}^N	-0.41	-0.31	-0.23	p_{comp}^N	-0.31	-0.19	-0.16
$C_{-0.48}$	-0.04	-0.04	-0.04	$C_{-0.31}$	-1.43	-1.53	-1.53	$C_{-0.19}$	-16.06	-17.49	-17.49

Table 10.10: Computed orders of convergence $p_\varepsilon^N(\frac{1}{V^*}D_x^- V_{M\varepsilon})$, $p^N(\frac{1}{V^*}D_x^- V_{M\varepsilon})$ and error constant $C_{p^*}^N$ generated by $(A_{M\varepsilon}^N)$ applied to problem $(P_{M\varepsilon})$ for various values of ε, N, v_i and $\beta = 0.8$.

From the data in Tables 10.8 and 10.9 we obtain the computed error bounds for $\sqrt{\varepsilon}D_y^- U_{M\varepsilon}$ and $D_y^- V_{M\varepsilon}$ for $N \geq 64$

$$
\begin{aligned}
v_i = -0.6 && \sqrt{\varepsilon}\|D_y^- U_{M\varepsilon} - \tfrac{\partial u_{M\varepsilon}}{\partial y}\|_{\Omega_\varepsilon^N} &\leq 0.56 N^{-0.14} \\
v_i = 2.0 && \sqrt{\varepsilon}\|D_y^- U_{M\varepsilon} - \tfrac{\partial u_{M\varepsilon}}{\partial y}\|_{\Omega_\varepsilon^N} &\leq 1.87 N^{-0.42} \\
v_i = 7.0 && \sqrt{\varepsilon}\|D_y^- U_{M\varepsilon} - \tfrac{\partial u_{M\varepsilon}}{\partial y}\|_{\Omega_\varepsilon^N} &\leq 4.32 N^{-0.18}
\end{aligned}
\tag{10.3}
$$

$$
\begin{aligned}
v_i = -0.6 && \|D_y^- V_{M\varepsilon} - \tfrac{\partial v_{M\varepsilon}}{\partial y}\|_{\Omega_\varepsilon^N} &\leq 0.52 N^{-0.19} \\
v_i = 2.0 && \|D_y^- V_{M\varepsilon} - \tfrac{\partial v_{M\varepsilon}}{\partial y}\|_{\Omega_\varepsilon^N} &\leq 2.93 N^{-0.38} \\
v_i = 7.0 && \|D_y^- V_{M\varepsilon} - \tfrac{\partial v_{M\varepsilon}}{\partial y}\|_{\Omega_\varepsilon^N} &\leq 14.92 N^{-0.42}.
\end{aligned}
\tag{10.4}
$$

10.5 Error analysis based on the Blasius solution

In this section, we compute ε-uniform maximum pointwise differences in the approximations generated by the direct numerical method described in Section 10.2.

For this case, we compare the parameter uniform maximum pointwise differences in the approximations generated by the direct numerical method of the previous section with the corresponding values of $\mathbf{U}_{MB}^{8192}$ generated be the method defined in Chapter 9. The scaled maximum pointwise differences $\|U_{M\varepsilon} - \overline{U_{MB}}^{8192}\|_{\overline{\Omega}_\varepsilon^N}$ and $\frac{1}{V^*}\|V_{M\varepsilon} - \overline{V_{MB}}^{8192}\|_{\overline{\Omega}_\varepsilon^N \backslash \Gamma_L}$

for various values of N, ε, v_i and $\beta = 0.8$ are given in Tables 10.11 and 10.12, respectively.

$\varepsilon \backslash N$	32	64	128	256	512	$\varepsilon \backslash N$	32	64	128	256	512
		$v_i = -0.6$						$v_i = 2.0$			
2^{-0}	1.68e-04	9.78e-05	6.21e-05	4.38e-05	3.47e-05	2^{-0}	6.91e-03	3.37e-03	1.55e-03	6.31e-04	1.69e-04
2^{-2}	3.75e-04	2.34e-04	1.56e-04	1.17e-04	9.85e-05	2^{-2}	2.16e-02	1.06e-02	5.13e-03	2.36e-03	9.57e-04
2^{-4}	1.43e-03	7.00e-04	3.53e-04	1.78e-04	1.16e-04	2^{-4}	4.83e-02	2.33e-02	1.07e-02	4.83e-03	2.16e-03
2^{-6}	4.33e-03	2.10e-03	1.01e-03	4.81e-04	2.25e-04	2^{-6}	7.14e-02	4.34e-02	2.11e-02	9.54e-03	4.08e-03
2^{-8}	5.30e-03	3.10e-03	1.76e-03	9.61e-04	4.76e-04	2^{-8}	7.14e-02	4.34e-02	2.40e-02	1.24e-02	6.02e-03
2^{-10}	5.28e-03	3.10e-03	1.76e-03	9.99e-04	5.62e-04	2^{-10}	7.14e-02	4.34e-02	2.40e-02	1.24e-02	6.02e-03
2^{-12}	5.25e-03	3.10e-03	1.76e-03	9.99e-04	5.62e-04	2^{-12}	7.14e-02	4.34e-02	2.40e-02	1.24e-02	6.02e-03
2^{-14}	5.23e-03	3.10e-03	1.76e-03	9.99e-04	5.62e-04	2^{-14}	7.14e-02	4.34e-02	2.40e-02	1.24e-02	6.02e-03
2^{-16}	5.22e-03	3.10e-03	1.76e-03	9.99e-04	5.62e-04	2^{-16}	7.14e-02	4.34e-02	2.40e-02	1.24e-02	6.02e-03
2^{-18}	5.21e-03	3.10e-03	1.76e-03	9.99e-04	5.62e-04	2^{-18}	7.13e-02	4.34e-02	2.40e-02	1.24e-02	6.02e-03
2^{-20}	5.20e-03	3.10e-03	1.76e-03	9.99e-04	5.62e-04	2^{-20}	7.13e-02	4.34e-02	2.40e-02	1.24e-02	6.02e-03
2^{-22}	5.20e-03	3.10e-03	1.76e-03	9.99e-04	5.62e-04	2^{-22}	7.13e-02	4.34e-02	2.40e-02	1.24e-02	6.02e-03
2^{-24}	5.20e-03	3.10e-03	1.76e-03	9.99e-04	5.62e-04	2^{-24}	7.13e-02	4.34e-02	2.40e-02	1.24e-02	6.02e-03
E^N	5.30e-03	3.10e-03	1.76e-03	9.99e-04	5.62e-04	E^N	7.14e-02	4.34e-02	2.40e-02	1.24e-02	6.02e-03

$\varepsilon \backslash N$	32	64	128	256	512
		$v_i = 7.0$			
2^{-0}	4.73e-02	2.23e-02	9.67e-03	3.70e-03	9.08e-04
2^{-2}	9.42e-02	5.01e-02	2.37e-02	1.02e-02	3.88e-03
2^{-4}	9.60e-02	5.69e-02	3.18e-02	1.65e-02	7.91e-03
2^{-6}	9.77e-02	5.75e-02	3.20e-02	1.66e-02	7.95e-03
2^{-8}	9.84e-02	5.78e-02	3.21e-02	1.67e-02	7.97e-03
2^{-10}	9.75e-02	5.78e-02	3.21e-02	1.67e-02	7.97e-03
2^{-12}	9.55e-02	5.75e-02	3.21e-02	1.67e-02	7.97e-03
2^{-14}	9.33e-02	5.71e-02	3.20e-02	1.67e-02	7.98e-03
2^{-16}	9.15e-02	5.67e-02	3.19e-02	1.67e-02	7.97e-03
2^{-18}	9.04e-02	5.63e-02	3.18e-02	1.66e-02	7.97e-03
2^{-20}	8.98e-02	5.61e-02	3.18e-02	1.66e-02	7.97e-03
2^{-22}	8.94e-02	5.60e-02	3.17e-02	1.66e-02	7.96e-03
2^{-24}	8.93e-02	5.59e-02	3.17e-02	1.66e-02	7.96e-03
E^N	9.84e-02	5.78e-02	3.21e-02	1.67e-02	7.98e-03

Table 10.11: Computed maximum pointwise difference $||U_{M\varepsilon} - \overline{U_{MB}}^{8192}||_{\overline{\Omega}_{\varepsilon}^N}$ where $U_{M\varepsilon}$ is generated by $(A_{M\varepsilon}^N)$ for various values of ε, N, v_i and $\beta = 0.8$.

In Tables 10.11 and 10.12 we see that the computed maximum differences for the velocity components decrease as the number of mesh points, N, increases.
In Table 10.11 the largest maximum differences of $||U_{M\varepsilon} - \overline{U_{MB}}^{8192}||_{\overline{\Omega}_{\varepsilon}^N}$ occur between $2^{-6} \leq \varepsilon \leq 2^{-10}$ for $\beta = 0.8$ and all N and v_i. The maximum differences stabilise to a fixed value when $\varepsilon \leq 2^{-10}$.

$\varepsilon \backslash N$	$v_i = -0.6$				
	32	64	128	256	512
2^{-0}	8.55e-03	4.54e-03	2.49e-03	1.42e-03	1.22e-03
2^{-2}	1.34e-02	6.73e-03	3.42e-03	1.78e-03	1.28e-03
2^{-4}	1.47e-02	7.61e-03	3.83e-03	1.94e-03	9.99e-04
2^{-6}	1.35e-02	6.31e-03	3.10e-03	1.57e-03	8.24e-04
2^{-8}	8.97e-03	4.81e-03	2.51e-03	1.26e-03	6.10e-04
2^{-10}	5.35e-03	2.82e-03	1.47e-03	7.58e-04	3.89e-04
2^{-12}	3.62e-03	1.88e-03	9.67e-04	4.94e-04	2.52e-04
2^{-14}	2.77e-03	1.41e-03	7.16e-04	3.63e-04	1.84e-04
2^{-16}	2.35e-03	1.18e-03	5.92e-04	2.98e-04	1.50e-04
2^{-18}	2.13e-03	1.06e-03	5.30e-04	2.66e-04	1.33e-04
2^{-20}	2.03e-03	1.00e-03	4.99e-04	2.49e-04	1.25e-04
2^{-22}	1.98e-03	9.73e-04	4.84e-04	2.41e-04	1.21e-04
2^{-24}	1.95e-03	9.58e-04	4.76e-04	2.37e-04	1.19e-04
E^N	1.47e-02	7.61e-03	3.83e-03	1.94e-03	1.28e-03

$\varepsilon \backslash N$	$v_i = 2.0$				
	32	64	128	256	512
2^{-0}	4.96e-02	4.00e-02	2.75e-02	1.59e-02	6.32e-03
2^{-2}	6.65e-02	5.14e-02	3.53e-02	2.21e-02	1.23e-02
2^{-4}	5.30e-02	3.76e-02	2.55e-02	1.73e-02	1.14e-02
2^{-6}	3.13e-02	2.50e-02	1.65e-02	1.03e-02	6.41e-03
2^{-8}	1.56e-02	1.25e-02	8.67e-03	5.62e-03	3.52e-03
2^{-10}	7.82e-03	6.25e-03	4.33e-03	2.81e-03	1.76e-03
2^{-12}	3.91e-03	3.13e-03	2.17e-03	1.41e-03	8.80e-04
2^{-14}	1.95e-03	1.56e-03	1.08e-03	7.07e-04	4.40e-04
2^{-16}	1.91e-03	9.33e-04	5.42e-04	3.54e-04	2.20e-04
2^{-18}	1.92e-03	9.38e-04	4.64e-04	2.31e-04	1.16e-04
2^{-20}	1.92e-03	9.40e-04	4.66e-04	2.32e-04	1.16e-04
2^{-22}	1.92e-03	9.42e-04	4.67e-04	2.33e-04	1.16e-04
2^{-24}	1.92e-03	9.43e-04	4.68e-04	2.33e-04	1.16e-04
E^N	6.65e-02	5.14e-02	3.53e-02	2.21e-02	1.23e-02

$\varepsilon \backslash N$	$v_i = 7.0$				
	32	64	128	256	512
2^{-0}	2.28e-01	1.74e-01	1.16e-01	6.72e-02	2.81e-02
2^{-2}	2.06e-01	1.71e-01	1.14e-01	6.34e-02	2.72e-02
2^{-4}	1.03e-01	9.44e-02	7.22e-02	4.52e-02	2.21e-02
2^{-6}	5.15e-02	4.72e-02	3.61e-02	2.27e-02	1.11e-02
2^{-8}	2.55e-02	2.36e-02	1.80e-02	1.13e-02	5.55e-03
2^{-10}	1.26e-02	1.18e-02	9.02e-03	5.66e-03	2.78e-03
2^{-12}	6.26e-03	5.88e-03	4.51e-03	2.83e-03	1.39e-03
2^{-14}	3.11e-03	2.94e-03	2.25e-03	1.42e-03	6.94e-04
2^{-16}	1.95e-03	1.47e-03	1.13e-03	7.08e-04	3.47e-04
2^{-18}	1.94e-03	9.48e-04	5.64e-04	3.54e-04	1.74e-04
2^{-20}	1.93e-03	9.46e-04	4.69e-04	2.34e-04	1.17e-04
2^{-22}	1.93e-03	9.45e-04	4.69e-04	2.33e-04	1.17e-04
2^{-24}	1.92e-03	9.45e-04	4.68e-04	2.33e-04	1.17e-04
E^N	2.28e-01	1.74e-01	1.16e-01	6.72e-02	2.81e-02

Table 10.12: Computed maximum pointwise difference $\frac{1}{V^*}||V_{M\varepsilon} - \overline{V_{MB}}^{8192}||_{\overline{\Omega}^N_\varepsilon \backslash \Gamma_L}$ where $V_{M\varepsilon}$ is generated by $(A^{\mathbf{N}}_{M\varepsilon})$ for various values of ε, N, v_i and $\beta = 0.8$.

In Table 10.12 the largest maximum differences of $\frac{1}{V^*}||V_{M\varepsilon} - \overline{V_{MB}}^{8192}||_{\overline{\Omega}^N_\varepsilon \backslash \Gamma_L}$ occur for $\varepsilon \geq 2^{-4}$, for $\beta = 0.8$ and all N and v_i. We see that the computed pointwise maximum errors for $\frac{1}{V^*}V_{M\varepsilon}$ tend to a fixed value as ε decreases for all $\varepsilon \leq 2^{-18}$, $N \geq 256$ and v_i considered. For $N < 256$ the computed pointwise maximum errors for $\frac{1}{V^*}V_{M\varepsilon}$ decrease as ε decreases for all v_i considered. Thus, Tables 10.11 and 10.12 indicate that the maximum differences for the velocity components are independent of ε for all v_i and N.

In a similar fashion to Tables 10.1 and 10.2 of the the maximum pointwise errors of velocity components, Tables 10.11 and 10.12 suggest that the method is ε-uniform for U_ε and $\frac{1}{V^*}V_\varepsilon$ for all v_i considered.
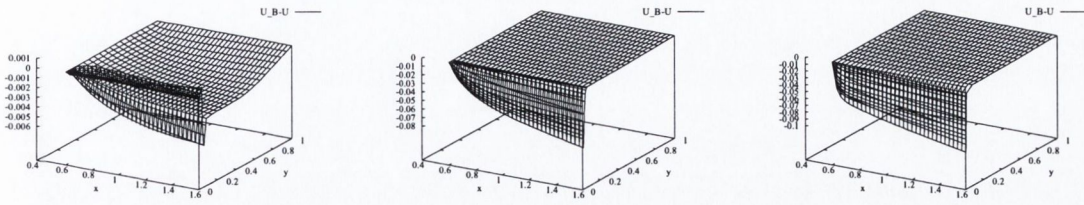
Figure 10-8: Graphs of $U_{M\varepsilon} - U_{MB}^{8192}$ for $\varepsilon = 2^{-12}$, N=32, $\beta = 0.8$ and $v_i = -0.6$, 2.0, 7.0.

The graphs of differences $U_{M\varepsilon} - U_{MB}^{8192}$ for $\varepsilon = 2^{-12}$, N=32, $\beta = 0.8$ and v_i=-0.6, 2.0, 7.0 in Figure 10-8 show that the largest difference occurs contained within the boundary layer along the surface of the wedge for all β considered. The graphs of differences $\frac{1}{V^*}(V_{M\varepsilon} - V_{MB}^{8192})$ for $\varepsilon = 2^{-12}$, N=32, $\beta = 0.8$ and $v_i = -0.6$, 2.0, 7.0 in Fig. 10-9 show that the largest difference occurs at the furthest point from the surface of the wedge and closest to the leading edge.

Figure 10-9: Graphs of $\frac{1}{V^*}(V_{M\varepsilon} - V_{MB}^{8192})$ for $\varepsilon = 2^{-12}$, N=32, $\beta = 0.8$ $v_i = -0.6$, 2.0 and 7.0.

The orders of convergence and the error constants of the scaled velocity components $U_{M\varepsilon}$ and $\frac{1}{V^*}V_{M\varepsilon}$ are given in Tables 10.13 and 10.14, respectively.

$v_i = -0.6$

$\varepsilon\backslash N$	32	64	128	256
2^{-0}	0.78	0.66	0.50	0.34
2^{-2}	0.68	0.59	0.42	0.25
2^{-4}	1.03	0.99	0.99	0.62
2^{-6}	1.04	1.05	1.08	1.09
2^{-8}	0.77	0.82	0.87	1.01
2^{-10}	0.77	0.82	0.82	0.83
2^{-12}	0.76	0.82	0.82	0.83
2^{-14}	0.76	0.82	0.82	0.83
2^{-16}	0.75	0.82	0.82	0.83
2^{-18}	0.75	0.82	0.82	0.83
2^{-20}	0.75	0.81	0.82	0.83
2^{-22}	0.75	0.81	0.82	0.83
2^{-24}	0.75	0.81	0.82	0.83
p^N_{comp}	0.77	0.82	0.82	0.83
$C_{0.82}$	0.21	0.21	0.22	0.22

$v_i = 2.0$

$\varepsilon\backslash N$	32	64	128	256
2^{-0}	1.04	1.12	1.30	1.90
2^{-2}	1.03	1.04	1.12	1.30
2^{-4}	1.05	1.12	1.15	1.16
2^{-6}	0.72	1.04	1.15	1.22
2^{-8}	0.72	0.85	0.95	1.04
2^{-10}	0.72	0.85	0.95	1.04
2^{-12}	0.72	0.85	0.95	1.04
2^{-14}	0.72	0.85	0.95	1.04
2^{-16}	0.72	0.85	0.95	1.04
2^{-18}	0.72	0.85	0.95	1.04
2^{-20}	0.72	0.85	0.95	1.04
2^{-22}	0.72	0.85	0.95	1.04
2^{-24}	0.72	0.85	0.95	1.04
p^N_{comp}	0.72	0.85	0.95	1.04
$C_{0.95}$	4.04	4.76	5.10	5.10

$v_i = 7.0$

$\varepsilon\backslash N$	32	64	128	256
2^{-0}	1.09	1.20	1.39	2.03
2^{-2}	0.91	1.08	1.21	1.40
2^{-4}	0.75	0.84	0.94	1.06
2^{-6}	0.77	0.85	0.94	1.06
2^{-8}	0.77	0.85	0.94	1.06
2^{-10}	0.76	0.85	0.95	1.06
2^{-12}	0.73	0.84	0.94	1.06
2^{-14}	0.71	0.83	0.94	1.06
2^{-16}	0.69	0.83	0.94	1.06
2^{-18}	0.68	0.82	0.94	1.06
2^{-20}	0.68	0.82	0.93	1.06
2^{-22}	0.68	0.82	0.93	1.06
2^{-24}	0.67	0.82	0.93	1.06
p^N_{comp}	0.77	0.85	0.94	1.06
$C_{0.94}$	5.41	6.12	6.54	6.54

Table 10.13: Computed orders of convergence $p^N_{\varepsilon,comp}$, p^N_{comp} and the error constant $C^N_{p^*_{comp}}$ for $U_{M\varepsilon} - U^{8192}_{MB}$ where $U_{M\varepsilon}$ is generated by (A^N_ε) for various values of ε, N, v_i and $\beta = 0.8$.

$v_i = -0.6$

$\varepsilon\backslash N$	32	64	128	256
2^{-0}	0.91	0.87	0.81	0.23
2^{-2}	0.99	0.97	0.94	0.48
2^{-4}	0.95	0.99	0.98	0.96
2^{-6}	1.10	1.03	0.98	0.93
2^{-8}	0.90	0.94	0.99	1.05
2^{-10}	0.92	0.94	0.96	0.96
2^{-12}	0.95	0.96	0.97	0.97
2^{-14}	0.98	0.97	0.98	0.98
2^{-16}	1.00	0.99	0.99	0.99
2^{-18}	1.01	1.00	1.00	0.99
2^{-20}	1.02	1.00	1.00	1.00
2^{-22}	1.02	1.01	1.00	1.00
2^{-24}	1.02	1.01	1.00	1.00
p^N_{comp}	0.95	0.99	0.98	0.60
$C_{0.60}$	0.35	0.27	0.21	0.16

$v_i = 2.0$

$\varepsilon\backslash N$	32	64	128	256
2^{-0}	0.31	0.54	0.79	1.33
2^{-2}	0.37	0.54	0.67	0.85
2^{-4}	0.50	0.56	0.56	0.60
2^{-6}	0.32	0.60	0.67	0.69
2^{-8}	0.32	0.53	0.62	0.68
2^{-10}	0.32	0.53	0.62	0.68
2^{-12}	0.32	0.53	0.62	0.68
2^{-14}	0.32	0.53	0.62	0.69
2^{-16}	1.04	0.78	0.62	0.69
2^{-18}	1.03	1.02	1.01	1.00
2^{-20}	1.03	1.01	1.01	1.00
2^{-22}	1.03	1.01	1.01	1.00
2^{-24}	1.03	1.01	1.01	1.00
p^N_{comp}	0.37	0.54	0.67	0.85
$C_{0.67}$	1.84	2.27	2.48	2.48

$v_i = 7.0$

$\varepsilon\backslash N$	32	64	128	256
2^{-0}	0.39	0.58	0.79	1.26
2^{-2}	0.26	0.59	0.85	1.22
2^{-4}	0.13	0.39	0.67	1.03
2^{-6}	0.13	0.39	0.67	1.03
2^{-8}	0.11	0.39	0.67	1.03
2^{-10}	0.10	0.38	0.67	1.03
2^{-12}	0.09	0.38	0.67	1.03
2^{-14}	0.08	0.38	0.67	1.03
2^{-16}	0.41	0.38	0.67	1.03
2^{-18}	1.03	0.75	0.67	1.03
2^{-20}	1.03	1.01	1.01	1.00
2^{-22}	1.03	1.01	1.01	1.00
2^{-24}	1.03	1.01	1.01	1.00
p^N_{comp}	0.39	0.58	0.79	1.26
$C_{0.79}$	8.29	10.91	12.57	12.57

Table 10.14: Computed orders of convergence $p^N_{\varepsilon,comp}$, p^N_{comp} and the error constant $C^N_{p^*_{comp}}$ for $\frac{1}{V^*}(V_{M\varepsilon} - V^{8192}_{MB})$ where $V_{M\varepsilon}$ is generated by $(A^N_{M\varepsilon})$ for various values of ε, N, v_i and $\beta = 0.8$.

From Tables 10.13 and 10.14 we see the order of convergence for the approximations to the scaled velocity components $U_{M\varepsilon}$ and $\frac{1}{V^*}V_{M\varepsilon}$ is at least 0.6 for $N \geq 128$ and all v_i considered. Using Tables 10.13-10.14 we obtain the following error bounds

for $N \geq 128$ and $\beta = 0.8$

$$
\begin{aligned}
v_i = -0.6 \quad & \|U_{M\varepsilon} - U_{MB}^{8192}\|_{\Omega_\varepsilon^N} \leq 0.22 N^{-0.82} \\
v_i = 2.0 \quad & \|U_{M\varepsilon} - U_{MB}^{8192}\|_{\Omega_\varepsilon^N} \leq 5.10 N^{-0.95} \\
v_i = 7.0 \quad & \|U_{M\varepsilon} - U_{MB}^{8192}\|_{\Omega_\varepsilon^N} \leq 6.54 N^{-0.94}
\end{aligned}
\tag{10.5}
$$

$$
\begin{aligned}
v_i = -0.6 \quad & \tfrac{1}{V^*}\|V_{M\varepsilon} - V_{MB}^{8192}\|_{\Omega_\varepsilon^N \backslash \Gamma_L} \leq 0.35 N^{-0.60} \\
v_i = 2.0 \quad & \tfrac{1}{V^*}\|V_{M\varepsilon} - V_{MB}^{8192}\|_{\Omega_\varepsilon^N \backslash \Gamma_L} \leq 2.48 N^{-0.67} \\
v_i = 7.0 \quad & \tfrac{1}{V^*}\|V_{M\varepsilon} - V_{MB}^{8192}\|_{\Omega_\varepsilon^N \backslash \Gamma_L} \leq 12.57 N^{-0.79}.
\end{aligned}
\tag{10.6}
$$

From Tables 10.11-10.14 we have shown that for the velocity components the method is ε–uniform for $v_i = -0.6$, 2.0 and 7.0. Further computations, not reported here, show that the errors for the velocity components for $v_i \in [-0.6, 7.0]$ and $\beta \in [0.0, 1.0]$ have similar behaviour, therefore the method can be said to be $(\varepsilon, v_i, \beta)$–uniform for the scaled velocity components.

		$v_i = -0.6$						$v_i = 2.0$		
$\varepsilon \backslash N$	32	64	128	256	512	$\varepsilon \backslash N$	32	64	128	256	512
2^{-0}	6.52e-03	3.44e-03	1.90e-03	1.13e-03	7.43e-04	2^{-0}	6.51e-02	3.46e-02	1.91e-02	1.11e-02	8.32e-03
2^{-2}	1.23e-02	6.24e-03	3.24e-03	1.74e-03	1.00e-03	2^{-2}	1.08e-01	6.51e-02	3.46e-02	1.91e-02	1.11e-02
2^{-4}	2.71e-02	1.24e-02	6.28e-03	3.25e-03	1.73e-03	2^{-4}	1.80e-01	8.57e-02	4.12e-02	2.47e-02	1.53e-02
2^{-6}	7.09e-02	3.33e-02	1.56e-02	7.23e-03	3.35e-03	2^{-6}	2.71e-01	1.64e-01	8.01e-02	3.68e-02	1.65e-02
2^{-8}	9.65e-02	5.69e-02	3.25e-02	1.72e-02	8.15e-03	2^{-8}	2.71e-01	1.64e-01	9.15e-02	4.81e-02	2.42e-02
2^{-10}	9.65e-02	5.69e-02	3.25e-02	1.80e-02	9.76e-03	2^{-10}	2.71e-01	1.64e-01	9.15e-02	4.81e-02	2.42e-02
2^{-12}	9.65e-02	5.69e-02	3.25e-02	1.80e-02	9.76e-03	2^{-12}	2.71e-01	1.64e-01	9.15e-02	4.81e-02	2.42e-02
2^{-14}	9.65e-02	5.69e-02	3.25e-02	1.80e-02	9.76e-03	2^{-14}	2.71e-01	1.64e-01	9.15e-02	4.81e-02	2.42e-02
2^{-16}	9.65e-02	5.69e-02	3.25e-02	1.80e-02	9.76e-03	2^{-16}	2.71e-01	1.64e-01	9.15e-02	4.81e-02	2.42e-02
2^{-18}	9.65e-02	5.69e-02	3.25e-02	1.80e-02	9.76e-03	2^{-18}	2.71e-01	1.64e-01	9.15e-02	4.81e-02	2.42e-02
2^{-20}	9.65e-02	5.69e-02	3.25e-02	1.80e-02	9.76e-03	2^{-20}	2.71e-01	1.64e-01	9.15e-02	4.81e-02	2.42e-02
2^{-22}	9.65e-02	5.69e-02	3.25e-02	1.80e-02	9.76e-03	2^{-22}	2.71e-01	1.64e-01	9.15e-02	4.81e-02	2.42e-02
2^{-24}	9.65e-02	5.69e-02	3.25e-02	1.80e-02	9.76e-03	2^{-24}	2.71e-01	1.64e-01	9.15e-02	4.81e-02	2.42e-02
E^N	9.65e-02	5.69e-02	3.25e-02	1.80e-02	9.76e-03	E^N	2.71e-01	1.64e-01	9.15e-02	4.81e-02	2.42e-02

		$v_i = 7.0$			
$\varepsilon \backslash N$	32	64	128	256	512
2^{-0}	3.66e-01	1.80e-01	1.14e-01	7.58e-02	6.27e-02
2^{-2}	6.48e-01	3.53e-01	1.75e-01	8.56e-02	6.20e-02
2^{-4}	6.43e-01	3.94e-01	2.27e-01	1.26e-01	6.75e-02
2^{-6}	6.37e-01	3.92e-01	2.26e-01	1.25e-01	6.74e-02
2^{-8}	6.35e-01	3.92e-01	2.26e-01	1.25e-01	6.74e-02
2^{-10}	6.38e-01	3.91e-01	2.26e-01	1.25e-01	6.74e-02
2^{-12}	6.44e-01	3.92e-01	2.26e-01	1.25e-01	6.74e-02
2^{-14}	6.51e-01	3.94e-01	2.26e-01	1.25e-01	6.74e-02
2^{-16}	6.56e-01	3.95e-01	2.27e-01	1.25e-01	6.74e-02
2^{-18}	6.60e-01	3.96e-01	2.27e-01	1.25e-01	6.74e-02
2^{-20}	6.61e-01	3.97e-01	2.27e-01	1.25e-01	6.74e-02
2^{-22}	6.62e-01	3.97e-01	2.27e-01	1.25e-01	6.74e-02
2^{-24}	6.63e-01	3.97e-01	2.27e-01	1.25e-01	6.74e-02
E^N	6.63e-01	3.97e-01	2.27e-01	1.26e-01	6.75e-02

Table 10.15: Computed maximum pointwise scaled difference $\sqrt{\varepsilon}\|D_y^- U_{M\varepsilon} - D_y U_{MB}^{8192}\|_{\overline{\Omega_\varepsilon^N} \backslash \Gamma_B}$ where $U_{M\varepsilon}$ is generated by $(A_{M\varepsilon}^{\mathbf{N}})$ for various values of ε, N, v_i and $\beta = 0.8$.

In Tables 10.15-10.17, we display the computed maximum pointwise differences

of the approximations to the scaled first order derivatives of the velocity components for various values of ε, N, v_i and $\beta = 0.8$.

The maximum scaled differences for $\sqrt{\varepsilon}D_y^- U_\varepsilon$ and $D_y^- V_\varepsilon$ in Tables 10.15 and 10.16 stabilise to a fixed value after $\varepsilon = 2^{-10}$ for all values of v_i and N considered for $\beta = 0.8$. In a similar fashion to Tables 10.5 and 10.6 of the maximum pointwise errors, Tables 10.15 and 10.16 show that the method is independent of ε for $\sqrt{\varepsilon}D_y^- U_\varepsilon$ and $D_y^- V_\varepsilon$, for all values of v_i and N considered for $\beta = 0.8$.

$v_i = -0.6$

$\varepsilon\backslash N$	32	64	128	256	512
2^{-0}	7.87e-03	4.21e-03	2.87e-03	2.78e-03	2.73e-03
2^{-2}	1.52e-02	7.87e-03	4.86e-03	4.35e-03	3.98e-03
2^{-4}	2.58e-02	1.52e-02	8.79e-03	7.36e-03	6.15e-03
2^{-6}	6.21e-02	2.89e-02	1.30e-02	9.80e-03	8.70e-03
2^{-8}	8.13e-02	4.81e-02	2.69e-02	1.37e-02	8.70e-03
2^{-10}	8.13e-02	4.81e-02	2.69e-02	1.44e-02	8.70e-03
2^{-12}	8.13e-02	4.81e-02	2.69e-02	1.44e-02	8.70e-03
2^{-14}	8.13e-02	4.81e-02	2.69e-02	1.44e-02	8.70e-03
2^{-16}	8.13e-02	4.81e-02	2.69e-02	1.44e-02	8.70e-03
2^{-18}	8.13e-02	4.81e-02	2.69e-02	1.44e-02	8.70e-03
2^{-20}	8.13e-02	4.81e-02	2.69e-02	1.44e-02	8.70e-03
2^{-22}	8.13e-02	4.81e-02	2.69e-02	1.44e-02	8.70e-03
2^{-24}	8.13e-02	4.81e-02	2.69e-02	1.44e-02	8.70e-03
E^N	8.13e-02	4.81e-02	2.69e-02	1.44e-02	8.70e-03

$v_i = 2.0$

$\varepsilon\backslash N$	32	64	128	256	512
2^{-0}	1.03e-01	7.91e-02	5.45e-02	3.36e-02	1.59e-02
2^{-2}	2.01e-01	1.65e-01	1.19e-01	7.95e-02	4.78e-02
2^{-4}	2.82e-01	1.94e-01	1.49e-01	1.15e-01	8.44e-02
2^{-6}	3.23e-01	2.51e-01	1.53e-01	1.16e-01	8.44e-02
2^{-8}	3.23e-01	2.51e-01	1.59e-01	1.16e-01	8.44e-02
2^{-10}	3.23e-01	2.51e-01	1.59e-01	1.16e-01	8.44e-02
2^{-12}	3.23e-01	2.51e-01	1.59e-01	1.16e-01	8.44e-02
2^{-14}	3.23e-01	2.51e-01	1.59e-01	1.16e-01	8.44e-02
2^{-16}	3.23e-01	2.51e-01	1.59e-01	1.16e-01	8.44e-02
2^{-18}	3.23e-01	2.51e-01	1.59e-01	1.16e-01	8.44e-02
2^{-20}	3.23e-01	2.51e-01	1.59e-01	1.16e-01	8.44e-02
2^{-22}	3.23e-01	2.51e-01	1.59e-01	1.16e-01	8.44e-02
2^{-24}	3.23e-01	2.51e-01	1.59e-01	1.16e-01	8.44e-02
E^N	3.23e-01	2.51e-01	1.59e-01	1.16e-01	8.44e-02

$v_i = 7.0$

$\varepsilon\backslash N$	32	64	128	256	512
2^{-0}	6.99e-01	5.32e-01	3.61e-01	2.30e-01	1.14e-01
2^{-2}	1.19e+00	1.02e+00	6.74e-01	3.63e-01	1.52e-01
2^{-4}	1.19e+00	1.12e+00	8.60e-01	5.33e-01	2.71e-01
2^{-6}	1.19e+00	1.12e+00	8.60e-01	5.34e-01	2.72e-01
2^{-8}	1.19e+00	1.12e+00	8.61e-01	5.34e-01	2.72e-01
2^{-10}	1.19e+00	1.12e+00	8.61e-01	5.34e-01	2.72e-01
2^{-12}	1.18e+00	1.12e+00	8.61e-01	5.34e-01	2.72e-01
2^{-14}	1.18e+00	1.12e+00	8.61e-01	5.34e-01	2.72e-01
2^{-16}	1.18e+00	1.12e+00	8.61e-01	5.34e-01	2.72e-01
2^{-18}	1.18e+00	1.12e+00	8.61e-01	5.34e-01	2.72e-01
2^{-20}	1.18e+00	1.12e+00	8.61e-01	5.34e-01	2.72e-01
2^{-22}	1.18e+00	1.12e+00	8.61e-01	5.34e-01	2.72e-01
2^{-24}	1.18e+00	1.12e+00	8.61e-01	5.34e-01	2.72e-01
E^N	1.19e+00	1.12e+00	8.61e-01	5.34e-01	2.72e-01

Table 10.16: Computed maximum pointwise difference $||D_y^- V_{M\varepsilon} - D_y V_{MB}^{8192}||_{\overline{\Omega_\varepsilon^N \backslash \Gamma_B}}$ where $V_{M\varepsilon}$ is generated by $(A_{M\varepsilon}^N)$ for various values of ε, N, v_i and $\beta = 0.8$.

Table 10.17 shows the maximum scaled difference for $\frac{1}{V^*}D_x^- V_{M\varepsilon}$ for various values of ε, N, v_i and β. From Table 10.17 note that the maximum pointwise scaled differences decrease as ε decreases.

		$v_i = -0.6$						$v_i = 2.0$			
$\varepsilon \backslash N$	32	64	128	256	512	$\varepsilon \backslash N$	32	64	128	256	512
2^{-0}	6.35e-02	1.18e-01	1.74e-01	2.47e-01	3.73e-01	2^{-0}	1.32e+00	1.67e+00	1.90e+00	1.96e+00	1.61e+00
2^{-2}	8.07e-02	1.41e-01	2.16e-01	3.19e-01	4.94e-01	2^{-2}	1.24e+00	1.77e+00	2.18e+00	2.51e+00	2.67e+00
2^{-4}	7.45e-02	1.52e-01	2.24e-01	3.17e-01	4.58e-01	2^{-4}	6.90e-01	9.10e-01	1.30e+00	1.79e+00	2.36e+00
2^{-6}	2.91e-02	7.62e-02	1.35e-01	2.14e-01	3.29e-01	2^{-6}	3.35e-01	4.33e-01	6.09e-01	8.73e-01	1.17e+00
2^{-8}	1.12e-02	3.77e-02	6.72e-02	1.04e-01	1.64e-01	2^{-8}	1.67e-01	2.16e-01	3.00e-01	4.32e-01	5.83e-01
2^{-10}	7.30e-03	1.88e-02	3.35e-02	5.21e-02	8.16e-02	2^{-10}	8.36e-02	1.08e-01	1.50e-01	2.16e-01	2.92e-01
2^{-12}	6.04e-03	9.40e-03	1.67e-02	2.60e-02	4.08e-02	2^{-12}	4.18e-02	5.41e-02	7.50e-02	1.08e-01	1.46e-01
2^{-14}	5.52e-03	4.70e-03	8.36e-03	1.30e-02	2.04e-02	2^{-14}	2.09e-02	2.70e-02	3.75e-02	5.52e-02	7.29e-02
2^{-16}	5.31e-03	2.68e-03	4.18e-03	6.50e-03	1.02e-02	2^{-16}	1.05e-02	1.35e-02	1.88e-02	2.76e-02	3.64e-02
2^{-18}	5.22e-03	2.69e-03	2.09e-03	3.25e-03	5.10e-03	2^{-18}	5.23e-03	6.76e-03	9.38e-03	1.38e-02	1.82e-02
2^{-20}	5.18e-03	2.75e-03	1.48e-03	1.63e-03	2.55e-03	2^{-20}	4.82e-03	3.38e-03	4.69e-03	6.90e-03	9.11e-03
2^{-22}	5.16e-03	2.79e-03	1.52e-03	8.13e-04	1.27e-03	2^{-22}	4.97e-03	2.36e-03	2.34e-03	3.45e-03	4.55e-03
2^{-24}	5.15e-03	2.84e-03	1.56e-03	8.15e-04	6.37e-04	2^{-24}	5.04e-03	2.46e-03	1.34e-03	1.73e-03	2.28e-03
E^N	8.07e-02	1.52e-01	2.24e-01	3.19e-01	4.94e-01	E^N	1.32e+00	1.77e+00	2.18e+00	2.51e+00	2.67e+00

		$v_i = 7.0$			
$\varepsilon \backslash N$	32	64	128	256	512
2^{-0}	5.31e+00	6.90e+00	7.85e+00	8.14e+00	6.80e+00
2^{-2}	4.27e+00	5.87e+00	6.10e+00	5.09e+00	3.35e+00
2^{-4}	2.12e+00	3.17e+00	3.61e+00	2.97e+00	1.63e+00
2^{-6}	1.06e+00	1.58e+00	1.81e+00	1.50e+00	8.34e-01
2^{-8}	5.27e-01	7.92e-01	9.04e-01	7.52e-01	4.17e-01
2^{-10}	2.65e-01	3.96e-01	4.52e-01	3.76e-01	2.09e-01
2^{-12}	1.33e-01	1.98e-01	2.26e-01	1.89e-01	1.04e-01
2^{-14}	6.68e-02	9.92e-02	1.13e-01	9.43e-02	5.21e-02
2^{-16}	3.35e-02	4.96e-02	5.65e-02	4.71e-02	2.61e-02
2^{-18}	1.68e-02	2.48e-02	2.82e-02	2.36e-02	1.30e-02
2^{-20}	8.39e-03	1.24e-02	1.41e-02	1.18e-02	6.51e-03
2^{-22}	5.11e-03	6.21e-03	7.06e-03	5.89e-03	3.26e-03
2^{-24}	5.12e-03	3.10e-03	3.53e-03	2.95e-03	1.63e-03
E^N	5.31e+00	6.90e+00	7.85e+00	8.14e+00	6.80e+00

Table 10.17: Computed maximum pointwise scaled difference $V^{*-1}\|D_x^- V_{M\varepsilon} - D_x V_{MB}^{8192}\|_{\overline{\Omega_\varepsilon^N}\backslash\Gamma_L\cup X_1}$ where $V_{M\varepsilon}$ is generated by $(A_{M\varepsilon}^N)$ for various values of ε, N, v_i and $\beta = 0.8$.

Graphs of the scaled differences $\sqrt{\varepsilon}(D_y^- U_{M\varepsilon} - D_y U_{MB}^{8192})$, $D_y^- V_{M\varepsilon} - D_y V_{MB}^{8192}$ and $\frac{1}{V^*}(D_x^- V_{M\varepsilon} - D_x V_{MB}^{8192})$ generated by (A_ε^N) are given in Figures 10-10, 10-11 and 10-13 for $N = 32$ $\varepsilon = 2^{-12}$, $\beta = 0.8$ and $v_i = -0.6$, 2.0 and 7.0.
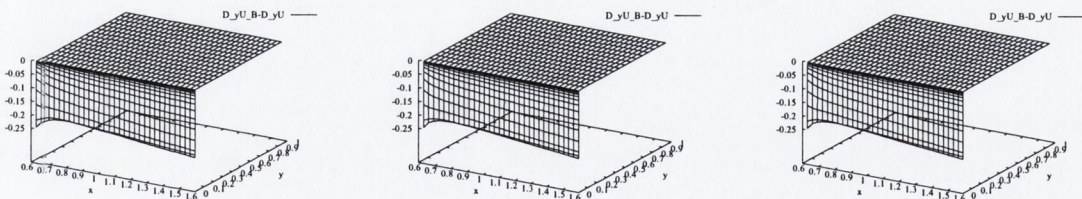
Figure 10-10: Graphs of $\sqrt{\varepsilon}(D_y^- U_{M\varepsilon} - D_y U_{MB}^{8192})$ for $\varepsilon = 2^{-12}$, $N=32$, $\beta = 0.8$ and $v_i = -0.6, 2.0$ and 7.0.
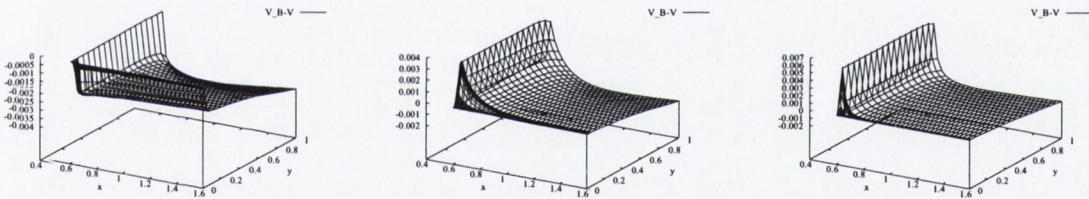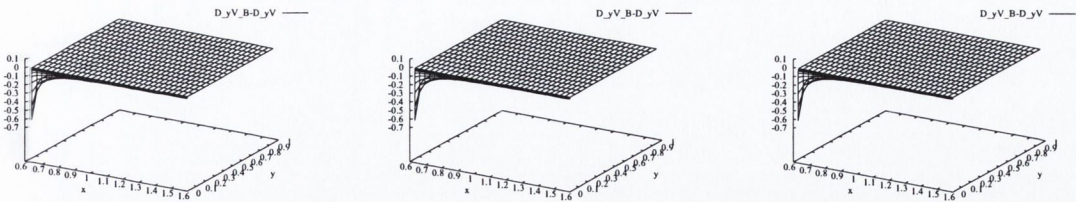
Figure 10-11: Graphs of $D_y^- V_{M\varepsilon} - D_y V_{MB}^{8192}$ for $\varepsilon = 2^{-12}$, $N=32$, $\beta = 0.8$ and $v_i = -0.6, 2.0$ and 7.0.

Graphs of $\sqrt{\varepsilon}(D_y^- U_{M\varepsilon} - D_y U_{MB}^{8192})$ and $D_y^- V_{M\varepsilon} - D_y V_{MB}^{8192}$ in Figures 10-10 and 10-11 show the largest differences to be contained within the boundary layer. The largest differences $D_y^- V_{M\varepsilon} - D_y V_{MB}^{8192}$ are at the points closest to the leading edge.

Figure 10-12: Graphs of $\frac{1}{V^*}(D_x^- V_{M\varepsilon} - D_x V_{MB}^{8192})$ for $\varepsilon = 2^{-12}$, $N=32$, $\beta = 0.8$ and $v_i = -0.6, 2.0$ and 7.0.

Graphs of $\frac{1}{V^*}(D_x^- V_{M\varepsilon} - D_x V_{MB}^{8192})$ in Figure 10-13 show the largest difference to be closest to the leading edge.

In Tables 10.18 -10.20 we display the computed orders of convergence for the approximations of the first order scaled derivatives of the velocity components $\sqrt{\varepsilon}D_y^- U_{M\varepsilon}$, $D_y^- V_{M\varepsilon}$ and $\frac{1}{V^*}D_x^- V_{M\varepsilon}$, respectively for various values of ε, N, v_i and $\beta = 0.8$.

	$v_i = -0.6$					$v_i = 2.0$					$v_i = 7.0$			
$\varepsilon \backslash N$	32	64	128	256	$\varepsilon \backslash N$	32	64	128	256	$\varepsilon \backslash N$	32	64	128	256
2^{-0}	0.92	0.86	0.75	0.60	2^{-0}	0.91	0.86	0.78	0.41	2^{-0}	1.02	0.66	0.59	0.27
2^{-2}	0.97	0.95	0.89	0.80	2^{-2}	0.73	0.91	0.86	0.78	2^{-2}	0.88	1.01	1.03	0.47
2^{-4}	1.13	0.98	0.95	0.91	2^{-4}	1.07	1.06	0.74	0.69	2^{-4}	0.71	0.80	0.85	0.90
2^{-6}	1.09	1.10	1.11	1.11	2^{-6}	0.72	1.04	1.12	1.16	2^{-6}	0.70	0.79	0.85	0.90
2^{-8}	0.76	0.81	0.91	1.08	2^{-8}	0.72	0.84	0.93	0.99	2^{-8}	0.70	0.79	0.85	0.89
2^{-10}	0.76	0.81	0.85	0.89	2^{-10}	0.72	0.84	0.93	0.99	2^{-10}	0.70	0.79	0.85	0.89
2^{-12}	0.76	0.81	0.85	0.89	2^{-12}	0.72	0.84	0.93	0.99	2^{-12}	0.72	0.79	0.85	0.89
2^{-14}	0.76	0.81	0.85	0.89	2^{-14}	0.73	0.84	0.93	0.99	2^{-14}	0.73	0.80	0.85	0.89
2^{-16}	0.76	0.81	0.85	0.89	2^{-16}	0.73	0.84	0.93	0.99	2^{-16}	0.73	0.80	0.85	0.90
2^{-18}	0.76	0.81	0.85	0.89	2^{-18}	0.73	0.84	0.93	0.99	2^{-18}	0.74	0.80	0.86	0.90
2^{-20}	0.76	0.81	0.85	0.89	2^{-20}	0.73	0.84	0.93	0.99	2^{-20}	0.74	0.80	0.86	0.90
2^{-22}	0.76	0.81	0.85	0.89	2^{-22}	0.73	0.84	0.93	0.99	2^{-22}	0.74	0.81	0.86	0.90
2^{-24}	0.76	0.81	0.85	0.89	2^{-24}	0.73	0.84	0.93	0.99	2^{-24}	0.74	0.81	0.86	0.90
p_{comp}^N	0.76	0.81	0.85	0.89	p_{comp}^N	0.73	0.84	0.93	0.99	p_{comp}^N	0.74	0.81	0.86	0.90
$C_{0.85}$	4.12	4.37	4.50	4.50	$C_{0.93}$	14.25	16.41	17.39	17.39	$C_{0.86}$	28.72	31.11	32.19	32.19

Table 10.18: Computed orders of convergence $p_{\varepsilon,comp}^N$, p_{comp}^N and the error constant $C_{p_{comp}^*}^N$ for $\sqrt{\varepsilon}(D_y^- U_{M\varepsilon} - D_y U_{MB}^{8192})$ where $U_{M\varepsilon}$ is generated by $(A_{M\varepsilon}^N)$ for various values of ε, N, v_i and $\beta = 0.8$.

	$v_i = -0.6$					$v_i = 2.0$					$v_i = 7.0$			
$\varepsilon \backslash N$	32	64	128	256	$\varepsilon \backslash N$	32	64	128	256	$\varepsilon \backslash N$	32	64	128	256
2^{-0}	0.90	0.55	0.04	0.03	2^{-0}	0.39	0.54	0.70	1.08	2^{-0}	0.39	0.56	0.65	1.01
2^{-2}	0.95	0.70	0.16	0.13	2^{-2}	0.28	0.47	0.58	0.73	2^{-2}	0.23	0.59	0.89	1.26
2^{-4}	0.76	0.79	0.26	0.26	2^{-4}	0.54	0.38	0.37	0.45	2^{-4}	0.09	0.38	0.69	0.98
2^{-6}	1.10	1.16	0.40	0.17	2^{-6}	0.37	0.71	0.40	0.45	2^{-6}	0.09	0.38	0.69	0.97
2^{-8}	0.76	0.84	0.97	0.66	2^{-8}	0.37	0.66	0.46	0.46	2^{-8}	0.09	0.38	0.69	0.97
2^{-10}	0.76	0.84	0.90	0.72	2^{-10}	0.37	0.66	0.46	0.46	2^{-10}	0.08	0.38	0.69	0.97
2^{-12}	0.76	0.84	0.90	0.72	2^{-12}	0.37	0.66	0.46	0.46	2^{-12}	0.08	0.38	0.69	0.98
2^{-14}	0.76	0.84	0.90	0.72	2^{-14}	0.37	0.66	0.45	0.46	2^{-14}	0.08	0.38	0.69	0.98
2^{-16}	0.76	0.84	0.90	0.72	2^{-16}	0.37	0.66	0.45	0.46	2^{-16}	0.08	0.38	0.69	0.98
2^{-18}	0.76	0.84	0.90	0.72	2^{-18}	0.37	0.66	0.45	0.46	2^{-18}	0.08	0.38	0.69	0.98
2^{-20}	0.76	0.84	0.90	0.72	2^{-20}	0.37	0.66	0.45	0.46	2^{-20}	0.08	0.38	0.69	0.98
2^{-22}	0.76	0.84	0.90	0.72	2^{-22}	0.37	0.66	0.45	0.46	2^{-22}	0.08	0.38	0.69	0.98
2^{-24}	0.76	0.84	0.90	0.72	2^{-24}	0.37	0.66	0.45	0.46	2^{-24}	0.08	0.38	0.69	0.98
p_{comp}^N	0.76	0.84	0.90	0.72	p_{comp}^N	0.37	0.66	0.45	0.46	p_{comp}^N	0.09	0.38	0.69	0.98
$C_{0.72}$	2.52	2.47	2.27	2.00	$C_{0.45}$	5.74	6.09	5.27	5.27	$C_{0.69}$	34.02	51.57	63.92	63.92

Table 10.19: Computed orders of convergence $p_{\varepsilon,comp}^N$, p_{comp}^N and the error constant $C_{p_{comp}^*}^N$ for $D_y^- V_{M\varepsilon} - D_y V_{MB}^{8192}$ where $V_{M\varepsilon}$ is generated by $(A_{M\varepsilon}^N)$ for various values of ε, N, v_i and $\beta = 0.8$.

The results in Tables 10.15 and 10.18 suggest that the method is an ε-uniform numerical method and of order at least 0.68 for $\sqrt{\varepsilon}D_y^- U_{M\varepsilon}$ for $N \geq 64$ for all v_i and $\beta = 0.8$.

The results in Tables 10.16 and 10.19 suggest that the method is an ε-uniform numerical method and of order at least 0.45 for $D_y^- V_{M\varepsilon}$ for $N \geq 64$ for all v_i and $\beta = 0.8$.

Using Tables 10.18-10.19, we obtain the following error bounds

$$
\begin{array}{lll}
v_i = -0.6 & \sqrt{\varepsilon}||D_y^- U_{M\varepsilon} - D_y U_{MB}^{8192}||_{\Omega_\varepsilon^N} & \leq 4.50 N^{-0.85} \\
v_i = 2.0 & \sqrt{\varepsilon}||D_y^- U_{M\varepsilon} - D_y U_{MB}^{8192}||_{\Omega_\varepsilon^N} & \leq 17.39 N^{-0.93} \\
v_i = 7.0 & \sqrt{\varepsilon}||D_y^- U_{M\varepsilon} - D_y U_{MB}^{8192}||_{\Omega_\varepsilon^N} & \leq 32.19 N^{-0.86}
\end{array}
\tag{10.7}
$$

$$
\begin{array}{lll}
v_i = -0.6 & ||D_y^- V_{M\varepsilon} - D_y V_{MB}^{8192}||_{\Omega_\varepsilon^N \backslash \Gamma_L} & \leq 2.52 N^{-0.72} \\
v_i = 2.0 & ||D_y^- V_{M\varepsilon} - D_y V_{MB}^{8192}||_{\Omega_\varepsilon^N \backslash \Gamma_L} & \leq 6.09 N^{-0.45} \\
v_i = 7.0 & ||D_y^- V_{M\varepsilon} - D_y V_{MB}^{8192}||_{\Omega_\varepsilon^N \backslash \Gamma_L} & \leq 63.92 N^{-0.98}.
\end{array}
\tag{10.8}
$$

Further computations, not reported here, show that the errors for the velocity components for $v_i \in [-0.6, 7.0]$ and $\beta \in [0.0, 1.0]$ have similar behaviour, therefore the method can be said to be $(\varepsilon, v_i, \beta)$–uniform for $\sqrt{\varepsilon} D_y^- U_{M\varepsilon}$ and $D_y^- V_{M\varepsilon}$.

The results in Table 10.20 do not suggest that the numerical method is ε-uniform for $\frac{1}{V^*}(D_x^- V_{M\varepsilon} - D_x V_{MB}^{8192})$ for all β on the domain $\overline{\Omega}_\varepsilon^N \backslash (X_1 \bigcup \Gamma_L)$. Hence we look at the results in Table 10.21 of the computed orders of convergence for $\frac{1}{V^*}(D_x^- V_{M\varepsilon} - D_x V_{MB}^{8192})$ in the subdomain $\overline{\Omega}_\varepsilon^N \backslash (X_1 \bigcup \Gamma_L) \bigcap [x_0 + 0.1, x_N] \times [0, 1]$. These results suggest that the method is ε-uniform for $\frac{1}{V^*} D_x^- V_{M\varepsilon}$ in the subdomain for all $\varepsilon \leq 2^{-2}$, all v_i and β.

$\varepsilon\backslash N$	$v_i = -0.6$				$\varepsilon\backslash N$	$v_i = 2.0$			
	32	64	128	256		32	64	128	256
2^{-0}	-0.89	-0.56	-0.51	-0.59	2^{-0}	-0.33	-0.19	-0.05	0.29
2^{-2}	-0.81	-0.61	-0.57	-0.63	2^{-2}	-0.52	-0.30	-0.20	-0.09
2^{-4}	-1.03	-0.56	-0.50	-0.53	2^{-4}	-0.40	-0.51	-0.46	-0.40
2^{-6}	-1.39	-0.82	-0.67	-0.62	2^{-6}	-0.37	-0.49	-0.52	-0.42
2^{-8}	-1.75	-0.83	-0.63	-0.65	2^{-8}	-0.37	-0.47	-0.52	-0.43
2^{-10}	-1.36	-0.83	-0.64	-0.65	2^{-10}	-0.37	-0.47	-0.52	-0.43
2^{-12}	-0.64	-0.83	-0.64	-0.65	2^{-12}	-0.37	-0.47	-0.52	-0.43
2^{-14}	0.23	-0.83	-0.64	-0.65	2^{-14}	-0.37	-0.47	-0.56	-0.40
2^{-16}	0.99	-0.64	-0.64	-0.65	2^{-16}	-0.37	-0.47	-0.56	-0.40
2^{-18}	0.95	0.37	-0.64	-0.65	2^{-18}	-0.37	-0.47	-0.56	-0.40
2^{-20}	0.91	0.89	-0.13	-0.65	2^{-20}	0.51	-0.47	-0.56	-0.40
2^{-22}	0.88	0.87	0.91	-0.65	2^{-22}	1.08	0.01	-0.56	-0.40
2^{-24}	0.86	0.87	0.93	0.36	2^{-24}	1.04	0.88	-0.37	-0.40
p^N_{comp}	-0.91	-0.56	-0.51	-0.63	p^N_{comp}	-0.42	-0.30	-0.20	-0.09
$C_{-0.63}$	-0.02	-0.02	-0.02	-0.02	$C_{-0.20}$	-4.53	-5.28	-5.68	-5.68

$\varepsilon\backslash N$	$v_i = 7.0$			
	32	64	128	256
2^{-0}	-0.38	-0.19	-0.05	0.26
2^{-2}	-0.46	-0.06	0.26	0.61
2^{-4}	-0.58	-0.19	0.28	0.87
2^{-6}	-0.59	-0.19	0.26	0.85
2^{-8}	-0.59	-0.19	0.27	0.85
2^{-10}	-0.58	-0.19	0.27	0.85
2^{-12}	-0.57	-0.19	0.26	0.86
2^{-14}	-0.57	-0.19	0.26	0.86
2^{-16}	-0.57	-0.19	0.26	0.86
2^{-18}	-0.57	-0.19	0.26	0.86
2^{-20}	-0.57	-0.19	0.26	0.86
2^{-22}	-0.28	-0.19	0.26	0.86
2^{-24}	0.72	-0.19	0.26	0.86
p^N_{comp}	-0.38	-0.19	-0.05	0.26
$C_{-0.05}$	-119.15	-149.40	-163.85	-163.85

Table 10.20: Computed orders of convergence $p^N_{\varepsilon,comp}$, p^N_{comp} and the error constant $C^N_{p^*_{comp}}$ for $\frac{1}{V^*}(D_x^- V_{M\varepsilon} - D_x V_{MB}^{8192})$ in the domain $\overline{\Omega}_\varepsilon^N \backslash (X_1 \bigcup \Gamma_L)$ where $V_{M\varepsilon}$ is generated by $(A_{M\varepsilon}^{\mathbf{N}})$ for various values of ε, N and β.

Figure 10-13: Graphs of $\frac{1}{V^*}(D_x^- V_{M\varepsilon} - D_x V_{MB}^{8192})$ for $\varepsilon = 2^{-12}$, N=32, $\beta = 0.8$ and $v_i = -0.6, 2.0$ and 7.0.
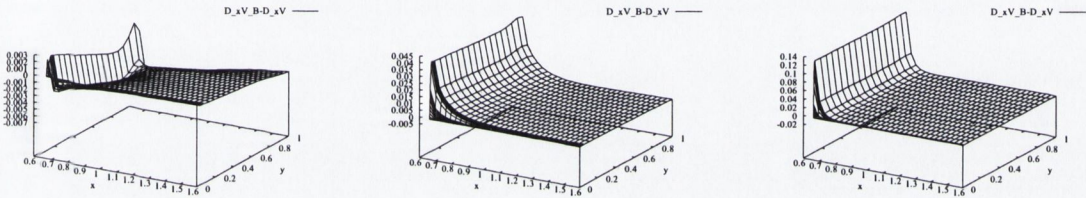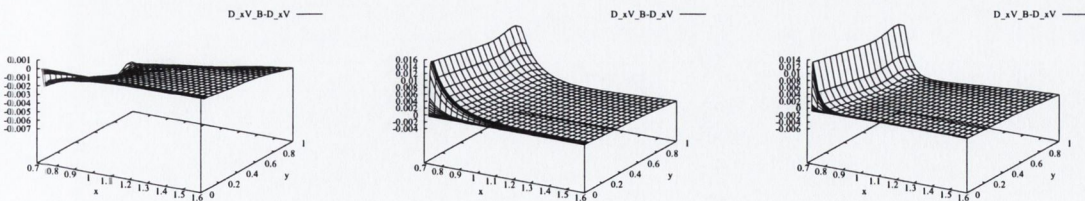
Graphs of $\frac{1}{V^*}(D_x^- V_{M\varepsilon} - D_x V_{MB}^{8192})$ in Figure 10-13 show the largest difference to be along the left hand edge of the subdomain.

$\varepsilon\backslash N$	$v_i = -0.6$			
	32	64	128	256
2^{-0}	0.67	0.41	0.32	-1.48
2^{-2}	1.03	1.02	0.64	-0.46
2^{-4}	0.85	1.08	1.13	1.09
2^{-6}	1.44	0.94	0.96	0.97
2^{-8}	1.03	1.33	1.13	1.15
2^{-10}	1.01	1.16	1.05	1.14
2^{-12}	1.01	1.04	1.00	1.07
2^{-14}	1.04	0.97	0.97	1.01
2^{-16}	1.07	0.92	0.95	0.98
2^{-18}	1.08	0.92	0.95	0.97
2^{-20}	1.08	0.92	0.94	0.96
2^{-22}	1.08	0.92	0.94	0.96
2^{-24}	1.08	0.92	0.94	0.96
p_{comp}^N	0.92	0.77	0.32	-1.48

$\varepsilon\backslash N$	$v_i = 2.0$			
	32	64	128	256
2^{-0}	1.38	1.41	1.54	-1.36
2^{-2}	1.12	1.08	1.23	1.34
2^{-4}	0.96	1.09	1.24	1.24
2^{-6}	0.56	0.92	1.18	1.26
2^{-8}	0.56	0.77	0.99	1.09
2^{-10}	0.56	0.77	0.99	1.09
2^{-12}	0.56	0.77	0.99	1.09
2^{-14}	0.56	0.77	0.99	1.09
2^{-16}	0.72	0.77	0.99	1.09
2^{-18}	1.07	1.04	1.02	1.01
2^{-20}	1.07	1.04	1.02	1.01
2^{-22}	1.08	1.04	1.00	0.93
2^{-24}	1.07	1.01	0.93	0.95
p_{comp}^N	1.06	1.09	1.24	0.33
$C_{0.33}$	3.27	1.96	1.16	0.62

$\varepsilon\backslash N$	$v_i = 7.0$			
	32	64	128	256
2^{-0}	1.66	1.61	2.07	1.43
2^{-2}	1.26	1.33	1.50	1.47
2^{-4}	1.06	1.04	1.22	1.14
2^{-6}	1.02	1.03	1.21	1.14
2^{-8}	0.98	1.02	1.21	1.14
2^{-10}	0.96	1.01	1.21	1.15
2^{-12}	0.96	1.00	1.21	1.14
2^{-14}	0.96	1.01	1.21	1.14
2^{-16}	1.06	1.03	1.01	1.00
2^{-18}	1.07	1.03	1.01	1.01
2^{-20}	1.07	1.03	1.02	0.94
2^{-22}	1.07	1.03	0.93	0.94
2^{-24}	1.07	0.98	0.93	0.95
p_{comp}^N	1.26	1.33	1.50	1.36
$C_{1.36}$	88.74	94.93	96.86	87.81

Table 10.21: Computed orders of convergence $p_{\varepsilon,comp}^N$, p_{comp}^N and the error constant $C_{p^*}^N$ for $\frac{1}{V^*}(D_x^- V_{M\varepsilon} - D_x V_{MB}^{8192})$ in the subdomain $\overline{\Omega}_\varepsilon^N \backslash (X_1 \bigcup \Gamma_L) \bigcap [x_0+0.1, x_N] \times [0,1]$ where $V_{M\varepsilon}$ is generated by $(A_{M\varepsilon}^N)$ for various values of ε, N and β.

10.6 Computational error bounds

In this section we use the computed error estimates, obtained in Section 9.5 for the quantities $(U_{MB}^{8192}, V_{MB}^{8192})$ and their scaled discrete derivatives, to estimate the error in the numerical approximations $(U_{M\varepsilon}, \frac{1}{V^*}V_{M\varepsilon})$ generated by the direct method $(A_{M\varepsilon}^N)$. Also, we present an independent estimate of the maximum pointwise errors in the numerical solutions generated by the direct algorithm. The resulting estimates are independent of those obtained in Section 10.3.

First, we use the triangle inequality to obtain

$$
\begin{aligned}
\|U_{M\varepsilon} - u_M\|_{\Omega_\varepsilon^N} &= \|U_{M\varepsilon} - u_{MB}\|_{\Omega_\varepsilon^N} \\
&\leq \|U_{M\varepsilon} - U_{MB}^{8192}\|_{\Omega_\varepsilon^N} + \|U_{MB}^{8192} - u_{MB}\|_{\Omega_\varepsilon^N} \quad (10.9)
\end{aligned}
$$

$$
\begin{aligned}
\frac{1}{V^*}\|V_{M\varepsilon} - v_{MB}\|_{\overline{\Omega}_\varepsilon^N \backslash \Gamma_L} &= \frac{1}{V^*}\|V_{M\varepsilon} - v_{MB}\|_{\overline{\Omega}_\varepsilon^N \backslash \Gamma_L} \\
&\leq \frac{1}{V^*}(\|V_{M\varepsilon} - V_{MB}^{8192}\|_{\overline{\Omega}_\varepsilon^N \backslash \Gamma_L} + \|V_{MB}^{8192} - v_{MB}\|_{\overline{\Omega}_\varepsilon^N}) \, (10.10)
\end{aligned}
$$

where $\mathbf{U}_{M\varepsilon} = (U_{M\varepsilon}, V_{M\varepsilon})$ is the solution generated by the direct algorithm $(A_{M\varepsilon}^N)$ on the mesh Ω_ε^N with $\mathbf{N} = (N, N)$. $\mathbf{u}_{MB} = (u_{MB}, v_{MB})$ is the exact solution of

the Prandtl problem constructed from the Blasius formulae (9.2) and (9.3) and $\mathbf{U}_{\mathrm{MB}}^{8192} = (U_{\mathrm{MB}}^{8192}, V_{\mathrm{MB}}^{8192})$ is the computed Blasius solution generated in the previous chapter on a mesh with 8192 intervals. We then observe that the first term on the right–hand side of (10.9) and (10.10) involves the computable quantities $U_{M\varepsilon}, U_{\mathrm{MB}}^{8192}$ and $V_{M\varepsilon}, V_{\mathrm{MB}}^{8192}$, respectively. Furthermore, the second term on each right–hand side involves the scaled pointwise errors $U_{\mathrm{MB}}^{8192} - u_{\mathrm{MB}}$, $\frac{1}{V^*}(V_{\mathrm{MB}}^{8192} - v_{\mathrm{MB}})$, which have already been estimated in Section 9.5 of the previous chapter. This shows that we can estimate the errors in the scaled numerical solutions and their scaled discrete derivatives, generated by the numerical method $(A_{M\varepsilon}^{\mathbf{N}})$ applied to problem $(P_{M\varepsilon})$, even though no theoretical error analysis is available for this numerical method.

We now compare the magnitudes of the two terms on the right–hand side of both (10.9) and (10.10). The first terms are the scaled maximum pointwise differences $\|U_{M\varepsilon} - U_{\mathrm{MB}}^{8192}\|_{\overline{\Omega}_\varepsilon^N}$ and $\frac{1}{V^*}\|V_{M\varepsilon} - V_{\mathrm{MB}}^{8192}\|_{\overline{\Omega}_\varepsilon^N \backslash \Gamma_L}$. These quantities are found immediately from the solutions $\mathbf{U}_{M\varepsilon}$ of $(A_{M\varepsilon}^{\mathbf{N}})$ and the solution $\mathbf{U}_{\mathrm{MB}}^{8192}$, respectively, computed in the previous section and chapter. Their numerical bounds are given in Tables 10.13 and 10.14 for various values of ε, N, v_i and $\beta = 0.8$. The second terms on the right–hand side of (10.9) and (10.10) are the scaled maximum pointwise errors $\|U_{\mathrm{MB}}^{8192} - u_{\mathrm{MB}}\|_{\Omega_\varepsilon^N}$ and $\frac{1}{V^*}\|V_{\mathrm{MB}}^{8192} - v_{\mathrm{MB}}\|_{\Omega_\varepsilon^N}$ in the computed Blasius solution. The corresponding error bounds (9.12) and (9.14), respectively, show that the second terms are bounded above by 1.822×10^{-3} and 1.136×10^{-3} for all v_i.

$$
\begin{aligned}
\|U_{M\varepsilon} - u_{\mathrm{M}}\|_{\Omega_\varepsilon^N} &= \|U_{M\varepsilon} - u_{\mathrm{MB}}\|_{\Omega_\varepsilon^N} \\
&\leq \|U_{M\varepsilon} - U_{\mathrm{MB}}^{8192}\|_{\Omega_\varepsilon^N} + \|U_{\mathrm{MB}}^{8192} - u_{\mathrm{MB}}\|_{\Omega_\varepsilon^N}
\end{aligned}
$$

$$
\begin{aligned}
v_i = -0.6 \quad &\leq \quad 0.22N^{-0.82} + 1.822 \times 10^{-3} \qquad (10.11) \\
v_i = 2.0 \quad &\leq \quad 5.10N^{-0.95} + 1.822 \times 10^{-3} \\
v_i = 7.0 \quad &\leq \quad 6.54N^{-0.94} + 1.822 \times 10^{-3}
\end{aligned}
$$

$$
\begin{aligned}
\frac{1}{V^*}\|V_{M\varepsilon} - v_{\mathrm{M}}\|_{\Omega_\varepsilon^N} &= \frac{1}{V^*}\|V_{M\varepsilon} - v_{\mathrm{MB}}\|_{\Omega_\varepsilon^N} \\
&\leq \frac{1}{V^*}\|V_{M\varepsilon} - V_{\mathrm{MB}}^{8192}\|_{\Omega_\varepsilon^N} + \frac{1}{V^*}\|V_{\mathrm{MB}}^{8192} - v_{\mathrm{MB}}\|_{\Omega_\varepsilon^N}
\end{aligned}
$$

$$
\begin{aligned}
v_i = -0.6 \quad &\leq \quad 0.35N^{-0.60} + 1.136 \times 10^{-3} \qquad (10.12) \\
v_i = 2.0 \quad &\leq \quad 2.48N^{-0.67} + 1.136 \times 10^{-3} \\
v_i = 7.0 \quad &\leq \quad 12.57N^{-0.79} + 1.136 \times 10^{-3}
\end{aligned}
$$

The computational error bounds for $U_{M\varepsilon}$ and $V_{M\varepsilon}$ in (10.11), (10.12), (10.1) and (10.2) give two workable formulas for each velocity component to ensure the error is below a desired value for all ε v_i and β. In a similar manner to the above we calculate computed error bounds for approximations of the scaled first derivatives $\sqrt{\varepsilon}D_y^- U_{M\varepsilon}$

and $D_y^- V_{M\varepsilon}$ by the bounds (9.21), (9.24), (10.7) and (10.8)

$$
\begin{aligned}
\sqrt{\varepsilon}\|D_y^- U_{M\varepsilon} - \partial_y u_{\mathrm{M}}\|_{\Omega_\varepsilon^N \backslash \Gamma_B} &= \sqrt{\varepsilon}\|D_y^- U_{M\varepsilon} - \partial_y u_{\mathrm{MB}}\|_{\Omega_\varepsilon^N \backslash \Gamma_M B} \\
&\leq \sqrt{\varepsilon}\|D_y^- U_{M\varepsilon} - D_y U_{\mathrm{MB}}^{8192}\|_{\Omega_\varepsilon^N \backslash \Gamma_M B} + \\
&\quad \sqrt{\varepsilon}\|D_y U_{\mathrm{MB}}^{8192} - \partial_y u_{\mathrm{MB}}\|_{\Omega_\varepsilon^N \backslash \Gamma_M B}
\end{aligned} \tag{10.13}
$$

$$v_i = -0.6 \qquad\qquad \leq\; 4.50 N^{-0.85} + 5.502 \times 10^{-2}$$
$$v_i = 2.0 \qquad\qquad \leq\; 17.39 N^{-0.93} + 5.502 \times 10^{-2}$$
$$v_i = 7.0 \qquad\qquad \leq\; 32.19 N^{-0.86} + 5.502 \times 10^{-2}$$

$$
\begin{aligned}
\|D_y^- V_{M\varepsilon} - \partial_y v_{\mathrm{M}}\|_{\Omega_\varepsilon^N \backslash \Gamma_B} &= \|D_y^- V_{M\varepsilon} - \partial_y v_{\mathrm{MB}}\|_{\Omega_\varepsilon^N \backslash \Gamma_M B} \\
&\leq \|D_y^- V_{M\varepsilon} - D_y V_{\mathrm{MB}}^{8192}\|_{\Omega_\varepsilon^N \backslash \Gamma_M B} + \\
&\quad \|D_y V_{\mathrm{MB}}^{8192} - \partial_y v_{\mathrm{MB}}\|_{\Omega_\varepsilon^N \backslash \Gamma_M B}
\end{aligned} \tag{10.14}
$$

$$v_i = -0.6 \qquad\qquad \leq\; 2.52 N^{-0.72} + 1.214 \times 10^{-3}$$
$$v_i = 2.0 \qquad\qquad \leq\; 6.09 N^{-0.45} + 1.214 \times 10^{-3}$$
$$v_i = 7.0 \qquad\qquad \leq\; 63.92 N^{-0.98} + 1.214 \times 10^{-3}.$$

10.7 Conclusion

In Chapters 5 and 6 we considered the Prandtl boundary layer equations for incompressible laminar flow past a wedge with suction/blowing of the flow rate density $v_0(x) = -v_i 2^{-1/2} Re^{-1/2} x^{-1/2}$, where the Reynolds number Re can be arbitrarily large, β is the angle of the wedge with arbitrary values in the segment $[0, 1]$ and v_i is the intensity of the mass transfer with arbitrary values in the segment $[-0.6, 7.0]$. When the Reynolds number is large the solution of this problem has a parabolic boundary layer at the surface of the wedge excluding its leading edge. We constructed a direct numerical method for computing approximations to the solution of this problem using a piecewise uniform fitted mesh technique appropriate to the parabolic boundary layer. To validate this numerical method the model Prandtl problem with self-similar solution was examined, for which a reference solution can be computed using the Blasius problem for a nonlinear ordinary differential equation. We considered the Prandtl problem in a finite rectangle, excluding the leading edge of the wedge, for various values of Re which can be arbitrarily large and for some values of v_i and β, when meshes with a different number of mesh points were used. To find reference solutions for the the velocity components and their derivatives with required accuracy, we solved the Blasius problem using a semi–analytical numerical method. By extensive numerical experiments we showed that the direct numerical

method constructed in this chapter allows us to approximate both the solution and its derivatives Re–uniformly for different values of v_i and β.

Chapter 11

Conclusion and future work

11.1 Conclusion

In this thesis, we have constructed four parameter-uniform numerical methods for four Prandtl problems.

In Chapters 3 and 4, we constructed a new numerical method for the Prandtl problem for flow past a wedge. In Chapter 3, we numerically solved the Falkner–Skan problem for f and its derivatives, and then used a variant of the semi-analytic approach of Falkner–Skan to generate numerical approximations of guaranteed pointwise accuracy to the velocity components and their scaled derivatives. In Chapter 4, we constructed a direct numerical method for the Prandtl problem to generate numerical approximations of guaranteed accuracy to the velocity components and their scaled derivatives for any given Reynolds number and angle of the wedge.

By means of extensive numerical experiments we showed that the constructed direct numerical method is (Re, β)-uniform for the velocity components.

In Chapters 5 and 6, we constructed a (Re, β)-uniform numerical method for the Prandtl boundary layer problem for flow past a three dimensional semi-infinite wedge using a similar approach to Chapters 3 and 4.

In Chapters 7 and 8, we constructed a (Re, Pr, β, n)–uniform numerical method for the Prandtl boundary layer problem for flow past a semi-infinite wedge with heat–transfer.

Finally, in Chapters 9 and 10, we constructed a (Re, β, v_i)-uniform numerical method for the Prandtl boundary layer problem for flow past a semi-infinite wedge with mass–transfer.

It is worth noting that the experimental error analysis technique used to calculate the bounds in Chapters 4, 6, 8 and 10 is not known to be applicable to the numerical

solutions generated by each algorithm applied to its problem. This is because there is no theoretical error analysis available currently. Nevertheless, it is clear from the results in this thesis that the experimental error analysis technique provides a means to estimate the accuracy of the numerical approximations to the unknown continuous solution and its derivatives even when no theoretical error estimates are known. This suggests the methods constructed in Chapters 3-10 are robust layer-resolving methods.

11.2 Future work

As an immediate consequence to work in this thesis these are some of the problems that have come to light:

- adapt the direct numerical method in Chapters 5 and 6 to construct a robust numerical method for more complex three dimensional shapes [46].

- investigate the use of a second transition point on linear equations.

- explore the complex nature of the thermal layer in Chapter 8 by looking at a linear coupled equation with similar properties to the Prandtl problem for heat transfer.

- attack the Prandtl problem with heat transfer with Neumann and Dirichlet boundary conditions [18] and the Prandtl problem with heat transfer including the effect of frictional heat [46].

- assault the Prandtl problem with heat transfer in natural flow [18].

- combine the methods in Chapters 8 and 10 to construct a numerical method for the Prandtl Problem with heat and mass transfer [43].

- construct a method for the Prandtl problem with heat and mass transfer in the boundary layers on an exponentially stretching continuous plate [37].

Our ultimate goal is this: after dealing with laminar flow, after addressing transitional flow, we dream of constructing a parameter-uniform method for turbulence of the water around the barge.

Appendix A

The choice of V^*

In this appendix we investigate the choice of the scaling factor for

$$v_{FS}(x,y) = -\sqrt{\frac{m+1}{2x}\frac{U}{Re}}\left(f(\eta) + \frac{m-1}{m+1}\eta f'(\eta)\right). \tag{A.1}$$

Using the extensions

$$f''(\eta) = 0, \text{ for all } \eta \geq L \tag{A.2}$$

$$f'(\eta) = 1, \text{ for all } \eta \geq L \tag{A.3}$$

$$f(\eta) = (\eta - L_N) + f(L_N), \text{ for all } \eta \geq L, \tag{A.4}$$

to look at $v_{FS}(x,y)$ for $\eta \geq L$. Rewriting A.1 we have

$$
\begin{aligned}
v_{FS}(x,y) \quad &= -\sqrt{\frac{m+1}{2x_n}\frac{U(x_n)}{Re}}\left(\eta - L_N + f(L_N) + \frac{m-1}{m+1}\eta 1\right) \quad \eta \geq L \\
&= -\sqrt{\frac{m+1}{2x_n}\frac{U(x_n)}{Re}}\left(-L_N + f(L_N) + (1 + \frac{m-1}{m+1})\eta\right) \quad \eta \geq L \\
&= -\sqrt{\frac{m+1}{2x_n}\frac{U(x_n)}{Re}}\left(-L_N + f(L_N) + \beta\eta\right) \quad \eta \geq L \\
&= -\sqrt{\frac{m+1}{2x_n}\frac{U(x_n)}{Re}}(-L_N + f(L_N)) - \sqrt{\frac{m+1}{2x_n}\frac{U(x_n)}{Re}}(y_n\sqrt{\frac{(m+1)Re}{2}\frac{U(x_n)}{x_n}}\beta) \quad \eta \geq L \\
&= -\sqrt{\frac{m+1}{2x_n}\frac{U(x_n)}{Re}}(-L_N + f(L_N)) - y_n\frac{m+1}{2x_n}U(x_n)\beta \quad \eta \geq L \\
&= O(\sqrt{\varepsilon}) + \beta O(1)
\end{aligned}
\tag{A.5}
$$

as a result of these calculations we choose V^*

$$V^* = \begin{cases} \sqrt{\varepsilon} & \text{for } \beta = 0 \\ 1 & \text{for } \beta \neq 0. \end{cases}$$

Using

$$\sqrt{\tfrac{m+1}{2x}\tfrac{U(x)}{Re}}(\|\overline{F}(\eta) - f(\eta)\|) \le \sqrt{\tfrac{m+1}{2x}U(x)}(\|\overline{F}(\eta) - f(\eta)\|)$$

we rearrange the inequality such that it does not contain Re,

$$
\begin{aligned}
\|V_{FS} - v_{FS}\|_{\overline{\Omega}} \;=\; & \sqrt{\tfrac{m+1}{2x}\tfrac{U(x)}{Re}}\|\overline{F}(\eta) + \tfrac{m-1}{m+1}\eta\overline{D^+F}(\eta) \\
& \quad -(f(\eta) + \tfrac{m-1}{m+1}\eta f')\|) \\
\le\; & \sqrt{\tfrac{m+1}{2x}\tfrac{U(x)}{Re}}(\|\overline{F}(\eta) - f(\eta)\| \\
& +\|\tfrac{m-1}{m+1}\eta\overline{D^+F}(\eta) - \tfrac{m-1}{m+1}\eta f'\|) \\
\le\; & \sqrt{\tfrac{m+1}{2x}\tfrac{U(x)}{Re}}(\|\overline{F}(\eta) - f(\eta)\| \\
& +\|\tfrac{m-1}{m+1}\eta\overline{D^+F}(\eta) - \tfrac{m-1}{m+1}\eta f'\|) \\
\le\; & \sqrt{\tfrac{m+1}{2x}\tfrac{U(x)}{Re}}(\|\overline{F}(\eta) - f(\eta)\|) \\
& +\sqrt{\tfrac{m+1}{2x}\tfrac{U(x)}{Re}\tfrac{m-1}{m+1}}y\sqrt{\tfrac{(m+1)Re}{2}\tfrac{U}{x}}\|\overline{D^+F}(\eta) - f'\|) \\
\le\; & \sqrt{\tfrac{m+1}{2x}\tfrac{U(x)}{Re}}(\|\overline{F}(\eta) - f(\eta)\|) \\
& +\tfrac{m+1}{2x}U(x)\tfrac{m-1}{m+1}y\|\overline{D^+F}(\eta) - f'\|) \\
\le\; & \sqrt{\tfrac{m+1}{2x}U(x)}(\|\overline{F}(\eta) - f(\eta)\|) \\
& +U(x)\tfrac{m-1}{2x}y\|\overline{D^+F}(\eta) - f'\|)
\end{aligned}
$$

We now investigate

$$\partial_x V_{FS} = \frac{m-1.0}{2x}\left(V_{FS} - \sqrt{\frac{(m+1)U(x)}{(2xRe)}}\left(\eta\overline{D^+}F + \eta\frac{m-1.0}{m+1.0}\left(\overline{D^+}F + \eta\overline{D^+D^+}F\right)\right)\right).$$
(A.6)

Using the same arguments we applied to v_{FS} we look at $\partial_x V_{FS}$ for $\eta \ge L$

$$
\begin{aligned}
\partial_x V_{FS} \;&=\; \tfrac{m-1.0}{2x_n}\left(V_{FS} - \eta\sqrt{\tfrac{(m+1)U(x_n)}{(2x_n Re)}}\left(1 + \tfrac{m-1.0}{m+1.0}\left(1 + \eta 0\right)\right)\right) \;\; \eta \ge L \\
&=\; \tfrac{m-1.0}{2x_n}\left(MaxV_{FS} - y_n\tfrac{(m+1)U(x_n)}{(2x_n)}\left(1 + \tfrac{m-1.0}{m+1.0}\left(1 + \eta 0\right)\right)\right) \;\; \eta \ge L \\
&=\; (\beta O(1) + O(\sqrt{\varepsilon}))
\end{aligned}
$$

As a result we can use the scaling factor V^* for $\partial_x v_{FS}$.

Rearranging the inequality such that it is free from *Re*,

$$
\begin{aligned}
\left\| \partial_x V_{FS} - \frac{\partial v_{FS}}{\partial x} \right\|_{\overline{\Omega}} &= \frac{m-1.0}{2x} \\
&\quad \left(\left\| V_{FS} - \sqrt{\frac{(m+1)U(x)}{(2xRe)}} \left(\eta \overline{D^+F} + \eta \frac{m-1.0}{m+1.0} \left(\overline{D^+F} + \eta \overline{D^+D^+F} \right) \right) \right.\right.\\
&\quad \left.\left. - v_{FS} + \sqrt{\frac{(m+1)U(x)}{(2xRe)}} \left(\eta f' + \eta \frac{m-1.0}{m+1.0} \left(f' + \eta f'' \right) \right) \right\| \right) \\
&\leq \frac{m-1.0}{2x} \left(\left\| V_{FS} - v_{FS} \right\|_{\overline{\Omega}} \right. \\
&\quad + \sqrt{\frac{m+1}{2x}\frac{U(x)}{Re}} \left\| (1 + \tfrac{m-1}{m+1})\eta \overline{D^+F} + \tfrac{m-1}{m+1}\eta^2 \overline{D^+D^+F} \right. \\
&\quad \left.\left. - (1 + \tfrac{m-1}{m+1})\eta f' + \tfrac{m-1}{m+1}\eta^2 f'' \right\|_{[0,\infty)} \right) \\
&\leq \frac{m-1.0}{2x} \left(\left\| V_{FS} - v_{FS} \right\|_{\overline{\Omega}} \right. \\
&\quad + \eta\sqrt{\frac{m+1}{2x}\frac{U(x)}{Re}} \left\| (1 + \tfrac{m-1}{m+1})\overline{D^+F} + \tfrac{m-1}{m+1}\eta \overline{D^+D^+F} \right. \\
&\quad \left.\left. - (1 + \tfrac{m-1}{m+1})f' + \tfrac{m-1}{m+1}\eta f'' \right\|_{[0,\infty)} \right) \\
&\leq \frac{m-1.0}{2x} \left(\left\| V_{FS} - v_{FS} \right\|_{\overline{\Omega}} \right. \\
&\quad + \tfrac{m+1}{2x}U(x) \left\| (1 + \tfrac{m-1}{m+1})\overline{D^+F} + \tfrac{m-1}{m+1}\eta \overline{D^+D^+F} \right. \\
&\quad \left.\left. - (1 + \tfrac{m-1}{m+1})f' + \tfrac{m-1}{m+1}\eta f'' \right\|_{[0,\infty)} \right) \\
&\leq \frac{m-1.0}{2x} \left(\left\| V_{FS} - v_{FS} \right\|_{\overline{\Omega}} \right. \\
&\quad + \tfrac{m+1}{2x}U(x) \left(\left\| (1 + \tfrac{m-1}{m+1})\overline{D^+F} - (1 + \tfrac{m-1}{m+1})f' \right\|_{[0,\infty)} \right.\\
&\quad \left.\left. + \left\| \tfrac{m-1}{m+1}\eta \overline{D^+D^+F} - \tfrac{m-1}{m+1}\eta f'' \right\|_{[0,\infty)} \right) \right) \\
&\leq \frac{m-1.0}{2x} \left(\left\| V_{FS} - v_{FS} \right\|_{\overline{\Omega}} \right. \\
&\quad + \tfrac{m+1}{2x}U(x)\beta \left\| \overline{D^+F} - f' \right\|_{[0,\infty)} \\
&\quad \left. + \tfrac{m-1}{m+1} \left\| \eta \overline{D^+D^+F} - \eta f'' \right\|_{[0,\infty)} \right).
\end{aligned}
$$

(A.7)

Appendix B

Theoretical tables

	$\beta = 0.5$							
N	128	256	512	1024	2048	4096	8192	16384
$N^{-1}lnN$	0.78	0.81	0.83	0.85	0.86	0.87	0.88	0.89
$2N^{-1}ln\frac{N}{2}$	0.74	0.78	0.81	0.83	0.85	0.86	0.87	0.88

Table B.1: Orders of local convergence p^N corresponding to different theoretical bounds for various values of N.

Appendix C

The choice of C

C.1 Introduction

In this Appendix we investigate the subtle choices of the constant C when defining the transition point. We use two simple examples to illustrate the choice of C.

Using the Prandtl problem for flow past a flat plate (see Chapter 2) we define the two approaches. When constructing a mesh in the rectangle Ω, it is important to note where the boundary layer occurs in order to define an appropriate transition point from the coarse to the fine mesh. Because the computational domain is rectangular the piecewise–uniform fitted mesh Ω_ε^N is a tensor product of two one–dimensional meshes. The mesh in the x direction is the uniform mesh

$$\Omega_u^{N_x} = \{x_i : x_i = 0.1 + iN_x^{-1}, 0 \leq i \leq N_x\}.$$

The mesh in the y-direction is a piecewise–uniform fitted mesh, which is defined by

$$\Omega_\varepsilon^{N_y} = \{y_j : y_j = \sigma j \frac{2}{N_y}, 0 \leq j \leq \frac{N_y}{2}; y_j = \sigma + (1-\sigma)(j - \frac{N_y}{2})\frac{2}{N_y}, \frac{N_y}{2} \leq j \leq N_y\}$$

The transition point σ is chosen so that there is a fine mesh in the boundary layer when required. The appropriate choice in this case is

$$\sigma = \min\{\frac{1}{2}, C\sqrt{\varepsilon}lnN_y\}.$$

The factor $\sqrt{\varepsilon}$ may be motivated from *a priori* estimates of the derivatives of the solution $\mathbf{u}_\varepsilon$ or from asymptotic analysis [46].

The two case we choose are:

- $C = 0.5$, which will reduce the value of σ;

- $C = 2.5$, which will enlarge the value of σ.

The rectangular mesh is then the tensor product $\Omega_\varepsilon^{\mathbf{N}} = \Omega_u^{N_x} \times \Omega_\varepsilon^{N_y}$, where $\mathbf{N} = (N_x, N_y)$. For simplicity we take $N_x = N_y = N$.

The systems of linearized equations are

$$
(A_\varepsilon^{\mathbf{N}}) \begin{cases}
\text{With the boundary condition } \mathbf{U}_\varepsilon^M = \mathbf{U}_{\mathrm{UB}}^{8192} \text{ on } \Gamma_{\mathrm{L}}, \\
\text{for each } i, 1 \le i \le N, \text{ use the initial guess } \mathbf{U}_\varepsilon^0|_{X_i} = \mathbf{U}_\varepsilon^0|_{X_{i-1}} \\
\text{and for } m = 1, \ldots, M \text{ solve the following} \\
\text{two point boundary value problem for } U_\varepsilon^m(x_i, y_j) \\
\\
-\varepsilon \delta_y^2 U_\varepsilon^m(x_i, y_j) + U_\varepsilon^{m-1}(x_i, y_j) D_x^- U_\varepsilon^m(x_i, y_j) + \\
V_\varepsilon^{m-1}(x_i, y_j) D_y^- U_\varepsilon^m(x_i, y_j) = 0 \\
\\
\text{with the boundary conditions } U_\varepsilon^m = U_{\mathrm{UB}} \text{ on } \Gamma_{\mathrm{B}} \cup \Gamma_{\mathrm{T}}, \\
\text{and the initial guess for } V_\varepsilon^0|_{X_1} = 0. \\
\text{Also solve the initial value problem for } V_\varepsilon^m(x_i, y_j) \\
\\
(\mathbf{D}^- \cdot \mathbf{U}_\varepsilon^m)(x_i, y_j) = 0, \\
\\
\text{with initial condition } V_\varepsilon^m = 0 \text{ on } \Gamma_{\mathrm{B}}. \\
\text{Continue to iterate between the equations for } \mathbf{U}_\varepsilon^m \text{ until } m = M, \\
\text{where } M \text{ is such that} \\
\max\left(|U_\varepsilon^M - U_\varepsilon^{M-1}|_{\overline{\Omega}_\varepsilon^N}, \frac{1}{\sqrt{\varepsilon}}|V_\varepsilon^M - V_\varepsilon^{M-1}|_{\overline{\Omega}_\varepsilon^N}\right) \le tol.
\end{cases}
$$

For notational simplicity, we suppress explicit mention of the iteration superscript M henceforth, and we write simply $\mathbf{U}_\varepsilon$ for the solution generated by $(A_\varepsilon^{\mathbf{N}})$. We take $tol = 10^{-6}$ in the computations.

C.2 Error Analysis

In this section we compute ε–uniform maximum pointwise differences in the approximations generated by the direct numerical method described in the previous section. For this case, we compare the parameter uniform maximum pointwise differences in the approximations generated by the direct numerical method with the corresponding values of $\mathbf{U}_{UB}^{8192}$.

The maximum pointwise differences $||U_\varepsilon - \overline{U_{UB}}^{8192}||_{\overline{\Omega}_\varepsilon^N}$ of N and ε for $C = 0.5$ and $C = 2.5$ are given in Tables C.1 and C.2, respectively. In Tables C.1 and C.2 we

see that the computed maximum differences decrease as the number of mesh points, N, increases. In Table C.1 we see that the maximum pointwise differences do not stabilise to a fixed value as ε decrease for $C = 0.5$. Thus we cannot say that the method is ε-uniform when $C = 0.5$.

			C=0.5		
$\varepsilon \backslash N$	32	64	128	256	512
2^{-0}	2.87e-03	1.66e-03	8.98e-04	4.51e-04	2.12e-04
2^{-2}	1.24e-02	6.22e-03	3.12e-03	1.57e-03	7.92e-04
2^{-4}	3.21e-02	1.67e-02	8.17e-03	4.04e-03	2.02e-03
2^{-6}	4.76e-02	2.10e-02	1.00e-02	5.41e-03	3.00e-03
2^{-8}	7.56e-02	3.35e-02	1.39e-02	6.14e-03	3.00e-03
2^{-10}	5.65e-02	4.93e-02	2.23e-02	8.88e-03	3.61e-03
2^{-12}	1.19e-01	4.58e-02	3.42e-02	1.55e-02	5.72e-03
2^{-14}	1.94e-01	1.12e-01	4.54e-02	2.46e-02	1.12e-02
2^{-16}	2.38e-01	1.61e-01	8.89e-02	3.77e-02	1.73e-02
2^{-18}	2.62e-01	1.89e-01	1.19e-01	6.45e-02	2.88e-02
2^{-20}	2.74e-01	2.05e-01	1.37e-01	8.25e-02	4.52e-02
E^N	2.74e-01	2.05e-01	1.37e-01	8.25e-02	4.52e-02

Table C.1: Computed maximum pointwise difference $||U_u - U_{UB}^{8192}||_{\overline{\Omega}_u^N}$ generated by (A_u^N) for various values of ε and N.

In Table C.2 we see that the maximum pointwise differences tend to a fixed value as ε decreases for $C = 2.5$. Table C.2 indicates that maximum errors are independent of ε, this suggests that the method is ε–uniform for U_ε for $C = 2.5$.

$$C=2.5$$

$\varepsilon \backslash N$	32	64	128	256	512
2^{-0}	2.87e-03	1.66e-03	8.98e-04	4.51e-04	2.12e-04
2^{-2}	1.24e-02	6.22e-03	3.12e-03	1.57e-03	7.92e-04
2^{-4}	3.52e-02	1.67e-02	8.17e-03	4.04e-03	2.02e-03
2^{-6}	7.25e-02	3.26e-02	1.56e-02	7.62e-03	3.78e-03
2^{-8}	1.89e-01	6.96e-02	3.16e-02	1.51e-02	7.43e-03
2^{-10}	2.23e-01	9.64e-02	4.98e-02	2.68e-02	1.46e-02
2^{-12}	2.23e-01	9.64e-02	4.98e-02	2.68e-02	1.46e-02
2^{-14}	2.23e-01	9.64e-02	4.98e-02	2.68e-02	1.46e-02
2^{-16}	2.23e-01	9.64e-02	4.98e-02	2.68e-02	1.46e-02
2^{-18}	2.23e-01	9.64e-02	4.98e-02	2.68e-02	1.46e-02
2^{-20}	2.23e-01	9.64e-02	4.98e-02	2.68e-02	1.46e-02
E^N	2.23e-01	9.64e-02	4.98e-02	2.68e-02	1.46e-02

Table C.2: Computed maximum pointwise difference $||U_u - U_{UB}^{8192}||_{\overline{\Omega}_u^N}$ generated by (A_u^N) for various values of ε and N.

Graphs of the velocity component U_ε and of the difference $U_\varepsilon - U_{UB}^{8192}$ with $N = 32$ and $\varepsilon = 2^{-12}$ for $C = 0.5$ and $C = 2.5$ are shown in Figures C-1 and C-2 respectively. In Figure C-1 we see that for $C = 0.5$ the fine mesh is contained within the boundary layer, which would lead to the erroneous results in Table C.1.
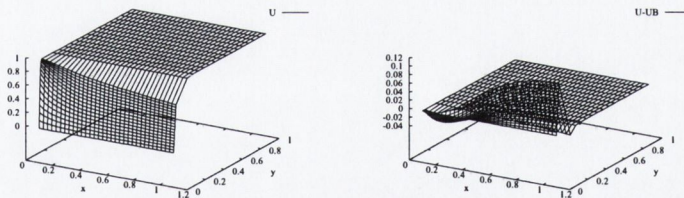
Figure C-1: Graphs of U_ε and $U_\varepsilon - U_{UB}$ for $\varepsilon = 2^{-12}$, $N=32$ and $C = 0.5$.

In Figure C-2 we see that for $C = 2.5$ the fine mesh contains the boundary layer but not optimising the fine mesh.

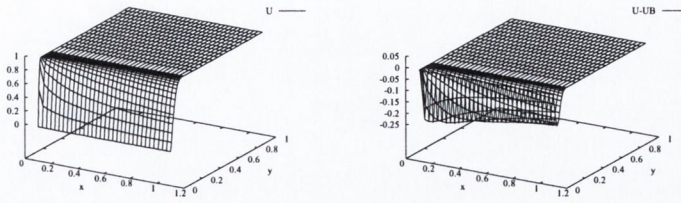Figure C-2: Graphs of U_ε and $U_\varepsilon - U_{UB}$ for $\varepsilon = 2^{-12}$, N=32 and $C = 2.5$.

C.3 The choice of C

From the two examples we have shown that the choice of C is significant. It is prudent to choose it such that is larger than 1.

Appendix D

A curious side effect of σ_2

D.1 Introduction

In this Appendix we investigate benefits of using a second transition point. The motivation for this is from Chapter 8, were the second transition point was used to resolve the thermal layer.

Using the Prandtl problem for flow past a flat plate (see Chapter 2) we define the piecewise compound mesh. When constructing a mesh in the rectangle Ω, it is important to note where the boundary layer occurs in order to define an appropriate transition point from the coarse to the fine mesh. Because the computational domain is rectangular the piecewise–uniform fitted mesh Ω_ε^N is a tensor product of two one–dimensional meshes. The mesh in the x direction is the uniform mesh

$$\Omega_u^{N_x} = \{x_i : x_i = 0.1 + iN_x^{-1}, 0 \leq i \leq N_x\}.$$

The mesh in the y-direction is a compound piecewise–uniform fitted mesh, which is defined by

$$\Omega_\varepsilon^{N_y} = \{y_j : y_j = \sigma_2 j\tfrac{4}{N_y}, 0 \leq j \leq \tfrac{N_y}{4}; y_j = \sigma_2 + (\sigma - \sigma_2)(j - \tfrac{N_y}{4})\tfrac{4}{N_y}, \tfrac{N_y}{4} \leq j \leq \tfrac{N_y}{2};$$
$$y_j = \sigma + (1 - \sigma)(j - \tfrac{N_y}{2})\tfrac{2}{N_y}, \tfrac{N_y}{2} \leq j \leq N_y\}.$$

The transition points σ and σ_2 are chosen so that there is a fine mesh in the boundary layer when required. The appropriate choices in this case are

$$\sigma = \min\{\tfrac{1}{2}, 1.2\sqrt{\varepsilon}lnN_y\} \tag{D.1}$$

$$\sigma_2 = \min\{\tfrac{1}{2}\sigma, \tfrac{1}{32}\sqrt{\varepsilon}lnN_y\}. \tag{D.2}$$

The factor $\sqrt{\varepsilon}$ may be motivated from *a priori* estimates of the derivatives of the solution $\mathbf{u}_\varepsilon$ or from asymptotic analysis [46]. The choice of $\frac{1}{32}$ is purely experimental. The rectangular mesh is then the tensor product $\Omega_\varepsilon^{\mathbf{N}} = \Omega_u^{N_x} \times \Omega_\varepsilon^{N_y}$, where $\mathbf{N} = (N_x, N_y)$. For simplicity we take $N_x = N_y = N$.

The systems of linearized equations are

$(A_{2\varepsilon}^{\mathbf{N}})$ $\begin{cases} \text{With the boundary condition } \mathbf{U}_\varepsilon^M = \mathbf{U}_{\mathrm{UB}}^{8192} \text{ on } \Gamma_{\mathrm{L}}, \\ \text{for each } i, 1 \le i \le N, \text{ use the initial guess } \mathbf{U}_\varepsilon^0|_{X_i} = \mathbf{U}_\varepsilon^0|_{X_{i-1}} \\ \text{and for } m = 1, \dots, M \text{ solve the following} \\ \text{two point boundary value problem for } U_\varepsilon^m(x_i, y_j) \\ \\ -\varepsilon \delta_y^2 U_\varepsilon^m(x_i, y_j) + U_\varepsilon^{m-1}(x_i, y_j) D_x^- U_\varepsilon^m(x_i, y_j) + \\ V_\varepsilon^{m-1}(x_i, y_j) D_y^- U_\varepsilon^m(x_i, y_j) = 0 \\ \\ \text{with the boundary conditions } U_\varepsilon^m = U_{\mathrm{UB}} \text{ on } \Gamma_{\mathrm{B}} \cup \Gamma_{\mathrm{T}}, \\ \text{and the initial guess for } V_\varepsilon^0|_{X_1} = 0. \\ \text{Also solve the initial value problem for } V_\varepsilon^m(x_i, y_j) \\ \\ (\mathbf{D}^- \cdot \mathbf{U}_\varepsilon^m)(x_i, y_j) = 0, \\ \\ \text{with initial condition } V_\varepsilon^m = 0 \text{ on } \Gamma_{\mathrm{B}}. \\ \text{Continue to iterate between the equations for } \mathbf{U}_\varepsilon^m \text{ until } m = M, \\ \text{where } M \text{ is such that} \\ \max\left(|U_\varepsilon^M - U_\varepsilon^{M-1}|_{\overline{\Omega}_\varepsilon^N}, \frac{1}{\sqrt{\varepsilon}}|V_\varepsilon^M - V_\varepsilon^{M-1}|_{\overline{\Omega}_\varepsilon^N}\right) \le tol. \end{cases}$

For notational simplicity, we suppress explicit mention of the iteration superscript M henceforth, and we write simply $\mathbf{U}_\varepsilon$ for the solution generated by $(A_\varepsilon^{\mathbf{N}})$. We take $tol = 10^{-6}$ in the computations.

D.2   Error Analysis

In this section we compute ε−uniform maximum pointwise differences in the approximations generated by the direct numerical method described in the previous section. For this case, we compare the parameter uniform maximum pointwise differences in the approximations generated by the direct numerical method with the corresponding values of $\mathbf{U}_{UB}^{8192}$.

The maximum pointwise differences $\|U_\varepsilon - \overline{U}_{UB}^{8192}\|_{\overline{\Omega}_\varepsilon^N}$ and $\sqrt{\varepsilon}\|V_\varepsilon - \overline{V}_{UB}^{8192}\|_{\overline{\Omega}_\varepsilon^N}$ for var-

ious values of N and ε are given in Tables D.1 and D.2, respectively. In Tables D.1 and D.2 we see that the computed maximum differences decrease as the number of mesh points, N, increases. In Tables D.1 and D.2 we see that the maximum pointwise differences stabilise to a fixed value as ε decreases.

$\varepsilon\backslash N$	32	64	128	256	512
2^{-0}	2.42e-03	1.49e-03	8.42e-04	4.38e-04	2.10e-04
2^{-2}	1.78e-02	8.29e-03	3.95e-03	1.91e-03	9.35e-04
2^{-4}	5.97e-02	2.69e-02	1.26e-02	6.05e-03	2.94e-03
2^{-6}	1.39e-01	5.78e-02	2.63e-02	1.25e-02	6.03e-03
2^{-8}	1.59e-01	8.15e-02	4.29e-02	2.30e-02	1.22e-02
2^{-10}	1.59e-01	8.15e-02	4.29e-02	2.30e-02	1.24e-02
.	.	.	.	.	.
2^{-20}	1.59e-01	8.15e-02	4.29e-02	2.30e-02	1.24e-02
E^N	1.59e-01	8.15e-02	4.29e-02	2.30e-02	1.24e-02

Table D.1: Computed maximum pointwise difference $||U_\varepsilon - U_{UB}^{8192}||_{\overline{\Omega}_\varepsilon^N}$ generated by $(A_{2\varepsilon}^{\mathbf{N}})$ for various values of ε and N.

$\varepsilon\backslash N$	32	64	128	256	512
2^{-0}	2.32e-01	1.15e-01	5.57e-02	2.74e-02	1.35e-02
2^{-2}	5.15e-01	2.49e-01	1.17e-01	5.51e-02	2.64e-02
2^{-4}	1.19e+00	5.11e-01	2.33e-01	1.07e-01	4.90e-02
2^{-6}	3.40e+00	1.22e+00	5.05e-01	2.22e-01	9.78e-02
2^{-8}	4.12e+00	1.87e+00	8.84e-01	4.33e-01	2.05e-01
2^{-10}	4.12e+00	1.87e+00	8.84e-01	4.33e-01	2.08e-01
.	.	.	.	.	.
2^{-20}	4.12e+00	1.87e+00	8.84e-01	4.33e-01	2.08e-01
E^N	4.12e+00	1.87e+00	8.84e-01	4.33e-01	2.08e-01

Table D.2: Computed maximum pointwise difference $\frac{1}{\sqrt{\varepsilon}}||V_\varepsilon - V_{UB}^{8192}||_{\overline{\Omega}_\varepsilon^N}$ generated by $(A_{2\varepsilon}^{\mathbf{N}})$ for various values of ε and N.

The orders of convergence and the error constants of the scaled velocity components are given in Tables D.3 and D.3, respectively.

$\varepsilon\backslash N$	32	64	128	256
2^{-0}	0.70	0.82	0.94	1.06
2^{-2}	1.10	1.07	1.05	1.03
2^{-4}	1.15	1.09	1.06	1.04
2^{-6}	1.26	1.13	1.08	1.05
2^{-8}	0.96	0.93	0.90	0.91
2^{-10}	0.96	0.93	0.90	0.89
.	.	.	.	.
2^{-20}	0.96	0.93	0.90	0.89
p_{comp}^{N}	0.96	0.93	0.90	0.89
$C_{0.89}$	7.60	7.23	7.06	7.02

Table D.3: Computed orders of convergence $p_{\varepsilon,comp}^{N}$, p_{comp}^{N} and the error constant $C_{p_{comp}^{*}}^{N}$ for $U_{\varepsilon} - U_{FS}^{8192}$ where U_{ε} is generated by (A_{ε}^{N}) for various values of ε, N and β.

$\varepsilon\backslash N$	32	64	128	256
2^{-0}	1.01	1.04	1.03	1.01
2^{-2}	1.05	1.09	1.09	1.06
2^{-4}	1.22	1.14	1.12	1.13
2^{-6}	1.48	1.27	1.18	1.19
2^{-8}	1.14	1.08	1.03	1.08
2^{-10}	1.14	1.08	1.03	1.06
.	.	.	.	.
2^{-20}	1.14	1.08	1.03	1.06
p_{comp}^{N}	1.14	1.08	1.03	1.06
$C_{1.03}$	286.33	265.98	256.13	256.13

Table D.4: Computed orders of convergence $p_{\varepsilon,comp}^{N}$, p_{comp}^{N} and the error constant $C_{p_{comp}^{*}}^{N}$ for $V_{\varepsilon} - V_{FS}^{8192}$ where V_{ε} is generated by $(A_{2\varepsilon}^{N})$ for various values of ε, N and β.

Tables D.1 -D.4 show that the method is ε-uniform for the scaled velocity components.

The maximum pointwise differences of the approximations to the scaled first order derivatives of the velocity components for various values of N and ε are given in Tables D.5-D.7, respectively. In Tables D.5-D.7 we see that the computed maximum differences decrease as the number of mesh points, N, increases. In Tables D.5 - D.7 we see that the maximum pointwise differences stabilise to a fixed value as ε decreases.

$\varepsilon \backslash N$	32	64	128	256	512
2^{-0}	1.80e-02	9.14e-03	4.71e-03	2.50e-03	1.39e-03
2^{-2}	7.22e-02	3.59e-02	1.78e-02	8.84e-03	4.40e-03
2^{-4}	1.31e-01	6.64e-02	3.29e-02	1.65e-02	8.28e-03
2^{-6}	2.64e-01	1.30e-01	6.77e-02	3.41e-02	1.71e-02
2^{-8}	2.82e-01	1.77e-01	1.08e-01	6.25e-02	3.48e-02
2^{-10}	2.82e-01	1.77e-01	1.08e-01	6.25e-02	3.53e-02
.	.	.	.	.	.
2^{-20}	2.82e-01	1.77e-01	1.08e-01	6.25e-02	3.53e-02
E^N	2.82e-01	1.77e-01	1.08e-01	6.25e-02	3.53e-02

Table D.5: Computed maximum pointwise difference $\sqrt{\varepsilon}\|D_y^- U_\varepsilon - D_y U_{UB}^{8192}\|_{\overline{\Omega}_\varepsilon^N}$ generated by $(A_{2\varepsilon}^{\mathbf{N}})$ for various values of ε and N.

$\varepsilon \backslash N$	32	64	128	256	512
2^{-0}	2.70e-01	1.35e-01	6.84e-02	3.48e-02	1.79e-02
2^{-2}	4.84e-01	2.48e-01	1.21e-01	5.87e-02	2.94e-02
2^{-4}	9.91e-01	4.94e-01	2.39e-01	1.14e-01	5.46e-02
2^{-6}	2.38e+00	1.11e+00	5.09e-01	2.34e-01	1.08e-01
2^{-8}	2.86e+00	1.70e+00	8.90e-01	4.54e-01	2.23e-01
2^{-10}	2.86e+00	1.70e+00	8.90e-01	4.54e-01	2.27e-01
.	.	.	.	.	.
2^{-20}	2.86e+00	1.70e+00	8.90e-01	4.54e-01	2.27e-01
E^N	2.86e+00	1.70e+00	8.90e-01	4.54e-01	2.27e-01

Table D.6: Computed maximum pointwise difference $\|D_y^- V_\varepsilon - D_y V_{UB}^{8192}\|_{\overline{\Omega}_\varepsilon^N}$ generated by $(A_{2\varepsilon}^{\mathbf{N}})$ for various values of ε and N.

$\varepsilon \backslash N$	32	64	128	256	512
2^{-0}	3.28e+00	1.86e+00	1.03e+00	6.86e-01	7.09e-01
2^{-2}	6.14e+00	3.60e+00	1.89e+00	9.48e-01	6.08e-01
2^{-4}	1.43e+01	7.86e+00	4.00e+00	1.68e+00	7.36e-01
2^{-6}	4.56e+01	2.12e+01	9.94e+00	3.87e+00	1.47e+00
2^{-8}	5.37e+01	3.40e+01	1.94e+01	9.09e+00	3.37e+00
2^{-10}	5.37e+01	3.40e+01	1.94e+01	9.09e+00	3.43e+00
.	.	.	.	.	.
2^{-20}	5.37e+01	3.40e+01	1.94e+01	9.09e+00	3.43e+00
E^N	5.37e+01	3.40e+01	1.94e+01	9.09e+00	3.43e+00

Table D.7: Computed maximum pointwise scaled difference $\frac{1}{\sqrt{\varepsilon}}\|D_x^- V_\varepsilon - D_x V_{FS}^{8192}\|_{\overline{\Omega}_\varepsilon^N \backslash \Gamma_L \bigcup X_1}$ where V_ε is generated by $(A_\varepsilon^{\mathbf{N}})$ for various values of ε and N.

The orders of convergence and the error constants of the scaled velocity components are given in Tables D.8-D.10, respectively.

$\varepsilon \backslash N$	32	64	128	256
2^{-0}	0.98	0.96	0.92	0.84
2^{-2}	1.01	1.01	1.01	1.01
2^{-4}	0.98	1.01	1.00	0.99
2^{-6}	1.02	0.95	0.99	0.99
2^{-8}	0.67	0.72	0.79	0.84
2^{-10}	0.67	0.72	0.79	0.82
.	.	.	.	.
2^{-20}	0.67	0.72	0.79	0.82
p_{comp}^N	0.67	0.72	0.79	0.82
$C_{0.67}$	7.80	7.80	7.56	6.99

Table D.8: Computed orders of convergence $p_{\varepsilon,comp}^N$, p_{comp}^N and the error constant $C_{p_{comp}^*}^N$ for $\sqrt{\varepsilon}(D_y^- U_\varepsilon - D_y U_{FS}^{8192})$ where U_ε is generated by (A_ε^N) for various values of ε and N

$\varepsilon \backslash N$	32	64	128	256
2^{-0}	1.00	0.98	0.98	0.96
2^{-2}	0.96	1.03	1.05	1.00
2^{-4}	1.00	1.05	1.07	1.06
2^{-6}	1.10	1.12	1.12	1.12
2^{-8}	0.75	0.93	0.97	1.02
2^{-10}	0.75	0.93	0.97	1.00
.	.	.	.	.
2^{-20}	0.75	0.93	0.97	1.00
p_{comp}^N	0.75	0.93	0.97	1.00
$C_{0.75}$	95.96	95.96	84.91	73.01

Table D.9: Computed orders of convergence $p_{\varepsilon,comp}^N$, p_{comp}^N and the error constant $C_{p_{comp}^*}^N$ for $(D_y^- V_\varepsilon - D_y V_{FS}^{8192})$ where U_ε is generated by (A_ε^N) for various values of ε and N

$\varepsilon \backslash N$	32	64	128	256
2^{-0}	0.82	0.85	0.59	-0.05
2^{-2}	0.77	0.93	0.99	0.64
2^{-4}	0.87	0.98	1.25	1.19
2^{-6}	1.10	1.09	1.36	1.39
2^{-8}	0.66	0.81	1.09	1.43
2^{-10}	0.66	0.81	1.09	1.41
.	.	.	.	.
2^{-20}	0.66	0.81	1.09	1.41
p_{comp}^{N}	0.66	0.81	1.09	1.41
$C_{0.66}$	1437.66	1437.66	1294.98	958.35

Table D.10: Computed orders of convergence $p_{\varepsilon,comp}^{N}$, p_{comp}^{N} and the error constant $C_{p_{comp}^{*}}^{N}$ for $\frac{1}{\sqrt{\varepsilon}}(D_x^- V_\varepsilon - D_x V_{FS}^{8192})$ in the domain $\overline{\Omega}_\varepsilon^N \backslash (X_1 \bigcup \Gamma_L)$ where V_ε is generated by $(A_\varepsilon^{\mathbf{N}})$ for various values of ε and N

The results in Tables D.5-D.10 suggest that the method is ε-uniform numerical method with orders of convergence of at least 0.66 for $\sqrt{\varepsilon}D_y^- U_\varepsilon$, $D_y^- V_\varepsilon$ and $\frac{1}{\sqrt{\varepsilon}}D_x^- V_\varepsilon$. It is important to note that without the second transition point, σ_2, the method does not give ε-uniform results for $\frac{1}{\sqrt{\varepsilon}}D_x^- V_\varepsilon$. The method is ε-uniform for flow past a flat plate. We also have greatly improved orders of convergence for the $D_x^- V_\varepsilon$. We can only speculate why the introduction of a second transition point has the effect.

Bibliography

[1] D.J. Acheson, *Elementary Fluid Dynamics*, Clarendon Press, (1990).

[2] Myron B Allen III, Eli L. Isaacson, *Numerical Analysis for Applied Science*, John Wiley and Sons, Inc. (1997).

[3] Ali R. Ansari, *On the use of Shishkin Meshes to Obtain Parameter Robust Numerical Solutions of Singularly Perturbed Differential Equations*, PhD Thesis, UL, (2001).

[4] Richard L. Burden, J. Douglas Faires, *Numerical Analysis*, Brooks/Cole, (1997).

[5] J. S. Butler , J.J.H. Miller, G.I. Shishkin, *A Reynolds–uniform numerical method for Prandtl's boundary layer problem for flow past a wedge*, International Journal for Numerical Methods in Fluids 2003; 43:903-913.

[6] J. S. Butler , J.J.H. Miller, G.I. Shishkin, *A Reynolds–uniform numerical method for Prandtl's boundary layer problem for flow past a plate with mass–transfer*, Recent Advances in Computational Science & Engineering, Eds. H.P. Lee, K. Kumar, Imperial College Press, 2002, 733-737. - submitted to Journal of Computational Methods in Sciences and Engineering.

[7] J. S. Butler , J.J.H. Miller, G.I. Shishkin, *A Reynolds uniform numerical method for Prandtl's boundary layer problem for flow past a three dimensional yawed wedge*, Trinity College Dublin, Maths. Dept. Preprint TCDMATH 04-11.

[8] J. S. Butler , J.J.H. Miller, G.I. Shishkin, *A Reynolds uniform numerical method for Prandtl's boundary layer problem for flow past a wedge with heat transfer* , Trinity College Dublin, Maths. Dept. Preprint TCDMATH 04-12.

[9] Yunus A Cenbal *Heat transfer : a practical approach*, 2nd ed. New York ; London : McGraw-Hill, (2003).

[10] Tuncer Cebeci, Peter Bradshaw, *Physical and Computational Aspects of Convective Heat Transfer*, Springer, (1988).

[11] Tuncer Cebeci, Jean Cousteix, *Modeling and Computation of Boundary-Layer Flows*, Springer, Horizons Publishing Inc, (1999).

[12] Tuncer Cebeci, *An Engineering Approach to the Calculation of Aerodynamic Flows*, Springer, (1999).

[13] P. Carragher, L J Crane *Heat Transfer on a Continuous Stretching Sheet*, ZAMM 62, 564-565 1982.

[14] Frank P. Incropera, David P. DeWitt, *Fundamentals of Heat and Mass Transfer*, Hemisphere Publishing Corporation, (1987).

[15] Edward P Doolan *Zero order asymptotic expansions for singularly perturbed problems and theis numerical calculation* MSc Thesis (TCD), (1977).

[16] Edward P Doolan *Uniform numerical methods for problems with initial and boundary layers*, Phd Thesis (TCD), (1980).

[17] Edward P Doolan, J J H Miller, W H A Schilders *Uniform numerical methods for problems with initial and boundary layers*, Boole Press, (1980).

[18] E. R. G. Eckert, Robert M. Drake, Jr, *Analysis of Heat and Mass Transfer*, Hemisphere Publishing Corporation, (1987).

[19] J. Etienne, J. J. H. Miller, G. I. Shishkin, *A Robust Layer Resolving Numerical method for a free convection problem*, Trinity College Dublin, Maths. Dept. Preprint TCDMATH 00-03.

[20] H L Evans, *Laminar Boundary-Layer theory*, Addison–Wesley Publishing Company, (1968).

[21] Paul A Farrell, *Uniformly convergent difference schemes for singularly perturbed turning and non–turning point problems*, Phd Thesis, TCD, (1983).

[22] Paul A Farrell, *A Higher Order Finite Element Method for the Solution of a Singularly Perturbed Differential equation*, MSc Thesis, TCD, (1978).

[23] P. Farrell, A. Hegarty, J.J.H. Miller, E. O'Riordan, G.I. Shishkin, *Computed realistic Reynolds–uniform error bounds for discrete derivatives of flow velocities in the boundary layer for Prandtl's problem*, International journal for Numerical Methods in Fluids 2003, 43:895-902.

[24] P. Farrell, A. Hegarty, J.J.H. Miller, E. O'Riordan, G.I. Shishkin, *Numerical Techniques for flow problems with singularities*, International journal for Numerical Methods in Fluids 2002, 00:1-27.

[25] P. Farrell, A. Hegarty, J.J.H. Miller, E. O'Riordan, G.I. Shishkin, *An iterative Re-uniform method for the Prandtl boudary–layer Problem*, Trinity College Dublin, Maths. Dept. Preprint TCDMATH 99-08.

[26] P. Farrell, A. Hegarty, J.J.H. Miller, E. O'Riordan, G.I. Shishkin, *Robust Computational Techniques for Boundary Layers*, CRC Press, (2000).

[27] Kevin. B. Farrell, *Numerical methods for astrophysical shock dynamics in one dimension*, Thesis (1998).

[28] B. Gahan, J.J.H. Miller, E. O'Riordan, G.I. Shishkin, *Accurate numerical method for Blasius' problem for flow past a flat plate with mass transfer*, Trinity College Dublin, Maths. Dept. Preprint TCDMATH 00-05.

[29] B. Gahan, J.J.H. Miller, E. O'Riordan, G.I. Shishkin, *Reynolds–uniform method for Prandtl's problem with suction–blowing based on Blasius' approach*, Trinity College Dublin, Maths. Dept. Preprint TCDMATH 00-05.

[30] Walter Gautschi, *Numerical Analysis an Introduction*, Birkhauser (1997).

[31] Curtis F. Gerald, Patrick O. Wheatley, *Applied Numerical Analysis*, Addison-Wesley (1994).

[32] Alan F. Hegarty, *Analysis of Finite Difference Methods for Two–Dimensional Elliptic Singular Perturbation Problems*, Phd Thesis, TCD, (1986).

[33] J. P. Holman *Heat transfer*. Boston [Mass.] ; London : McGraw-Hill, c2002.

[34] Cheng-Hsing Hsu, Kai-Long Hsiao, *Conjugate heat transfer of a plate fin in a second-grade fluid flow*, Int. J. Heat Mass Transfer, Vol. 41 Nos 8-9, pp 1087-1102, (1988).

[35] Ian Jaques and Colin Judd, *Numerical Analysis*, Chapman and Hall Ltd, (1987).

[36] C. A. Long, *Essential Heat Transfer*, Pearson Education Limited (1999).

[37] E Magyari, B Keller, *Heat and mass transfer in the boundary layers on an exponentially stretching continuous plate*, J. Phys D: Phys 32 (1999) 577-585.

[38] J.J.H. Miller, A. P. Musgrave, G.I. Shishkin, *A Reynolds–uniform method for the Prandtl solution and its derivatives for stagnation line flow*, International journal for Numerical Methods in Fluids 2003, 43:881-894.

[39] J.J.H. Miller, E. O'Riordan, G.I. Shishkin, *Fitted Numerical Methods for Singular Pertubation problems*, World Scientific Publishing Co. Pte. Ltd., (1996).

[40] J. J. H. Miller, G. I. Shishkin, B. Koren, L. P. Shishkin *Grid approximation of singularly perturbed boundary value problem modelling heat transfer in the case of flow over a flat plate with suction of the boundary layer*,Journal of Computational and applied mathematics 166 (2004) 221-232.

[41] O. A. Oleink, V. N. Samokhin, *Mathematical Models in Boundary Layer Theory*, Chapman & Hall\ CRC, (1999).

[42] H. Oertel, *Prandtl's Essentials of Fluid Mechanics*, Springer 2nd, (2004).

[43] D.F. Rogers, *Laminar Flow Analysis*, Cambridge University Press, (1992).

[44] H.-G. Roos, L. Tobiska M. Stynes, *Numerical methods for singularly perturbed differential equations : convection-diffusion and flow problems*, Berlin ; London : Springer, (1996).

[45] L. Rosenhead, *Laminar Boundary Layers*, Clarendon Press, (1963).

[46] H. Schlichting, *Boundary Layer Theory*, 7th edition, McGraw Hill, (1951).

[47] I J Sobey, *Introduction to Interactive Boundary Layer Theory*, Oxford University Press (2000).

[48] J. Stoer and R. Bulirsch, *Introduction to Numerical Analysis*, Springer-Verlag (1980).

[49] G D Smith *Numerical Solution of Partial Differential Equations: Finite Difference Method*, Oxford (1992).

[50] Z. U. A Warsi, *Fluid dynamics : theoretical and computational approaches*, Boca Raton ; London : CRC Press, (1993).